HYDROLOGICAL MODELLING OF A TROPICAL WATERSHED UNDER LAND USE AND CLIMATE CHANGE SCENARIOS

Ph.D. THESIS

by

AYUSH CHANDRAKAR

DEPARTMENT OF WATER RESOURCES DEVELOPMENT & MANAGEMENT
INDIAN INSTITUTE OF TECHNOLOGY ROORKEE
ROORKEE - 247 667 (INDIA)
DECEMBER, 2019

HYDROLOGICAL MODELLING OF A TROPICAL WATERSHED UNDER LAND USE AND CLIMATE CHANGE SCENARIOS

A THESIS

Submitted in partial fulfilment of the requirements for the award of the degree

of

DOCTOR OF PHILOSOPHY

in

WATER RESOURCES DEVELOPMENT AND MANAGEMENT

by

AYUSH CHANDRAKAR

DEPARTMENT OF WATER RESOURCES DEVELOPMENT & MANAGEMENT
INDIAN INSTITUTE OF TECHNOLOGY ROORKEE
ROORKEE - 247 667 (INDIA)
DECEMBER, 2019

INDIAN INSTITUTE OF TECHNOLGY ROORKEE

STUDENT'S DECLARATION

I hereby certify that the work which is being presented in the thesis entitled "**HYDROLOGICAL MODELLING OF A TROPICAL WATERSHED UNDER LAND USE AND CLIMATE CHANGE SCENARIOS"** is my own work carried out during a period from July, 2013 to December, 2019 under the supervision of Dr. Deepak Khare, Professor, Department of Water Resources Development and Management, Indian Institute of Technology Roorkee, Roorkee.

The matter presented in this thesis has not been submitted for the award of any other degree of this or any other Institute.

(AYUSH CHANDRAKAR)

This is to certify that the above mentioned work is carried out under my supervision.

(Deepak Khare)
Supervisor

The Ph.D. Viva-Voce Examination of Ayush Chandrakar, Research Scholar, has been held on December 17, 2019.

Chairman, SRC **External Examiner**

This is to certify that the student has made all corrections in the thesis.

(Deepak Khare)
Supervisor **Head of the Department**

Dated: December 17, 2019

ABSTRACT

Water is one of the essential components of our environment. Therefore, proper planning and management are essential to achieve sustainable utilization. Changes in climate and land use have significantly altered the hydrological cycle which in turn has affected the water resources. Due to increased uncertainty in both climate and land-use change projections, improved knowledge of watershed hydrology and resource availability are indispensable for current and future policy formulation and sustainable development of the water sector.

The present study has been carried out to ascertain the availability of water and its distribution under the impact of climate change projection and anthropogenic intervention in the Kharun watershed, India. This study investigated the changes in water balance components under varied land use and climate change projections over the Kharun watershed. Kharun watershed lies in the tropical region of central India. Trend changes in meteorological parameters of the past and the future constituted the climate change aspect of the study. The land use land cover (LULC) change dynamics constituted the anthropogenic intervention aspect of the study. Keeping into account the changes in climatic conditions and land change patterns, a hydrological impact assessment was carried out over the study area.

Trend analysis is one of the most significant tools to analyze the global warming problem as it quantifies the past and future changes in meteorological and hydro-climatological parameters. In the present study, trend detection was carried out for two metrological parameters namely, long term temperature (maximum, minimum and mean) and precipitation using regression analysis and Modified Mann-Kendall (MMK) test. The magnitude of change was estimated using the Sen's slope estimator over 22 grids in and around the study area. Cumulative sum (Cusum) and sequential Mann-Kendall (SQMK) test was used to identify the climatic shift (change per year) over the meteorological time series. Significant findings of the study stated an increase in average maximum temperature during summer (0.19ºC), post-monsoon (0.21ºC), and winter (0.61ºC) seasons. A significant reduction in average yearly minimum temperature (-0.68ºC) was also observed. The annual precipitation decreased by almost 210 mm over 115 years.

Similar statistics were computed over 23 indices of meteorological extremes derived from long term precipitation and temperature time series. Out of these 23 indices, five were proposed in the study

based on the precipitation intensity indices suggested by India Meteorological Department (IMD). Long term trend changes in these indices were computed for both historical as well as future periods.

For reproduction of meteorological parameters in order to study changes in extreme value indices in the future, regional climate model (RCMs) were evaluated. Four RCMs were identified as the most suitable models to determine future times series data of precipitation and temperature (maximum and minimum) for the study viz. CCCma, CSIRO, MIROC5 and NorESM. The distribution mapping technique was used to remove systematic biases present in the data. MMK test statistic was used to evaluate the presence of any trend while the magnitude of the trend was quantified using Sen's slope estimator over the entire period (2011-2100) and for three climate periods, namely CC1 (2011-2041), CC2 (2041-2070) and CC3 (2071-2100). These tests were applied over two scenarios viz. RCP 4.5 and RCP 8.5.

After the computation of long term variation in meteorological extremes, it can be inferred that the gap between the minimum and maximum temperature is increasing over the study period at an average rate of 0.09ºC/decade (4.6%), which explains the increasing trend in Diurnal Temperature Range (DTR). This precisely precedes the fact that the days are getting hotter, and the nights are getting colder and its effects can be seen over the rainfall intensities in the region. As per the results obtained, there is a reduction observed in the number of light rainy days (-10.2%), moderate rainy days (-17.8%) in contrast to heavy and heavy rainy days (-25.5 and -18.4%). The number of cumulative dry days in the study area has also increased by 19.5%, which explains the reduction in rainy days. The overall result indicates an increase in DTR in the future along with an increase in days with heavy rainfalls in the case of both scenarios for the study area.

Evaluation of land use land cover is critical and must be monitored to assess the impact on the environment. For this purpose, LULC mapping was carried out for the region using satellite imageries (LANDSAT 5, 7, and 8), remote sensing (RS), and geographical information system (GIS) tools. The LULC maps were classified into six different classes namely water bodies, urban areas, agricultural land, barren land, mixed forest, and sand/open rocks. Significant findings in the study state a decrease in vegetation (agricultural land and mixed forest) in the region due to the rise in the urban area and barren land. After the analysis of historical trend patterns in LULC, the land use land cover map for the near future (2030) was projected using the CA-Markov model. The model was validated and simulated with the classified LULC map of 2015. The projected LULC map of 2030

indicated the continuation of the same trend of the past. These future projections indicate the expected changes in the near future. Therefore, the LULC changes concerning different classes in the near future will help in cautioning the concerned authorities for proper planning and management of the study area.

In order to investigate the effect of land use land cover change and historical and future climate variability on water availability of Kharun watershed, Soil and Water Assessment Tool (SWAT), a semi-distributed hydrological model was calibrated and validated for the area. Parameters namely Baseflow Alpha Factor (ALPHA_BF), Plant uptake compensation factor (EPCO), and Deep aquifer percolation fraction (RCHRG_DP), were found to be the most sensitive parameters for the Kharun watershed. For monthly simulations, the values of Coefficient of determination (R^2), Nash-Sutcliffe efficiency (NSE), and Percent bias (PBIAS) were found to be 0.84, 0.8, and -9.4% during calibration, and 0.85, 0.79 and -9.2% during validation respectively. The results indicated a very good model performance for Kharun watershed. Based on these results, it is concluded that the SWAT model can be successfully employed for the hydrological simulation purposes over Kharun watershed. In order to compute the hydrological components under the dynamics of land use land cover and climate change, 29 simulations were carried out under different variations of land use and climate parameters. Results indicated that the increase in settlement (urban and barren land) for real estate development, accompanied by a decrease in vegetation (agricultural land and mixed forest), has resulted in an increased water yield but the evapotranspiration (ET) reduced due to reduction of vegetation. It is observed that ET reduced with time due to a decrease in vegetation, earlier it used to be 326.71 mm in 1990 but it declined to 298.39 mm during the projected the year of 2030. Due to an increase in overland flow, the water yield increased from 781.58 mm in 1990 to 881.84 mm in the projected the year of 2030. During the last two decades (2010-2030), LULC change increased water yield by 45.88 mm and accounted for 5.48% of the total change (881.84 mm).

Moreover, ET decreased by 4.19% in the same duration. Reduction in precipitation was observed for both RCP scenarios in the period CC1 (2011-2040) by -16.83% for NorESM and by -16.29% for MIROC5. The simulation result suggests that the evapotranspiration (ET) in the region is going to increase between 2011 and 2100 but when compared to IMD simulation as a reference, it was observed that the ET has decreased. The maximum change in ET was obtained in CC3. For RCP 4.5, it was 3.99% (MIROC5) and for RCP 8.5, it was 7.26% (MIROC5). While the minimum change

in ET was observed in CC1. The maximum increase in water yield was observed in CC3, 37.36% for CSIRO (RCP 4.5), and 77.10% for CCCma (RCP 8.5).

In summary, the study provided a scientifically essential and practically relevant approach towards identifying the historical climate variability and hydrological assessment under land use and climate change scenarios considering representative climate models output, in contributing to water resources planning and management in the context of a small tropical watershed.

Keywords: Climate change; LULC; SWAT; MMK; Extreme value indices; SQMK; Cusum; Water balance components; CA-Markov model

ACKNOWLEDGEMENT

I wish to express my deep sense of gratitude to my supervisor Dr. Deepak Khare, Professor, Department of Water Resources Development and Management, Indian Institute of Technology Roorkee, for his invaluable guidance, thought-provoking discussions, and untiring efforts throughout this work. His timely help, encouragement, constructive criticism and painstaking efforts made it possible to present the work carried out by me in the form of this thesis. Prof. Khare taught me how to respond positively to comments in research and publication and taught me to channel the same positivity towards different aspects of life.

I am thankful to Prof. Ajit Kumar Chaturvedi, Director, IIT Roorkee; Prof. M. L. Kansal, Head, Department of WRD&M; Prof. S. K. Mishra, Department of WRD&M & Internal Member (SRC); Dr. R. D. Garg, Department of Civil Engineering & External Member (SRC); and other faculty members at IIT Roorkee, for providing support, constructive suggestions and boosting morale during the study period.

I thankfully acknowledge the moral and technical support received from my mentors and friends, Dr. Santosh Pingale, Dr. Brij Kishor Pandey, Dr. Tesfa Worku, Dr. Santosh palmate, Dr. Sushil Kr. Himanshu, Dr. Amrit Upadhyay, Dr. Subash Rai, Dr. Shailendra Kr. Kumre and Mr. Radha Krishan. A special thanks go to my fellow researchers and lab mates in the Dept. of WRD&M namely, Ms. Tanmoyee, Ms. Sakshi, Ms. Osheen, Mr. Deen Dayal, Mr. Sabyasachi, Mr. Gagan, Mr. Ishan, Mr. Praveen and Mr. Rahul. A wholesome thanks goes to my fellow friends in Azad Bhawan, Mr. Abhishek, Mr. Phani, Mr. Dinesh, Mr. Shishant and Mr. Rajesh; I would also like to acknowledge my empathetic friends in IIT Roorkee who treated me just as I was part of their family, Dr. Aditya, Dr. Ashu and Mrs. Preeti, Dr. Hitesh and Dr. Shambhavi, Dr. Prateek and Mrs. Purnima, Mr. Gopal and Mrs. Deepmala and Mrs. Ruchi. A shoutout goes to "KGP K Boys" for their constant encouragement and friendly support.

It will be unjust on my part to bind in words the spirits of unparalleled sacrifices made by my parents, Mr. Dilip Kumar Chandrakar and Mrs. Manju Chandrakar, for their blessings and moral support. I want to thank my elder brother Mr. Piyush Chandrakar and my sister in law Mrs. Ankita Thawani for their unconditional love and support. My life and my work would not have taken shape as it is now, without the involvement of the love of my life and soon to be my wife Ms. Pooja Bhatt. She is the driving force of my life and always keeps me motivated. I also feel obliged to my family

members who have always supported me spiritually throughout writing this thesis and my life in general.

I thankfully acknowledge the financial support received from the Government of India through the MHRD fellowship during the period of study. The scholarship provided by the 'American Geophysical Union' and IIT Roorkee to attend the AGU Fall Meeting 2018.

Further, my humble thanks are due to all those who, in any manner, directly or indirectly, put a helping hand in every bit of completion of this research work.

(Ayush Chandrakar)

TABLE OF CONTENTS

LIST OF TABLES

LIST OF FIGURES

LIST OF ABBREVIATIONS AND SYMBOLS

S. NO.	Abbreviation	Description
1	Alpha_bf	Baseflow Alpha Factor
2	AMC	Antecedent Moisture Condition
3	ANN	Artificial Neural Network
4	AR5	Assessment Report 5
5	BIOMIX	Biological mixing efficiency
6	CA	Cellular Automata
7	CDF	Cumulative Distribution Function
8	CH_K2	Effective hydraulic conductivity in main channel alluvium
9	CMIP	Coupled Ocean-Atmosphere Model
10	CN	Curve Number
11	CN2	SCS runoff curve number
12	CORDEX	Coordinated Regional Downscaling Experiment
13	Cusum	Cumulative Sum
14	DEM	Digital Elevation Model
15	DTR	Diurnal Temperature Range
16	EPCO	Plant uptake compensation factor
17	ERDAS	Earth Resource Data Analyzing System
18	ESCO	Soil Evaporation Compensation Factor
19	ETM	Enhanced Thematic Mapper
20	FAR	False Alarm Ratio
21	GCM	Global Climate Model
22	GCMs	Global Climate Models
23	GDP	Gross Domestic Product
24	GHGs	Green House Gases
25	GIS	Geographic Information System
26	GPS	Global Positioning System
27	GW_DELAY	Groundwater Delay Time
28	GW_REVAP	Groundwater Revap Coefficient
29	GWQMN	Water depth (threshold) in shallow aquifer for return flow to occur

HRUs	Hydrological Response Units
IMD	India Meteorological Department
IPCC	Intergovernmental Panel on Climate Change
IWRM	Integrated Water Resources Management
km	Kilometer
LANDSAT	Land Satellite
LHOAT	Latin Hypercube One Factor At a Time
LULC	Land Use Land Cover
MCA	Multi-Criteria Analysis
MCM	Million Cubic Meters
mm	Millimeters
MMK	Modified Mann-Kendall
MSL	Mean Sea Level
NASA	National Aeronautical and Space Administration
NSE	Nash–Sutcliffe Efficiency
OLI_TIRS	Operational Land Imager and Thermal Infrared Sensor
PBIAS	Percent Bias
PET	Potential Evapo-transpiration
R^2	Coefficient of Determination
RCHRG_DP	Deep aquifer percolation fraction
RCM	Regional Climate Models
RCP	Representative Concentration Pathways
RMSE	Root Mean Square Error
ROC	Rate of Change
RS	Remote Sensing
SCS	Soil Conservation Service
SLSUBBSN	Average slope length
SOL_AWC	Available Water Capacity
SOL_BD	Moist Bulk Density
SOL_K	Saturated hydraulic conductivity
SOL_Z	Soil depth

61	SQMK	Sequential Mann-Kendall
62	SRTM	Shuttle Radar Topography Mission
63	SUFI	Sequential Uncertainty Fitting
64	SURLAG	Surface runoff lag coefficient
65	SWAT	Soil and Water Assessment Tool
66	SWAT-CUP	SWAT Calibration and Uncertainty Programs
67	TM	Thematic Mapper
68	TN, T_{min}	Minimum Temperature
69	TX, T_{max}	Maximum Temperature
70	TXN, T_{mean}	Mean Temperature
71	WMO	World Meteorological Organization

CHAPTER 1

INTRODUCTION

1.1 GENERAL

Availability of fresh water is indispensable in the socio-economic development and preservation of a healthy environment. It is impossible to imagine the development of any country without access to adequate water for various purposes (viz., drinking, irrigation, environment and ecosystems). In the recent past, there is a remarkable change in nature on the global discussion of issues of climate change and land use/land cover (LULC) change and its effect on water resource availability. These issues, in particular, are disturbing the sustainable development planning and management of water resources. Water resources are vital for the agricultural sector, power generation, ecosystem and human health; moreover its requirement is raising day by day with population growth. However, an increase in water demand is anticipated, but changes in the environment and its impacts on humans and other ecosystems are locally unpredictable. Therefore, it is crucial to plan and manage water resources, considering the anthropogenic effect and environmental changes. Climate projections for the 21st century indicate that rising temperatures and changing precipitation regimes are likely to affect the hydrological cycle and water resources availability. Assessment of water resources availability under climate change impact and anthropogenic activity at a regional and global scale has always been an intriguing issue to the hydrologic research community in the recent past. It is essential to assess the exact knowledge of water availability for policymakers to accomplish sustainable development and management for providing various adaptation strategies.

Global Climate Models (GCMs) are the essential tools and sole means to detect and evaluate the climate change impact. GCMs have been developed to assess the current climate as well as to project the future climatic conditions at the synoptic scale (300 to 450 km spatial resolution). Moreover, GCMs accuracy decreases by increasing finer resolution, which is not suitable to evaluate significant impact studies at the local scale. It is a complex numerical model to formulate the global climate system. However, due to climate change, the temperature is rising and altering the frequency and intensity of precipitation extreme values, which advances the flood and drought events. In the recent past, many studies indicate that global warming has reduced water availability in many regions. Moreover, water is the basic need for development at a regional or local scale, but its availability

influenced by many factors, including hydro-meteorological and climate variability and anthropogenic activities. This study aims to identify the contribution of climate change, human intervention and its combined effect on the future projection of water resources of a tropical watershed.

1.2 BACKGROUND OF THE STUDY

The impact of climate change and anthropogenic activity on climatological parameters influence the hydrological processes and water resources availability. Under global warming, the occurrence of extreme events is altered, which causes water scarcity and hurdles in sustainable development. In the recent past, many studies indicated that global warming had altered water availability in many regions of India. Many researchers and the scientific community have proved that global warming is caused by rising greenhouse gas (GHGs) concentrations and it is the primary reason for the rise in temperature and. Under projected climate change, extreme events (flood and drought) usually will rise across most of the Indian River. In India, during the monsoon season, floods are the most vulnerable natural disasters and affect the settlement as well as cropland. In the recent past, many researchers highlighted the climate change impact on Indian rivers (Gosain et al. 2006; Mall et al. 2006; Pandey et al. 2017).

1.2.1 Long Term Effects of Climate Change over Water Resources

The mean annual precipitation in India is about 1170 mm, and it varies from 100 mm (Rajasthan) to 11000 mm (Meghalaya). Most of the rainfall occurs in monsoon season. Moreover, the average surface runoff estimated to be about 1869 billion cubic meters from rainfall and snowmelt. It is expected that water demand will increase around two times (552 to 1050 billion cubic meters) by 2025 from 1997 (Chatterjee et al. 2014). Climate change and climate variability are altering the intensity and frequency of extreme events. Instrumental and proxy observations indicate global warming due to the emission of greenhouse gases, particularly in the last four-five decades of the 20^{th} century. Mearns et al. (2001) indicated that the surface temperature is rising in the global hydrological cycle which will alter the frequency and intensity of annual precipitation and weather extreme. It is expected that a change in annual precipitation will likely increase flood magnitude and frequency (Bhaskar et al. 1997).

Moreover, change in climatic conditions and LULC dynamics will affect the surface discharge, water yield and water availability, particularly on catchment or basin scale (Rai et al. 2017). Gosain et al.

(2011) simulated the runoff of 12 Indian River basins under climatic conditions of a different scenario. Authors presented the worst affected two river basins (Krishna and Mahanadi), one is under droughts and others concerning floods under climate change effect. Narsimlu et al. (2013) assessed the impact of climate change on water availability of the Upper Sind River Basin and found that the mean annual runoff would increase by 94% at the end of the 21st century.

1.2.2 Effects of Land Use/Land Cover Change due to Anthropogenic Activities

Large scale deforestation, expansion of urbanization and industrialization due to increasing Population growth contributes to global warming. Moreover, increasing urbanization and population alter the ecological system, environment, groundwater recharge, surface water flow, water demand for agriculture, power generation and other purposes. Human interference and GHGs emission are the driving forces behind climate change (Zakaria et al. 2004). Increasing population and their livelihood demands exert the pressure on existing LULC resources. Thus, it is vital to monitor the information about the dynamics of LULC along with population growth and rising requirement. In central India, due to the rising population, there is a continuous over-exploitation of natural resources such as the expansion of cropland at the cost of deforestation and subsequent urbanization from cropland and deforestation. Due to the modification of LULC, many problems generated, such as deficit in soil moisture, high rate of soil loss, depletion of groundwater level and scarcity of water demand. Thus, it is crucial to assess the dynamics of LULC for long term land resources planning and management for decision-makers. Currently, there are many tools such as remote sensing technologies available to assess and develop the LULC map (Nagarajan et al. 1998; Wakode et al. 2013; Samal et al. 2015;). Jaiswal et al. (1999) suggested that geospatial tools and remote sensing data, along with topo sheets obtained from the Survey of India, are appropriate tools to analyze and mapping to LULC. Mondal et al. (2015) examined part of the Narmada River Basin in Madhya Pradesh, India considering different GHGs emission scenarios and show that the rise in precipitation will increase soil erosion.

1.3 PROBLEM IDENTIFICATION

In recent times, various literature from worldwide indicates climatic change, and anthropogenic activities are significantly affecting the water resources availability at regional and basin scale. In India, water resources demand has already raised manifold in the field of agriculture, ecological life, power generation, domestic and industries due to rapid growth in population. In the current scenario, a rise in temperature, change in cropping pattern, overexploitation of groundwater and stream water

has dramatically altered the hydrological cycle and precipitation rate in many climatic zones and water availability of river basins in India. In terms of climate impact on the agriculture field, many crops such as rice, wheat, maize and sorghum are the worst hit by extreme weather conditions. Considering food security, climate change affects 4-9% per year production on a different crop, and 15% to India's Gross Domestic Product (GDP) (Mall et al. 2006b). Therefore, it is vital to assess the water availability under the climate change and dynamics of LULC for long term strategic planning and sustainable development of a region or basin for the country.

1.3.1 Research Gaps

An increased concentration of GHGs and anthropogenic activities are expected to change the climatic conditions causing a rise in temperature and change in precipitation frequency and intensity. The following research gaps are summarized:

1. In most of the studies, annual average precipitation and mean temperature were considered for trend detection; extreme values are rarely considered to measure the climate change impact. Additionally, very few studies were focused on periodicity rather than trend and shifting.
2. There are limited studies based on the selection of best suitable GCMs/RCMs, considering the six climatic variables. To project the future climate and water availability, it is vital to identify representative climate models for the region.
3. Due to mismatches between hydrological model requirements and GCMs ability, it is not suitable to couple hydrological models with crude spatial resolution GCMs output to assess the impact studies at the local scale. To bridge the gap between GCMs output and hydrological model inputs, RCMs with finer resolution have been used in the study.
4. There are very few studies available to project the trend pattern of water yield and evapotranspiration in a tropical watershed.

1.3.2 Research Objectives

The general aim of this study is to evaluate the water availability under climate change impact, and LULC Change, on Kharun watershed, a relatively small watershed in the tropical region of central India. The following specific objectives are outlined in the present study:

i. To analyze the historical trends, shifting (change year), and periodicity of climatic variables such as precipitation and temperature of Kharun watershed.

ii. To evaluate the pattern of trends for precipitation and temperature in the future using Regional Climate Model (RCM) data.

iii. To assess the pattern of LULC and project the near future LULC changes.

iv. To estimate the changes in the hydrological response under the dynamics of LULC and projection of virtual water for three climatic periods of the 21st century under climate change scenarios.

1.3.3 Methodologies

In order to achieve objectives, statistical analysis and hydrological modeling approaches were considered in this study. Identification of long term changes in meteorological parameters such as temperature and precipitation, as well as an assessment of changes in meteorological extremes (proposed by ETCCDMI), have been done considering various parametric and non-parametric tests. While few indices based on various rainfall intensities were proposed in the study. Modified Mann-Kendall (MMK), Sen's slope test, and linear regression were employed to detect the presence of trend and to quantify its magnitude. To identify the climatic shift in the meteorological series, Sequential Mann Kendall (SQMK) and Cumulative Sum (CUSUM) test were used. For future climate projection, Regional climate model (RCM) data was used, it was corrected for all the systematic biases using the technique of distribution mapping and the above mentioned parametric and non-parametric tests were applied over the corrected data to determine the changes in future trend patterns. LULC classification was carried out by unsupervised classification, whereas LULC for the near future were simulated by Markov and Cellular Automata (CA). The hydrological model, Soil and Water Assessment Tool (SWAT) was calibrated and validated using SWAT-CUP at a monthly time step applying a multisite calibration approach. The calibrated model was used to evaluate the water balance components under climate and LULC change.

1.4 STRUCTURE OF THESIS

The outline of the chapters and framework of objectives are as follows:

Chapter One explains the background and importance of the subject in the context of climate change's impact on water availability. This chapter also identifies the specific objectives considering the research gaps based on previous studies over central India.

Chapter Two presents the review on the assessment of climate change at a regional and local scale, including the studies based on trend detection and identification of change year. Studies based on

global climate models (GCMs) and regional climate model (RCMs) outputs were considered in this literature review chapter. This chapter includes the assessment of previous studies of land use/ land cover mapping and future projection by geospatial tools. Moreover, this chapter covers the hydrological modeling studies based on a different hydrological model, especially SWAT.

Chapter Three covers information about the study area. Kharun watershed is located in Chhattisgarh state, Central India. Additionally, this chapter describes the information about data collection, such as the distribution of LULC, soil type etc.

Chapter Four Discuses long term trend and shifting year of precipitation and temperature (maximum, minimum, and mean) detection along with detection of a trend in meteorological extremes using various parametric and non-parametric tests. The spatial and temporal distribution of climatic parameters were also plotted using geospatial tools.

Chapter Five covers the trend of meteorological extremes for the future at representative concentration pathways (RCPs) 4.5 and 8.5. Techniques of BIAS correction of the RCMs as well also discussed in this chapter. Along with the identification of trends for the entire period (2011-2100), trends for three distinct climate periods were also identified, namely CC1 (2011-2040), CC2 (2041-2070) and CC3 (2071-2100).

Chapter Six describes the change in the LULC pattern for the last 25 years (1990 to 2015), both decadal as well as demi decadal changes were discussed in this chapter. The technique of unsupervised classification was used to classify the classes. The classifications were verified with ground truth data points observed during the site visit. This chapter also discusses the projection of the LULC map for 2030 by Markov and Cellular Automata (CA-Markov) approach.

Chapter Seven includes the hydrological model (SWAT) setup for Kharun watershed. Model calibration and validation were performed by using SWAT-CUP (SWAT Calibration and Uncertainty Programs) based on monthly time-setup. The sequential uncertainty fitting algorithm version 2 (SUFI-2) of SWAT- CUP was applied with multiple sets of SWAT parameters to assess the performance of the model in terms of coefficient of determination (R^2), Nash–Sutcliffe Efficiency (NSE) and Percent BIAS (PBIAS). The calibrated model was used to simulate the response of Kharun watershed under climate change scenarios and LULC dynamics. Future projection (2011-2100) of hydro-meteorological components were assessed using representatives

RCM outputs, under moderate and high emission scenarios (RCP 4.5 and RCP 8.5), for three climatic periods (CC1: 2011-2040, CC2: 2041-2070, CC3: 2071-2100).

Chapter Eight discusses the summary and important conclusions drawn from the study. Additionally, the chapter also focuses on the limitation and future scope of the study.

The overall structure (chapter-wise) of the thesis has been illustrated in Figure 1.1.

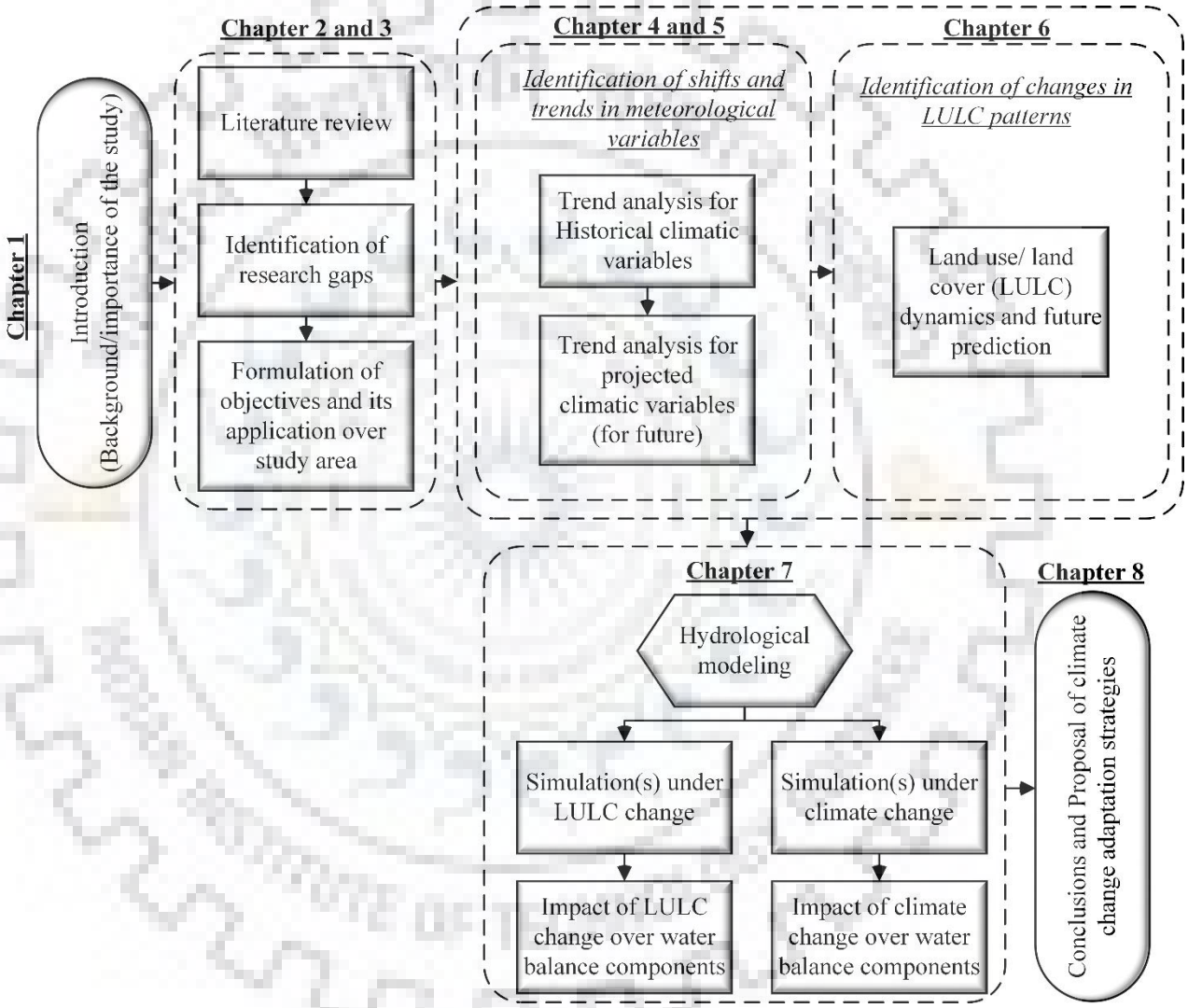

Figure 1.1 Illustration of chapter wise structure of the thesis.

CHAPTER 2

LITERATURE REVIEW

2.1 GENERAL

In the rainfall dependent agrarian countries of the globe, productivity is insufficient, erosion and degradation of natural resources are intensive, which has worsened the livelihoods and condition of the people. Since the natural resources are depleting, the concept and idea of watershed management is considered as a relief for rainfall dependent agriculture. As indicated by Intergovernmental Panel on Climate Change Fifth Assessment Report (IPCC AR5), the current global average temperature increased by 0.85ºC from 1880 to 2012, and by the end of the 21st century, it may rise by 2ºC (IPCC 2013). The increase in global temperature due to the emission of greenhouse gases and anthropogenic activities has induced higher evapotranspiration rates that alter the rainfall rate globally. Change in temperature influences the hydrological process and hydrological events such as floods and droughts (Mishra and Nagarajan 2013). In order to get a better understanding of the hydrological process, many hydrological tools have been used to assess the water balance under climate change scenarios.

This chapter mainly focuses on a rigorous review of available literature related to the present study. Based on the proposed main objectives for this study, a literature review has been addressed in the following sections. The first section presents a review related to climatic variability and changes. It also includes trend analysis of rainfall and temperature and different approaches used to manage climatic variability. Section two details the various uses and practices of the climate model and assessment of their inputs. Section three illustrates the various issues related to the assessment of LULC changes, the uses of Geographic Information System (GIS) and Remote Sensing (RS) for LULC changes using different methods and application of different methods and models for future LULC changes prediction. Section four includes hydrological modeling approaches such as the SWAT model, application of the SWAT model, and LULC change dynamics implication on surface runoff process as well as various adaptation and coping measures undertaken across the globe. Finally, concluding remark from the reviewed literature is presented.

2.2 DETECTION OF LONG TERM CHANGES IN METEOROLOGICAL VARIABLES

Long-term average increase and decrease in values of temperature and precipitation time series constitute the trend change. It is the oscillation in time series. In the recent past, many researchers have analyzed the trend of hydro-climatic variables. Numerous studies have been carried out in the past at regional as well as local scale to examine the trend periodicity and change point in climatic variables such as precipitation and temperature. Also, several types of research related to long-term trend detection of hydrological and climatic variables have conducted studies using various parametric and non-parametric techniques (Parida 1999). Parametric techniques are based on the hypothesis that the long-term time series data with normal distribution follows the error. It used to quantify the data variations. Therefore, compared to the non-parametric technique, the parametric technique is more powerful to check the trend test, based on the notion that the time-series data is both independent as well normally distributed. When the long-term series data variables and the errors do not follow the normal distribution, re-sampling time series analysis is used to test the level of significance at various significance levels.

Non-parametric techniques are usually employed to identify the monotonic trends in the long series of hydrological, environmental, and climatic data. It does not quantify the size of the trend as well as quantifies the change. As compared to parametric techniques, the reason for applying the non-parametric statistical techniques is believed to be more appropriate for non-distributed available data which is commonly encountered in the hydro-meteorological long term series data and the test has less sensitive to unexpected disruptions due to not homogeneous long term time series (Tabari et al. 2011).

Some of the parametric techniques are (I) t-test (Longobardi and Villani 2010), it is used to assess and test the slope of the linear regression coefficient, and if it considerably differs from zero value, it indicates the presence of the trend of linearity. Hence, the slope sign coefficient shows either a positive or negative time series trend. (II) Analysis of variance (Diaconis and Efron 1985) and (III) Linear regression. Some of the non-parametric techniques which are applied to test trends of long term series are (I) Mann-Whitney test (II) Mann-Kendall test (MK test), (III) Wilcoxon Signed Rank test, (IV) Anderson-Darling test (Anderson 1952) (V) Cohen's Kappa (Smeeton 1985; Parida 1999), (VI) Kandall's tau (Kendall 1975) and (VII) Spearman's rho (SR). However, the MK test is popularly used in order to assess the trend of long-term time series climatic variables. It confirms either positive or negative trends at a given statistical significance level. This section covers the

review of previous works regarding the assessment of long term change in rainfall and temperature time series using different tools and approaches.

2.2.1 Rainfall

Rainfall is the most prominent component of the hydrological cycle; hence, it is very crucial to know about its variability and intensity. The vast agrarian economy of India is mainly dependent on rainfall for irrigation purposes. Therefore, information related to rainfall variability and intensity in time and space is necessary for better planning and development of appropriate policies and strategies for the country. In many parts of the world, various studies have been undertaken based on climatic variables trend change detection (Kampata et al. 2008; Byakatonda et al. 2015). Some of the studies related to precipitation trends have been summarized in Table 2.1, while detailed explanations about various researches have been described below.

Xu et al. (2003) observed the monotonic long-term trends and step change in rainfall data time series over Japan, by using parametric method (student t-test) and nonparametric methods (Mann-Kendall and Mann-Whitney test). The limitation of the study is that in this investigation, only 46 rain gauges were used with long data records. Results specify that although many shift changes occurred in Japan but the time series did not display significant evidence of monotonic trends during the previous century. However, magnitude outcome indicates that if the step change extents up to one or two times of the standard deviation of the time series, the previous fifty years of the record together with five years or more of new data will be obtainable for detecting the probable trend. This decision may be helpful for the revealing step changes in the regions where the rainfall has near-normal distributions.

Xu et al. (2010) investigated the trend detection on rainfall and streamflow over the Naoli River basin, northeast China. Rainfall and streamflow data of 160 climatological stations were chosen for the study. Results suggested that from 1951 to 2000, overall rainfall increased in the southern regions and declined in the northern stretch. Partal and Kahya (2006) studied the long term trend in average annual monthly Turkish rainfall data series using Mann- Kendall and Sen's slope test. The autocorrelation method is applied to determine the significant level in the outcome of the Mann Kendall test. In this study, 96 rainfall stations are used, which reflect the turkey regional hydro-climatic conditions. The study concludes that rainfall trend detection results give some significant trends in September, January, and February, and the average annual. However, outputs of trend

analysis confirm the decrease in average annual rainfall in the western and southern parts of turkey and also in coasts of the black sea.

Basistha et al. (2008) evaluated the spatial trends of precipitation over India for 133 years (1872-2005) using the MMK test. The outcomes show falling trends of precipitation in North India (except Punjab, Haryana, West Rajasthan and Saurashtra) and increasing trends in south India (except Kerala and Maharashtra). Further, the MMK test and PMW test were used to detect the shift in rainfall patterns from the year 1901 to 1980. The increasing trend of rainfall was found up to the year 1964 and decreasing trend during the year 1965-1980. The year 1964 was observed as the year of most probable annual and seasonal change in rainfall in the region.

De and Rao (2004) have assessed the rainfall trends for major Indian cities, namely, Ahmedabad, Bangalore, Chennai, Hyderabad, Jaipur, Kanpur, Kolkata, Lucknow, Mumbai, Nagpur, New Delhi, Patna, Pune, and Surat, with more than one million population. The significant increasing trends were identified over annual and monsoon time series of rainfall over the four metro cities viz. Mumbai, Chennai, New Delhi and Kolkata.

Table 2.1 Observation of precipitation trends.

Author's Name	Regions	Data used	Methods	Results obtained
Lázaro et al. (2001)	A semi-arid area in South East Spain	31 years (1967 to 1997)	Sen's slope estimator, Thom test cumulative sums of deviations (CSD) and MT test	Annual as well as monthly rainfall has been lower than the average with 36% inter-annual variability and up to 20.7% inter-annual variability, respectively.
Boyles and Raman (2003)	North Carolina, USA	50 years (1949 to 1998)	Long-term linear time series slope	Precipitation during the winter season shown an increasing trend and shown a decreasing trend during summer in the given periods.
Da Silva (2004)	North East Brazil	78 years (1913 to 1990)	MK test	The decreasing trend has shown in rainfall.
Longobardi and Villani (2010)	Campania region, Southern Italy	81 years (1918 to 1999)	MK test and Student's *t*-test	Annual and seasonal rainfall has shown a decreasing trend except for the summer season.

Garbrecht et al. (2004)	Grate plain of USA	71 years (1930 to 2001)	Moving average techniques	Positive slope (upward trend of precipitation has been indicated).
Modarres and da Silva (2007)	Arid and Semi-Arid region of Iran	40 years (1959 to 1999)	Mann-Kendall trend test	High variability in precipitation, increasing, and decreasing (up and down oscillation) trend has been observed.
Some'e et al. (2012)	28 stations	40 years (167 to 2006	Mann-Kendall trend test	Downward trend (negative) of annual rainfall with magnitude and intensity ranged from 2.53 mm/annum to 3.43 mm/annum.
Mondal et al. (2015)	Orissa	40 years (1971 to 2010)	Mann-Kendall trend test	An increasing trend of monthly rainfall has been shown during Jan, May, Sept, Oct, and Nov. whereas, a decreasing trend of monthly rainfall with a parallel decrease of Sen's slope has shown during Feb, Mar, Apr, Jul, Aug and Dec.
Pingale et al. (2014)	Rajasthan	109 years (1904 to 2012)	Mann-Kendall trend test	During the study periods, up and down oscillation of mean and extreme events of rainfall was observed.
(Garbrecht et al. 2004)	Great plains of USA	1992 to 2001	Moving average method (11 years)	Insignificant or no changes were observed during the summer season, while during winter and spring months, the annual rainfall has been increased.
Cheung et al. (2008)	Ethiopia	42 years (1960 to 2002)	Regression and t-test statistics	From June to Sep., precipitation has shown a declining trend for Southern Blue Nile, Omo-Ghibe Rift valley, and Baro-Akobo. However, a decreasing trend is not necessarily indicated at the regional level.

2.2.2 Temperature

In recent experience and recently as well, climate change is recognized as the global agenda tied with growth, food security, and poverty. Overall production, employment contribution, and export earnings are significantly dependent on the agricultural sector; therefore, the country can be considered prone to climate change; events like recurrent drought, frequent flooding, and increasing temperature are commonly experienced.

Recently, it is evident that the global temperature has shown an increasing trend, though the magnitude and intensity are variable in different regions and seasons. According to Solomon et al. (2007), in an IPCC report, in the late 19th century, there has been a continuous rising in surface temperature by 0.6 ± 0.2ºC and increased by 0.2 to 0.3ºC in the last two and half decades and hence rainfall amount of the globe has declined. Different scholars in their observation in many parts of the world confirmed that in the last 20th-century global climate has been changed (Kenabatho et al. 2012). Nicholls and Collins (2006), reported that the annual average maximum temperature rises at the rate of 0.6ºC for Australia. Likewise, the annual minimum temperature increased by about 1.2ºC during the year 1950 to 2004.

Kruger and Shongwe (2004), observed the spatial and temporal trend of the average temperature of Africa from 1960 to 2003. The trend of mean seasonal temperature has shown variable throughout the mentioned periods with maximum and minimum mean temperature was recorded for autumn and spring, respectively. Evans and McCabe (2010), observed using the evaluation of the regional climatic model using weather forecast model in order to simulate the south-eastern part of Australia's climatic condition during the periods of 1984 to 2010 and confirmed in the report average temperature of the area was continuously rising.

Tabari and Talaee (2011), reported that during the periods of 1966 to 2005, there had been a rising trend of maximum and minimum temperature of Iran during the summer season. , Keller (2009) found in his study that the temperature of Ethiopia has increased by about 0.2ºC/decade. Fazzini et al. (2015), reported that during the year 1981 to 2010, the average temperature has increased by about 1.1ºC (which is 0.04ºC/year). Ezber et al. (2007) used a statistical and numerical modeling technique to temperature data in urban, suburban and rural areas to find the urbanization effect on the climate of Istanbul. The MK test was used to determine the significance of trends and the years in which changes were started. The effect of urbanization on climate was studied using a mesoscale atmospheric model. Both the statistical and atmospheric models have found significant warming in the atmosphere over the urbanized area. The MK test found a significant positive trend in the average monthly minimum temperature over urban and rural areas. The seasonal analysis shows that the effect of urbanization was more pronounced in the summer season. The significant changes in temperature were observed in the year 1970 and 1980 due to dramatic increase in population.

Arora et al. (2005) detected the temporal trends of temperature at both annual as well as seasonal scale, by employing the MK test statistics at regional as well as country level. It was found that the increase in annual average, average maximum, and average minimum temperatures were at a rate of 0.42, 0.92 and 0.09ºC per 100 years respectively. In the case of a regional basis, stations present in southern and western India show an increasing trend of 1.06ºC and 0.36ºC per 100 years, respectively, while North Indian plains stations show a decreasing trend of 0.38ºC per 100 years. The seasonal average temperature increased by almost 0.94ºC per 100 years for the post-monsoon season and during the winter season, it increased by 1.1ºC per 100 years.

Jhajharia and Singh (2011) observed declining trends in the daily diurnal temperature range (DTR). DTR is the difference between the maximum and minimum temperatures over some time. In the study, DTR was assessed at four stations in northeast India for almost all time scales. Results showed that there was a significant increase in DTR trends for the annual time scale, for both pre-monsoon and monsoon, and the months May to November apart from October. Significant rising trends in DTR are observed at three stations in October and the monsoon and post-monsoon seasons. Four sites showed significant increasing trends for T_{mean} in monsoon and post-monsoon seasons. However, post-monsoon changes for T_{max} and T_{min} were more than the monsoon season, indicating an element of a seasonal cycle. Significant decreasing trends in the sunshine duration were noticed at annual, seasonal (winter and pre-monsoon), and monthly (January–March) time scales.

2.3 CLIMATE MODELS AND ASSESSMENT OF ITS OUTPUT

Based on an analysis of thousands of studies in the recent past, many researchers from several research communities across the globe have assessed that most of the aspects of life form on planet Earth are affected by global warming. The assessment of climate change impacts on hydrology and water resources availability is usually evaluated by deriving the scenarios (Pandey et al. 2017). Moreover, these scenarios based on the emission of greenhouse gases scenarios (GHGs) for changes in climatic inputs for the hydrological model, these varied scenarios of the future greenhouse gas emission act as an input for its evaluation. The world's socio-economic projections form the basis for the development of emission scenarios. Climate model output at different emission scenarios is required to assess and predict future water availably.

2.3.1 Global and Regional Climate Models

As confirmed by the previous researches, the climate is altering very rapidly and the rate of change of climatic parameters is going to increase in the future which will further worsen the living

conditions. To assess the futuristic projection and impact, the scientific community and research institute develop the mathematical model named Global climate model (GCM). Global climate models (GCMs) represent the coupling of atmosphere, oceans, sea ice and land surface and have substantial potential for assessment of climate change. GCMs are the models for the evaluation of climate change based on the emission of greenhouse gas concentration. GCMs grids data are available at a coarse resolution so it is not able to predict the most crucial features reliably at local and regional impact analyses.

Moreover, various climate change prediction models are available for the assessment and modeling of climate change. The greenhouse effects are included in all of these models, which are based on physical laws, the phenomenon of atmospheric and oceanic effect (WMO report survey). Global climate model is represented as GCM, while RCM means the regional climate model, whereas MHM is the macro scale land-surface hydrological model, the macro scale water balance model is denoted by MWB and the catchment scale hydrological model is denoted by CHM (Xu and Singh 2004). These models are useful to assess, model and simulate the future climate change scenarios either at the global or regional level.

In order to analyze local and regional climate impact study, it is required to downscale the GCM data at coarser resolution to finer resolution. To solve this problem, two downscaling techniques viz., dynamic and statistical downscaling have been proposed. Transforming coarser scale information to finer scale and making it available is downscaling. Therefore, downscaling methods available in the literature vary from the secure rule-based method to sophisticated modelling of the spatial dynamics downscaling. In general, the downscaling techniques can be classified as the dynamic downscaling technique and the statistical downscaling technique. Both techniques have their weaknesses and strengths but are complementary.

Dynamic downscaling or regional climate modeling (RCM) is the methodology to scale the coarser GCM data grid into the local data grid at finer resolution by applying the complex algorithms. Dynamic downscaling can be further subdivided into one-way nesting and two-way nesting (Anandhi and Nanjundiah 2014). RCMs represent the tropical cyclones, extreme events, etc. and very useful in the study on regional climate change.

Statistical downscaling techniques based on the development of a statistical (linear or nonlinear) relationship between regional-scale climate variables and local hydrologic variables. In order to

calibrate the statistical downscaling model, observed or reanalysis climate data required. There are many advantages of statistical downscaling methodologies over dynamical downscaling approaches such as low cost, rapid assessments of regional climate change impacts. Statistical downscaling is the process of empirical relationships that transform large scale features of GCM (predictors) to regional-scale climate variables (predicted). The statistical regression model is the most popular model among the other statistical downscaling methods, which are employed to estimate a linear and nonlinear relationship between the predictor directly and predicted. It is now widely conceived that long term climate change will impact water resources availability and it might become to manage available resources across the globe. The agriculture, urban sector and hydropower production are the primary sectors that are affected by climate change (IPCC 2013).

According to Wilby and Harris (2006), the uncertainty is related to the downscaling method, global climate model (GCM) structure and climate change scenario (which is associated with future civilization). With this point of view, several studies have tried to address the anomalies mentioned above. McAlpine et al. (2007) reported the impact of regional climate change on the vegetative cover. They found significant changes in regional climate, with a shift from humid and colder conditions to warmer and drier conditions, particularly in southeast Australia. These changes in Australia's regional climate advocated that land cover change is probably a contributing factor to the observed trends in temperature and rainfall at the regional scale. Kay et al. (2009) studied the impact of climate change on flood frequency over two river basins in England. The authors used four scenarios (A1F1, B2, B1 and A2) of five GCMs to estimate GCM uncertainty using the delta change downscaling approach. They reported that the majority of the uncertainty is due to climate modeling, i.e., selection of GCM and RCM structures. Other research studies have also investigated the different arrangement of above-stated sources of uncertainty, the work by Wilby and Harris (2006) examined the climate change based on the comparative study of one conceptual model and two physically-based models. They reported that the difference in structure complexities of models might play a vital role in the assessment of model outcomes.

To explore climate change modeling and the use of General Climate Models (GCMs) with different downscaling methods, the following research has been discussed. Loaiciga et al. (1996) have studied the necessary process of the hydrological cycle and examined the current predictive capability of GCM that simulate the regional and local hydrologic regime under global warming. This study suggests that GCM is used on a large scale. The climate change effect on meteorological parameters

using the Canadian Climate Centre General Circulation Model (CCCGCM) and the University of British Columbia (UBC) watershed model for two hydro-meteorologically different watersheds was studied by Loukas and Quick (1996). Other meteorological variables (like cloud cover, albedo, wind speed, evaporation etc.) were also considered along with precipitation and temperature in the hydrologic model to the study climate change. Kondratyev and Cracknell (2017) reviewed some of the priority areas in the context of global climate change in Japan. Authors discussed global climate change and a particular emphasis was given to the water cycles and global energy. The author suggested that considerations of process, which are overcoming the current uncertainties of numerical climate models, climate prediction and modelling.

Matondo and Msibi (2001) had presented a case study of assessment of water resources and hydrology under the changing climate in Swaziland at the country level. The WatBall hydrologic model and General circulation model (GCM) were used to assess the water resources i.e. streamflow and found that the WatBall model is suitable for assessing the climate change impact on water resources. First, the climatic parameters were derived from selected GCMs (i.e., precipitation, temperature and potential evapotranspiration). Streamflow was predicted from the WatBall model using GCMs output for the year 2075 under changing climate scenarios. Also, streamflow was predicted considering the effects of population increase and agricultural activities on water resources considering climate change impacts. Various adaptation strategies were suggested to cope with climate change. This study did not consider the combined effects of population increase, expanded high growth of industries, commercial activities and land-use change on water availability. This study assesses water resources on the country level, which could not represent the accurate picture of climate change at the local level.

Xu et al. (2006) reviewed the different existing techniques for assessing water availability in changing the climate. Climate change impact on hydrological regimes was identified both for process research for water and catchment management strategies. It was concluded that climate change-related studies include: 1) Use of GCMs data to provide future climate scenarios under different GHG emission, 2) Use of downscaling techniques (both dynamic downscaling method and statistical methods) to downscale the GCM output to the local scales for hydrological models, and 3) Use of hydrologic models to simulate the effects of climate change. The authors suggested that climate change models should represent the land-surface process in the prediction of future climate change. They also found that results should be simulated at local sites or regions using RCMs.

Caramelo and Manso (2007) analyzed the spatial and temporal behavior of winter precipitation using principal component analysis (PCA). The monthly observed data from 34 weather stations and a subset of daily precipitation used. The first three PCs represent the winter precipitation pattern. So, the data of these three stations were further analyzed. The precipitation variability was assessed using PCA for winter precipitation. Parekh and Suryanarayana (2012) studied the impact of climatological parameters on crop yield using neural network fitting and extended their studies to other climatological variables to understand the effect of various parameters overproduction of wheat.

Ojha et al. (2010) formulated the downscaling model by using the Linear Multiple Regression (LMR) and Artificial Neural Networks (ANN) methods to downscale the GCM precipitation for Pichola lake area in Rajasthan, India. Predictor variables data are taken out from; NCEP (National Centers for Environmental Prediction) reanalysis dataset, 1948-2000 years, and replications from CGCM3 (Canadian Coupled Global Climate Model, third-generation) for scenarios A2, B1, A1B and COMMIT for 2001-2100 years. In this study, the cross-correlations are utilized to check the consistency of the GCM predictor variables. The downscaling outcome demonstrates that precipitation is expected to rise in the future for A2 and A1B situations, while, it is minimum for COMMIT and B1 scenarios. Ghosh (2010) reported that at a local and regional scale, the hydrological parameter could be downscaled by using GCM (General Circulation Model) outputs. In this study, SVM (Support Vector Machine) technique was used to downscale the predictor variable and also to develop the best relationship between the predictor and predicted variables. During the calibration and validation process in the SVM model, the values of specific parameters need to be fixed; for this purpose PGSL (Probabilistic Global Search Algorithm) technique is used to give the optimum output. By this, the obtained relationship between large scale predictor variables and local scale predicted variables is used to calculate the climate scenarios for multiple GCMs. This multiple GCMs provides the uncertainty condition and that outcome has to be further modified by the averaging method. Overall, the performance of the model is evaluated by comparing the earlier developed SVM based downscaling models.

Yang et al. (2012) evidence the potentiality in downscaling extreme precipitation, evaporation, and temperature in South China using, SDSM (statistical downscaling method). They downscaled the large scale GCM output to regional scale in direction to inquire about the spatial-temporal changes in extreme precipitation, evaporation, and temperature over the Dongjiang River basin for the period of 2010 to 2099 under H3A2 and H3B2 radiation scenarios. The consequences for

downscaling extreme temperature events would be more substantial from 2010 to 2099 for both scenarios. Nevertheless, the projections of change in extremes precipitation and pan evaporation were not coherent. Therefore, the performance evaluation of the SDSM shows good results in case of extreme temperature and evaporation while in case of extreme precipitation model performance, not as much satisfactory.

Hassan et al. (2012) applied the SDSM (Statistical Downscaling Model) to downscale precipitation from the GCMs into a fine-scale. Single gauge station data of Kurau River located in Malaysia are used as input in the SDSM model. The study evidence that the SDSM model can perform well during the calibration and validation process. For the future (2010-2099), models determine that there is a rise in the sum of mean annual precipitation, and the study area becomes drizzlier.

Duhan and Pandey (2013) studied three downscaling methods least square support vector machine (LS- SVM), artificial neural network (ANN) and multiple linear regression (MLR) to formulate the downscaling model for the future projections of average minimum and maximum air temperature for the central region of India. The A2 emission scenario from CGCM3 (Canadian Coupled Global Climate Model) is used in this study during the period 2001 to 2100. The reason being, to evaluate the analytical performance of MLR, ANN and LS-SVM models is to downscale the future temperature. This study revealed that the calibration and verification outcome of the models are good, but the performance of LS-SVM is outstanding as compared to MLR and AAN model.

2.3.2 Climate Model Selection

Evaluation of future projection of climate change impact is very important for the human and natural systems. For the future projection of climatic variables in different scenarios, climate models have been introduced (Meehl et al. 2007). Climate models are based on mathematical and physical principles that are capable of reproducing the present and future climatic parameters. They provide reasonable confidence in producing future climatic conditions by using the numerically coupled Atmospheric Ocean General Circulation Model (AOGCM) (Moss et al. 2010; Su et al. 2013).

For impact studies, climate models output being used. The impact of climate change on climatic variables has been assessed by many researchers (Chen et al. 2012; Camici et al. 2013; Haddeland et al. 2014; Miao et al. 2014; Mondal et al. 2014; Niraula et al. 2015). For certain impact studies of climate change, it is necessary to evaluate the model with observed datasets, and model output should perform close to the observed data. The study based on GCM climatic variables has been

examined for future projection for 2046-2065 and 2081-2100 time slice. Model results for Malaprabha catchment, India indicated that there is no significant change in rainfall for the future (Mehrotra et al. 2013). Climate impact on agriculture and crop production can also be carried out using GCM output (Mall et al. 2006a).

Several studies have been carried out for inter-comparison of the model output with observation (Perkins et al. 2007; Errasti et al. 2011; Kodra et al. 2012; Fu et al. 2013b; Anandhi and Nanjundiah 2014). The output of GCMs is very uncertain, so it is required to compare them with the past data and apply bias correction (Ojha et al. 2012). The performance of 10 GCM models for simulating the summer monsoon rainfall variation over the Asian-western pacific region assessed by Kang et al. (2002). Johnson and Sharma (2009) used a variable convergence score (VCS) methodology which is based on the coefficient of variation. The authors used this methodology to evaluate the eight different variables from nine GCM output for two emission scenarios for Australia. This skill score methodology can be used to evaluate any GCM in any region. Radić and Clarke (2011) evaluated 22 GCMs for North America using several statistical parameters. Evaluation has been carried out by comparing the model output with reanalysis data for period 1980-99.

Frei et al. (2003) conducted daily precipitation simulation for European Alps by using five regional climate models. Model evaluation using the climatic statistics is important than mean values. Several recent studies are using climatic indices and the probability density function (PDF) for examining the best (Frei et al. 2003; Perkins et al. 2007; Radić and Clarke 2011; Ojha 2013; Anandhi and Nanjundiah 2014; Parth Sarthi et al. 2015). Perkins et al. (2007) carried a model evaluation for 12 regions of Australia using Probability density function (PDFs). Evaluation of model on study area has been performed considering daily simulation data of maximum temperature, minimum temperature and precipitation. There are many approaches to compare the simulated or model output with observed values or reanalysis values. Teng et al. (2012) analyzed the datasets from 10 GCM for Australia. After bias correction, data were used for runoff evaluation using the hydrological model. A very popular model Taylor diagram has been used for several studies based on the correlation coefficient and root mean square error (RMSE) and variance ratio to compare the model output with observed values (Li et al. 2014).

(Fennessy 1994) Conducted the sensitivity experiment of the observed seasonal Indian Monsoon with the GCM model output considering the changes in vegetation, soil moisture, and cloudiness. For the evaluation of 10 atmospheric variables over India, the VCS method was used by Ojha et al. (2012). VCS curve generated for quantifying the variable performance for different GCMs (Ojha et al. 2013). Das et al. (2012) investigated about six conventional models from Intergovernmental Panel on Climate Change (IPCC), Second, Third and Fourth Assessment Report - SAR, TAR and AR4 respectively. These models have been considered for the performance evaluation of a model for the Gangetic West Bengal region of east India. In the results, it has been found that the MICRO, Japanese model is the best model for the region. GCM ranking of India region carried out using multi-criteria analysis by (Raju and Kumar 2014). The authors used the five performance indicators for the evaluation of eleven GCMs. The study carried at 73 grid points of $2.5^{o} \times 2.5^{o}$ resolution covering the whole of India. The entropy method used for weight the performance indicator, and for removing the systematic bias, nested bias correction has been used (Ojha et al. 2013; Raju and Kumar 2014)

In this study, Intergovernmental Panel on Climate Change (IPCC), Fourth Assessment Report (AR4) of global climate model output datasets are evaluated using RMSE and skill score for the Indian region considering six climatic variables. Ranking of the model has been carried out for each climatic variable using Akaike Information Criteria (AIC) and combined ranking using Multi-Criteria Analysis (MCA) method. This study has been carried for monsoon (June to October), non-monsoon (January to May, November, December), and annual (January to December) basis. The Indian monsoon season has an enormous socioeconomic impact on the development of the country. Variation in monsoon rainfall affects the flood, drought, agriculture, and economy of the country. There are several factors viz. Indian Ocean Dipole (IOD), El Ni˜no-Southern Oscillation (ENSO), and sea-surface temperature (SST) responsible for the inter-annual variation in Indian monsoon (Srinivas et al. 2013).

2.3.3 Bias Correction on Climate Model Outputs

The GCMs are used for the projections of future climate change caused by natural variability or anthropogenic activities (IPCC 2007a). Regardless of numerous efforts to improve the capability of GCM's in order to simulate historical climates, the usage of bias correction methods is quite essential to perform impact assessment studies of climate change for more improved projections (Gan et al. 2016; Vallam and Qin 2017). The significance of bias correction methods has been

detailed in the special report produced by IPCC (Seneviratne et al. 2012). In estimating probable hydrologic impacts of climate change (Arnell 1999), a suitable bias correction has been applied to projected temperature and precipitation for error-free estimation of projections. Dettinger et al. (2004) carried out the climate change impact assessment study in the Sierra Nevada of California to study the climate change impact on river flow by using bias-corrected on GCM projected temperature and precipitation data.

Several bias correction methods have been used in the past in order to improve the regional climate downscaling model. Lynch and Arcsym (2000) examined the impact of climate change on the seasonal carbon cycle in the Alaskan region through a process of dynamical downscaling approach in which linear bias correction (LBC) method was constructed for an RCM by adding projected changes of specific humidity and temperature in GCM simulation to reanalyze climate. Also, a similar technique was adopted by Sato et al. (2007) to examine the effect of global warming on regional rainfall over Mongolia. The bias correction has also been applied to correct the projected wind speed temperature, geopotential height, specific humidity, and sea surface temperature. The results reveal that the rainfall intensity predicted with new method has been closer to observations than the traditional method, Patricola and Cook (2010) also employed a similar method as applied by Sato et al. (2007). The climatological LBCs in the above mentioned studies maintain deviations on the seasonal time scales but eliminate the diurnal and synoptic effects. Huang et al. (2011) proposed a complicated bias correction method for hurricane simulation. The bias correction developed by Holland et al. (2010) maintained the diurnal, synoptic effect and the inter-annual variation in the LBC by correcting GCM climatological mean bias with six-hourly, National Center for Atmospheric Research (NCAR) reanalysis data and GCM output. They recommended that the dynamical downscaling prediction with GCM bias correction can generate realistic tropical cyclone frequency because the bias correction reduced the impracticable high vertical wind shear over the tropical Atlantic. Huang et al. (2011) proposed a statistical regression model between GCM and reanalysis data to reduce the GCM climatological bias, and the bias corrected GCM output data have been used to force an RCM to predict winter precipitation over the western United States. Several studies are carried out worldwide to determine the changes in mainly temperature and rainfall and also other climatic parameters its connection with climate change.

2.4 ASSESSMENT OF LAND USE/LAND COVER (LULC) CHANGES

During the past few decades, LULC changes detection was employed by using conventional techniques, which is time-consuming and tedious as well as cost-ineffective methods. However, due to the advancement of technology and innovations of powerful computers, Remote Sensing (RS) and Geographic Information System (GIS) software are recognized as excellent tools in the study of LULC dynamics (Mishra and Nagarajan 2010). Remotely sensed data could be employed for several applications in the area of LULC dynamics, water resources management, catchment management and other many more analysis throughout the globe.

In the last few decades, due to anthropogenic effects, LULC dynamics are significantly under pressure. Therefore, it is essential to detect LULC changes starting from the microscale to larger catchment for effective and sustainable management. To this effect, remotely sensed satellite data are necessary to assess natural resources and observing the changes in the time series results derived from the integration of RS and GIS, which are substantially crucial in the planning and monitoring of resources based activities. Therefore, the focus of this section is on the assessment of historical LULC change dynamics studies and LULC's future prediction.

2.4.1 Use of GIS and RS for LULC by Different Methods

In most parts of the globe, land cover classes are dynamic. Under this situation, the availability of accurate and significant data related to land and other natural resources (such as land cover class data, Landsat images, GIS, and satellite remote sensing) is significantly important to take action. The dynamics of land cover classes from one class to other classes, and hence mapping of land cover dynamics establish the baseline to predict future LULC class dynamics, current natural resources management and other reclamation practices. The dynamic component of mapping is helpful to indicate the dynamics of the LULC change in the catchment. In order to identify LULC change dynamics from satellite imagery, various studies have been undertaken using different methods. The change of LULC dynamics is a locally influential and significant ecological and environmental trend (Burns et al. 2007; Samal et al. 2015). Some scholars across the globe have conducted various studies in order to evaluate the reliability of change dynamic detection techniques to recommend significant methods for LULC change dynamic detection; essential studies are presented in subsequent sections.

Mendis and Wadigamangawa (1996) detected LULC changes by using the existed and use survey data for the year 1983, Thematic Mapper (TM) data for the year 1992, an aerial photograph of the

year 1994 for Nilwala River watershed in Sri Lanka. The maximum likelihood classifier was employed in order to classify Thematic Mapper image of band combination 3, 5, and 7. The focus of this study was to explore the dynamics of LULC classes due to the application of the Nilwala Ganda Flood Protection Scheme. The results revealed that plantations had replaced cultivation.

Kucukmehmetoglu and Geymen (2008) explored the land-use dynamics using Landsat imagery for the year 1990 to 2005. Application of RS and GIS techniques were employed to assess the water resources of Istanbul (Turkey). Using this technique, the impacts of urbanization on water resources of Istanbul city was carried out. When classifying the images, the main focus was settlement areas and changes of respective settlement areas were analyzed. However, this study ignored the association between land-use change dynamics, temperature and rainfall of urban areas to explore the water resources in considering the climate changes and variability scenario.

Balamurugan et al. (2014), assessed LULC change dynamics for the coastal area of Odisha state using RS and GIS for the period 1990 to 2014 and explored various land use classes such as settlement areas, farmland, water bodies, and forestland in order to create RS and GIS database. This study arrived at a conclusion in which settlement areas and industrial growth expansion were identified whereas a continuous decline of forest resources has been observed. Prakasam (2010) detected the LULC changes in Kodaikanal, Western Ghats (Tamilnadu), India, for noticing changes during the period of 1969 to 2008 (40 years) by using Landsat satellite data and performing supervised classification techniques.

Given the above studies undertaken in various parts of the world, it can be concluded that several techniques and methods are available for LULC classes' exploration and classification. Generally, some of the most essential LULC dynamics classification methods are presented in Table 2.2.

Table 2.2 Land Use/Land Cover change dynamic classification techniques.

Authors and Year	Title of work	Major Findings
Meshesha et al. (2016)	LULC change dynamics using RS and GIS in the Beressa watershed, Ethiopia	Farmland was expanded at the rate of 71.6 ha/year, while settlement areas expanded by about 16.8 ha/year in the last three decades (1984 to 2015). Whereas, forestland was reduced at the rate of 5 ha/year while water bodies have reduced at the rate of 0.03 ha/year in the first periods (1984 to1999). The alarming rate in the growth of the population is the responsible factor for the alteration of LULC.
Asres et al. (2016)	Analyses of LULC changes in the upper Blue Nile Basin Highland Watersheds.	Interpolation of Landsat imageries for 1973, 1986, 2000, and 2013 have been done using GIS and RS. The results showed that at the expense of pastureland and forestland, cultivated land was increased.
Minale and Rao (2011)	Impacts of LULC change in the catchment of Gilgel Abbay, Lake Tana, on climate variability.	GIS and RS tools were used in order to assess the trend of change detection in LULC. The results revealed that forestland (72.3%), glass land (55%), wetlands (47.2%), and lake areas (6.3%) had been altered into farmland and settlement areas.
Lin et al. (2007)	LULC classes dynamics impact on hydrology and the pattern of LULC in the Wu-Tu watershed and Northern Taiwan.	Employed an integrated approach in which is used to integrate the LULC model and hydrological model to explore the future influence of LULC dynamic scenarios on hydrology as well as the future land use pattern. It confirmed that variability, distribution, intensity as well as magnitude in future hydrological components were substantially affected by LULC changes particularly the runoff process.
Kiran (2013)	GIS and RS tools have been employed to identify the LULC dynamics of Mahananda catchment of West Bengal.	The results revealed that due to anthropogenic effects, coverage of dense forest reduced continuously from 58% -33% jus with eight years (1990 to 2000).
Jat et al. (2009)	RS and GIS-based urbanization assessment and watershed degradation.	RS and GIS techniques have been employed to verify the condition of two urbanized sub-watersheds over 29 years (1977 to 2005). The study indicated that significant alteration had been found in essential watershed characteristics consequently to the decline of

		its health. In this, regards RS and GIS tools are essential RS, and GIS tools are convenient for such studies.

2.4.2 Use of Different Methods/Models for LULC Prediction

In the past few decades, many researchers have used different methods to predict future LULC change dynamics based on historical maps and Landsat imagery (Kuemmerle et al. 2006). The magnitude of LULC change dynamics in response to an alarming rate of population growth, and consequently to the environment merit detail explorations of these alterations are necessary. Land-use models are the primary focus in the LULC. In the last few decades, many researchers created a vast set of operating models, which is crucial in the future, LULC prediction. However, models are useful not only in assisting the consideration of future land-use change dynamics, analysis of scenarios using land-use models but also is used to assist planning the land use and policy formulation as well (Samal et al. 2015). In general, land use prediction model is grouped into three main classes, and these are statistical as well as empirical models like Markov chains and regression model (Hu and Lo 2007); Cellular Automata (CA) model (Mitsova et al. 2011); Agent-based model as well as system dynamic; integrated model like conversion of land use and its effects (CLUE) (Kamusoko et al. 2009).

Kamusoko et al. (2009) forecasted future LULC change dynamics for Zimbabwe. The results indicated that barren land continuously increasing and a risk to the sustainability for the community up to 2030. Zhu et al. (2015) explored the influence of preserving farmland policies on urban sprawl as well as food availability in many parts of China. The results derived a conclusion that future urban land use could further expand, consequently would result in negative impacts on future land and other natural resources. Guan et al. (2011) identified a decrease in farmland and forest area; consequently, the settlement area could be increased for the period 2015 to 2042 in the Saga area of Japan. Relevant studies on the Markov chain model to predict future LULC change are presented in Table 2.3.

Table 2.3 Land Use/Land Cover change, future prediction models in different parts of the world.

Authors and year	Title and Study area	Methods	Major finding
Kamusoko et al. (2009)	Sustainability of rural area under tension in Zimbabwe- Simulation of LULC dynamics prediction of Bindura district	MC automata model	The MC automata model has employed to simulate future LULC dynamics to 2030. Prediction results revealed that woodland areas are continuously decreasing, whereas, increasing trend of barren land was observed.
Memarian et al. (2012)	Validation of CA-MCM for Simulation of LULC dynamics in the Langat Basin of Malaysia	CA-MCM validation has done using validation metrics	CA-MCM has applied and due to uncertainties of the source data, showed poor performance was observed for LULC changes.
Mitsova et al. (2011)	A CA- model of LULC changes to integrate urban growth with open space conservation	CA-MCM	Using the model LULC changes was developed in the process of integration, the preservation of environmentally most sensitive areas into projections of urban expansion both at the regional and national level. The scenarios of baseline data is a continuation of the present patterns.
Al-sharif and Pradhan (2014)	Monitoring and forecasting LULC an integrated MCM and CA in the GIS tool for the Tripoli Metropolitan City	Integrated Markov chain and cellular automata	CA-MCM has been used in the process of simulating and predicting quantitative LULC changes. The results of the study obtained acceptable model performance and it signifies rapid urban sprawl consequently remarkable reduction of agricultural lands.

2.5 HYDROLOGICAL MODEL

Hydrological models are the tools that provide an understanding of active interactions between climatic parameters and land-surface hydrology. Moreover, available water and atmospheric temperature affect the hydrological cycle and water budget components. Thus, it is vital to select a suitable hydrological model to assess the dynamic interaction between climatic parameters and

surface hydrology. It is also helpful in assessing the climate change impact on regional water availability and cropland productivity. To date, several models have been developed to estimate the peak flow for the design of several hydraulic structures, irrigation and drainage system.

2.5.1 Soil and Water Assessment Tool (SWAT Model)

According to Arnold et al. (1998), SWAT is a semi-distributed, physical algorithm developed in order to estimate runoff and sediment in daily and monthly time step at catchment level. The catchment of an area is divided into the smaller watershed and sub-watershed level using Hydrological Response Units (HRUs) based on different situations viz., soil type, slope classes and land use classes used to allow an acceptable and high level of detail simulation. Different inputs like rainfall, topography, LULC map, soil texture and properties are some of the required data used to calculate sediment yield and runoff generation using curve number equation (Abbaspour et al. 2007; Ghani and Azamathulla 2014). The necessity to assess sediment yield, runoff, and to develop management practices in the smaller and larger watershed and the catchment resulted in the development of SWAT (Guy et al. 1987; Arnold et al. 1998; Gassman et al. 2007; Ghani et al. 2008). Weather, land management, plant growth, water movement, hydrology, sediment movement and stream routing are some of the major components included in the SWAT model. The interface of SWAT is compatible with ArcGIS (ArcSWAT) which has been developed to use the geodatabase approach. Various types of techniques have been developed to support the implementation of the SWAT model simulation. For instance, the interactive SWAT software (i-SWAT), conservation reserve program decision support system (CRP-DSS) which was established by Kumar et al. (2006), and generic interface program (i-SWAT) (Abbaspour et al. 2007), that is important for choice of automates parameter and aggregation for continuous iteration of SWAT model calibration and simulation. Presently ArcSWAT 2012 is compatible with ArcGIS 10.2.2 interface.

2.5.2 Adaptation and Application of SWAT Model

Following SWAT model development, in order to obtain further improved and accurate prediction of specific process improved SWAT models have been adjusted. SWAT-G (river basin scale model developed for functioning daily), Extended SWAT (ESWAT), soil, and integrated model (SWIM) are some examples of the model. A physical-based model (Arnold et al. 1998; Lenhart et al. 2002), which have been established to forecast the influence of management practices in the small (meso) to large (macroscale) basins scale level accurately. According to

Lenhart et al. (2002), SWAT 9.2 was modified to predict flow characteristics due to changes in percolation, interflow and hydraulic conductivity.

SWAT model simulates the watershed system based on how concurrent watershed processes are presented in the model, as well as how well the watershed to be defined by input parameters in the model. Many of the erosion, runoff, sediment and flow models need the watershed to be subdivided into sub-watershed scale or meso (smaller). Even though the size of watershed implication on the homogeneity, the assumption of each of watershed is homogeneous, and parameters represent the entire meso and sub watershed. According to Singh et al. (2004) and Tripathi et al. (2006), size reduction with an increasing number of subwatershed, affect model simulation results on the runoff process and sediment yield reduction of the whole watershed.

Several studies have been undertaken using the SWAT model by various researchers in different ways for different purposes. Tripathi et al. (2006), used SWAT to simulate the runoff process as well as sediment yield generation for smaller Nagwan watershed in the eastern part of India using generated rainfall data. It confirmed that the ability of the SWAT model to simulate and evaluated satisfactorily for generated rainfall during the periods of 18 years. Study by Van Liew et al. (2007), in the USDA ARS on experimental watersheds, applied SWAT in the process of simulating the influence of subdivision of watershed on simulated water balance components (surface runoff process, sediment yield, and evapotranspiration, and percolation loss). The results of the study confirmed the perfect water balance for the experimental watershed.

Rosenthal et al. (2013), in their study, found that the various properties of watershed related to the runoff process and sediment yield generation affected by the size of watershed. In order to relate the channel hydraulic properties to the size of the watersheds; therefore, the authors derived different parameters. On the contrary, Kuhnle et al. (1996), used SWAT to simulate runoff generation and sediment yield generation from Goodwin Creek watershed. Results confirmed that numbers, including watershed and sub-watershed size, do not have any implication on runoff volume. However, the response of annual sediment yield for the watershed subdivision was sensitive.

Easton et al. (2010), in order to forecast runoff generation as well as sediment loss in Ethiopia, Blue Nile Basin of Ethiopia, modified SWAT model has developed. Using daily water balance, the model used to simulate the excessive runoff process from the landscape. The spatial and temporal

distribution erosion from the landscape is therefore, simulated successfully. As can be seen in Table 2.4, SWAT has been used for different applications in different parts of the globe.

Table 2.4 Application of SWAT model in different categories.

Researcher/s (year)	Broad application category	Study area	Major findings/Remarks
Gebremicael et al. (2013)	Runoff process and sediment yield fluxes	In the Blue Nile Basin, Ethiopia	SWAT has been applied to analyze the influences of land use dynamics on sediment yield and runoff. Calibrated and validated results indicated that SWAT and LULC dynamics detection are reliable with the assumption; therefore, LULC dynamics have been the primary cause for the runoff process and sediment yield generation in the Blue Nile basin. This finding has a substantial contribution to water resources management.
Rosenthal et al. (2013)	GIS linkage with SWAT	Lower Colorado River Basin	Urbanization significantly affects the downstream flow; therefore, the SWAT model underestimates the extreme events.
Kuhnle et al. (1996)	Surface runoff process and sediment yield generation	Northern Mississippi, USA (Goodwin Creek Research Watershed)	For daily and annual runoff and sediment yield, the reliable result was obtained for multiple sub watershed and sub-basin.
Chu and Shirmohammadi (2004)	Surface and sub-surface runoff and sediment yield	Maryland (Warner Creek watershed)	SWAT model result on a monthly basis for sediment yield and flow was poorly simulated.
Alibuyog et al. (2009)	Runoff process and sediment yield generation	Manupali River subwatershed and test watersheds, Philippines	SWAT has applied in the process of modeling the outcome of land-use dynamics in the Philippine watersheds. Results from simulation indicated that LULC changes significantly affects runoff and sediment yield (conversion

			of pasture, forest and grassland to agricultural land resulted in increased in runoff generation, increased sediment yield and in reverse decreased in base flow).
Santhi et al. (2008)	Surface runoff variation	Ohio and Arkansas White River Basin, U.S.	Spatially and temporally distributed calibration and validation at sub-watershed and stream gauges level respectively reasonably good for a spatiotemporal hydrological pattern for larger river basin scale.
Pisinaras et al. (2010)	Management scenario	Kosynthos River Watershed, N-E Greece	The validated and calibrated results were used to test the implication of various LULC changes on the runoff process and sediment yield generation. It is a very flexible and reliable technique for water and related decision-making. Therefore, if the SWAT model is calibrated correctly and validated used for successful testing of various management scenarios.
Bharati and Jayakody (2011)	Water balance	Gorai River catchment, Bangladesh	They concluded that the significant change in the LULC classes significantly affect runoff and sediment yield
Khoi and Suetsugi (2014)	Climatic data effects	Dak Bla River central Vietnam	Land use/cover dynamics, as well as changes of climate on surface runoff process, sediment yield and water balance component, are affected by each other. Nevertheless, the components of subsurface flow are more response to LULC change than climate change. Significant results to plan rainfall-runoff and sediment management for data-scarce regions/ areas.

2.5.3 Impact Assessment on Water Availability Employing SWAT

Several hydrological models have been utilized in the past for computation of water availability and water deficits for present and future scenarios (Saulnier et al. 1997; Minale and Rao 2011;

Azamathulla and Zahiri 2012; Huong and Pathirana 2013). In general, hydrological models represent the dynamic cycle of water balance components (precipitation, evapotranspiration, surface water, groundwater recharge percolation and water utilization by vegetation). Jha et al. (2004) examined the climate change impact on discharge using RCMs output in the Upper Mississippi River Basin. A hydrological model, SWAT were calibrated and validated against measured discharge utilizing observed climate data from the U.S. Environmental Protection Agency Better Assessment Science Integrating Point and Nonpoint Sources (BASINS). Model outputs were evaluated based on an annual scale considering the observed climate series as the lateral boundary condition in RCM. Impacts of climate change on water availability and other hydrologic components were evaluated by driving SWAT with current and future scenario climates. Results indicated that a 21% increase in future precipitation simulated by the RCM produced 18%, 51%, 43%, and 50% increase in snowfall, surface runoff, groundwater recharge and net water yield, respectively in the Upper Mississippi River Basin.

Matondo et al. (2004) expected the increasing greenhouse gas effect which raises the temperature by 1-3.5ºC, resulting in a change in precipitation by ±20%. The impact of anticipated global warming will strike nearly all the sectors of human endeavor. However, this study was to evaluate the impact of climate change on water resources availability for Swaziland. The computation of the impact of climate change on hydrology and water resources in Swaziland was implemented in three watersheds namely: Mbuluzi, Komati and Ngwavuma. The gaps in discharge data have been filled by applying rainfall-runoff modeling techniques (Panchal et al. 2013). MAGICC-model was applied to simulate the climate parameters for Swaziland given the baseline scenarios.

Moreover, three GCMs were used to project the temperature and precipitation changes for Swaziland for the year 2075. The model was calibrated and results indicate that there is an annual streamflow change of ±5% in the Komati watershed and ±2% in the Mbuluzi watershed given climate change scenarios. Projected results indicate a negative annual streamflow change ranging from 4% to 23% in the Ngwavuma watershed under climate change scenarios.

Dibike and Coulibaly (2005) noted that global warming has significant impact on local and regional hydrological regimes, which will, in turn, affect ecological, social and economic systems. However, a more steady precipitation series of future climate scenarios can be derived from GCM outputs using downscaling techniques. The downscaled data is used as input to two different hydrologic

models to simulate the corresponding future flow regime in the Chute-du-Diable and Saguenay watershed, Canada. Moreover, the water availability impact analysis was carried out with the downscaled precipitation and temperature time series as input to the two hydrological models advise an overall rising trend in average annual river flow and reservoir inflow. Fischer et al. (2007) investigated the climate change impact on irrigation demand for regional and local scale considering with and without mitigation of greenhouse gases emission. Future regional and globally irrigation water demands were calculated as a function of both projected irrigated land and climate change and simulations were performed from 1990 to 2080. Future trends for extents of farmland, irrigation water use, and withdrawals were calculated, with specific care given to the implications of climate change mitigation. Renewable water-resource availability was calculated under present and future climate scenarios. Results advise that mitigation of climate change may have substantial convincing effects compared with unmitigated climate change. Moreover, mitigation measures can cut down the impacts of climate change on farmland water demands by about 40% or 125–160 billion cubic meters (BCM) equated with unmitigated climate.

Guo et al. (2008) examined the occurrence and damages of the flood in 1990 due to climate change in the Poyang Lake basin in China. In order to evaluate these issues, it was crucial to get information about climate variability, land-use and land-cover changes in the area impact the yearly and seasonal fluctuations of basin hydrology and streamflow. Moreover, this study is crucial for long-term planning for LULC to protect water resources and to effectively handle floods in the Poyang Lake basin and lower basins. Additionally, it is also crucial for ecological and socio-economic implications for the area. Franczyk (2000) investigated the climate changes effect on the hydrology of the Pacific Northwest during the 21st century. Several GCMs were used to simulate the output, and simulated temperature and precipitation indicate the higher projection. In the last 30 years, due to sudden growth in urbanization, there is a change in climate and LULC alter the surface runoff and water availability. A combining of global warming and LULC change for 2040 with the semi-distributed, ArcView SWAT hydrological model was used to evaluate the changes in mean runoff depths in the 2040s (2030–2059) from the baseline period (1973–2002) at the monthly, seasonal, and annual scales. Climate model ECHAM5 outputs were downscaled for the region and it was noticed that the region would experience an increase of 1-2°C in the average annual temperature and a 2% increase in average annual precipitation from the baseline period.

Liu et al. (2011) investigated the climate change impact on streamflow in the Yellow River Basin. A semi-distributed hydrological model (SWAT) is calibrated and validated with records at Huayuankou, Lanzhou, and Huaxian hydrological stations. Outputs from climate model HadCM3 were downscaled with SDSM and delta statistical approach to generate the daily temperature and precipitation data from 1961 to 2099. In order to get the change in runoff due to climate change, hydrological model SWAT was used. In results, it is noticed that annual mean maximum and minimum temperature may rise by 5°C in the 2080s, and annual precipitation would increase by 54 mm to 150 mm. Additionally, raising streamflow in spring and summer can help in crop growth, and raising annual precipitation and runoff can facilitate water demand stress to some degree in the Yellow River Basin.

Due to the scarcity of observed data and heterogeneousness of the system, discharge, and soil loss evaluation in river basin or catchment is one of the most ambitious tasks in water resources studies (Sinha 2015). However, SWAT is a semi-distributed and physical model that can simulate the discharge as well as soil loss for the catchment. SWAT is a physically-based model. It requires specific information about the topography, vegetation, land management practices, hydro-meteorological data (precipitation, maximum & minimum temperature, relative humidity, wind speed, solar radiation), soil physical properties in the catchment. The physical processes associated with water movement, sediment movement, crop growth, nutrient cycling, etc. are directly modeled by SWAT using these input data The SWAT model is designed to assess streamflow and sediments from the individual watershed (Table 2.5).

Table 2.5 Studies related to climate change impact and anthropogenic activities on water availability using SWAT.

Authors (Year)	Study Area	Hydrological Model	Major Finding /Remarks
Murty et al. (2014)	Ken Basin, India (Area 28574 km^2)	SWAT	• SWAT applied for Ken River basin • Water balance components calculated (1985-2009)
Gessesse et al. (2015)	Modjo Watershed, Ethiopia	SWAT	• Climate and LULC change • Sediment loss and transport estimation • Characterization of runoff estimation

Heo et al. (2015)	Neches River (Area: 2221 km^2), Eastern Texas (US)	SWAT	• Climate and LULC change considered • Water budget components evaluated
Liu and Lu (2015)	Changle River basin	SWAT	• Nutrient and Pollution estimation • Application of Best Management Practices (BMPs)
Singh et al. (2015)	Satluj River Basin (48598 km^2) and Tungbhadra River Basin (14429 km^2), India	SWAT, SWAT-CUP	• Model uncertainties with streamflow (peak and low flow) • Separation of sequential peak and low flow using multicriteria evaluation • Temperature and snowmelt identified as sensitive parameters in the region
Chattopadhyay and Jha (2016)	Haw river (4000 km^2), North Central Carolina (U.S.)	SWAT	• SWAT model calibrated and validated • Water balance components evaluated due to climate variability
Pandey et al. (2017)	Armur watershed, Narmada River, India	SWAT	• SWAT applied for Armur watershed • Water balance components computed for baseline (1961-1990) and future climate scenarios (2071-2100) • Positive changes in annual average temperature and rainfall in future projection
Marhaento et al. (2017)	Samin river basin (278 km^2), Indonesia	SWAT	• LULC changes and climate change considered • Ratio of surface runoff to streamflow increase • Ratio of base flow to streamflow and lateral flow to streamflow decrease
Omer et al. (2017)	Hutuo River, China	SWAT	• Integrated effect of Anthropogenic and climate change • Climate change and LULC change reduced the runoff • Proposed framework for

			sustainable development cause of runoff uncertainties
Trang et al. (2017)	3S transboundary The river basin (Sekong, Sesan, Srepok), of countries (Laos, Vietnam, and Cambodia)	SWAT	• Climate study under RCP 4.5 and RCP 8.5. • Discharge and nutrient increase in the wet season and decrease in the dry season

2.6 CONCLUDING REMARKS

In recent studies, long term changes in time series of climatological and hydrological data have received immense interest. Different aspects of climate change impact and effect of the anthropogenic intervention on hydrology were discussed worldwide. Long term changes in any historical series often occur in the form of shifting (change year) and trends. Moreover, the trend in precipitation, temperature and other hydro-meteorological parameters were identified, applying various parametric and non-parametric tools. Furthermore, climate variability and land-use changes identified for abrupt shifts and trends. In this manner, it was hard to separate and measure the individual impacts of various land-use changes inside the catchment areas based on observed hydrological response evidence.

Many researchers found reasonable uncertainty in projections of future climate change and its impacts on hydro-meteorological responses, particularly on regional or basin scale. The spatial resolution of the climate models is too coarse to simulate the impact of global change on the local scale. The major hurdle in the case of evaluation of the effects of future projection of climate on water balance components is the uncertainties in global climate models and its scenarios. Based on the research above discussed, plenty of work has been carried out to simulate the hydrological response considering different scenarios of General Circulation Models output. Therefore, the performance of GCMs is still required to assess for a particular region. Based on the research discussed above, climate and hydrological model was selected to project the water balance for tropical river basin of central India.

Based on the literature review, the following research gaps were identified which were further established as the objectives of the present study:

1. Study of extreme values are rarely considered to measure the climate change impact. Moreover, very few studies focused on trend and shifting
2. There are limited studies based on the selection of best suitable GCMs/RCMs, considering the six climatic variables.
3. It is not suitable to couple hydrological models with crude spatial resolution GCMs output to assess the impact studies at the local scale. To bridge the gap between GCMs output and hydrological model inputs, RCMs with finer resolution have been used in the study.
4. There are very few studies available to project the trend pattern of water yield and evapotranspiration in a tropical watershed.

CHAPTER 3

STUDY AREA

3.1 GENERAL

The detailed description of the study area and data collection are presented in this chapter. This chapter covers the general aspects of location, extent, topography, climate, drainage, soil, agriculture and hydrological issues over the study area. In other parts of the chapter description of data collection and processing are discussed.

In this research, Kharun watershed - a tropical river watershed of central India has been considered for long term trend analysis of climatic variables, change detection in land use/land cover (LULC), and hydrological modeling to evaluate the water availability in the watershed. Comprehensive descriptions of the study area have been mentioned in the given sections.

3.2 STUDY AREA DESCRIPTION

Kharun watershed, considered in the present study, is at the heart of Chhattisgarh and passes directly through the state capital. Kharun River is the major tributary of the Seonath River, which is a major tributary of Mahanadi River. The index map showing the study area and its cutoff from Mahanadi River are shown in Figure 3.1. Kharun River originates at Petechua in Balod district and lies between the geographical coordinates of 20° 33′ 30″N – 21° 33′ 38″ N latitude and 81° 17′ 51″ E – 81° 55′ 25″ E longitude. It can be seen from Figure 3.1 that the study area exhibits a flat topography and does not have much elevation difference throughout its stretch. The total length of the river is 164 km and its catchment area is approximately 4191 km^2.

3.2.1 Topography

The study area exhibits a relatively flat topography ranging from 212 to 453 m above sea level. The study area lies in the state of Chhattisgarh, which is the most populated state in India, with a population of 25.5 million. Being the primary producer of steel and power, it is considered to be the fastest-growing state of India. The state is enclosed by six other states, namely Orissa, Madhya Pradesh, Uttar Pradesh, Jharkhand, and Telangana. Speaking of physiographic characteristics, almost two-third of the area is broad and fertile, suitable for cultivation. The southern part of the study area has a forest cover. While the Northcentral part of the watershed is heavily urbanized due to the presence of state capital in that region.

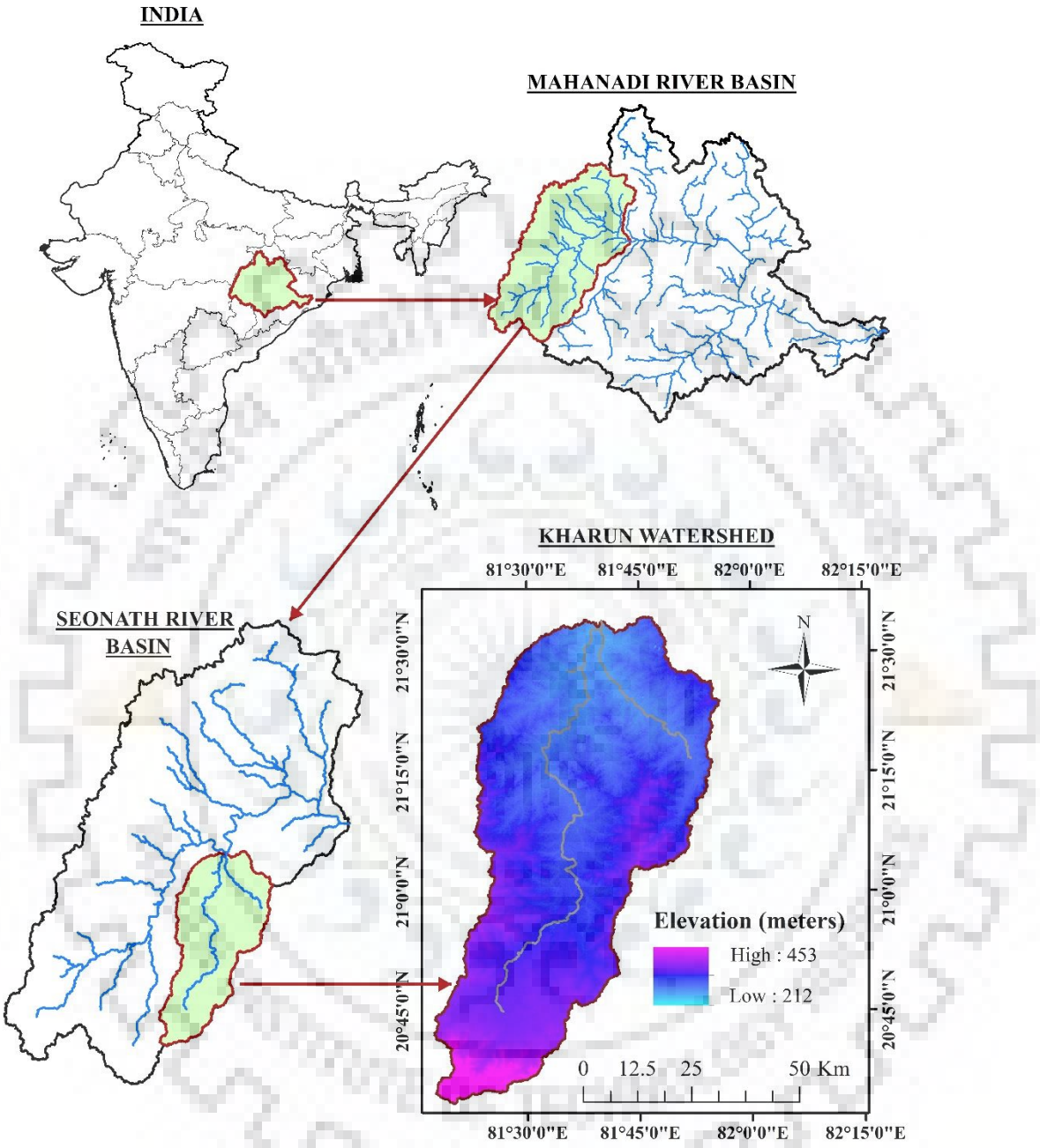

Figure 3.1 Index map of the study area.

The digital elevation model (DEM) of Kharun watershed is also given in Figure 3.1, which depicts that the elevation gradually declines from South to North. The highest elevation is towards the Southern part of the watershed and is about 453 m, while the Northern part has the least elevation in the watershed, which is about 212 m. The slope distribution of the Kharun watershed is shown in Figure 3.2.

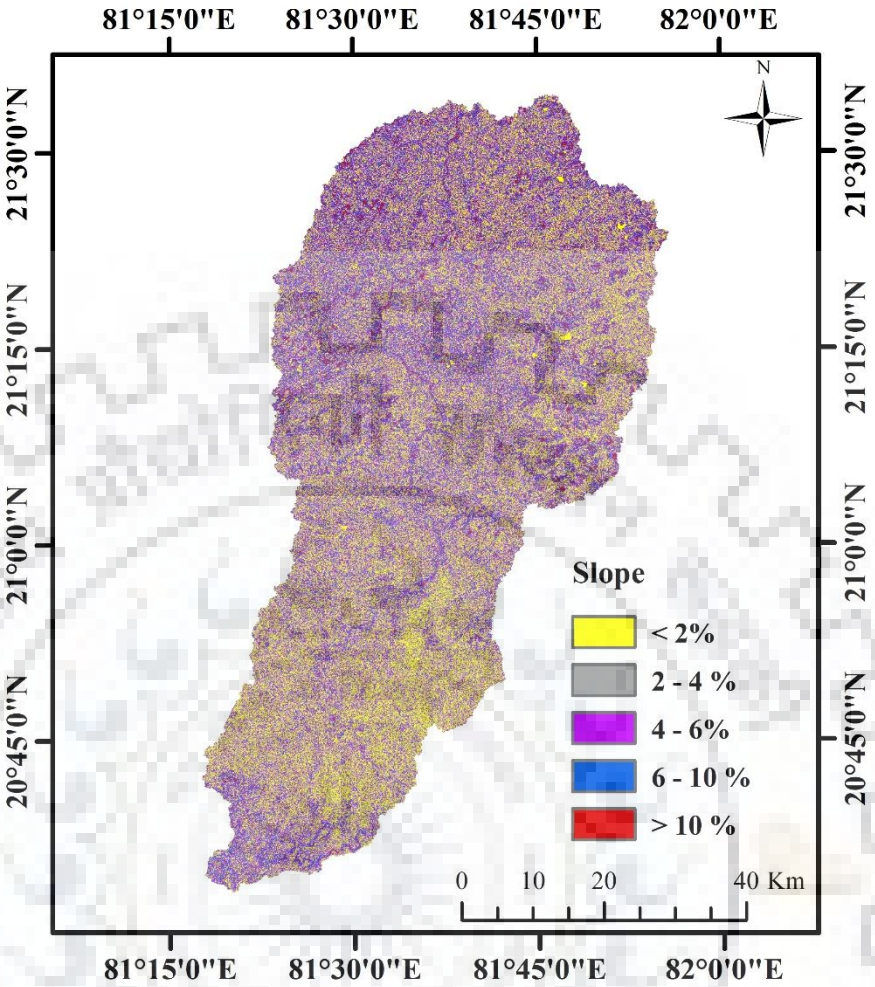

Figure 3.2 Slope map of the study area.

3.2.2 Climatology

The climate in and near the watershed is tropical. Because of its proximity to the tropic of cancer, the area is quite hot and humid. Kharun watershed experiences extreme temperature variation throughout the year. Summer temperatures can go as high as 46ºC in May, while in winter, the temperature is moderately low, 9ºC recorded in January. The study area receives an average of 1,292 millimeters of rainfall, much of it (almost 85%) is received in the monsoonal period (late June to September) (Chandrakar et al. 2017). The significant share of rainfall is due to the south-west monsoon, while a minor share is of retreating monsoon due to cyclonic depression in the Bay of Bengal. For climate, the study area can be considered to have four seasons, as described in Table 3.1, along with the maximum/minimum temperature in a day and cumulated precipitation in those seasons.

Table 3.1 Characteristics of various seasons in the study area.

S. No.	Season	Months	Max. /Min. temp. (ºC)	Precipitation (mm)
1	Monsoon	June -September	43/22	1099
2	Post-monsoon	October-November	34/16	64
3	Winter	December – February	25/8	35
4	Summer	March-May	46/30	94

3.2.3 Land use /Land Cover Distribution

The vast majority of the land in the study area can be categorized as cultivable land, vegetation (or mixed forest), barren land, sand and open rocks, water bodies and urban settlement. Almost 76% of the area in Kharun watershed can be characterized as cultivable land, which is more than two-thirds the total area of the watershed, hence it is the most dominant class. The Indian cropping season is primarily classified into two seasons (i) Kharif (June to October) and (ii) Rabi (October to March). Paddy is grown in almost entire cultivable land of the study area during the Kharif season, while lintels and wheat are grown in some parts of the area during Rabi season. Apart from the cultivable land, almost 4% of the area can be characterized as an urban settlement, which is expanding at a decent pace due to the presence of state capital in the watershed. A sudden surge in the emergence of barren land has been observed, and currently, it is around 11% of the total study area, owing to the conversion of agricultural land into real estate properties because of massive urbanization of the area in recent years. Almost 6% of the area is covered by vegetation, while water bodies (including ponds, lakes, and river stretch), sand, and open rocks span over 3% of the total study area.

3.2.4 Soil Types and Their Distribution

Soil can be described as a composite of various minerals and organic matters, which differ from their parent constituents concerning their color, texture, consistency, structure, and other such characteristics. A clear understanding of the soil properties in the region is one of the primary aspects which is quite essential when it comes to hydrological modeling of the watershed. Soil characteristics and properties in any area are mainly dependent on its relief, which majorly influences the variation in soil formation. The soil around the Kharun River is very fertile and is quite suitable for agricultural practices. The spatial distribution of the soil types in the region are shown in Figure 3.3.

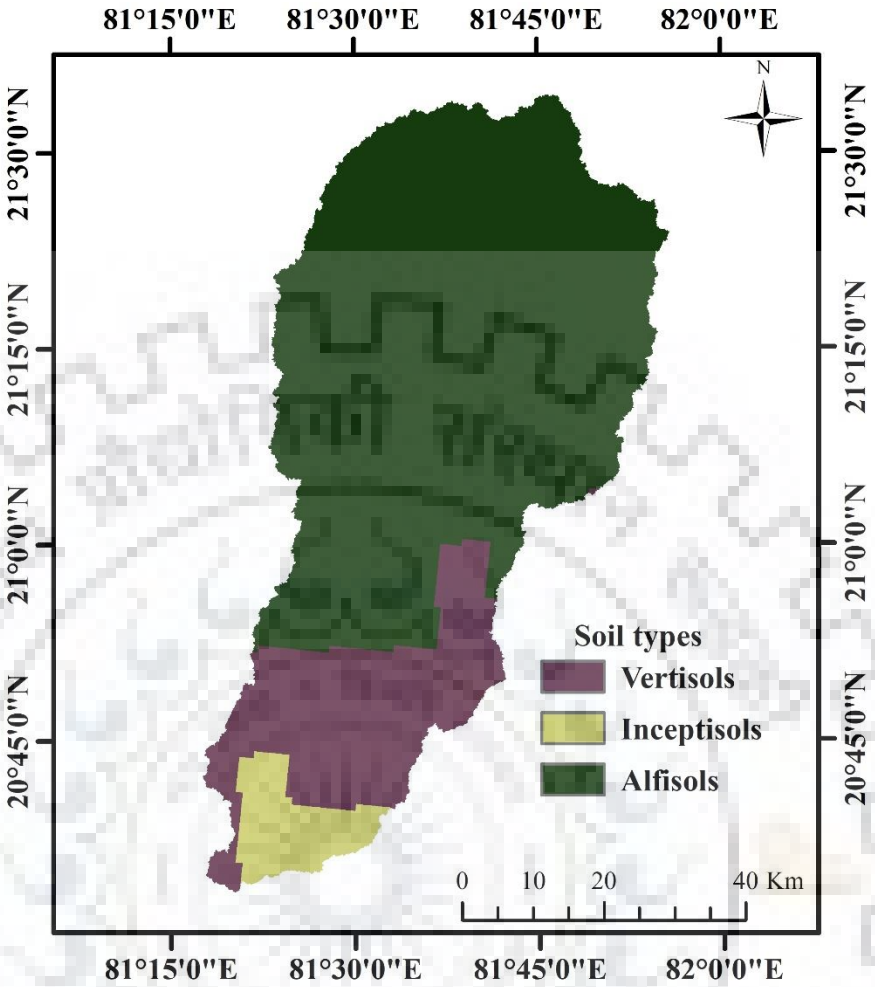

Figure 3.3 Spatial distribution of soil types in the study area.

The study area has mainly three different types of soils, i.e., Vertisols (32.9%), Inceptisols (21.3%), and Alfisols (45.5%). Apart from these three soil types, a tiny percentage of Mollisols (0.3%) are also found in the region. The description of various soil types that are found in the Kharun watershed is listed in Table 3.2.

Since mass agricultural practices are prevalent in the study area, erosion of soil is a common phenomenon because of the loosening of topsoil. Soil erosion is quite severe in the plains regions of the Kharun watershed. Severe erosion also occurs throughout the river in the lower plains.

Table 3.2 Description of soil types found in Kharun watershed.

S. No.	Soil type	Code	Local name	Suborder	Description	Area (%)
1	Vertisols	ert	Kanhar	Invert	Soils having swell- shrink type clays, having more than 30% clay up to 0.5 to 2 m depth, lithic / paralithic contact.	22.9
2	Inceptisols	ept	Matasi	Inception	Soils representing an early stage in soil formation and no spodic, argillic, nitric, petrocalcic, plinthite, but have a cambic-B horizon.	11.3
3	Alfisols	alf	Dorsa	Pedalfer	Soils of the humid and sub-humid regions, high base status (>35%), and having ochric epipedon.	65.5
4	Mollisols	oll	-NA-	Mollify	Dark color, high base (>50%) soils of grassland vegetation with a mollic epipedon that is no hard and massive when dry.	0.3

3.3 DATA COLLECTION AND PROCESSING

Hydro-meteorological and spatial data have been collected from the India Meteorological Department (IMD) Pune, India Water Portal (Indian Meteorological Datasets), and other resources.

3.3.1 Hydro-Meteorological Data

Daily temperature (minimum and maximum) and precipitation values were extracted using $1^{o} \times 1^{o}$ and $0.25^{o} \times 0.25^{o}$ gridded datasets, respectively, which was provided by IMD, Pune (Pai et al. 2014). The study of climate change demands long term data series, keeping that in view, precipitation data of 115 years (1901-2015) was considered for the study at $0.25^{o} \times 0.25^{o}$ scale. However, due to the unavailability of data for temperature for the entire period, 64 years (1951-2014) were considered for the evaluation of trends in temperature extremes (minimum and maximum). Moreover, as the temperature data provided by IMD was at $1^{o} \times 1^{o}$ scale, it was further resampled and interpolated using kriging (Gaussian process regression), which is an advanced geospatial procedure for interpolation of spatial data and was resampled at $0.25^{o} \times 0.25^{o}$ (Pai et al. 2014). Generally, resampling reduces the accuracy of the data. Nevertheless, as the study area has flat topography with the absence of any hilly region in the watershed, such technique can be used without altering the

data. In order to encompass the entire study area, 22 grids were identified in and around the watershed, as it is clear from Figure 3.4.

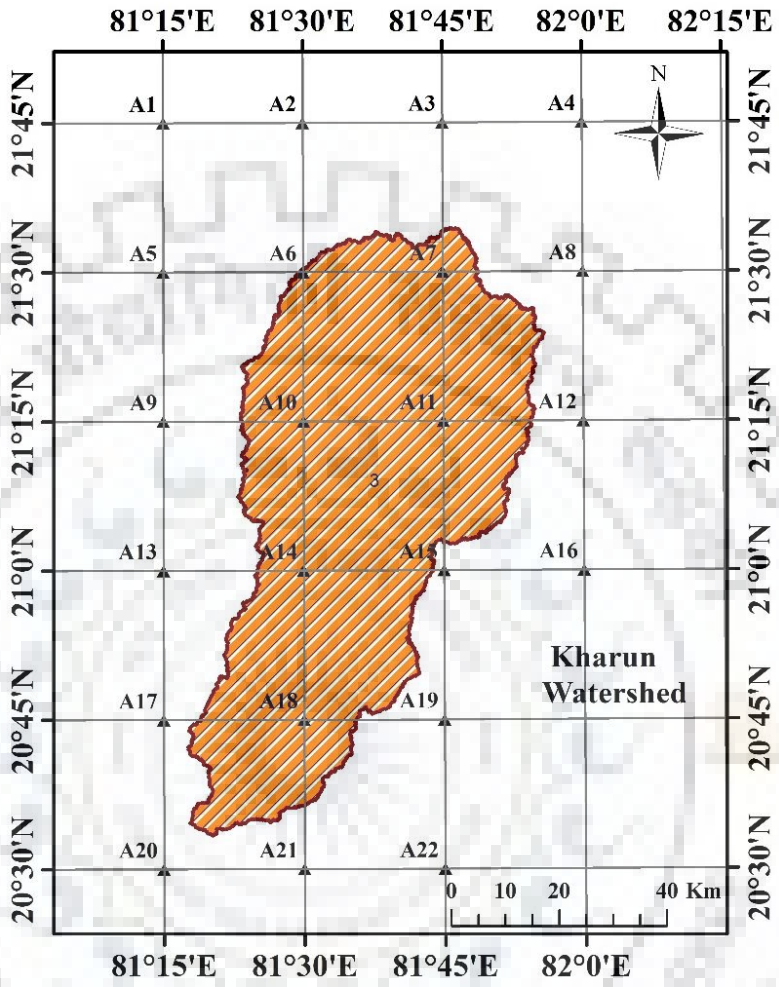

Figure 3.4 Selected grids in and around the study area.

3.3.2 Soil Map

The soil map for the study area at a scale of 1:25,00,000 was obtained from NBSSLUP (National Bureau of Soil Survey and Land Use Planning), Nagpur. It has been carefully scanned and exported to ArcGIS 10.2.2 environment. For the study area, three distinct soil types were traced and the polygons representing different soils were filled with different colors for their identification. The detailed description of the spatial variation of soil in the study area is already represented in Figure 3.3.

3.3.3 Digital Elevation Model

The Shuttle Radar Topography Mission (SRTM) data are digital elevation on a horizontal grid spacing of 30 m resolution. The elevation of Kharun watershed varies from about 212 m to 453 m

from mean sea level (MSL) by Digital Elevation Model (DEM). Southern parts of the catchment have the highest elevation ranges (Kharun watershed) and the lower range is located towards the Northern part of the catchment area, respectively. In the study area, the DEM, of 30 x 30 m pixel size was loaded to the system in an Arc Info grid format. The DEM properties were set up to verify the projection and the horizontal and vertical units of measure were verified. The DEM is acquired to generate the drainage network for the study area.

3.3.4 Observed Discharge

Observed discharge and sediment data are necessary for evaluating the hydrological model. Discharge data of Kharun watershed have been collected to calibrate and validate the model. For Kharun watershed, discharge data for 27 years was acquired from Patherdihi Gauge discharge site of Central Water Commission (CWC) on Kharun river located at Latitude 21º 20' 28'' N and Longitude 81º 35'48'' E near village Kumhari.

3.4 CONCLUDING REMARKS

To investigate the long term changes in the hydrological balance of an area (basin/watershed), it is essential to know about the history, climatology, topography and demography of that area. Kharun watershed was opted for the present study. The study area of Kharun watershed is vital as the state of Chhattisgarh was formed in the year 2000. Raipur, the capital city of Chhattisgarh, lies within the watershed, and the Kharun River bisects the capital due west of the city. Massive urbanization and industrialization have been observed after the formation of Chhattisgarh state. Due to real estate development, forest areas and agricultural land have given way to residential and industrial complexes. These extensive development and urbanization have altered the hydrological balance in the region. To investigate the extent of imbalances caused by the alteration in the hydrological balance, this study was carried out in one of the major watersheds in the tropical region of Chhattisgarh.

In this research, investigations on the climatic variables have been made over Kharun watershed to understand the relationship between spatial scale severities of climate change on water availability. Analysis of the trend and periodicity of precipitation and temperature and selection of climate model for hydrological studies have been done for the study area. Kharun watershed was selected for trend analysis of climatic variables and evaluation of water balance components at different emission scenarios. Kharun watershed was considered as a study area to demonstrate the application of

integrated hydrological modeling with changing climate scenarios. Salient features of the selected study area are described briefly, which includes the location map, topography, climatology, LULC distribution, and soil map. The spatial, non-spatial and meteorological data have also been briefly described and presented in subsequent chapters.

CHAPTER 4

SHIFT AND TRENDS IN METEOROLOGICAL VARIABLES

4.1 GENERAL

Numerous studies in the past have proved that planet Earth is warming day by day and at a faster rate in the past few decades (IPCC 2007a; Tilman et al. 2011a). For decades, the prime focus was centered around the study of climate change using mean values of meteorological data, while very few studies have highlighted changes in climate extremes (Shrestha et al. 1999; Zhang et al. 2013; Patel et al. 2018). Since the issue of climate change has become quite conspicuous, studies related to historical climate change has advanced immensely in recent years, especially for temperature and precipitation (Klein Tank and Können 2003; Muller 2007; UN Habitat 2011; Pingale et al. 2014; Sun et al. 2016; Pandey and Khare 2018). With the due acceleration of the global hydrological cycle ignited due to climate warming, incidences of extreme events (precipitation and temperature) have increased worldwide (Zhao et al. 2014). This exceedance in climatic extremes has significantly caused damage to ecology, infrastructure and agricultural sector (Pavan et al. 2008; Marengo et al. 2010; Penalba and Robledo 2010). As a result of which various studies have been carried out in many regions around the world in order to bring attention towards extreme weather, its causes and effects (Rusticucci and Barrucand 2004; Alexander et al. 2006; Min et al. 2011; Sun et al. 2016; Zhou et al. 2016). Extreme weather and its societal and ecological impacts have grabbed attention in many areas across the globe, such as in North America (Kunkel 2003), Central America (Aguilar et al. 2005), Middle East (Zhang et al. 2005), Western and Southern Africa (New et al. 2006), in various European countries like Germany and Greece (Trömel and Schönwiese 2007; Kioutsioukis et al. 2010) and in Asian countries like China (You et al. 2011; Liang et al. 2011; Fu et al. 2013b; She et al. 2015), Nepal (Shrestha et al. 2017) and India (Kothawale et al. 2010; Pingale et al. 2014). It was observed globally that increasing trends of temperature and precipitation extremes are present in most of the study areas, but downward trends were observed in Germany, while there was no significant trend observed in parts of Africa.

With a rapid rise in urban influx in major cities of Asia (especially in developing countries), rapid industrialization to fulfill the demographic demand accompanied by climate change has resulted in occurrences of the off-seasonal unusual climatic phenomena. Speaking of South-East Asian countries, China as a whole experienced increasing trends of precipitation extremes, but decreasing

trends were observed in northern, northeastern and central China (Zhai et al. 2005; Wang et al. 2014; Li et al. 2015). Study was carried out to compute the trends and observe the changes in daily temperature and precipitation extremes (in terms of extreme weather indices) over the Koshi river basin (Ganges sub-basin, shared among China, Nepal, and India). It was observed that the intensity and frequency of weather extremes (both temperature and precipitation) have increased over the Indo-Gangetic plains (Shrestha et al. 2017). Statistically significant trends of precipitation (in terms of extreme weather indices) were observed in South-western Ghats, India (adjacent to Bangladesh) (Iskander et al. 2014).

Although studies were carried out over very large areas, further analysis of the variations in meteorological extremes (precipitation and temperature) over a small watershed (Kharun River) forms the primary objective of this study. In the present study, 18 extreme precipitation and temperature indices out of 27 were considered for the study. These extreme indices were generated by the joint WMO Commission for Climatology (CCl) /World Climate Research Program (WCRP) Climate Variability and Predictability (CLIVAR) project's Expert Team on Climate Change Detection, Monitoring and Indices (ETCCDMI) (http://etccdi.pacificclimate.org/list_27_indices), which is a widely used methodology. Additionally, five more indices were proposed in the study, which is based on the precipitation intensity indices suggested by IMD.

In this chapter, outcomes of the study regarding long term trend changes in meteorological extremes have been discussed, along with that the methods, results, and implication of trend changes of extremes before and after the climatic shift have also been discussed. This study was carried out over 22 grids in and around the Kharun watershed. Long term data series of temperature (1951-2014) and precipitation (1901-2015) were considered to determine the variability of different extreme indices using parametric and nonparametric techniques. Cumulative sum (Cusum) and sequential Mann-Kendall (SQMK) test was applied to identify the climatic shift (change year) and to analyze the variation of climatic extremes Modified Mann-Kendall (MMK) was applied over the data series. Along with the MMK test statistic, Sens' slope estimator was applied to determine the magnitude of change for the study period. After this rate of change was calculated to quantify the extent of change, this study was conducted with the main objectives of spatiotemporal analysis of climatic parameters (rainfall and temperature) and the impact of variation in climatic extremes on crop production using various analysis techniques.

4.2 MATERIALS AND METHODS

4.2.1 Description of Study Area and Data Used

Detail description of the study area and the data used for the study have been already discussed in Chapter 3.

4.2.2 Methodology

Three different datasets, namely precipitation (1901-2015), minimum and maximum temperature (1951-2014), were used to identify long term changes in the meteorological extremes for all the grids (22 in number). To identify the trend statistics for extremes values indices in question, first of all, linear regression was administered over various indices computed from precipitation (PCP), maximum temperature (TX), and minimum temperature (TN) time series (Sharma et al. 2016). To have a precise idea about the trend displayed by various indices, the Modified Mann Kendall test (MMK) was applied. Statistic Z (obtained by MMK) was tested for significance of trend at the threshold level of 1.96 for a positive trend and -1.96 for negative trends (5% significance level). The magnitude of trend statistics was quantified using Sen's slope estimator, which is a tool to determine the variability of time series data. To know about the influence of trends shown by various indices over the study area, the spatial plot was obtained using an inverse distance weighted interpolation (IDW) technique.

For the purpose study, 23 indices were carefully selected for the study. Out of the five indices (*****) were proposed in the present study based on the precipitation intensity indices suggested by IMD to have a better understanding of variation in extremes, as shown and are presented in Table 4.1. Since the indices were developed by ETCCDMI and climatic conditions of North America (precisely Canada) were considered while deciding the temperature and precipitation thresholds. In this study climatic condition of India was considered while allotting threshold values. Upper and lower threshold values for temperature were defined as average temperatures of MAMJ (March, April, May, June) and average temperatures of NDJ (November, December, January), respectively. The average of daily rainfall between JJAS (June, July, August, and September) was considered to define daily precipitation thresholds. As per IMD, a day is considered as wet if it receives precipitation of 2.5mm or more, so this value was taken into account while computing indices this criterion was kept in mind while formulating different indices (Table 4.1).

Table 4.1 List of indices used for the analysis.

S. No.	Index ID	Index name	Description	Units
1	TN10P	Cool nights	Percentage of days when TN < 10^{th} percentile	%
2	TX90P	Hot days	Percentage of days when TX > 90^{th} percentile	%
3	TX10P	Cool days	Percentage of days when TX < 10^{th} percentile	%
4	TN90P	Warm nights	Percentage of days when TN > 90^{th} percentile	%
5	TR	Number of tropical nights	Annual count when TN > 24°C	Days
6	SU	Number of summer days	Annual count when TX > 40°C	Days
7	WSDI	Warm spell duration indicator	Annual count of days with at least 6 consecutive days when TX > 90th percentile	Days
8	CSDI	Cold spell duration indicator	Annual count of days with at least 6 consecutive days when TN < 10th percentile	Days
9	DTR	Diurnal temperature range	Monthly mean difference between TX and TN	°C
10	RX1day	Max. 1-day precipitation amount	Monthly maximum 1-day precipitation	mm
11	RX5day	Max. 5-day precipitation amount	Monthly maximum consecutive 5-day precipitation	mm
12	PRCPTOT	Annual total wet-day precipitation	Annual total PRCP in wet days (RR≥2.5mm)	mm
13	R95pTOT	Very Wet days	Annual total PRCP when RR>95th percentile	mm
14	R99pTOT	Extremely Wet days	Annual total PRCP when RR>99th percentile	mm
15	SDII	Simple daily intensity index	Ratio of annual total precipitation and number of wet days in a year	Days
16	CDD	Consecutive dry days	Maximum number of consecutive days with RR<2.5mm	Days
17	CWD	Consecutive wet days	Maximum number of consecutive days with RR >=2.5mm	Days
18	RW	Wet days	Days with minimum precipitation of 2.5mm or more	Days
19	*RL	Light rainy days	Days with precipitation between 2.5 to 7.5 mm	Days
20	*RM	Moderate rainy days	Days with precipitation between 7.6 to 35.5 mm	Days
21	*RRH	Rather heavy rainy days	Days with precipitation between 35.6 to 64.4 mm	Days
22	*RH	Heavy rainy days	Days with precipitation between 64.5 to 124.4 mm	Days
23	*RVH	Very heavy rainy days	Days with precipitation between 124.5 to 244.4 mm	Days

Where, TX and TN refer to maximum and minimum temperature, respectively.

4.2.2.1 Identification of shift

4.2.2.1.1 Cumulative Sum (Cusum) technique

In order to find the climatic shift in the long-term series of precipitation data (1901-2015), the Cusum test was applied over the data series. In case of such historical datasets, the mean hence, statistic S is given as:

$$S = \sum \left(x_t - x_m \right) \tag{4.1}$$

where X_t is the data point in the series and X_m is the mean

Change in the local mean is identified by the change in the slope of the Cusum chart, where a positive slope indicates rainfall above average and contrariwise in case of negative slope (Mansell 1997). The turning point of the slope signifies the change (shift) point of the data series.

4.2.2.1.2 Sequential Mann-Kendall (SQMK) test

The identification of shift in the time series of rainfall data using SQMK test comprises of four key steps:

1) Comparison of the values of P_j mean time series (j = 1, ..., n) with P_i (i = 1, …, j - 1). At every comparison step, the number of events where $P_j > P_i$ is summed up and is given by n_j.
2) Compute the test statistic t by:

$$t_j = \sum_{1}^{j} n_j \tag{4.2}$$

3) Compute the mean and variance of the statistic t by:

$$E(t_j) = \frac{j(j-1)}{4} \ , \ Var(t_j) = \frac{j(j-1)(2j+5)}{72} \tag{4.3}$$

4) Computation of sequential progressive value Z_t by:

$$Z_t = \frac{t_j - E(t)}{\sqrt{Var(t_j)}} \tag{4.4}$$

Similarly, the backward progressive sequential statistic (Z'_t) is computed, and the shift is identified at the intersection of statistic Z_t and Z'_t.

4.2.2.2 Identification of trend

4.2.2.2.1 Linear regression

Linear regression is one of the few renowned methods to detect the linear trend in any data series (Mirza et al. 1998; Jain et al. 2013; Rahmani et al. 2015). A Regression line was drawn for both before (1901-1958) and after (1958-2015) shift periods. According to the null hypothesis, the slope is zero; on the contrary, the alternative hypothesis suggests that the slope is a non-zero value. In any regression line β refers to the slope while intercept is denoted by λ, as shown in Eq. 4.5

$$y = \beta x + \lambda \tag{4.5}$$

To quantify the extent of trend, the slope of linear regression for all the indices was fitted to their respective time series.

4.2.2.2.2 Modified Mann-Kendall (MMK) test

In order to detect the trend in any time-series data, the following procedure is followed: By assuming that the time series data is independent, the MK statistic S can be computed as:

$$S = \sum_{i=1}^{n-1} \sum_{j=i+1}^{n} sign(x_j - x_k) \tag{4.6}$$

where n is the size of the sample, X_i and X_j are denoted as the sequential data points at *i*th and *j*th terms:

$$Sign\left(X_j - X_k\right) = \begin{cases} +1, \ldots\ldots\ldots if\ \left(X_j - X_k\right) > 0 \\ 0, \ldots\ldots\ldots if\ \left(X_j - X_k\right) = 0 \\ -1, \ldots\ldots\ldots if\ \left(X_j - X_k\right) < 0 \end{cases} \tag{4.7}$$

When n=18 the behavior of statistic S is more or less Gaussian, mean E(*S*) and Variance Var(*S*) of statistic *S* are described as:

$$E(S) = 0\ ,\ Vars(S) = \frac{n(n-1)(2n+5)}{18} \tag{4.8}$$

However, if the existence of ties is found in the data series, Var(*S*) can be readjusted as:

$$Vars(S) = \frac{\left\{ n(n-1)(2n+5) - \sum_{p=1}^{q} t_p (t_p - 1)(2t_p + 5) \right\}}{18} \tag{4.9}$$

The variables q and t_p in the above equation are respectively, the counts of tied groups and counts of data values in the pth group. The standardized test statistic 'Z' is computed by the following formula:

$$Z_{mk} = \begin{cases} \frac{S-1}{\sqrt{Var(S)}} & if \quad S > 0 \\ 0 & if \quad S = 0 \\ \frac{S+1}{\sqrt{Var(S)}} & if \quad S < 0 \end{cases} \tag{4.10}$$

If Z_{mk} is positive, there is a presence of a positive trend, whereas there is a negative trend if Z_{mk} is negative.

Since there it is a prerequisite for MK trend statistic that there must be no correlation present in the data series, if there is any trace of correlation present, pre-whitening of data series should be done to make it fit for analysis. In such cases, Modified Mann Kendall (MMK) can be used since it removes the effect of all autocorrelation coefficients (Hamed and Rao 1998). In the analysis Var(S) is modified as Var(S)* and is given as:

$$Var(S)^* = V(S)\frac{n}{n^*} \tag{4.11}$$

where n* is the effective size of the sample, the ratio n/n* is calculated from the following equation:

$$\frac{n}{n^*} = 1 + \frac{2}{n(n-1(n-2)} \sum_{i=1}^{n-1} (n-1)(n-i-1)(n-1-2)r_i \tag{4.12}$$

where n is the actual tally of observations, and r_i = lag-i is the significant autocorrelation of rank i of time series. Var(S) (Eq. 4.9) gets replaced by Var(S)* (Eq. 4.11) after its computation. Lastly, the MK statistic Z was tested for the significance of trend at threshold levels of 1.96 for positive trend and -1.96 for negative trends (5% significance level).

4.2.2.3 The magnitude of trend (Sen's slope)

Sen's method was used to compute the magnitude of the trend in various extreme value indices. It is a widely used method to determine the magnitude of the trend in time series data (Jain and Kumar 2012; Duhan and Pandey 2013). Firstly, slopes (T_i) of entire data pairs are computed by:

$$T_i = \frac{x_j - x_k}{j - k} \text{ for } i = 1,2,\ldots,N \quad (4.13)$$

where x_j and x_k refer to the data entries at time j and k (j>k), respectively. The median of these N value of T_i is termed as Sen's estimator of slopes and is computed by:

$$\beta = \frac{1}{2}\left(\frac{T_N}{2} + \frac{T_{N+2}}{2}\right) \quad \ldots \text{ if } N \text{ is even} \quad (4.14)$$

$$\beta = \left(\frac{T_{N+1}}{2}\right) \quad \ldots \text{ if } N \text{ is odd} \quad (4.15)$$

A Positive value of β signifies an upward trend, while negative values represent a negative trend (Shukla and Khare 2011; Pingale et al. 2014). The rate of change (ROC) or in other words change in magnitude (Gocic and Trajkovic 2013) can be calculated by an elementary formula given by:

$$ROC = \frac{N \times \beta \times 100}{\bar{X}} \quad (4.16)$$

where N is the length of the period, and $\bar{X}$ is the simple mean of the observations.

4.3 RESULTS AND DISCUSSIONS

4.3.1 Preliminary Analysis

Before the assessment of trends in meteorological (precipitation and temperature) extremes, variations in various classifications of precipitation intensity as well as day to day temperature aberrations, in meteorological parlance were computed based on IMD guidelines (Table 4.2). Linear trends in long term precipitation (PCP) and temperature variations for the study area are presented in Figure 4.1 and Figure 4.2, respectively. Figure 4.1 shows the yearly temperature aberrations for the study area. From Figure 4.1(a), it can be inferred that the maximum temperature (TX) over the study area between 1951 and 2014 has increased considerably. It should also be noted that departure from the normal was towards the negative half for most of the period, while in recent years, it has shifted towards the positive half. Similarly, Figure 4.1(b) depicts that minimum temperature (TN) during the investigation period has decreased further in recent years, as signified by the departure of values from the normal. It can be seen from Figure 4.2(a) that the annual precipitation over the region has decreased considerably over the past years which accounted for an increase in days having no

rain (Figure 4.2b), which in turn has resulted in decrease in rainy/wet days and days of heavy rain (Figure 4.2). Days with heavy rains have increased slightly (even though it is not that prominent), as visible from Figure 4.2(e), which may be due to recent rapid climate change over the globe.

Table 4.2 Classification of precipitation intensity and temperature aberrations as per IMD guidelines.

Parameter	Description
No rain	Precipitation amount realized in a day is 0.0 mm
Rainy/Wet Day	Precipitation amount realized in a day is 2.5 mm or more
Heavy rain	Precipitation amount realized in a day is between 64.5 to 124.4 mm
Very Heavy rain	Precipitation amount realized in a day is between 124.5 to 244.4 mm
Normal	Departure of minimum/maximum temperature from normal is +1ºC to -1ºC

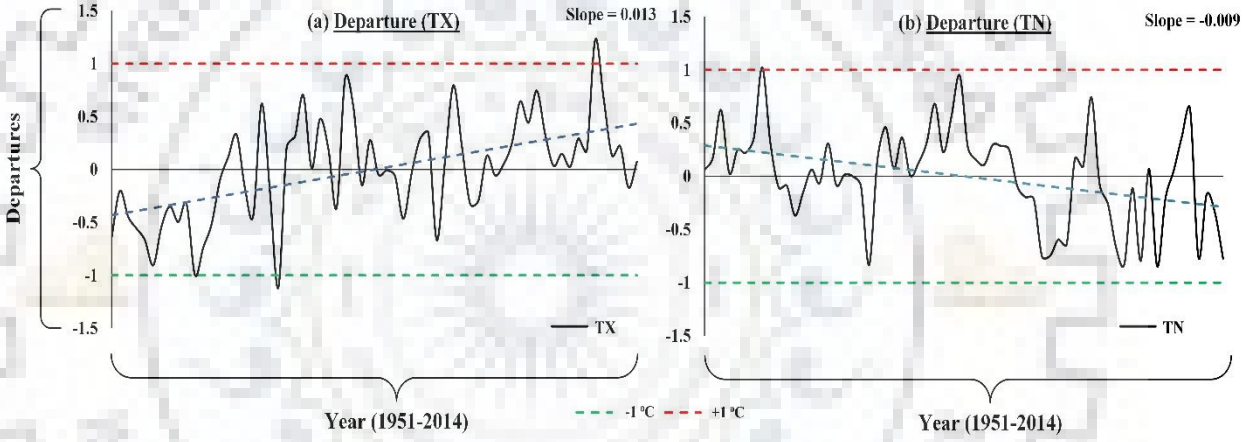

Figure 4.1 Departure of minimum/maximum temperature from normal is +1ºC to -1ºC, where TX is the daily maximum temperature, and TN is the daily minimum temperature.

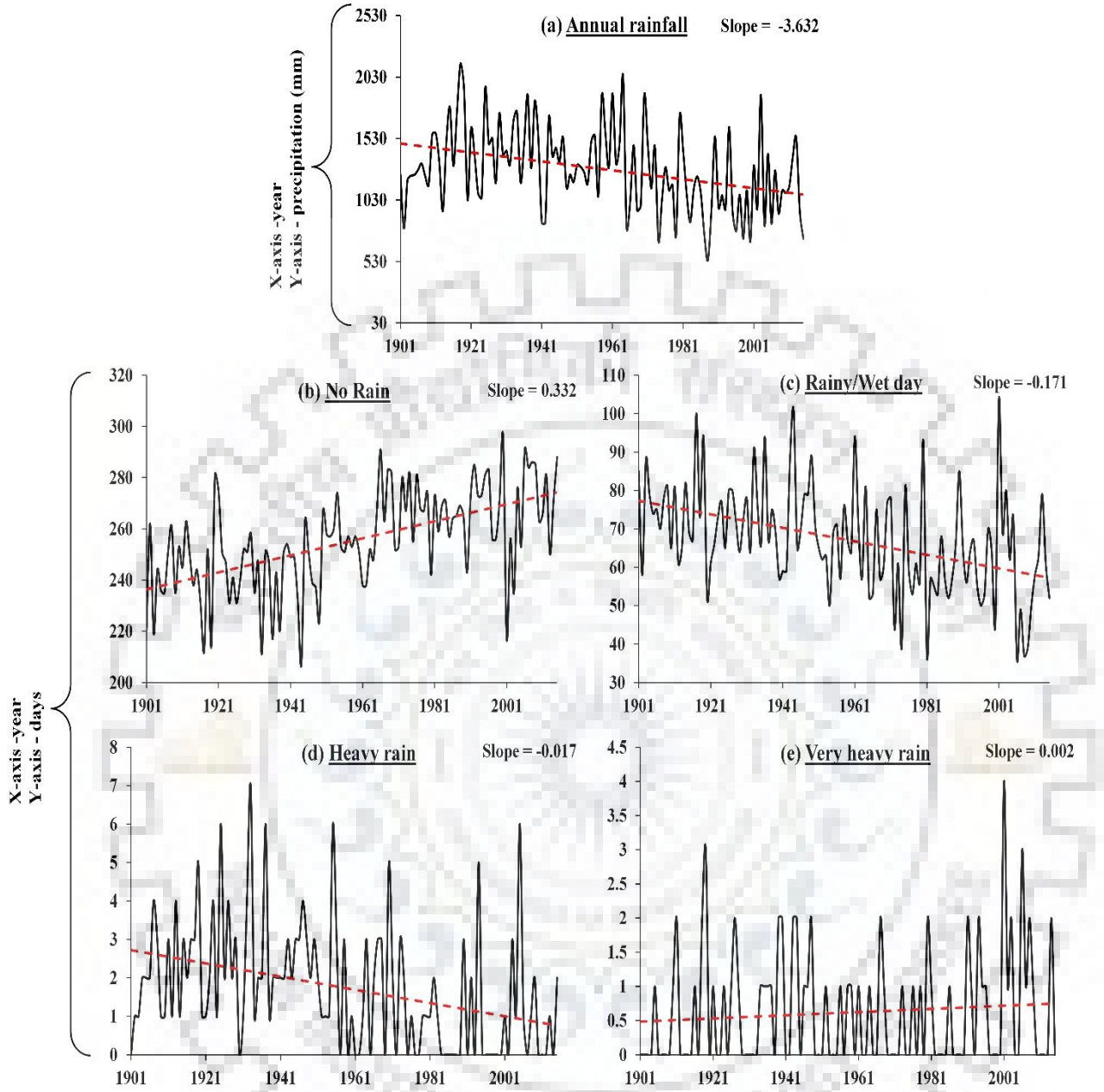

Figure 4.2 Figure showing long term variation of different rainfall intensities (IMD specified).

4.3.2 Elementary Statistics of Grids

Primary statistical constraints (mean, standard deviation (SD), coefficients of variance (C_v), skewness (C_s), and kurtosis (C_k)) were computed for annual precipitation (1901-2015) and temperature (1951-2014) for all the grids. Average annual precipitation varied between 1160 mm/year (Grid-A7) and 1367 mm/year (Grid-A13). Annual averaged maximum temperature (TX) varied between 31.8-32.4ºC across all the grids. Similarly, the variation of minimum temperature (TN) was in the range of 19.8-20.5ºC. Standard deviation (SD) for annual precipitation varied between 245-338 mm (grids 7 and 15, respectively). Similarly, the standard deviation of annual averaged TX and TN varied between 0.43-0.47ºC and 0.37-0.40ºC respectively, as shown in Table 4.3. A very small variation in the values may be due to the proximity of the grids and relatively less elevation difference among them.

The skewness (C_s) measures the asymmetry in frequency distribution around the normal, which varied between -0.04-0.58, -0.14-0.03 and 0.03-0.19 in case of annual average precipitation, TX and TN respectively. Positive values of C_s signify that the values of the parameters in question are asymmetric and are inclined towards the right of a mean for almost all the grids. The kurtosis (C_k) measures whether data series is peaked or flat relative to a normal frequency distribution, it varies between -1.43-0.48, -0.05-0.26 and -0.40--0.23 for annual average precipitation, TX and TN respectively. C_v is the ratio SD over the mean of data series. C_v varied between 21-27, 1.34-1.46 and 1.8-2.0 for annual average precipitation, TX, and TN, respectively, as shown in Table 4.3.

Table 4.3 Elementary statistics of annual rainfall (1901-2015), annual averaged maximum (TX), and minimum (TN) temperature (1951-2014).

Statistics	Coordinates		Elevation	Mean			SD			C_v			C_s			C_k		
Grid index	Lat.	Long.	(m)	PCP	TX	TN	PCP	TX	TN	PCP	TX	TN	PCP	TX	TN	PCP	TX	TN
Grid-A1	20.50	81.25	391	1301.87	32.32	19.82	292.62	0.46	0.38	22.48	1.42	1.94	0.52	0.02	0.19	0.24	0.26	-0.34
Grid-A2	20.75	81.25	321	1273.45	32.38	19.91	306.56	0.46	0.38	24.07	1.41	1.93	0.40	-0.01	0.17	0.05	0.22	-0.39
Grid-A3	21.00	81.25	288	1184.57	32.44	20.53	269.60	0.46	0.39	22.76	1.41	1.90	0.44	-0.03	0.14	0.48	0.19	-0.23
Grid-A4	21.25	81.25	284	1218.46	32.44	20.52	265.96	0.46	0.38	21.83	1.41	1.83	0.25	-0.03	0.16	0.19	0.19	-0.29
Grid-A5	21.50	81.25	311	1161.42	32.40	20.51	258.23	0.46	0.37	22.23	1.43	1.80	0.25	-0.01	0.14	-0.18	0.11	-0.32
Grid-A6	21.75	81.25	311	1163.79	32.36	20.29	264.05	0.46	0.37	22.69	1.43	1.84	0.58	0.02	0.13	0.43	0.16	-0.36
Grid-A7	21.75	81.50	288	1160.73	32.44	20.05	245.64	0.46	0.39	21.16	1.43	1.96	0.44	-0.03	0.07	0.29	0.06	-0.29
Grid-A8	21.50	81.50	291	1171.63	32.44	20.05	252.46	0.46	0.39	21.55	1.43	1.96	0.33	-0.03	0.07	-0.15	0.06	-0.29
Grid-A9	21.25	81.50	286	1285.99	32.39	20.06	284.62	0.47	0.38	22.13	1.44	1.90	0.47	0.03	0.11	0.03	0.06	-0.35
Grid-A10	21.00	81.50	302	1227.51	32.42	20.06	291.10	0.47	0.38	23.71	1.45	1.88	0.14	-0.01	0.13	-0.19	0.01	-0.39
Grid-A11	20.75	81.50	316	1214.49	32.44	19.81	271.28	0.47	0.40	22.34	1.46	2.01	0.14	-0.04	0.03	0.03	-0.05	-0.29
Grid-A12	20.50	81.50	362	1288.47	32.44	19.82	291.20	0.47	0.39	22.60	1.46	1.95	0.43	-0.04	0.09	0.25	-0.05	-0.36
Grid-A13	20.50	81.75	395	1367.65	32.32	19.81	332.49	0.45	0.40	24.31	1.41	2.01	0.25	-0.02	0.03	0.01	0.08	-0.29
Grid-A14	20.75	81.75	305	1355.44	32.27	19.84	328.30	0.45	0.38	24.22	1.41	1.93	0.22	-0.05	0.12	-0.15	0.04	-0.40
Grid-A15	21.00	81.75	303	1281.30	32.22	19.90	338.47	0.46	0.39	26.42	1.42	1.97	0.25	-0.07	0.07	-0.43	0.01	-0.36
Grid-A16	21.25	81.75	294	1248.48	32.25	19.90	303.65	0.44	0.39	24.32	1.37	1.97	0.16	-0.08	0.07	-0.29	0.09	-0.36
Grid-A17	21.50	81.75	280	1196.85	32.13	19.87	302.15	0.44	0.38	25.25	1.37	1.93	0.38	-0.09	0.13	-0.15	0.08	-0.39
Grid-A18	21.75	81.75	240	1188.73	32.01	19.83	329.78	0.44	0.38	27.74	1.38	1.92	0.05	-0.10	0.16	0.05	0.08	-0.40
Grid-A19	21.75	82.00	254	1177.50	32.17	20.00	295.90	0.43	0.39	25.13	1.35	1.95	0.22	-0.14	0.13	-0.43	0.09	-0.39
Grid-A20	21.50	82.00	273	1180.37	31.98	20.00	311.91	0.43	0.39	26.42	1.34	1.95	0.43	-0.13	0.13	-0.14	0.11	-0.39
Grid-A21	21.25	82.00	266	1265.67	32.22	20.29	316.23	0.46	0.38	24.98	1.42	1.86	0.07	-0.07	0.13	-0.40	0.01	-0.33
Grid-A22	21.00	82.00	277	1304.28	31.79	20.29	312.65	0.43	0.39	23.97	1.34	1.93	-0.04	-0.13	0.10	-0.36	0.13	-0.27

Where SD refers to the standard deviation, C_v, C_s, C_k are coefficients of variation (in percentage), skewness and kurtosis respectively, PCP, TX, and TN refer to precipitation, maximum, and minimum temperature.

4.3.3 Change Point Detection

The shift year for long-term PCP data was identified as of 1958 (Figure 4.3). Almost all the grids displayed shift year of 1958 (Figure 4.3 (b)) in case of SQMK test statistics, while majority of the grids displayed the shift year of 1961 in case of Cusum test (Figure 4.3 (a)) as shown in Table 4.4, but for the ease of the analysis year 1958 was considered as the shifting year due to widespread industrialization in and around the study area during that year.

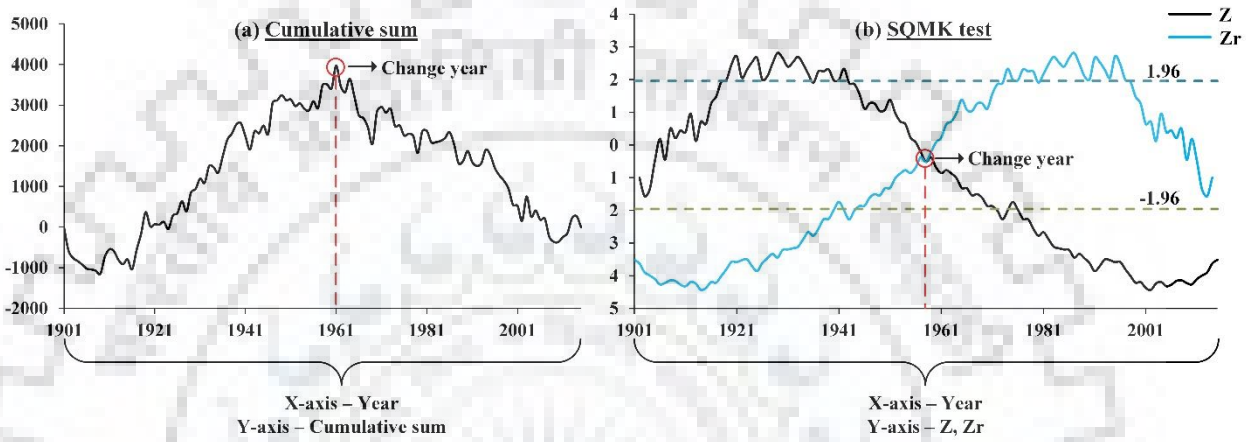

Figure 4.3 Detection of climatic shift using (a) Cumulative sum and (b) SQMK test.

Table 4.4 Change (shift) years obtained from Cusum and SQMK tests.

	Cusum			SQMK	
Change year	**1961**	**1962**	**1964**	**1957**	**1958**
Grids	6,7,10,12, 13,14,15, 17,21,22	3,5,8,18	1,4,9,11, 16,19,20	1	2,3,4,5,6,7,8,9,10, 11,12,13,14,15,16, 17,18,19,20,21,22

4.3.4 Trend Statistics

4.3.4.1 Trend statistics of maximum (TX), minimum (TN), and mean (TXN) temperature.

Modified Mann-Kendall (MMK) test statistic was applied for the entire data series to define the trend by implementing a two-tailed hypothesis at a 5% significance level. Long term trends in the study area for maximum, minimum, and mean temperatures during 1951-2014 at 5% significance level are presented in Figures 4.4, 4.5, and 4.6 respectively, while the results of their linear trends are represented in Figure 4.8. A slight increase in average yearly maximum temperature was observed (Figure 4.8a). The maximum temperature (TX) increased in all the seasons except the monsoon season (Figure 4.7). Significantly negative trends were observed across all grids in case of minimum temperature (TN) for yearly scale (Figure 4.5a). Similarly, significant negative trends were observed across all grids for the monsoon, post-monsoon and winter season (Figure 4.5), while no significant

trend was observed during the summer season (Figure 4.5b). The same can be confirmed from Figure 4.8 that shows negative trends for yearly averaged minimum temperature for all the time scales. In case of yearly mean temperature (TXN), only two grids showed significant decreasing trends for yearly time scale while only one grid showed significant decreasing trend during monsoon period (Figure 4.6), while none of the grids showed any significant trend during summer, post-monsoon and winter seasons (Figure 4.6). These results match the patterns of linear trends, which show a significant negative trend during the yearly and monsoon period (Figure 4.8), the negative trend during summer and winter seasons (Figure 4.8), and no trend during the post-monsoon period (Figure 4.8n).

4.3.4.2 Trend statistics of precipitation (PCP)

Modified Mann-Kendall (MMK) test statistic was applied to identify the trends in precipitation over the whole data series by implementing a two-tailed hypothesis at a 5% significance level and the results are presented in Figure. 4.7. The results of the linear trends are presented in Figure 4.9. Few of the grids showed a significantly decreasing trend in case of precipitation for yearly time scale (Figure 4.7a) as well during the summer and monsoon season (Figure 4.7), while no significant trend was obtained during the post-monsoon and winter season (Figure 4.7). The linear trends also showed a significant decrease in annual rainfall over the entire study period (Figure 4.7a) also rainfall has reduced during summer, monsoon and post-monsoon season (Figure 4.7) while there is a very slight increase in rainfall during the winter season (Figure 4.9).

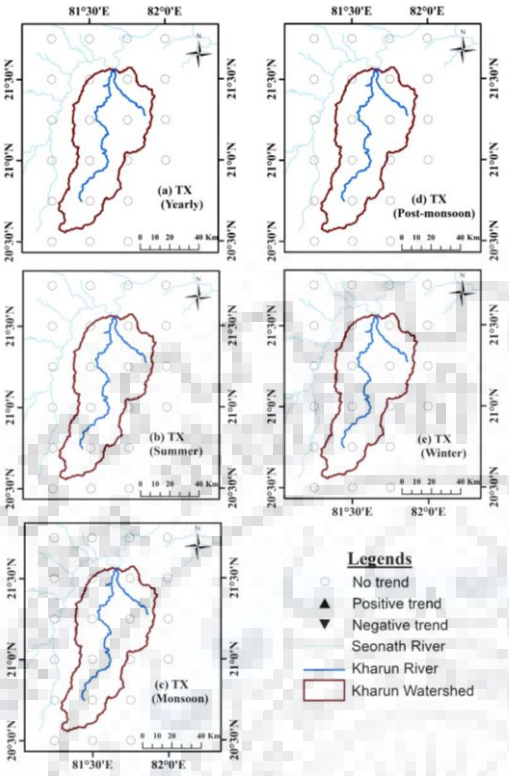

Figure 4.4 MMK trend statistics of maximum temperature (TX).

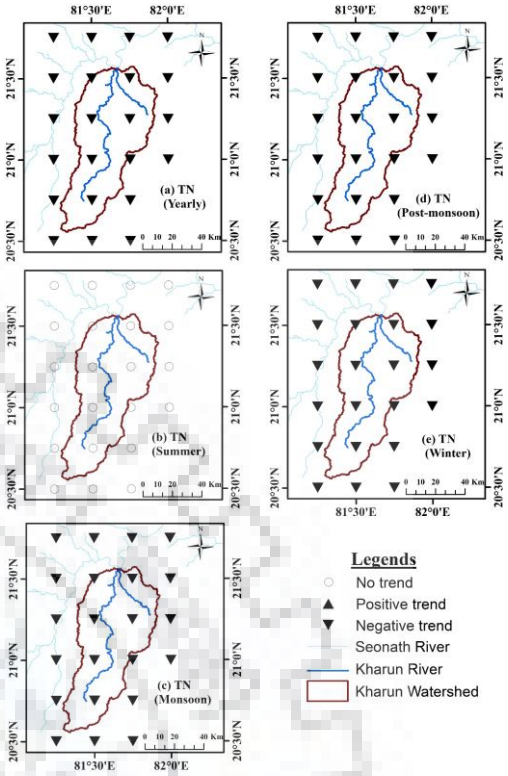

Figure 4.5 MMK trend statistics of minimum temperature (TN).

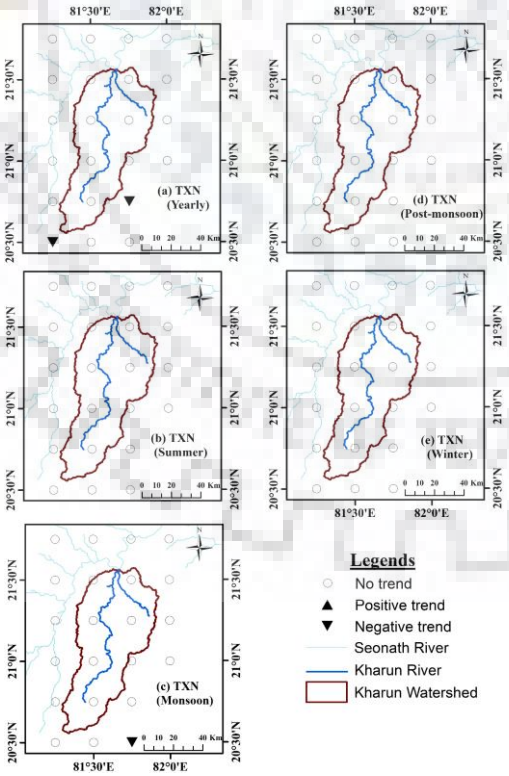

Figure 4.6 MMK trend statistics of mean temperature (TXN).

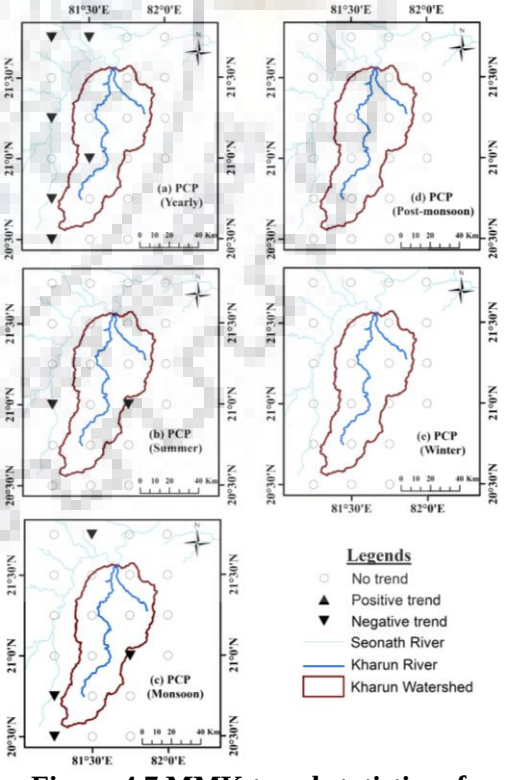

Figure 4.7 MMK trend statistics of precipitation (PCP).

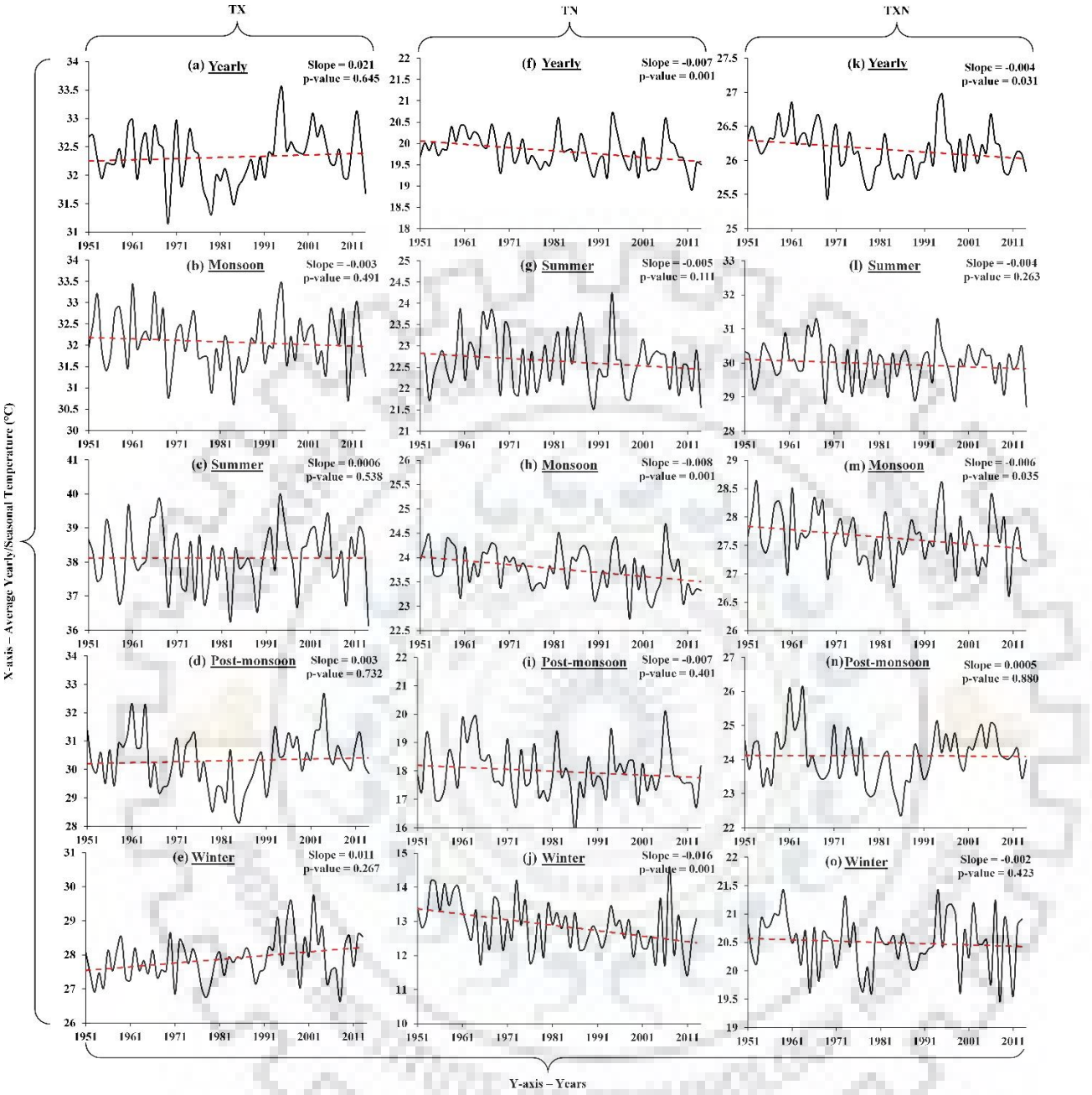

Figure 4.4 Linear trends of TX, TN, and TXN at a yearly and seasonal time scale.

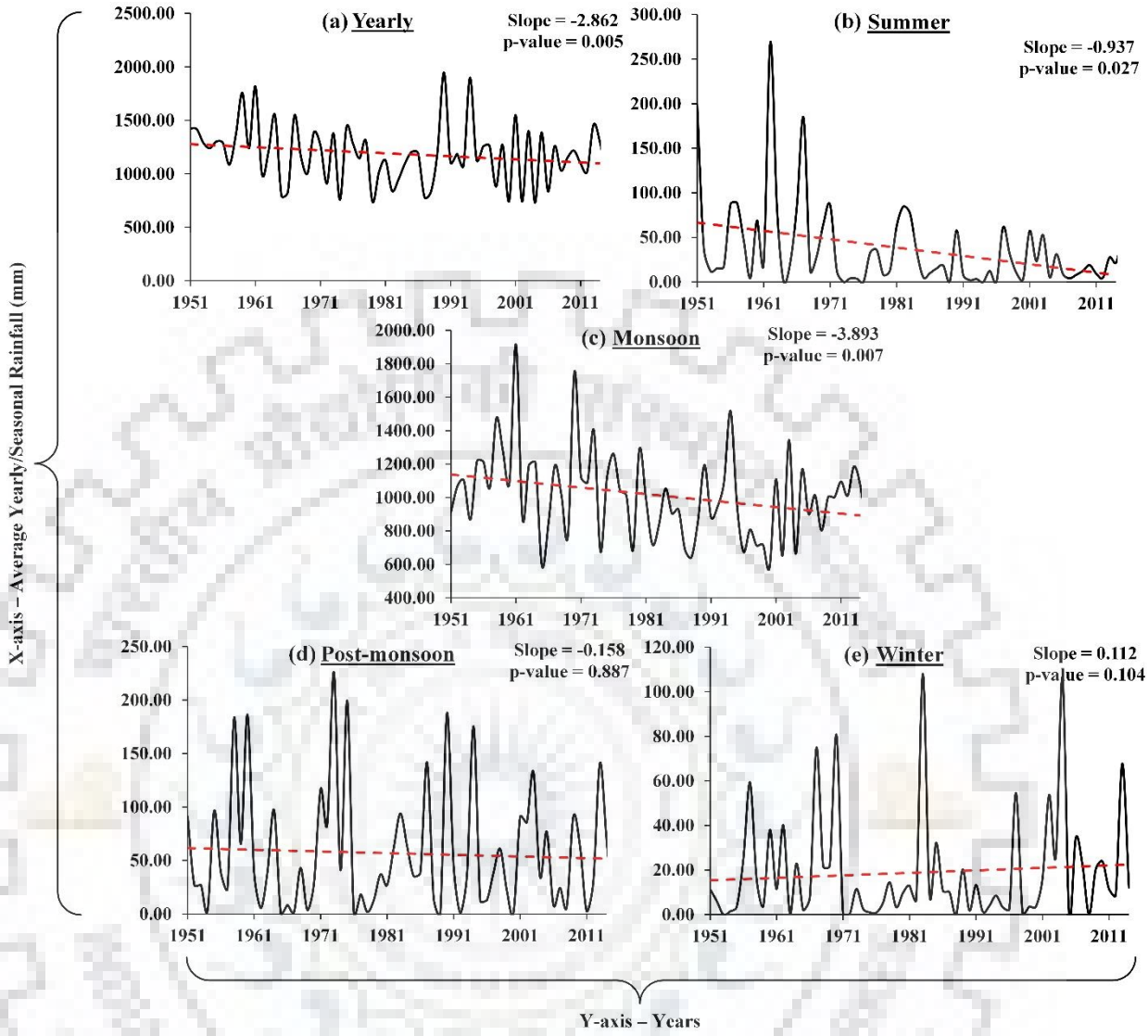

Figure 4.5 Linear trends of PCP at a yearly and seasonal time scale.

4.3.4.3 Trend statistics of extreme value indices

Modified Mann-Kendall (MMK) test was applied over different meteorological extreme indices using two-tailed hypotheses at a 5% significance level. MMK test statistic was applied initially over all the indices for all the grids, both pre-defined and over the proposed indices. Before the computation of trend through MMK and determination of its magnitude, the slope of linear regression for all the indices was fitted over their respective time series to visualize the extent of the trend (Figures 4.10, 4.11, and 4.12). Also, the p-value for each index was computed and fitted in the linear regression plot that itself describes their trend significance. After analyzing Figures 4.10, 4.11 and 4.12, it can be seen that index TX10P, TX90P, TN90P and SU (Figure 4.10) exhibited non-significant trend, but the main observation is that even though very marginally, but the number

of summer days (SU) per year has increased. Index TN10P and TR showed a significant decreasing trend for almost all the grids. Very few grids showed a significant decreasing trend for WSDI and CSDI. Similarly, for indices computed from precipitation data (Figure 4.11 and 4.12 respectively), only RVH (Figure 4.12b) exhibited a non-significant trend, but it can be seen that the number of very heavy rain days (RVH) in a year has increased in recent years. Index CWD, RW, RL and RM (Figure 4.11) showed a significant decreasing trend, while all other indices showed a significantly increasing trend (Figures 4.11 and 4.12 respectively).

The results obtained from MMK test statistics for indices computed from TX and TN, and their respective rate of change (ROC) are shown in Tables 4.5 and 4.6. The indices representing warm nights (TX10P) and hot days (TX90P) did not show any significant trend. Index of cool nights (TN10P) showed a significantly decreasing trend, none of the grids with maximum ROC of -35.4%. Few of the grids showed a significantly increasing trend for warm nights (TN90P), with a maximum ROC of 34.1%. Almost all the grids exhibited a predominantly decreasing trend for the number of tropical nights (TR), with a maximum ROC of -41.6%. There was no significant trend observed for the number of summer days (SU), but a ROC of 1.3% signifies that even though it might be less, but there is an increase in SU. Speaking of warm and cold spell duration index (WSDI and CSDI, respectively), both WSDI and CSDI showed a significantly increasing trend for very few grids. The maximum ROC for WSDI was found out to be 37.3%, while there was no quantifiable rate observed for CSDI. Index for Diurnal temperature range (DTR) showed a significantly increasing trend for most of the grids, with a maximum ROC of 6%.

The results of Indices computed from long term precipitation time series and their respective ROC are shown in Tables 4.7 and 4.8. There was a significantly increasing and decreasing trend that was observed for maximum 1-day precipitation (RX1day) at few grids, similar was the case for maximum 5-day precipitation (RX5day), with maximum ROC's of -43 and -24.7% respectively. An index representing annual wet day precipitation (PRCPTOT) showed a significantly decreasing trend for almost all the grids, with a maximum ROC of -33.8%. Indices for very wet days (R95TOT), extremely wet days (R99PTOT), simple precipitation intensity index (SDII) and consecutive wet days (CWD) showed significantly decreasing trend for few grids, while very few of the grids showed a significantly positive trend for these indices, with ROC's of -29.5, -37.5, -26.8 and -40%, respectively represent a quantifiable change in the indices. An index representing consecutive dry days (CDD) showed a significantly increasing trend for almost all the grids, with a maximum ROC

of 30.9%. As for the indices which were proposed in the study, almost half of the grids showed a significantly decreasing trend for number of wet days (RW), light rainy days (RL), moderate rainy days (RM) and rather heavy rainy days (RRH) in a year, with maximum ROC's of -30.6, -57, -31.7 and -49.8%. Few of the grids showed a significant increasing trend for the index of heavy rainy days (RH), which is quite a definite outcome; a maximum ROC of 89.4% further complimented it. Index for very high rainy days (RVH) did not show any significant trend; neither any change in its rate was observed.

Spatial distribution plot of MMK test statistics for all the indices over study area is shown in Figure 4.13 was made using an inverse distance weighted interpolation (IDW) technique using ArcGIS 10.2.2 to have a better understanding of variations of trends among different grids.

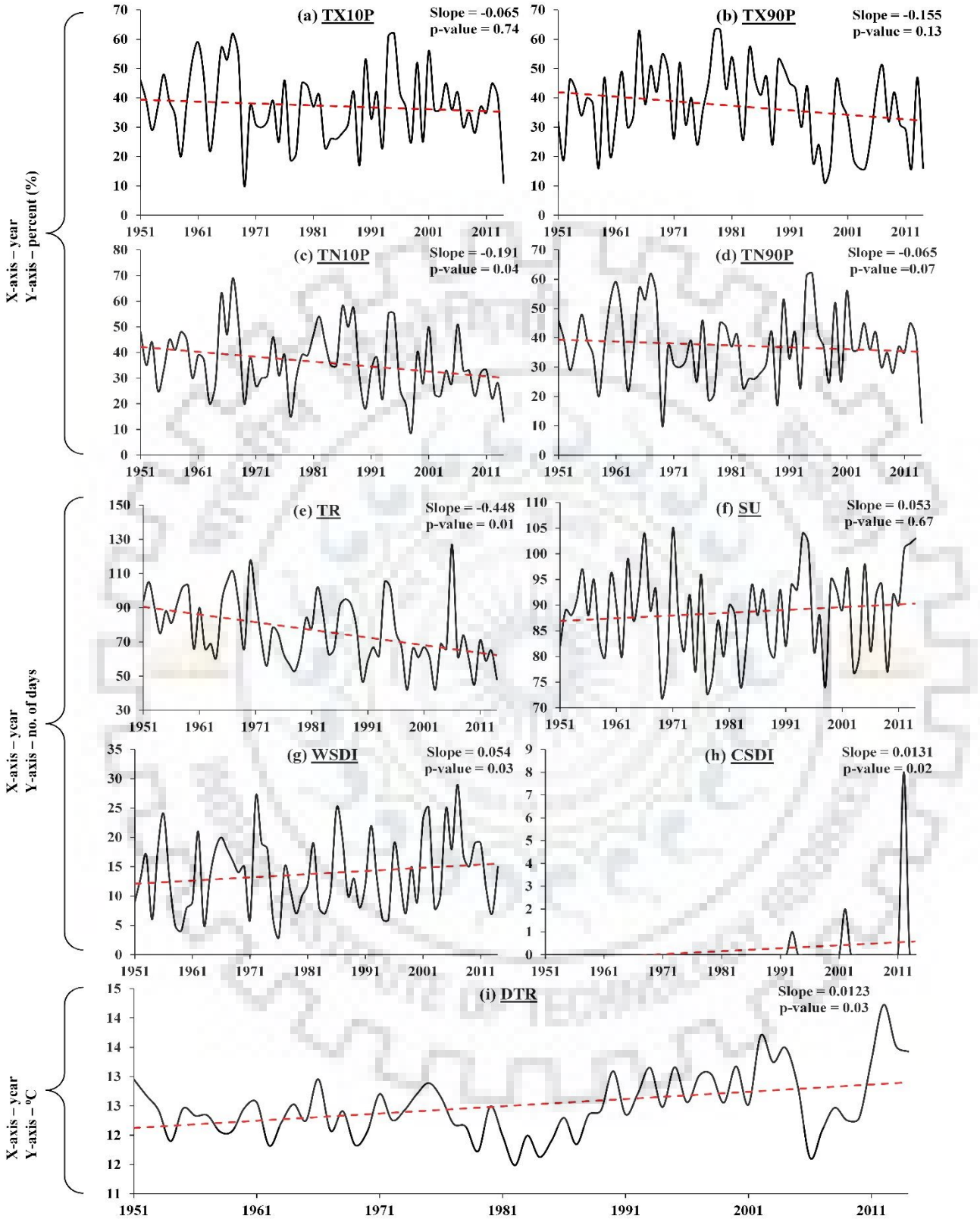

Figure 4.6 Linear trends for pre-defined extreme value indices of long term temperature series.

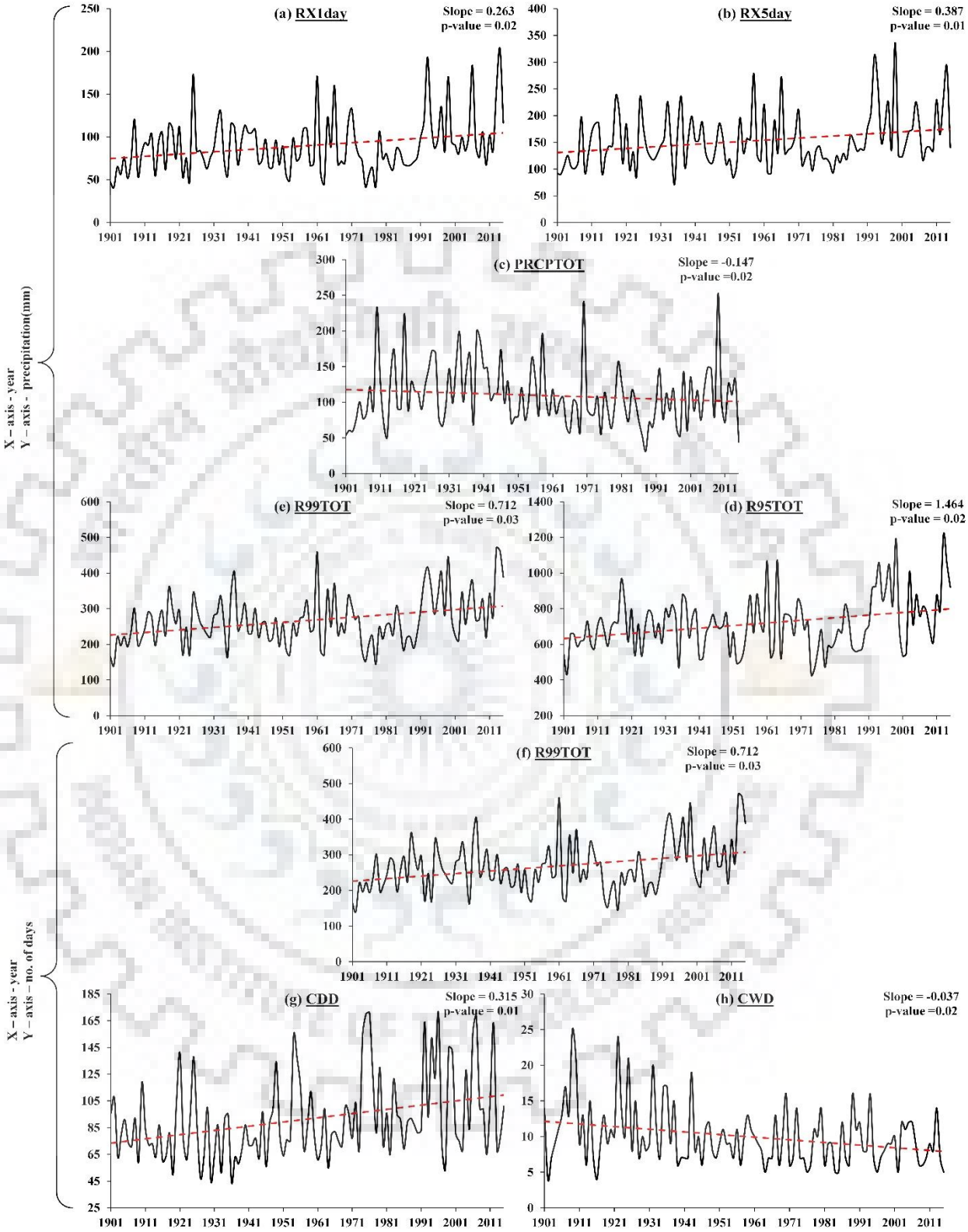

Figure 4.7 Linear trends for pre-defined extreme value indices of long term precipitation series.

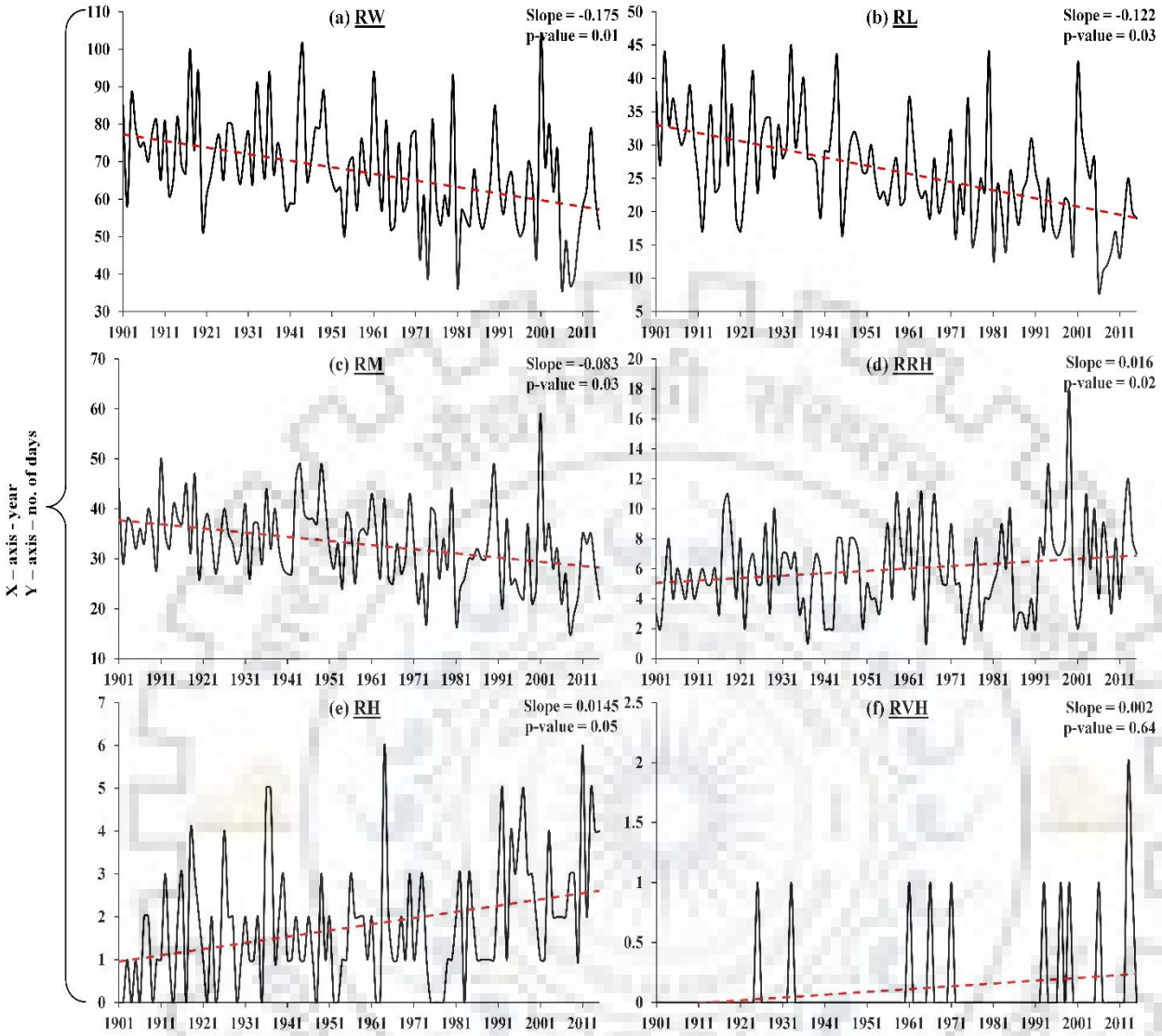

Figure 4.8 Linear trends for proposed extreme value indices of long term precipitation series.

Table 4.5 MMK statistics (Z) temperature extreme indices over the Kharun watershed (1951-2014).

Indices→	TX10P	TX90P	TN10P	TN90P	TR	SU	WSDI	CSDI	DTR
Grid-A1	-0.33	-1.51	**-2.18**	1.18	**-2.72**	0.45	1.08	1.32	**2.00**
Grid-A2	-0.12	-1.55	-1.76	1.56	**-3.43**	0.40	1.86	1.37	1.90
Grid-A3	-0.28	-1.59	**-2.06**	1.65	**-3.66**	0.05	1.42	1.36	**2.14**
Grid-A4	-0.28	-1.59	**-2.06**	1.65	**-3.66**	0.05	1.42	1.36	**2.14**
Grid-A5	-0.12	-1.59	**-2.04**	1.46	**-2.96**	0.11	0.72	1.41	1.69
Grid-A6	-0.18	-1.33	**-2.35**	1.48	**-2.85**	0.13	0.96	**1.96**	1.85
Grid-A7	-0.38	-1.39	**-2.52**	1.84	**-3.94**	0.12	1.57	**2.30**	**2.12**
Grid-A8	-0.38	-1.42	-1.91	1.43	**-2.86**	0.12	1.57	**2.30**	**2.12**
Grid-A9	-0.22	-1.19	**-2.52**	1.84	**-3.94**	0.26	0.64	1.44	1.44
Grid-A10	-0.30	-1.21	**-2.26**	1.64	**-3.50**	0.43	0.79	1.70	1.86
Grid-A11	-0.37	-1.52	**-2.35**	1.74	**-3.54**	0.50	0.86	1.57	**2.17**
Grid-A12	-0.37	-1.52	**-1.97**	1.42	**-3.54**	0.50	0.86	1.57	**2.17**
Grid-A13	-0.34	-0.89	**-1.97**	1.32	**-3.44**	0.04	1.36	0.68	1.30
Grid-A14	-0.39	-0.93	**-2.21**	1.87	**-3.07**	0.11	1.22	0.87	1.52
Grid-A15	-0.53	-0.83	**-2.30**	1.87	**-3.31**	0.18	1.22	0.87	1.78
Grid-A16	-0.53	-0.83	**-2.30**	1.87	**-3.31**	0.18	1.22	0.87	1.78
Grid-A17	-0.49	-0.88	**-2.07**	1.23	**-2.33**	-0.40	1.85	0.15	1.26
Grid-A18	-0.48	-0.85	**-2.01**	1.32	**-2.84**	-0.15	**2.47**	0.15	1.45
Grid-A19	-0.57	-0.94	**-4.20**	1.55	**-2.53**	-0.09	**2.23**	0.23	1.75
Grid-A20	-0.56	-1.05	**-2.49**	1.36	**-3.15**	-0.29	1.72	0.05	1.19
Grid-A21	-0.74	-1.02	-1.91	1.60	**-2.64**	-0.32	1.91	0.05	1.47
Grid-A22	-0.77	-0.72	**-4.64**	1.76	**-2.49**	-0.56	1.63	0.05	1.70

Figures in bold specify significant values at 95% confidence (5% significance) level.

Table 4.6 ROC for temperature extreme indices over the Kharun watershed (1951-2014).

Indices	TX10P	TX90P	TN10P	TN90P	TR	SU	WSDI	CSDI	DTR
Grid-A1	-3.6	-26.3	**-23**	18.6	**-33.9**	0.6	22.5	0	**6**
Grid-A2	0	-24.4	-27.2	20.7	**-36.4**	0	30.6	0	4.9
Grid-A3	-4.1	-25.5	**-29.3**	20.9	**-39.4**	0	37.3	0	**5.2**
Grid-A4	-4.1	-25.5	**-29.3**	20.9	**-39.4**	0	37.3	0	**5.2**
Grid-A5	0	-25.5	**-24.4**	20.9	**-28.8**	0	21.6	0	4.3
Grid-A6	0	-23.5	**-27.7**	21.9	**-35.7**	0	20.3	**0**	4.7
Grid-A7	-5.3	-23.4	**-28.5**	24.7	**-41.6**	0	36.4	**0**	**5.2**
Grid-A8	-5.3	-21.3	-22	20.4	**-27.2**	0	36.4	**0**	**5.2**
Grid-A9	0	-21.2	**-28.5**	24.7	**-41.6**	0	15.6	0	4.2
Grid-A10	-3.3	-21.1	**-27.8**	24.2	**-34.9**	1.3	16.9	0	4.8
Grid-A11	-5.7	-22.6	**-27**	26	**-40.9**	1.3	17.2	0	**5.4**
Grid-A12	-5.7	-22.6	**-22**	20.5	**-40.9**	1.3	17.2	0	**5.4**
Grid-A13	0	-21.3	**-22**	20.3	**-25.1**	0	14.3	0	3.9
Grid-A14	-3.6	-19.1	**-27.5**	28	**-31**	0	26.3	0	4.6
Grid-A15	-5.9	-20.3	**-31.5**	28	**-37.6**	0	25.8	0	5.1
Grid-A16	-5.9	-20.3	**-31.5**	28	**-37.6**	0	25.8	0	5.1
Grid-A17	-5.6	-20.2	**-25.5**	18.1	**-20.8**	0	23.6	0	3.6
Grid-A18	-6.9	-18.6	**-28.2**	22.9	**-27.7**	0	**27.2**	0	4.2
Grid-A19	-8.5	-19.3	**-32.9**	31.4	**-36**	0	**24.4**	0	4.8
Grid-A20	-7.9	-20.4	**-27.4**	25.8	**-16.3**	0	14	0	3.4
Grid-A21	-11.1	-25	-29.6	28.7	**-23.8**	-1.5	19.9	0	4.2
Grid-A22	-9.4	-21.4	**-35.4**	34.1	**-35**	-3	16.4	0	4.9

Where ROC is the rate of change.
Figures in bold specify values with significant trend statistics at a 5% significance level.

Table 4.7 MMK statistics (Z) of precipitation extreme indices over the Kharun watershed (1901-2015).

Indices→	RX1day	RX5day	PRCPTOT	R95PTOT	R99PTOT	SDII	CWD	CDD	RW	RL	RM	RRH	RH	RVH
Grid-A1	-0.65	-0.27	**-2.56**	**-2.25**	**-2.11**	**-2.05**	0.09	**1.99**	-0.84	**1.96**	-1.06	**-2.49**	**-2.25**	-0.14
Grid-A2	-1.29	-0.86	**-3.50**	**-3.56**	**-2.18**	**-3.00**	-1.09	**2.46**	**-3.55**	0.22	**-2.00**	**-2.36**	**-2.58**	-0.69
Grid-A3	-1.32	0.37	**-2.26**	**-3.29**	**-2.86**	**-3.16**	**2.95**	0.45	0.78	1.77	1.06	**-2.89**	**-2.44**	-1.11
Grid-A4	-0.01	0.47	**-2.10**	-0.24	0.34	1.77	-1.64	**1.98**	**-4.65**	**-3.35**	**-3.97**	0.02	0.74	-0.28
Grid-A5	1.59	1.72	-1.21	1.13	1.52	**3.93**	**-3.51**	**3.51**	**-2.46**	**-2.12**	**-3.06**	0.44	1.32	0.57
Grid-A6	**2.99**	**2.88**	0.12	**2.20**	**2.68**	**3.86**	**-3.50**	**3.29**	**-6.63**	**-7.35**	**-4.73**	1.67	**3.81**	0.62
Grid-A7	0.06	0.17	**-2.81**	-0.57	0.36	-0.18	-1.71	**2.52**	**-3.01**	**-1.98**	**-4.31**	-0.39	0.05	0.04
Grid-A8	**1.99**	0.29	**-2.05**	-0.39	1.17	-0.07	-1.39	1.58	**-2.64**	-1.86	**-3.42**	-0.82	-0.06	0.51
Grid-A9	-0.39	0.56	-1.42	-1.51	-1.21	-1.48	1.61	-0.68	-1.39	0.05	-0.52	**-1.98**	-0.60	-0.31
Grid-A10	0.38	0.27	**-2.88**	-1.19	-0.42	-1.09	0.74	**2.61**	**-2.08**	0.30	**-2.13**	-1.28	-1.64	-0.34
Grid-A11	-1.52	-0.01	-1.69	-0.94	-0.79	-1.00	1.05	0.05	-0.71	0.98	-1.27	-1.34	0.09	-0.24
Grid-A12	-0.56	-0.48	**-2.25**	-1.61	-1.02	-0.86	**-2.30**	1.74	**-2.97**	-0.89	**-2.41**	-1.83	-1.74	-0.10
Grid-A13	0.64	0.04	**-1.96**	-1.05	0.07	0.20	-1.32	1.68	**-2.63**	-0.64	**-2.88**	**-2.12**	-0.72	0.47
Grid-A14	0.56	0.25	**-2.28**	-0.59	0.13	0.80	-1.53	**2.49**	**-4.69**	**-2.29**	**-3.32**	-1.65	-0.03	0.20
Grid-A15	-0.96	-1.53	**-3.26**	**-2.67**	-1.92	0.80	**-2.15**	1.47	**-8.68**	**-2.63**	**-3.55**	**-2.57**	-1.18	-0.73
Grid-A16	-1.40	-1.16	**-3.66**	**-2.57**	-1.53	-1.72	-1.32	1.18	**-4.21**	-1.29	**-2.28**	**-3.28**	-0.28	-1.23
Grid-A17	-1.79	**-2.33**	**-4.69**	**-3.29**	**-2.67**	**-2.24**	-1.07	-0.17	**-3.63**	-0.05	-1.94	**-3.59**	-0.93	-1.27
Grid-A18	-1.50	-1.72	**-5.49**	-1.72	-1.03	-0.40	**-2.67**	**2.52**	**-5.96**	**-2.69**	**-3.24**	**-2.35**	-1.02	-0.25
Grid-A19	**-2.39**	**-2.69**	**-4.03**	**-3.16**	**-3.08**	**-2.57**	-1.69	**2.43**	**-2.84**	-1.17	-1.92	-1.60	**-4.86**	-0.14
Grid-A20	-1.87	**-2.28**	**-3.31**	**-2.20**	**-2.47**	-1.10	0.86	**2.67**	**-4.17**	**-2.81**	**-3.36**	-1.53	**-2.05**	-0.35
Grid-A21	-1.47	-0.84	**-2.85**	**-2.43**	-1.71	-1.81	0.86	**2.67**	**-4.18**	**-4.08**	-1.83	**-2.96**	-0.62	-1.01
Grid-A22	-0.99	-0.58	**-3.07**	-1.73	-1.23	-1.03	-0.77	**2.76**	**-4.97**	**-2.75**	**-3.79**	**-2.19**	-0.13	-0.59

Figures in bold specify significant values at 95% confidence (5% significance) level.

Table 4.8 ROC for precipitation extreme indices over the Kharun watershed (1901-2015).

Indices	RX1day	RX5day	PRCPTOT	R95PTOT	R99PTOT	SDII	CWD	CDD	RW	RL	RM	RRH	RH	RVH
Grid-A1	-6.5	-2	**-17.4**	**-15.8**	**-8.8**	**-12**	0	**17.1**	-3.9	**11.1**	-6.2	**-23.4**	**0**	0
Grid-A2	-12.1	-7.5	**-27.3**	**-21.7**	**-15.3**	**-13.7**	0	**20.7**	**-14.8**	0	**-15.6**	**-19**	**0**	0
Grid-A3	-16.2	4	**-16.5**	**-23**	**-20.6**	**-26.8**	**27.1**	5.1	9.4	30.9	11.8	**-44.3**	**0**	0
Grid-A4	-0.2	4.4	**-12.7**	-1.2	2.4	7.3	0	**17.5**	**-22.3**	**-22.2**	**-24.3**	0	0	0
Grid-A5	17.2	15.6	-9.3	8.3	17.4	**18.1**	**-40.8**	**30.9**	**-28**	**-37.4**	**-30.7**	0	0	0
Grid-A6	**26.7**	**24.1**	1	**19.5**	**24.9**	**35.6**	**-28.6**	**30.2**	**-30.6**	**-57**	**-31.7**	20.3	**67.2**	0
Grid-A7	0.7	1.7	**-15.2**	-4	3.1	-1	0	**22.8**	**-16**	**-13.2**	**-22.3**	0	0	0
Grid-A8	**17.5**	2.1	**-15.7**	-2.8	8.6	-0.5	-13.9	9.2	**-16.4**	-8.9	**-22.5**	0	0	0
Grid-A9	-5.9	5	-10.7	-10.3	-9.4	-7.3	0	-4.8	-4.9	0	0	**0**	0	0
Grid-A10	4.2	2.3	**-18.4**	-9.3	-3.4	-7.3	0	**9.7**	**-11**	0	**-16.5**	0	0	0
Grid-A11	-14	-0.1	-12	-7.6	-6.9	-6.3	0	0	-3	8	-6.3	0	0	0
Grid-A12	-5.5	-5.8	**-20.4**	-13	-10.3	-6.4	**-30.2**	12.6	**-16.8**	-6.1	**-17**	-19.2	0	0
Grid-A13	8.2	0.5	**-18.6**	-8.6	0.9	1.1	-13.6	18.7	**-15.2**	-5	**-23**	**-21**	0	0
Grid-A14	7.1	1.6	**-17.7**	-4.9	1.7	5.3	-12.9	**22.6**	**-19.9**	**-21.8**	**-23.7**	-18.2	0	0
Grid-A15	-13.1	-15.1	**-33.2**	**-23.4**	-16.8	5.3	**-13.9**	12.5	**-21.8**	**-15.4**	**-22.4**	**-29.5**	0	0
Grid-A16	-19.8	-12.7	**-28.6**	**-19.4**	-16.1	-12.6	0	9.5	**-18.5**	-11.5	**-17**	**-40.8**	0	0
Grid-A17	-33.8	**-23**	**-30.5**	**-25.9**	**-27.7**	**-18.2**	0	0	**-16.9**	0	-12.8	**-49.8**	0	0
Grid-A18	-21.8	-19.1	**-26.8**	-14.6	-11.8	-2.4	**-25**	**20.6**	**-27.6**	**-25.9**	**-26.9**	**-31.8**	0	0
Grid-A19	**-43**	**-24.7**	**-33.8**	**-29.5**	**-37.5**	**-18.4**	0	**16**	**-15.1**	-6.9	-12.8	0	**89.4**	0
Grid-A20	-29.9	**-23.8**	**-31.2**	**-19.8**	**-29.1**	-7.6	0	**20.6**	**-23.4**	**-25.1**	**-16.3**	0	**0**	0
Grid-A21	-28.1	-11.6	**-29.5**	**-26.4**	-25.9	-16.4	0	**20.6**	**-15.8**	**-6.7**	-12.4	**-47.6**	0	0
Grid-A22	-13.6	-8	**-27.3**	-18	-13.4	-6.7	0	**30.4**	**-23.3**	**-18.1**	**-24**	**-27.9**	0	0

Where, ROC is the rate of change.
Figures in bold specify values with significant trend statistics at a 5% significance level.

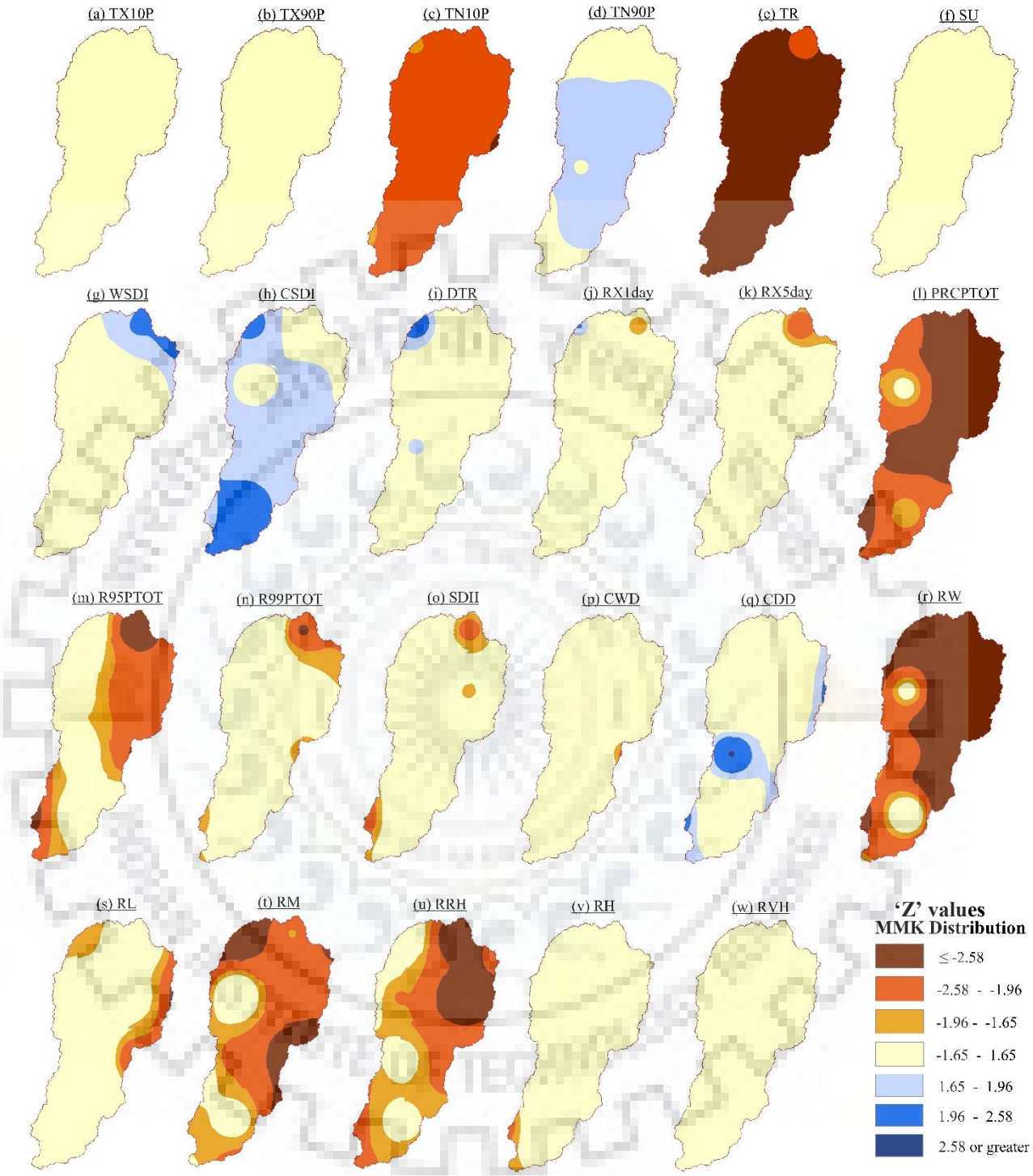

Figure 4.9 Spatial distribution plot of MMK test for all the indices between 1901-2015 (for precipitation) and 1951-2014 (for temperature).

After the computation of MMK trend statistics for indices derived from precipitation, the longtime series of precipitation was divided into two independent time series based on the computed shift year (the year 1958), as discussed in section 4.3.3. MMK test statistics and their respective ROC were computed for the indices obtained using precipitation data (both before and after the shift).

The results for MMK and ROC before the shift period are represented in Tables 4.9 and 4.10, respectively. Very few grids showed a significantly increasing trend for Indices RX1day, RX5day, R95TOT, R99TOT, SDII, and RH with maximum ROC of 33.8, 36.4, 24.1, 20.47 and 70% respectively. Few of the grids showed a significantly decreasing trend for CWD, RW, RL, and RM with maximum ROC of -28.8, -23.98, -34.92, and -34.13%, respectively. Only one grid exhibited a significantly increasing trend for PRCPTOT and a decreasing trend for index CDD, with maximum ROC of 20.14 and -25.23%, respectively, while RRH and RVH did not show any significant trend for any grid.

For the results of MMK and ROC after the shift period, represented in Tables 4.11 and 4.12 respectively, very few grids showed significantly increasing trend for RX1day, RX5day, R99TOT, CDD and RH with maximum ROC of 41.4%, 33.2, 35.5, 36.6 and 88%. Index PRCPTOT, SDII, CWD, RW, RM showed a significantly decreasing trend for few grids, with maximum ROC of -33.88, -23.1, -40.19, -27.7 and -37.8 % respectively. At very few grids significantly decreasing trend was observed for R95PTOT, CWD and RRH, while a significantly increasing trend was observed for CDD, with maximum ROC of -31.82, -40.19, -60 and 36.6% respectively. As for the index RVH, one grid exhibited a significant trend, but the ROC was non-measurable.

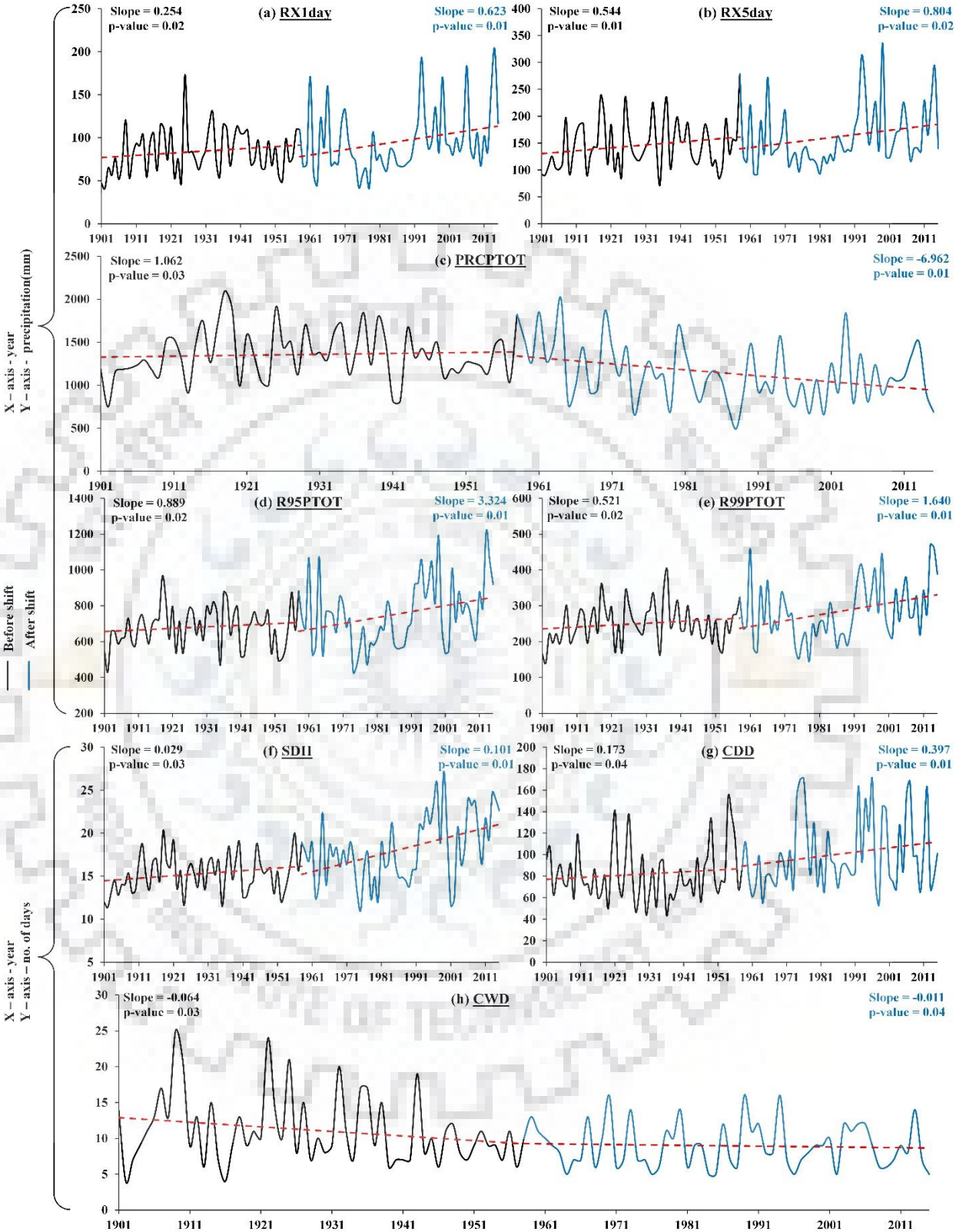

Figure 4.10 Linear trends for pre-defined extreme value indices of long term precipitation series, both before and after shift (the year 1958).

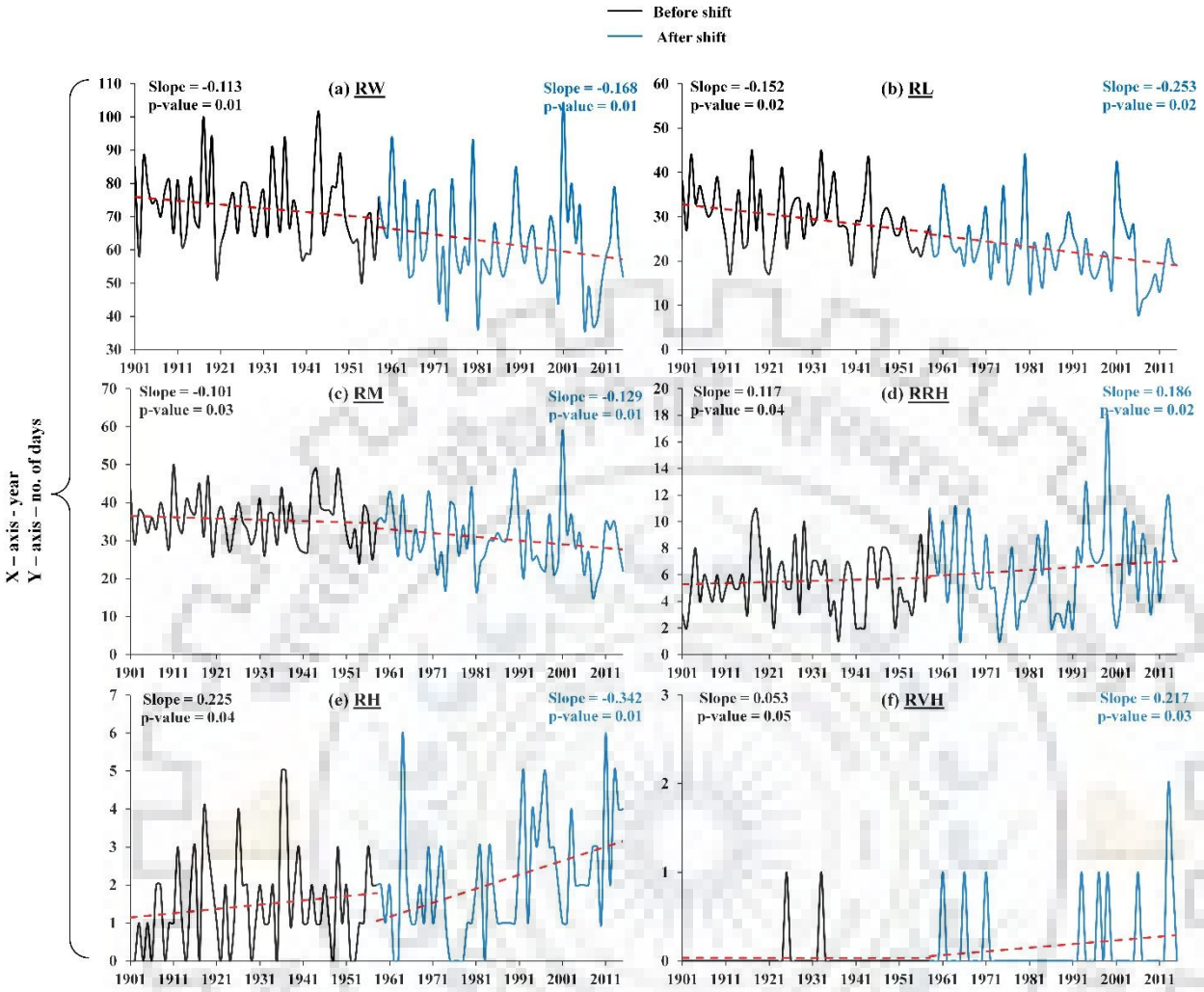

Figure 4.11 Linear trends for proposed extreme value indices of long term precipitation series, both before and after shift (the year 1958).

Table 4.9 MMK statistics (Z) of precipitation extreme indices over the Kharun watershed before shift (1901-1958).

Indices→	RX1day	RX5day	PRCPTOT	R95PTOT	R99PTOT	SDII	CWD	CDD	RW	RL	RM	RRH	RH	RVH
Grid-A1	**3.03**	**2.60**	0.90	0.76	1.64	1.00	-0.22	-0.85	0.14	0.48	0.54	0.35	-0.34	1.29
Grid-A2	0.92	1.91	0.20	0.12	0.73	-0.06	0.35	-0.44	0.68	1.06	0.24	0.40	-0.58	-0.01
Grid-A3	1.73	**2.46**	1.18	1.03	1.21	-1.16	**2.11**	**-2.08**	1.84	1.92	1.07	-0.30	0.00	1.26
Grid-A4	-0.41	0.83	1.47	1.72	0.85	**3.30**	0.07	-0.20	-1.58	**-2.39**	-1.07	1.60	1.65	-0.08
Grid-A5	**2.47**	**3.31**	0.40	**2.23**	**3.09**	**2.84**	**-1.98**	0.46	**-3.43**	**-3.70**	**-2.67**	0.63	**3.19**	0.06
Grid-A6	1.36	1.69	0.65	1.15	1.19	1.84	-1.07	0.55	-1.52	**-2.81**	-0.76	0.49	1.28	-0.01
Grid-A7	-1.00	0.31	-0.76	-0.76	-1.02	-1.68	-0.09	0.00	0.71	**-2.62**	-1.25	-0.31	-0.56	-0.15
Grid-A8	-0.82	0.59	-0.50	-0.50	-0.41	-1.50	-0.38	-0.32	1.08	**3.68**	-0.52	-0.04	-0.50	-0.13
Grid-A9	-0.32	1.19	1.61	0.84	0.05	0.62	**2.52**	-1.28	1.06	0.03	1.89	-0.64	1.57	-0.18
Grid-A10	1.93	1.38	1.60	1.92	1.52	1.83	0.13	0.00	0.09	0.36	-0.81	0.36	1.10	0.90
Grid-A11	1.04	-0.26	0.78	0.32	0.37	1.27	-0.24	-0.36	-0.33	**-2.12**	1.56	0.46	0.47	0.68
Grid-A12	1.54	0.95	0.53	0.99	1.56	1.30	-1.78	-0.45	-1.40	-0.91	-1.53	0.43	1.23	0.29
Grid-A13	1.36	1.15	0.93	0.60	0.99	0.49	0.17	-0.43	1.40	0.99	0.77	1.16	-0.10	1.11
Grid-A14	**2.01**	1.13	1.33	1.24	1.32	**3.29**	-0.67	-1.32	0.81	1.11	-0.07	0.68	0.27	1.34
Grid-A15	**1.98**	1.35	0.54	1.33	1.50	**3.29**	**-3.02**	-1.13	-0.64	-1.17	-0.69	-0.55	**3.12**	1.26
Grid-A16	-0.09	1.65	1.00	0.97	0.81	0.17	0.40	-0.87	0.54	0.88	-0.57	-0.47	1.66	0.37
Grid-A17	1.21	1.71	0.30	**2.02**	1.39	**1.97**	**-2.22**	-0.42	**-3.00**	-1.23	**-2.71**	-0.18	**2.79**	0.02
Grid-A18	1.17	1.20	-1.10	1.13	**2.01**	**2.16**	-1.95	-0.76	**-3.22**	**-2.16**	**-3.88**	-0.82	1.09	0.49
Grid-A19	0.28	**2.10**	1.29	**2.01**	0.58	1.18	-0.01	-1.34	0.68	-0.26	0.70	0.90	0.87	0.92
Grid-A20	1.17	**2.57**	**2.27**	**2.78**	1.43	**3.08**	0.95	-0.63	-0.16	-1.54	-0.11	1.22	**2.81**	0.57
Grid-A21	0.34	**1.99**	1.46	1.40	0.70	0.83	0.95	-0.63	-0.55	0.34	-0.29	0.48	**2.34**	-0.48
Grid-A22	0.91	1.31	0.63	1.31	1.07	1.58	0.12	0.25	-1.07	-0.80	-1.00	1.07	0.65	0.79

Figures in bold specify significant values at 95% confidence (5% significance) level.

Table 4.10 ROC of precipitation extreme indices over the Kharun watershed before shift (1901-1958).

Indices→	RX1day	RX5day	PRCPTOT	R95PTOT	R99PTOT	SDII	CWD	CDD	RW	RL	RM	RRH	RH	RVH
Grid-A1	**26.67**	**21.63**	7.65	8.36	12.92	7.53	0.00	-12.53	0.00	0.00	3.47	0.00	0.00	0.00
Grid-A2	12.11	18.55	1.44	2.02	3.57	-0.49	0.00	-5.56	3.97	13.44	0.00	0.00	0.00	0.00
Grid-A3	20.72	**25.96**	10.73	6.20	11.48	-11.72	**18.24**	**-25.23**	21.74	48.71	12.07	0.00	0.00	0.00
Grid-A4	-5.16	11.93	7.52	9.85	9.80	**16.36**	0.00	-2.50	-9.58	**-23.96**	-8.32	27.56	0.00	0.00
Grid-A5	**26.99**	**31.32**	3.38	**20.06**	**30.27**	**20.47**	**-28.84**	2.76	**-23.93**	**-34.92**	**-26.14**	0.00	**87.06**	0.00
Grid-A6	20.62	21.45	5.31	10.52	11.86	12.52	-12.35	5.17	-9.84	**-24.48**	-5.63	0.00	0.00	0.00
Grid-A7	-15.04	4.24	-6.27	-7.18	-8.65	-11.42	0.00	0.00	4.83	**19.34**	-6.97	0.00	0.00	0.00
Grid-A8	-13.21	6.77	-3.37	-4.51	-4.75	-11.43	0.00	-3.51	4.76	**20.92**	0.00	0.00	0.00	0.00
Grid-A9	-8.62	15.34	9.19	5.28	0.92	4.65	**22.55**	-17.67	4.27	0.00	8.72	0.00	38.47	0.00
Grid-A10	28.52	17.94	7.21	**11.53**	16.01	10.77	0.00	0.00	0.00	0.00	-4.93	0.00	0.00	0.00
Grid-A11	9.11	-2.93	7.00	1.70	3.74	9.15	0.00	-5.02	0.00	**-16.50**	11.40	0.00	0.00	0.00
Grid-A12	20.18	12.92	3.91	11.49	16.04	12.61	-23.82	-5.45	-10.16	-8.05	-11.84	0.00	0.00	0.00
Grid-A13	23.87	16.81	8.86	5.97	12.51	3.65	0.00	-3.94	7.66	11.55	9.26	0.00	0.00	0.00
Grid-A14	**33.83**	15.14	10.17	12.65	19.17	**8.69**	0.00	-10.74	3.94	8.75	0.00	0.00	0.00	0.00
Grid-A15	**32.26**	17.41	5.61	13.81	19.44	**8.69**	**-14.83**	-15.20	-3.04	-9.80	-6.71	0.00	**0.00**	0.00
Grid-A16	-2.13	22.84	8.05	9.66	10.82	1.34	0.00	-11.22	2.59	12.34	0.00	0.00	0.00	0.00
Grid-A17	19.38	23.01	1.99	**15.09**	18.38	**14.43**	**-28.37**	-5.47	**-16.42**	-12.40	**-25.11**	0.00	**72.50**	0.00
Grid-A18	17.74	15.02	-7.43	11.29	**19.19**	**14.21**	-23.74	-9.52	**-21.65**	**-18.02**	**-34.13**	0.00	0.00	0.00
Grid-A19	3.68	**27.80**	11.23	**8.62**	5.61	7.99	0.00	-15.47	4.23	0.00	4.61	0.00	0.00	0.00
Grid-A20	18.05	**36.37**	**20.14**	**24.12**	15.34	**18.39**	0.00	-6.86	0.00	-10.69	0.00	19.72	**70.01**	0.00
Grid-A21	6.90	**25.19**	10.06	10.90	11.90	7.69	0.00	-6.86	-2.10	0.00	0.00	0.00	**0.00**	0.00
Grid-A22	12.86	18.67	5.87	12.87	12.20	9.68	0.00	2.13	-7.35	-5.55	-7.64	18.37	0.00	0.00

Where, ROC is the rate of change.

Figures in bold specify values with significant trend statistics at a 5% significance level.

Table 4.11 MMK statistics (Z) of precipitation extreme indices over the Kharun watershed after shift (1958-2015).

Indices→	RX1day	RX5day	PRCPTOT	R95PTOT	R99PTOT	SDII	CWD	CDD	RW	RL	RM	RRH	RH	RVH
Grid-A1	-0.07	-0.11	-1.29	-0.64	0.11	-1.56	0.20	-0.13	0.06	**2.35**	-0.66	-1.44	-0.22	0.26
Grid-A2	-0.08	-0.16	-1.73	-0.90	-0.47	-1.56	0.32	-0.84	-1.27	**1.97**	-1.60	-0.80	-0.42	-0.28
Grid-A3	0.37	0.75	-0.31	-1.66	-0.91	**-2.33**	1.14	-0.94	1.30	1.28	**2.54**	**-3.32**	-0.79	-0.39
Grid-A4	0.06	1.18	-0.34	-0.24	0.56	-0.18	0.72	0.13	-0.62	1.29	-0.49	-0.57	0.42	-0.14
Grid-A5	-0.36	1.01	0.93	0.16	-0.65	-0.91	1.36	0.07	1.60	1.67	1.16	0.56	-1.70	0.30
Grid-A6	**3.51**	**3.18**	0.92	1.76	**2.09**	**2.35**	-1.17	1.47	-1.71	**-3.07**	-1.79	0.53	**3.19**	0.41
Grid-A7	1.36	1.23	0.17	1.26	1.72	1.60	-0.26	0.49	-1.76	-1.27	-1.92	0.01	1.15	0.32
Grid-A8	1.49	0.91	0.58	1.15	1.11	1.02	0.45	-0.04	-0.87	-0.03	-1.40	0.36	-0.44	1.03
Grid-A9	**2.36**	**2.11**	0.09	0.47	1.37	0.59	-0.61	0.14	-1.28	-1.12	0.22	-0.73	-0.74	1.11
Grid-A10	0.64	0.00	**-2.31**	-1.93	-1.03	**-2.21**	-0.45	-1.06	-1.29	0.50	-0.30	**-2.22**	**-2.28**	-0.62
Grid-A11	1.06	1.15	-1.44	0.09	0.72	-0.22	-0.15	-1.62	-0.99	0.55	**-2.30**	-0.58	0.27	1.00
Grid-A12	0.19	0.56	-0.94	-0.34	0.15	-1.22	-0.44	-0.89	0.00	**3.28**	-1.10	-0.03	0.13	-0.07
Grid-A13	**2.11**	1.33	-1.03	0.89	**2.43**	**2.02**	-1.63	**3.98**	**-6.96**	**-2.90**	**-19.58**	0.01	1.05	0.61
Grid-A14	**3.58**	**3.05**	-1.30	0.63	**2.43**	1.69	-0.82	**2.23**	**-4.92**	**-2.33**	**-4.30**	-1.08	0.77	0.71
Grid-A15	0.51	-0.46	**-2.01**	-1.60	-0.28	1.69	-1.72	-0.01	**-2.52**	-0.62	**-2.06**	-1.32	-0.78	0.76
Grid-A16	**2.86**	1.42	-0.42	0.55	1.77	1.09	**-3.00**	0.30	**-2.16**	-1.67	-1.64	-0.97	0.30	1.96
Grid-A17	-0.25	-0.93	**-2.04**	-1.62	-0.93	-1.58	0.19	-0.08	**-2.01**	0.12	-1.71	-1.78	-1.82	1.37
Grid-A18	-1.10	-1.31	**-3.98**	**-2.68**	-1.27	**-2.27**	-0.07	0.22	-0.95	0.92	0.19	**-2.11**	-1.53	-0.32
Grid-A19	0.90	-0.53	-1.33	-0.18	0.60	-0.19	-1.30	0.26	-1.71	-0.06	**-2.72**	0.24	-1.53	1.07
Grid-A20	0.30	-1.36	-1.56	-0.04	0.16	0.34	**-2.44**	1.03	**-2.22**	-1.59	**-2.99**	-1.04	-0.11	0.12
Grid-A21	0.81	1.09	-0.43	0.62	1.02	0.70	**-2.44**	1.03	-1.88	-1.46	-1.41	-0.26	1.55	**2.07**
Grid-A22	1.33	0.82	-0.32	0.52	1.36	0.60	-0.91	0.60	-1.89	-0.63	-1.61	-0.35	**2.43**	1.05

Figures in bold specify significant values at 95% confidence (5% significance) level.

Table 4.12 ROC of precipitation extreme indices over the Kharun watershed after shift (1958-2015).

Indices→	RX1day	RX5day	PRCPTOT	R95PTOT	R99PTOT	SDII	CWD	CDD	RW	RL	RM	RRH	RH	RVH
Grid-A1	-0.89	-1.06	-10.56	-6.62	1.34	-11.99	0.00	-1.41	0.00	**18.96**	-6.25	-23.45	0.00	0.00
Grid-A2	-1.28	-2.87	-12.57	-10.14	-7.73	-12.15	0.00	-12.35	-8.02	**19.07**	-20.16	0.00	0.00	0.00
Grid-A3	5.65	9.72	-4.18	-19.46	-8.85	**-23.00**	0.00	-21.33	18.99	29.95	**31.81**	**-60.02**	0.00	0.00
Grid-A4	1.57	17.87	-5.10	-1.54	4.89	-0.93	0.00	1.40	-4.58	0.00	-4.48	0.00	0.00	0.00
Grid-A5	-3.67	13.15	13.02	2.22	-7.42	-7.16	21.32	0.00	17.29	24.81	13.32	0.00	0.00	0.00
Grid-A6	**39.43**	**28.46**	14.34	25.28	**35.56**	**32.11**	0.00	17.45	-16.01	**-31.41**	-22.40	0.00	**88.95**	0.00
Grid-A7	18.90	14.98	2.41	14.13	16.60	13.27	0.00	6.09	-13.62	-13.48	-17.05	0.00	0.00	0.00
Grid-A8	22.77	11.21	7.71	12.75	14.56	9.07	0.00	0.00	-6.68	0.00	-13.96	0.00	0.00	0.00
Grid-A9	**32.70**	**33.19**	1.15	5.54	16.07	5.94	0.00	1.81	-8.76	-10.69	0.00	0.00	0.00	0.00
Grid-A10	7.98	-0.12	**-30.71**	-23.75	-14.69	**-21.72**	0.00	-8.60	-11.05	0.00	0.00	**-53.01**	**0.00**	0.00
Grid-A11	17.02	18.22	-9.93	0.65	9.56	-1.22	0.00	-15.77	-7.90	4.37	**-16.28**	0.00	0.00	0.00
Grid-A12	3.14	10.09	-11.65	-3.66	1.91	-10.63	0.00	-12.45	0.00	**21.58**	-12.76	0.00	0.00	0.00
Grid-A13	**36.64**	22.71	-11.71	10.11	**31.71**	**16.92**	-26.35	**36.60**	**-27.70**	**-29.97**	**-37.80**	0.00	0.00	0.00
Grid-A14	**41.45**	**32.48**	-17.08	6.21	**29.05**	14.17	0.00	**30.29**	**-26.60**	**-25.34**	**-33.40**	-18.78	0.00	0.00
Grid-A15	10.26	-6.00	**-32.92**	-20.64	-2.92	14.17	-25.62	0.00	**-21.91**	-5.22	**-27.07**	-28.44	0.00	0.00
Grid-A16	**39.65**	30.22	-6.65	4.88	19.73	9.82	**-21.99**	2.27	**-17.17**	-20.44	-17.11	0.00	0.00	0.00
Grid-A17	-4.08	-10.75	**-28.37**	-19.57	-16.55	-14.30	0.00	0.00	**-17.23**	0.00	-17.85	-34.44	0.00	0.00
Grid-A18	-24.97	-25.09	**-33.88**	**-31.82**	-24.13	**-20.38**	0.00	2.03	-10.73	14.23	0.00	**-55.29**	0.00	0.00
Grid-A19	12.85	-7.67	-19.73	-2.25	9.15	-1.79	-19.62	3.27	-18.51	0.00	**-32.01**	0.00	0.00	0.00
Grid-A20	3.49	-20.52	-18.83	-0.99	2.27	3.77	**-40.19**	13.82	**-22.27**	-18.92	**-18.94**	0.00	0.00	0.00
Grid-A21	22.01	28.99	-7.38	12.26	25.99	10.99	**-40.19**	13.82	-18.57	-14.05	-22.15	0.00	0.00	**0.00**
Grid-A22	29.31	17.03	-5.58	8.54	22.37	5.71	-14.00	9.82	-13.58	-7.46	-20.32	0.00	**0.00**	0.00

Where, ROC is the rate of change.

Figures in bold specify values with significant trend statistics at a 5% significance level.

Significant negative trends were observed in minimum temperature (TN) over the study area, accompanied by an increasing trend maximum temperature (TX), as shown in Table 4.13. It can also be inferred that the average yearly maximum temperature increased by 0.15ºC over 64 years (1951-2014). An increase in average maximum temperature was observed during summer (0.19ºC), post-monsoon (0.21ºC), and winter (0.61ºC) seasons. Significant reduction in average yearly minimum temperature (-0.68ºC) was observed over the study area, a similar reduction in average minimum temperature during summer (-0.39ºC), monsoon (-0.60ºC) and post-monsoon (-0.32ºC) season. The most significant reduction in average minimum temperature was seen during the winter season (-1.10ºC). Similar trends were also observed in case of averaged mean temperature with the reduction in averaged mean temperature for all the seasons. It further supports the argument of global warming (Linden 2007; Sun et al. 2016) with a more precise explanation that the days are getting hotter and the nights are getting colder. Various studies around the world have also supported such arguments (Alexander et al. 2006; Marengo et al. 2010; Sun et al. 2016).

The effects of these anomalies in long term temperature trends can be subsequently seen over precipitation. The annual precipitation seems to be decreasing over the study area by almost 210 mm over 115 years. Since the monsoon season receives a significant share of rainfall (almost 90-95%) annually, the significant effect of this change can be seen in monsoon season as one of the grids showed a reduction of almost 222 mm of rainfall during the monsoon season during the entire study period. Similar trends were also seen for summer (16.85 mm), post-monsoon (3.26 mm), and winter (2.69 mm).

Table 4.13 Results of Z, p-value, β, and ROC of TX, TN, TXN, and PCP over the study area.

Parameters	Seasons	Z	p-value	Sen's slope (β)	ROC (%)	Magnitude
TX	Yearly	0.46	0.64	0.00	0.46	0.15
	Summer	0.62	0.54	0.00	0.49	0.19
	Monsoon	-0.69	0.49	0.00	-0.53	-0.17
	Post-monsoon	0.37	0.71	0.00	0.70	0.21
	Winter	1.11	0.27	0.01	2.18	0.61
TN	Yearly	**-4.61**	0.01	-0.01	-3.41	-1.10
	Summer	-1.59	0.11	-0.01	-1.74	-0.56
	Monsoon	**-4.38**	0.00	-0.01	-2.51	-0.81
	Post-monsoon	-1.06	0.29	-0.01	-1.80	-0.58
	Winter	**-3.69**	0.01	-0.02	-8.66	-2.80
TXN	Yearly	**-2.15**	0.03	-0.01	-1.23	-0.40
	Summer	-1.12	0.26	0.00	-0.96	-0.31
	Monsoon	**-2.10**	0.04	-0.01	-1.43	-0.46
	Post-monsoon	0.15	0.88	0.00	0.42	0.14
	Winter	-0.80	0.42	0.00	-1.41	-0.45
PCP	Yearly	**-2.79**	0.01	-3.06	-16.76	-5.42
	Summer	**-2.21**	0.03	-0.32	-56.15	-18.15
	Monsoon	**-2.68**	0.01	-3.36	-21.57	-6.97
	Post-monsoon	-1.85	0.06	-0.05	-5.93	-1.92
	Winter	-1.52	0.13	-0.03	-9.97	-3.22

Where *Z* is the MMK trend statistics, β is the Sen's slope,
Figures in bold specify significant values at 95% confidence (5% significance) level.

Significant negative trends were observed in the case of index TN10P, TR, PRCPTOT, RW, RL, RM, RRH, and RH for the entire study period (Table 4.14). From these results, it can be inferred that there is a reduction in the percentage of cool nights (-27.3%), which explains that even though the minimum temperature in the region has decreased, the number of days with lesser temperatures has reduced. The number of tropical nights (TR) in a year has also reduced significantly (-33.9%). It seems to reduce with an average rate of 4.20 days/decade. Also, the gap between the minimum and maximum temperature seems to be increasing over the study period at an average rate of 0.09ºC/decade (4.6%), which explains the increasing trend in the Diurnal Temperature Range (DTR). It further supports the argument of global warming (IPCC 2007b; Sun et al. 2016) with a more precise explanation that the days are getting hotter, and the nights are getting colder, but overall, there is an increase in the mean temperature. The annual precipitation seems to be decreasing over the study area along with the reduction in annual total wet day precipitation, almost 242 mm (-20.2%) over 115 years. The number of wet days and extremely wet days have also reduced by

-17.1 (1 day/decade) and -4.5% (1.18 days/decade), respectively. It was also observed that there was reduction observed in the number of light rainy days (-10.2%), moderate rainy days (-17.8%), rather heavy and heavy rainy days (-25.5 and -18.4%). The number of cumulative dry days in the study area has increased by 19.5%, which in itself explains the reduction in rainy days. As the trend statistics of temperature and precipitation extremes tend to get severe after shift (as discussed in the results above), the phenomenon due to the variation in these extreme indices will have a more adverse effect on the study area.

Table 4.14 Results of Z, p-value, β, and ROC of all the indices over the study area.

Indices	Z	p-value	β	ROC (%)	Overall change	Decadal change
TX10P (%)	-0.42	0.67	-0.03	-5.9	-2.21	-0.35
TX90P (%)	-1.15	0.25	-0.14	-24.0	-9.02	-1.41
TN10P (%)	**-2.43**	0.02	-0.15	-27.3	-9.89	-1.55
TN90P (%)	1.58	0.12	0.13	22.9	8.48	1.32
TR (days)	**-3.32**	0.00	-0.42	-33.9	-26.91	-4.20
SU (days)	0.26	0.79	0.01	0.8	0.69	0.11
WSDI(days)	1.27	0.20	0.06	26.5	3.86	0.60
CSDI (days)	0.62	0.53	0.00	0.0	0.00	0.00
DTR (ºC)	1.82	0.07	0.01	4.6	0.57	0.09
RX1day (mm)	-0.70	0.48	-0.06	-6.2	-6.61	-0.57
RX5day (mm)	-0.16	0.87	-0.02	-1.0	-1.75	-0.15
PRCPTOT (mm)	**-3.01**	0.00	-2.11	-20.2	-242.22	-21.06
R95PTOT (mm)	-1.76	0.08	-0.76	-11.3	-87.48	-7.61
R99PTOT (mm)	-0.78	0.43	-0.12	-4.5	-13.59	-1.18
SDII (days)	-0.96	0.34	-0.01	-4.3	-0.75	-0.07
CWD (days)	-1.42	0.15	-0.01	-11.9	-1.10	-0.10
CDD (days)	**3.36**	0.00	0.16	19.5	17.97	1.56
RW (days)	**-3.5**	0.00	-0.10	-17.1	-11.76	-1.02
RL (days)	**-5.47**	0.00	-0.02	-10.2	-2.61	-0.23
RM (days)	**-3.12**	0.00	-0.05	-17.8	-5.96	-0.52
RRH (days)	**-2.65**	0.01	-0.01	-25.5	-1.53	-0.13
RH (days)	-1.72	0.09	0.00	-18.4	-0.39	-0.03
RVH (days)	-0.48	0.63	0.00	0.0	0.00	0.00

Where *Z* is the MMK trend statistics, β is the Sen's slope,
Figures in bold specify significant values at 95% confidence (5% significance) level

4.4 CONCLUDING REMARKS

The ecosystem and landscape change mainly influence long term changes in meteorological distribution. However, changes in precipitation rate and temperature are the main causes of climate change, which drastically varies the flow in the river. For the planning and management of water resources, it is quite essential to understand the distribution and variability of meteorological parameters.

Trend analysis is one of the most significant tools to analyze the global warming problem that quantifies the past and future changes in meteorological, hydro-climatological parameters. In this chapter, trend detection has been carried out for long term temperature (maximum, minimum, and mean) and precipitation data by applying regression analysis, MMK test, and the magnitude of change has been found out using Sen's slope estimator over 22 grids in and around the study area. Apart from finding the nature and extent of trend (using MMK and Sen's method respectively), the magnitude of changes was also computed to quantify the change in terms of the respective units of the parameters. Similar statistics were also performed over 23 indices of meteorological extremes computed from long term precipitation and temperature time series, 18 extreme precipitation and temperature indices out of 27 developed by ETCCDMI (as discussed in section 4.1) were considered for the study. Additionally, five more indices were proposed in the study, which is based on the precipitation intensity indices suggested by IMD. Also, Cumulative sum (Cusum) and sequential Mann-Kendall (SQMK) test were applied to identify the climatic shift (change year) over the meteorological time series

The significant findings of the study state that there is an increase in average maximum temperature during summer (0.19ºC), post-monsoon (0.21ºC), and winter (0.61ºC) seasons. Significant reduction in average yearly minimum temperature (-0.68ºC) was observed over the study area, similar reduction in average minimum temperature during summer (-0.39ºC), monsoon (-0.60ºC) and post-monsoon (-0.32ºC) season. The most significant reduction in average minimum temperature was seen during the winter season (-1.10ºC). The annual precipitation seems to be decreasing over the study area by almost 210 mm over 115 years. Similar trends were also seen for summer (16.85 mm), post-monsoon (3.26 mm), and winter (2.69 mm).

After the computation of long term variation in meteorological extremes, it can be inferred that the gap between the minimum and maximum temperature seems to be increasing over the study period

at an average rate of 0.09ºC/decade (4.6%), which explains the increasing trend in Diurnal Temperature Range (DTR). This precisely explains the fact that the days are getting hotter, and the nights are getting colder and its effects can be seen over the rainfall intensities in the region. As per the results obtained, there was reduction observed in the number of light rainy days (-10.2%), moderate rainy days (-17.8%), rather heavy and heavy rainy days (-25.5 and -18.4%). The number of cumulative dry days in the study area has increased by 19.5%, which in itself explains the reduction in rainy days. As the trend statistics of temperature and precipitation extremes tend to get severe after shift (as discussed in the results above), the phenomenon due to the variation in these extreme indices will have a more adverse effect on the study area.

The findings in this study provide a new understanding of extreme events trend evaluation that could probably the cause of flood and drought in the area. This will help in short or long term planning and development in water resources of the region. This information can also assist in managing the agriculture water supply and in updating the engineer and stakeholders for decision making.

CHAPTER 5

CLIMATE MODELS AND FUTURE TREND ANALYSIS

5.1 GENERAL

Global Climate Models (GCMs) are based on numerical and physical principles aimed at reproducing the present and future meteorological parameters. It provides considerable confidence in producing future climate conditions by using the numerically coupled Atmospheric Ocean General Circulation Model (AOGCM) (Moss et al. 2010; Su et al. 2013). Several inter-comparison studies have been done between model outputs and observed data all over the world (Perkins et al. 2007; Errasti et al. 2011; Kodra et al. 2012; Fu et al. 2013a; Anandhi and Nanjundiah 2014). However, the GCMs output is very uncertain due to the initial condition, boundary condition, model structure, and emission (Ojha et al. 2012). The performance of 10 GCM models for simulating the summer monsoon rainfall variation over the Asian-western pacific region was assessed by Kang et al. (2002). Johnson and Sharma (2009) used a variable convergence score (VCS) methodology based on the coefficient of variation to evaluate the eight different variables from nine GCM outputs for two emission scenarios for Australia. Radić and Clarke (2011), evaluated 22 GCMs for North America using several statistical parameters. An evaluation has been carried out by comparing the model output with reanalysis data for the period 1980-99.

Frei et al. (2003) investigated daily precipitation simulation for European Alps by using five regional climate models. There is a number of recent studies based on indices and probability density function (PDF) to identify the best model (Frei et al. 2003; Perkins et al. 2007; Radić and Clarke 2011; Ojha et al. 2013; Anandhi and Nanjundiah 2014; Parth Sarthi et al. 2015). Perkins et al. (2007) conducted a model evaluation for 12 regions in Australia using probability density function (PDFs). Evaluation of the model in the study area has been performed considering daily simulation data of maximum temperature, minimum temperature and precipitation. There are many approaches to compare the simulated or model output with observed values (when data are available) or reanalysis values (for poorly gauged regions with missing or no observed data). For impact studies of climate change, it is necessary to evaluate the model with observed datasets, and the model output should be close to the observed data.

The resolution of the GCM's is very coarse, even though there are methods to bring down the resolution of the GCM's (like statistical and dynamic downscaling), in some cases synthetic time series of weather data have been produced using stochastic weather generator (Wang and Ding 2003; Dibike and Coulibaly 2005; Vallam and Qin 2017). However, even then, those methods are quite cumbersome and involve a high level of skill set and heavy types of machinery to process huge amounts of data. Hence, to address this anomaly Regional Climate Model (RCM) can be used, which is produced by dynamic downscaling of GCM data to simulate regional climate (Graham et al. 2007a; Kumar et al. 2013; Varikoden et al. 2018). These are various projects in existence which have been established to provide high-resolution regional climate change scenarios, which are specific to particular area, RCM's are developed and produced by research institutes that are well capable of handling such big data and have sufficient computational capacity and technical expertise (Sanjay et al. 2017; Singh et al. 2017; Sanjay 2018; Varikoden et al. 2018).

Before the application of RCM data, it needs to be corrected of all the errors, which is referred to as BIAS correction (Lafon et al. 2013; Duhan and Pandey 2015). There are eight different methods for BIAS correction of RCM data, such as linear scaling, quantile mapping, power transformation, distribution mapping etc. as suggested by Teutschbein and Seibert (2012). In this study, the RCM data have been corrected for all the systematic biases using the distribution mapping technique, based on the application of the technique adopted by many researchers in the past (Lafon et al. 2013; Bhavani et al. 2017). Apart from the process of selection of RCM data for the study, the trend analysis of future predicted data has been carried out in this chapter. The magnitude of the trend was found out using Modified Mann Kendall (MMK) and the magnitude of the change was quantified using Sen's slope estimator. These test statistics were performed over the meteorological extreme indices, which have already been thoroughly discussed in the previous chapter.

5.2 MATERIALS AND METHODS

5.2.1 Description of the Study Area and Data Used

Detail description of the study area and the data used for the study have been already discussed in Chapter 3.

5.2.2 Methodology

Three different datasets, namely precipitation, minimum, and maximum temperature, were used to identify long term changes in the meteorological extremes for all the grids (22 in number) for the future (2011-2100). To identify the trend statistics for extremes values indices in question, first of all, linear regression was administered over various indices computed from precipitation (PCP), maximum temperature (TX), and minimum temperature (TN) time series (Sharma et al. 2016). To have a precise idea about the trend displayed by various indices, the Modified Mann Kendall test (MMK) was applied. Statistic Z (obtained by MMK) was tested for significance of trend at a threshold level of 1.96 for a positive trend and -1.96 for negative trends (5% significance level). The magnitude of trend statistics was quantified using Sen's slope estimator, which is a tool to determine the variability of time series data. For the study, 23 indices have opted, the details of which have been discussed in section 4.2.2 along with the statistics for trend analysis. Apart from determining the trend and its magnitude for the entire period of the future (2011-2100), three different climate cycles were identified in the future climate period and trends of all the parameters were computed for these three distinct periods also, the series was divided equally as CC1 (2011-2040), CC2 (2041-2070) and CC3 (2071-2100).

As the resolution of the GCM data is very coarse, RCM data was obtained from the Coordinated Regional Climate Downscaling Experiment (CORDEX) archive on a daily scale for the years 2005 to 2100. The CORDEX-RCM data has a very fine spatial resolution of the order of 0.2^{o} - 0.5^{o}, varying from model to model. Four RCM's were selected based on an extensive literature review to obtain meteorological parameters (precipitation, minimum and maximum temperature) for the future (2005-2100) time scale and also for representative concentration pathways (RCPs) 4.5 and 8.5 scenarios. RCP 2.6 was not considered, as the study was primarily focused towards the changes in extreme climatic conditions of the future, and the effect of RCP 2.6 is quite insignificant towards the study, as many reports have suggested in the past. The description of the selected RCM's is represented in Table 5.1.

Table 5.1 Description of the RCMs used in the study.

S. No.	RCM's	Resolution / Data period	Preferred Model name
1	NCC-NorESM1-M	0.44º × 0.44º (2006-2100)	NorESM
2	CCCma-CanESM2	0.44º × 0.44º (2006-2100)	CanESM2 or CSIRO
3	QCCCE-CSIRO Mk3.6	0.44º × 0.44º (2006-2100)	CSIRO MK3.6 or CSIRO
4	MIROC-MIROC5	0.44º × 0.44º (2006-2100)	MIROC5

Before the application of data for trend analysis of meteorological extremes, the RCM data was corrected for systematic errors (biases). These biases may be present in the raw RCM data due to the limited spatial resolution, various simplified physical and thermodynamically processes, different numerical schemes and also due to insufficient knowledge about climate system processes (Hay et al. 2002; Teutschbein and Seibert 2012; Lafon et al. 2013). Hence, it is essential to perform the bias-correction of raw climate data for future periods. There are various measures for BIAS correction of RCM data such as linear scaling, quantile mapping, power transformation, distribution mapping etc. (Teutschbein and Seibert 2012). In this study, distribution mapping has been used for BIAS correction of RCM outputs.

5.2.2.1 Identification of trend and its magnitude

To identify the trends, the Modified Mann Kendall test (MMK) was applied. Statistic Z (obtained by MMK) was tested for significance of trend at a threshold level of 1.96 for a positive trend and -1.96 for negative trends (5% significance level), the details of which have already been discussed thoroughly in sections 4.2.2.2 and 4.2.2.3, respectively.

5.2.2.2 BIAS correction of RCM outputs

The process of Bias correction applies a transformation algorithm to correct RCM outputs. To evaluate the biases in the control period (or baseline) of the RCM climate variable, a simple approach is adopted; RCM variables are compared with the observed climate variables. This approach is also applied to correct the baseline as well as RCP scenarios. In this study, dynamical downscaled GCMs output (RCM data) of driving representative GCMs were selected with the integration of the hydrological model. The RCM data from Coordinated Regional Downscaling Experiment (CORDEX) was used to assess the climate projections over the river watershed under IPCC AR5, representative concentration pathways (RCPs) 4.5 and 8.5 scenarios. The CORDEX-RCM outputs represent a daily average at the spatial resolution of 0.44º x 0.44º (50 km x 50 km approximately) for regional climate impact studies. However, these outputs are not being used directly for

hydrological models to assess the local scale studies because of systematic biases. These biases are the results of imperfect conceptualization, discretization while downscaling and spatial averaging within grid cells (Graham et al. 2007b). Therefore, distribution mapping (a BIA correction approach) was applied to precipitation and temperature series to remove the inherent systematic biases. The baseline for the observed series was considered as 1971-2000 and IMD gridded data at 0.25º x 0.25º scale.

5.2.2.1.1 Distribution mapping

BIAS correct method of distribution mapping was used to correct the raw RCM output variables for the study. The idea behind distribution mapping is to alter the distribution function of the raw climate variables (RCM data) so that it would fit with the observed distribution function of the observed data by developing a transform function (Teutschbein and Seibert 2012). Gamma distribution (Eq. 5.1), as well as Gaussian distribution (Eq. 5.2), are found to be best suited to correct the RCM outputs.

$$f\left(x \mid \alpha, \beta\right) = x^{\alpha-1} \frac{1}{\beta^{\alpha}.\Gamma\left(\alpha\right)}.e^{-\frac{x}{\beta}}; \qquad x \geq 0; \alpha, \beta > 0 \tag{5.1}$$

where the terms α and β are the shape and scale parameters respectively (Lafon et al. 2013; Teutschbein and Seibert 2012).

$$f\left(x \mid \mu, \sigma^2\right) = x^{\alpha-1} \frac{1}{\sigma\sqrt{2\pi}}.e^{\frac{-(x-\mu)^2}{2\sigma^2}}; \qquad x \in R \tag{5.2}$$

where the terms μ and σ are the location and scale parameters respectively (Teutschbein and Seibert 2012; Christensen et al. 2013).

Initially, the development of cumulative distribution functions (CDFs) was done for observed series as well as for the baseline RCM outputs. CDFs were developed for all days of their respective months. After the development of CDFs, the baseline simulated CDF was shifted to observed CDF (Teutschbein and Seibert 2012). Hence, similar CDFs were used to correct baseline as well as future projected series. Gaussian CDFs transfer for precipitation is given by Eq. 5.3 and Eq. 5.4.

$$P_{bl}^{'}\left(d\right) = F_G^{-1}\left[F_G\left(P_{bl}\right)\left(d\right) \mid \alpha_{bl,m}, \beta_{bl,m} \mid \alpha_{obs,m}, \beta_{obs,m}\right] \tag{5.3}$$

$$P_{bl}^{'}\left(d\right) = F_G^{-1}\left[F_G\left(P_{rcp}\right)\left(d\right) \mid \alpha_{rcp,m}, \beta_{rcp,m} \mid \alpha_{obs,m}, \beta_{obs,m}\right] \tag{5.4}$$

Whereas, Gaussian CDFs transfer for temperature is given by Eq. 5.5 and Eq. 5.6

$$T_{bl}^{'}(d) = F_G^{-1}\left[F_G(T_{bl})(d) \mid \mu_{bl,m}, \sigma_{bl,m}^2 \mid \mu_{obs,m}, \sigma_{obs,m}^2 \right] \quad (5.5)$$

$$T_{rcp}^{'}(d) = F_G^{-1}\left[F_G\left(T_{rcp}\right)(d) \mid \mu_{rcp,m}, \sigma_{rcp,m}^2 \mid \mu_{rcp,m}, \sigma_{rcp,m}^2 \right] \quad (5.6)$$

where the terms F and F^{-1} are the CDF and its inverse of CDF, respectively. Gamma CDF (F_G) was used in the case of precipitation time series, whereas for temperature time series Gaussian CDF (F_N) was used (Teutschbein and Seibert 2012; Lafon et al. 2013).

During the BIAS correction of the precipitation and temperature time series, cumulative distribution function (CDFs) were developed for both observed series (1981-2010) as well as baseline RCM output series (1981-2010) for all days of corresponding month and baseline simulated CDF shifted to the observed CDF. Therefore, the same CDFs was used for the correction of baseline and future projection, namely CC1 (2011-2040), CC2 (2041-70) and CC3 (2071-2100). It is an assumption that bias correction approaches are stationary, which indicates correction algorithm and parameterization are applicable for future scenarios as well.

5.3 RESULTS AND DISCUSSIONS

In this study, trend statistics of extreme value indices for the future (2011-2100) were evaluated over 22 grids in and around the study area considering two distinct scenarios (RCP 4.5 and RCP 8.5). First of all, the Regional Climate Model (RCM) data were acquired. Four representative models were selected for this study to have a better understanding of the future patterns of extreme value indices. The idea behind choosing more than one model for the study was to have a better understanding of future trend patterns. After the selection of the RCM's, the models were corrected for all the systematic biases using the distribution mapping technique. After the process of selection of RCM data and removal of all the systematic biases from the data, Modified Mann Kendall (MMK) was applied over the data to check the presence of any trend at 5% significance level, while the magnitude of trend change was quantified using Sen's slope estimator.

The whole time series (2011-2100) of precipitation, temperature (minimum and maximum) was further split into three distinct climate periods of 30 years each viz. CC1 (2011-2040), CC2 (2041-2070) and CC3 (2071-2100). Over each climate period, MMK and Sen's slope estimator

statistics were applied to check the presence of trends and to quantify the change for all the extreme value indices. The results of which have been presented in the subsequent sections.

5.3.1 Selection of Representative Grids

The study was conducted over two scenarios (RCP 4.5 and RCP 8.5) for 92 years (2011-2100) over 22 grids in and around the study area. Since, it was quite cumbersome to show the results of each grid, the results of only two representative grids among the 22 grids were shown for the entire study period, and the result of a single grid was shown for various climate periods. The question might arise as to why only two grids of the possible 22 were chosen for the representation purpose. As the study area exhibits a relatively flat topography with the absence of any hills or deeps valleys, such practice can be adopted for the study area. The idea behind choosing only a few grids for representing the whole area is also justified by Figure 5.1 that shows minimal variation among the MMK 'Z' statistics across the grids for all the indices.

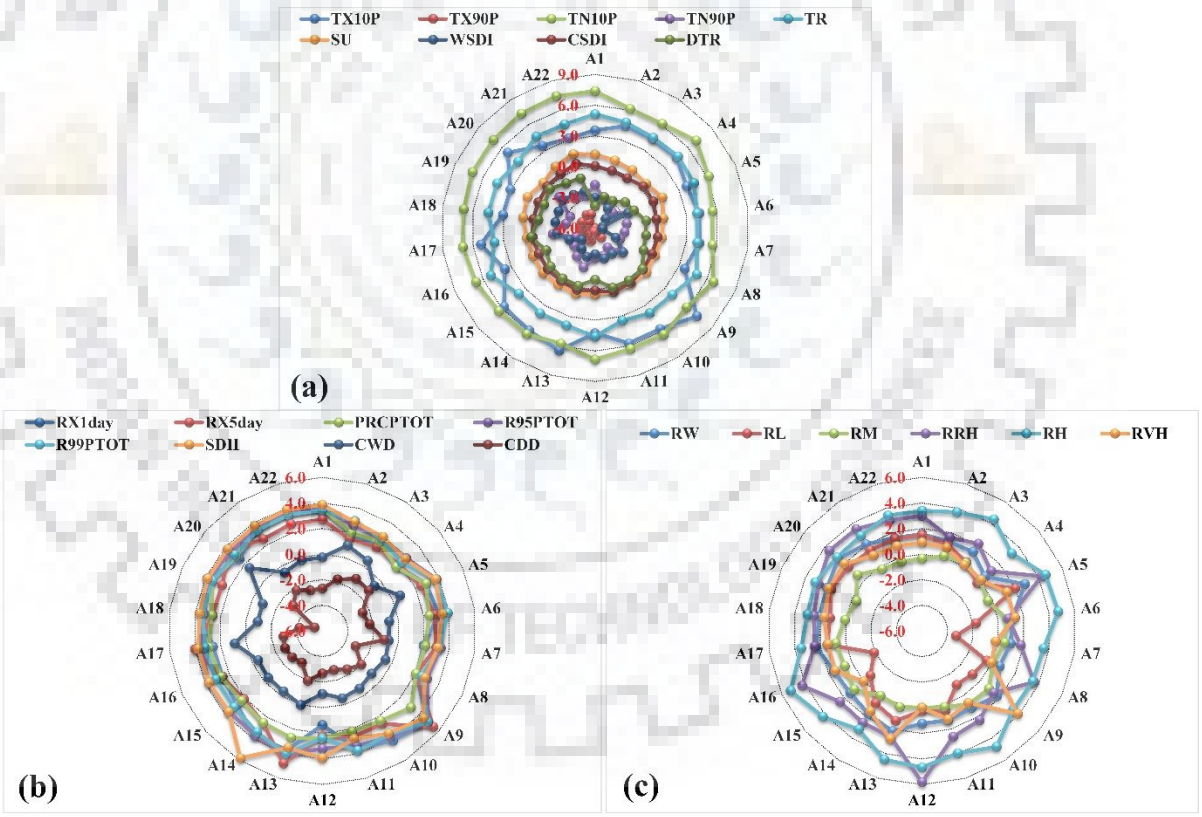

Figure 5.1 Variation of MMK 'Z' values of the grids.

5.3.2 Trend Statistics of Extreme Value Indices

Modified Mann-Kendall (MMK) test was applied over different meteorological extreme indices using two-tailed hypotheses at a 5% significance level over the entire study period (2011-2100) and for different climate periods CC1, CC2 and CC3. The results of all the indices for scenarios RCP 4.5 and RCP 8.5 have been discussed in subsequent sections, along with the results of the spatial distribution of temporal changes (in percentage) of indices based on temperature and precipitation time series. Linear trends for all the climate periods have also been represented to understand the behavioral pattern of trends in different climate periods.

5.3.2.1 Climate projections under RCP 4.5

MMK results of all the indices for scenarios RCP 4.5 are represented in Tables 5.2 and 5.3 for all study periods. Linear trends of extreme value indices considering long term temperature and precipitation series for the three climate periods (CC1, CC2, and CC3) have been represented in Figures 5.2, 5.3(a), and 5.3(b). Also, the results of the spatial distribution of temporal changes (in percentage) of indices based on temperature and precipitation time series are represented in Figures 5.4 and 5.5 respectively.

Upon the analysis of the results, it was observed that almost all the grids exhibited more or less similar results in the case of MMK trend statistics. Hence only the results of any two representative stations have been displayed. A significant increasing trend was observed in the case of index TX10P, TN10P, TR, SU and DTR, while significant decreasing trends were observed in the case of TX90P, TN90P, and WSDI for all the RCMs with few exceptions. Non-significant trends were found to exist in the case of TN10P (MIROC5), SU (CCCma and MIROC5), and WSDI (CSIRO, MIROC5 and NorESM) while index CSDI did not show any significant trend for any RCMs. Conflicting results were observed in the case of index SU, where CSIRO showed a significant increasing trend while NorESM showed a significant decreasing trend. Significant increasing trends were observed for indices RX1day, Rx5day, PRCPTOT, R95TOT, R99PTOT, SDII, RW, RL, RM, RRH, RH and RVH in case of all the RCMs except in the case of index RL, where NorESM did not show any significant trend and for RM where CSIRO and MIROC5 did not show any significant trend. Whereas, no significant trend was observed in the case of index CWD as represented in Tables 5.2 and 5.3.

As for the climate periods, significant increasing trends were observed during all three climate periods for all the RCMs in the case of TX10P and TR. Significant increasing trends were observed in the case of TN10P for the period CC1 (CCCma and CSIRO), CC2 (CSIRO and NorESM) and CC3 (CCCma, CSIRO and NorESM). Similar trends were observed for index SU, where significant increasing trends were observed for the period CC1 (CCCma and CSIRO), and period CC3 (CCCma), conflicting results were obtained for index SU (NorESM) that displayed significant decreasing trend for period CC3. Significant decreasing trends were observed for index TX90P and TN90P; a point of observation was that almost all the RCMs predicted the significant decreasing trend for both the indices for only period CC3, while only a few RCMs predicted decreasing trends for periods CC1 and CC2. Only CSIRO predicted the significant decreasing trend for period CC3 for index WSDI, while no trend was observed for any other period. Similarly, no significant trend was observed for index CSDI. Indifferent results were observed for index DTR, where significant increasing trends were observed for climate period CC1 (CCCma), while significant decreasing trends were observed for period CC3 (MIROC5 and NorESM) as represented in Table 5.2.

From Table 5.3, it can be observed that no significant trends were observed for all the indices in climate periods CC1 and CC2 with few exceptions. Such as a significant increasing trend was observed in case of R95PTOT for period CC2 (MIROC5), RW for period CC1 (NorESM0 and CC2 (MIROC5), RL for period CC1 (CSIRO and NorESM), RRH for period CC2 (CSIRO) and RH for period CC1 (CSIRO). The conflicting result was obtained for index RH for period CC1, where CCCma showed a significant decreasing trend. For period CC3, significant increasing trends were observed for RX1day, RX5day, PRCPTOT, R95PTOT, R99PTOT, SDII, RRH, and RH for all RCMs. For index RVH, models MIROC5 and NorESM showed a significant increasing trend. Significant decreasing trends were observed for index CWD (CCCma), CDD (CSIRO and NorESM), and RM (CCCma).

Linear trends of all the extreme value indices considering long term temperature and precipitation series have been presented in Figures 5.2, 5.3(a) and 5.3(b) for different climate periods, which further justify the trend results obtained in the study. The spatial distribution of temporal changes (in percentage) in precipitation and temperature-based indices for RCP 4.5 are shown in Figures 5.4 and 5.5, respectively.

Table 5.2 MMK statistics (Z) of indices based on temperature for RCP 4.5.

Entire period (2011-2100)										
RCM's	Grids	TX10P	TX90P	TN10P	TN90P	TR	SU	WSDI	CSDI	DTR
CCCma	Grid-A6	**7.08**	**-6.45**	**4.78**	-1.78	**5.12**	1.20	**-3.05**	0.05	**3.85**
	Grid-A16	**9.02**	**-7.00**	**4.11**	**-3.74**	**4.70**	0.60	**-4.65**	0.23	**2.13**
CSIRO	Grid-A9	**6.43**	**-3.65**	**7.10**	**-4.18**	**5.08**	**4.60**	-0.50	0.10	**2.41**
	Grid-A13	**5.55**	**-4.22**	**6.59**	**-3.39**	**6.00**	**4.52**	0.89	-0.06	**2.21**
MIROC5	Grid-A12	**6.78**	**-2.45**	-0.48	**-2.69**	**7.24**	0.05	0.80	-0.14	**7.13**
	Grid-A13	**6.67**	**-3.89**	-0.69	**-2.88**	**8.86**	0.07	1.39	0.17	**2.30**
NorESM	Grid-A14	**5.33**	**-4.81**	**4.59**	**-2.12**	**4.68**	**-3.11**	1.32	0.45	**4.80**
	Grid-A16	**6.35**	**-4.85**	**5.34**	-1.60	**3.86**	**-3.51**	0.25	0.38	**4.50**
Climate periods (CC1, CC2, CC3)										
Periods	RCM's	TX10P	TX90P	TN10P	TN90P	TR	SU	WSDI	CSDI	DTR
CC1	CCCma	**2.98**	-0.06	**2.77**	**-2.34**	**5.58**	**1.99**	0.99	0.52	**2.49**
	CSIRO	**3.25**	-0.73	**3.75**	-0.54	1.38	**2.80**	-1.18	0.02	-0.20
	MIROC5	**2.10**	-1.68	0.73	**-2.02**	**3.57**	0.14	0.24	-0.23	-1.27
	NorESM	**2.50**	**-2.26**	1.01	-0.84	**3.95**	-0.44	-0.74	-0.25	-0.86
CC2	CCCma	**2.10**	**-3.27**	0.89	**-2.05**	**2.12**	1.90	0.51	1.11	0.89
	CSIRO	**2.45**	**-1.97**	**2.24**	-0.34	**2.11**	0.90	-0.31	-0.42	-0.50
	MIROC5	**2.44**	-1.05	-1.16	-0.55	**3.21**	0.32	0.04	-0.16	-1.76
	NorESM	**2.27**	-1.71	**2.34**	-1.43	**4.48**	-0.26	-0.24	-0.86	-0.68
CC3	CCCma	**5.85**	**-3.70**	**6.47**	**-3.73**	**3.28**	**4.24**	-0.92	0.16	1.83
	CSIRO	**6.78**	**-4.67**	**6.96**	**-3.25**	**4.90**	0.20	**-3.43**	0.05	-1.19
	MIROC5	**6.00**	**-2.70**	-1.32	**-2.52**	**6.51**	-0.76	1.25	0.22	**-7.80**
	NorESM	**4.60**	**-4.95**	**4.15**	-1.71	**3.48**	**-3.70**	1.49	0.42	**-5.32**

Figures in bold specify significant values at 95% confidence (5% significance) level.

Table 5.3 MMK statistics (Z) of indices based on precipitation for RCP 4.5.

Entire period (2011-2100)															
RCMs	Grids	RX1day	RX5day	PRCPTOT	R95PTOT	R99PTOT	SDII	CWD	CDD	RW	RL	RM	RRH	RH	RVH
CCCma	Grid-A6	**2.02**	**3.44**	1.83	**5.83**	**2.23**	**5.75**	-1.65	-1.57	**2.41**	-0.11	**3.04**	1.50	**4.07**	**2.28**
	Grid-A16	0.97	1.92	**5.30**	**4.40**	**2.29**	**3.66**	-0.59	**-2.22**	0.18	**2.32**	-0.82	**3.04**	1.66	**2.12**
CSIRO	Grid-A9	**4.81**	**6.45**	**3.14**	**4.90**	**4.86**	**4.42**	-0.92	**-1.98**	1.74	-0.81	0.90	1.39	**3.41**	**3.88**
	Grid-A13	**3.70**	**4.79**	**2.69**	**4.06**	**4.02**	**3.50**	0.02	-1.96	**2.15**	1.32	0.19	**2.64**	**4.47**	**2.80**
MIROC5	Grid-A12	**3.58**	**2.68**	**4.69**	**6.12**	**5.43**	**6.21**	0.93	-1.96	**2.39**	**4.49**	0.82	**3.18**	**2.83**	**4.84**
	Grid-A13	**3.12**	**2.71**	**4.24**	**3.89**	**3.19**	**4.19**	-0.51	0.00	**3.44**	0.99	1.79	**3.44**	**2.62**	**2.87**
NorESM	Grid-A14	**2.29**	**3.26**	**5.07**	**4.60**	**3.22**	**3.85**	0.95	**-3.29**	**3.04**	-0.48	0.81	**5.54**	**3.22**	**2.45**
	Grid-A16	**3.09**	**2.80**	**4.83**	**6.76**	**3.78**	**3.37**	0.11	**-6.69**	**3.15**	0.00	**2.51**	**3.87**	1.66	**2.86**
Climate periods (CC1 , CC2, CC3)															
Periods	RCMs	RX1day	RX5day	PRCPTOT	R95PTOT	R99PTOT	SDII	CWD	CDD	RW	RL	RM	RRH	RH	RVH
CC1	CCCma	-0.88	-1.32	-1.69	-1.50	-1.03	-0.14	-0.58	0.16	-1.23	0.14	-1.72	0.48	**-3.05**	0.97
	CSIRO	0.86	0.61	0.50	0.86	1.14	0.43	0.23	-0.87	0.39	**2.19**	-0.29	0.41	**2.40**	-1.00
	MIROC5	-0.43	0.29	1.03	1.93	0.04	0.32	-0.35	0.75	1.05	0.65	1.24	0.16	0.57	-0.31
	NorESM	0.14	1.03	0.68	0.50	0.18	0.00	0.63	1.17	**2.02**	**3.11**	0.56	1.21	0.45	1.42
CC2	CCCma	-1.32	-0.95	-1.28	-1.00	-1.45	-0.43	-1.12	-0.96	-1.00	-0.10	-1.52	-0.29	-0.42	-0.85
	CSIRO	0.32	1.43	1.43	1.64	1.21	1.43	1.14	-0.66	0.50	0.22	-0.38	**1.98**	1.20	0.45
	MIROC5	1.50	1.00	1.93	**2.10**	1.27	0.89	1.28	-0.05	**2.80**	0.10	0.93	0.94	0.86	1.34
	NorESM	0.86	1.68	1.21	0.75	0.50	0.71	0.65	0.25	1.88	1.17	1.38	1.31	1.26	0.72
CC3	CCCma	**1.97**	**4.34**	**5.12**	**4.42**	**2.82**	**4.19**	**-2.18**	-0.86	-1.66	-0.58	**-2.51**	1.64	**4.25**	1.53
	CSIRO	**3.17**	**2.45**	**2.02**	**3.18**	**3.43**	**2.82**	-0.57	**-2.81**	1.01	0.11	0.02	**2.56**	**3.79**	0.65
	MIROC5	**2.97**	**2.44**	**4.14**	**3.84**	**2.98**	**4.56**	-0.61	-0.11	**3.29**	0.65	1.47	**3.53**	**2.67**	**2.60**
	NorESM	**1.99**	**3.17**	**4.89**	**4.42**	**2.96**	**3.96**	1.01	**-3.36**	**2.75**	-0.87	0.60	**5.56**	**3.12**	**2.25**

Figures in bold specify significant values at 95% confidence (5% significance) level.

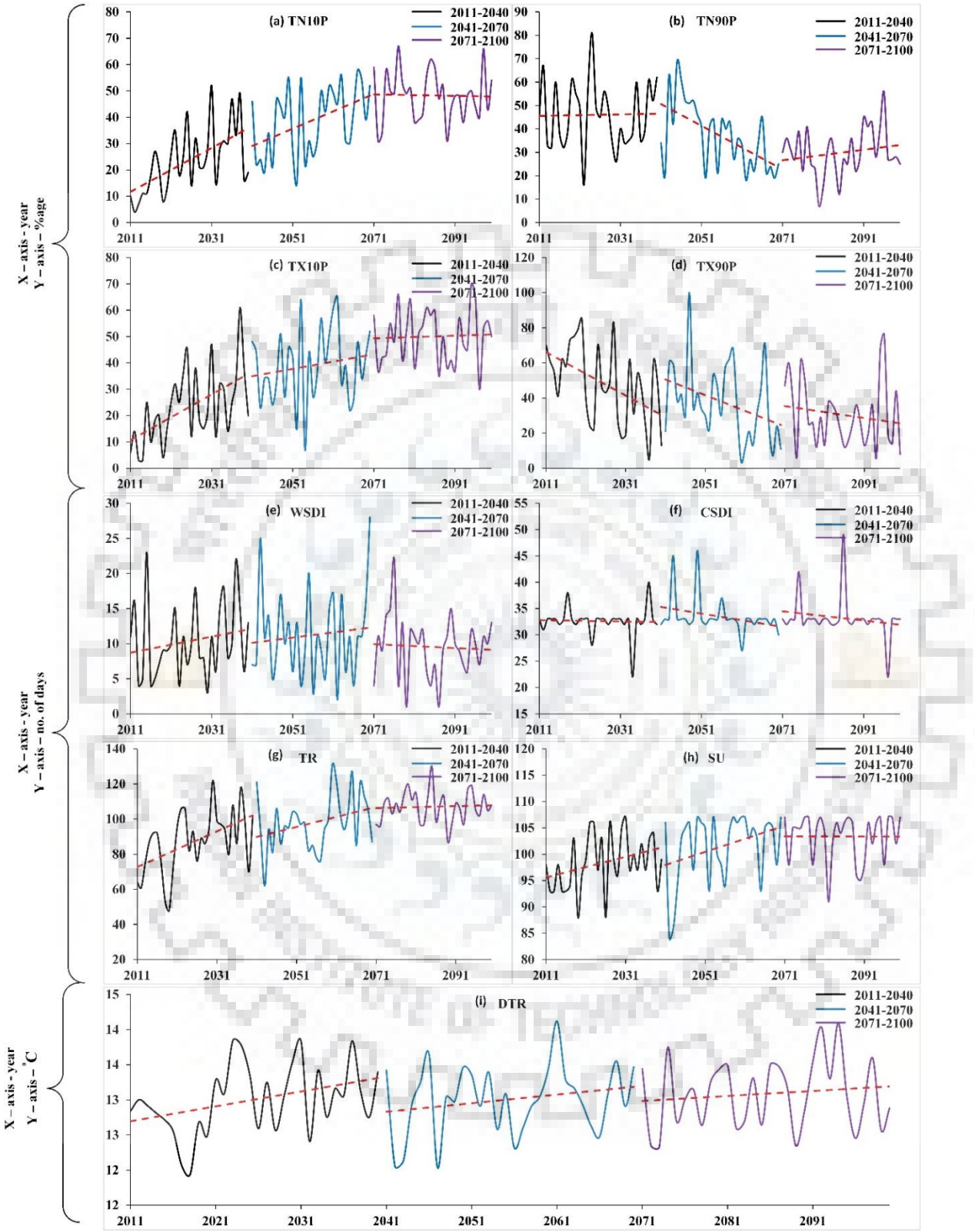

Figure 5.2 Linear trends for extreme value indices of long term temperature series for all climate periods for RCP 4.5.

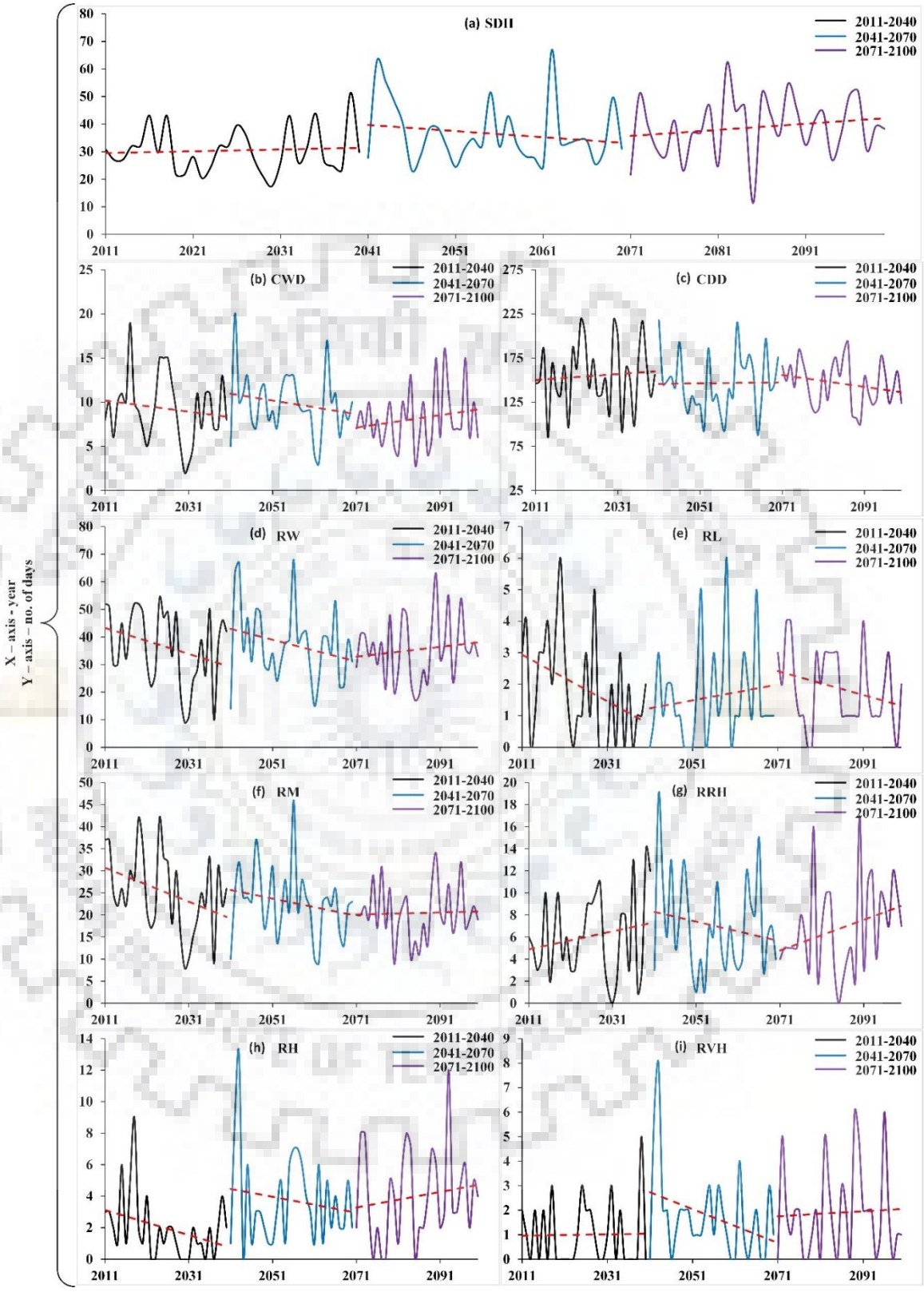

Figure 5.3(a) Linear trends for extreme value indices of long term precipitation series for all climate periods for RCP 4.5.

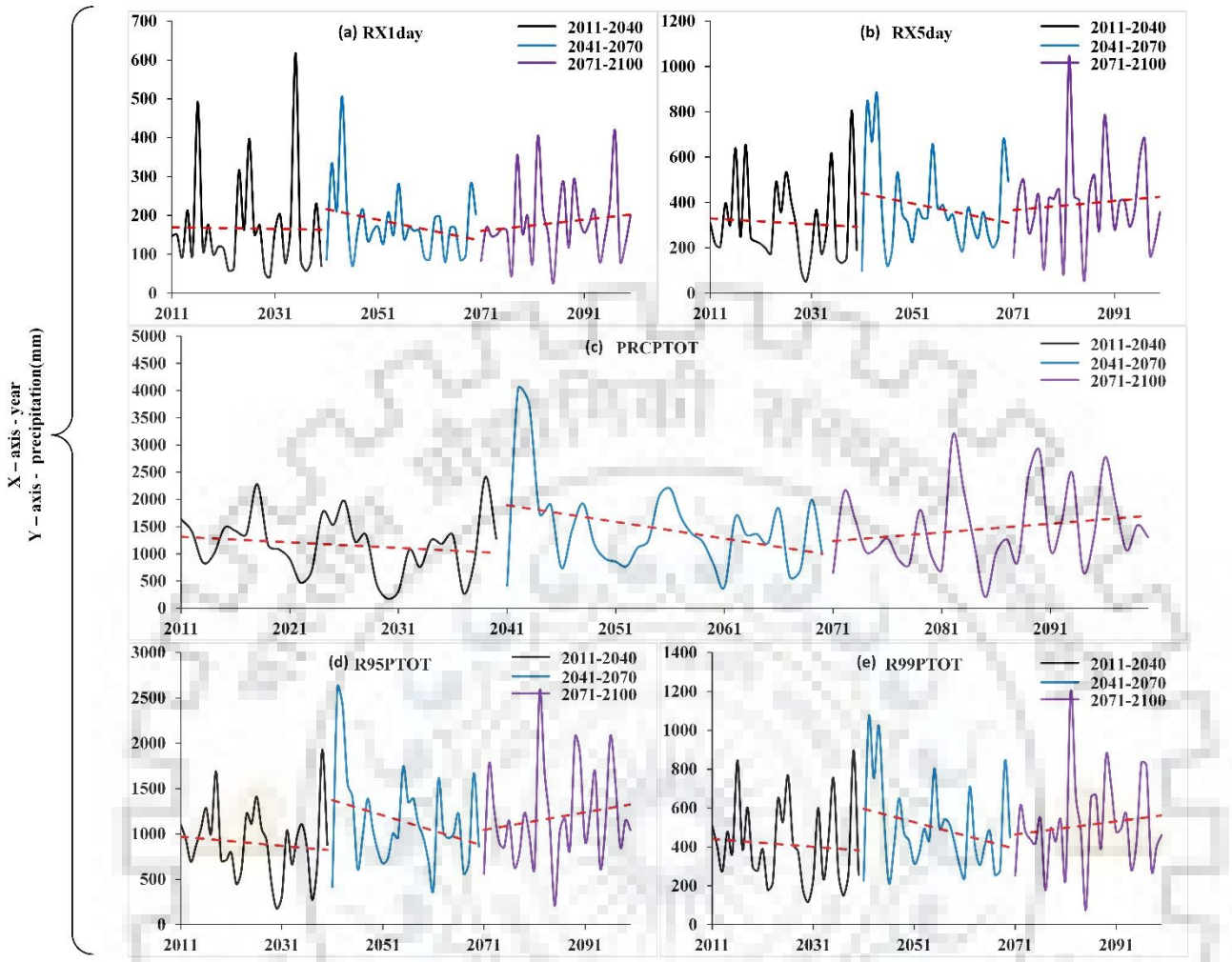

Figure 5.3(b) Linear trends for extreme value indices of long term precipitation series for all climate periods for RCP 4.5.

From the results discussed above and from Figures 5.4 and 5.5, some inferences were drawn for the study area. An increase in the percentage of a number of cool days (TX10P) will be observed in the future, along with an increase in cool nights (TN10P), tropical nights (TR), and summer days (SU). Significant reductions were observed in hot days (TX90P), warm nights (TN90P) and warm spell duration indicator (WSDI). Also, a significant increase in the Diurnal Temperature Range (DTR) was observed which shows that there will be an increase in the difference of maximum and minimum temperature over the region. An increase in DTR seriously affects rainfall intensities, as discussed in the previous chapters. It was also justified by the results obtained for different rainfall intensities, days with heavy rain (RH), very heavy rain (RVH) might increase as per the study. The study also suggested that there will be an increase in total wet-day precipitation (PRCPTOT), along with very wet days (R95PTOT) and extremely wet days (R99PTOT) for the study area. Also, the consecutive wet days (CWD) might decrease in the future which explains that even though there will be more

rainfall in the future the amount of that rain will be received in lesser number of days, hence the variability in rainfall days will be less and the intensity of rainfall might increase.

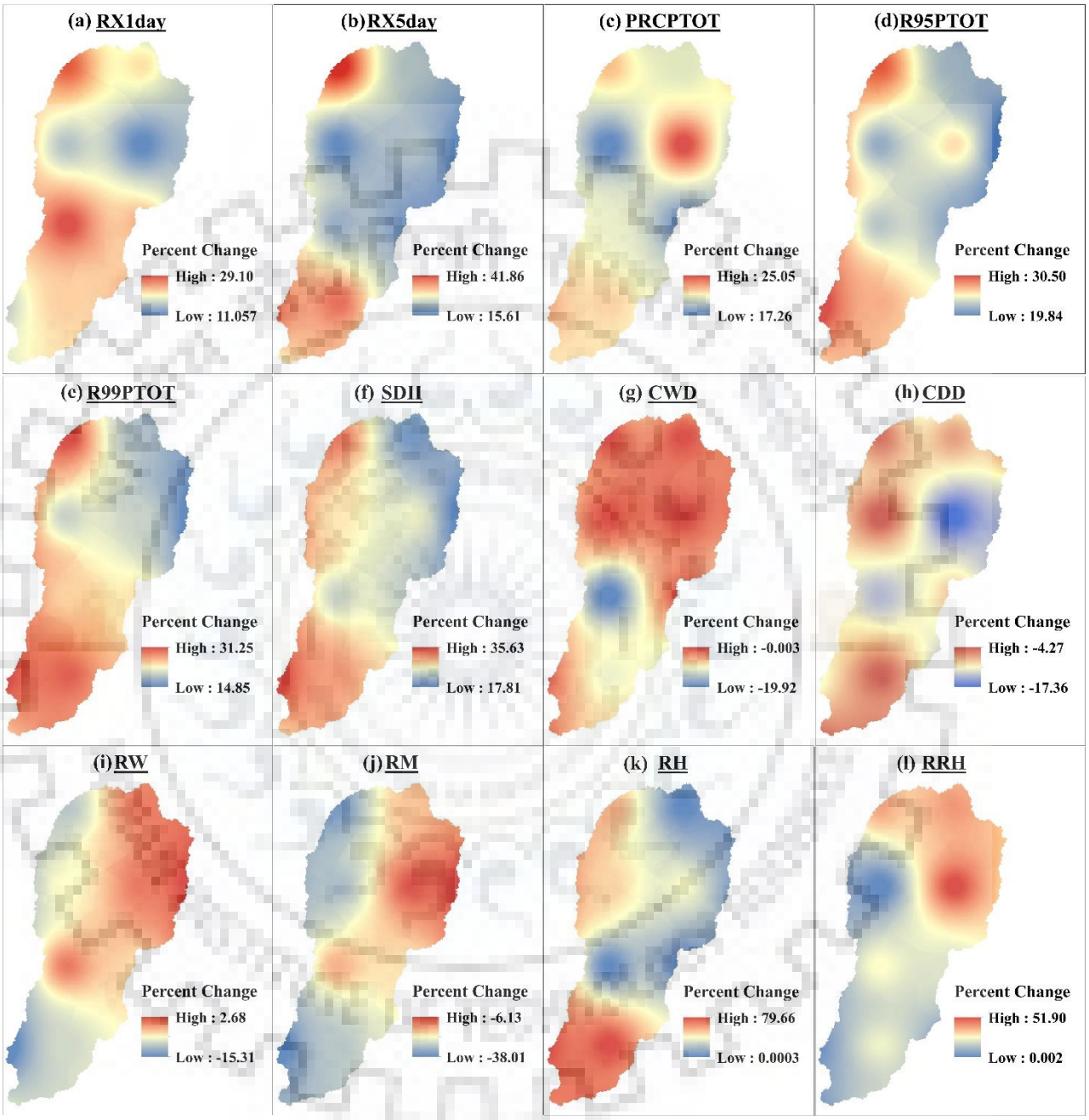

Figure 5.4 Spatiotemporal changes (%) in average precipitation based indices for RCP 4.5 of four RCMs (CCCma, CSIRO, NorESM, MIROC5).

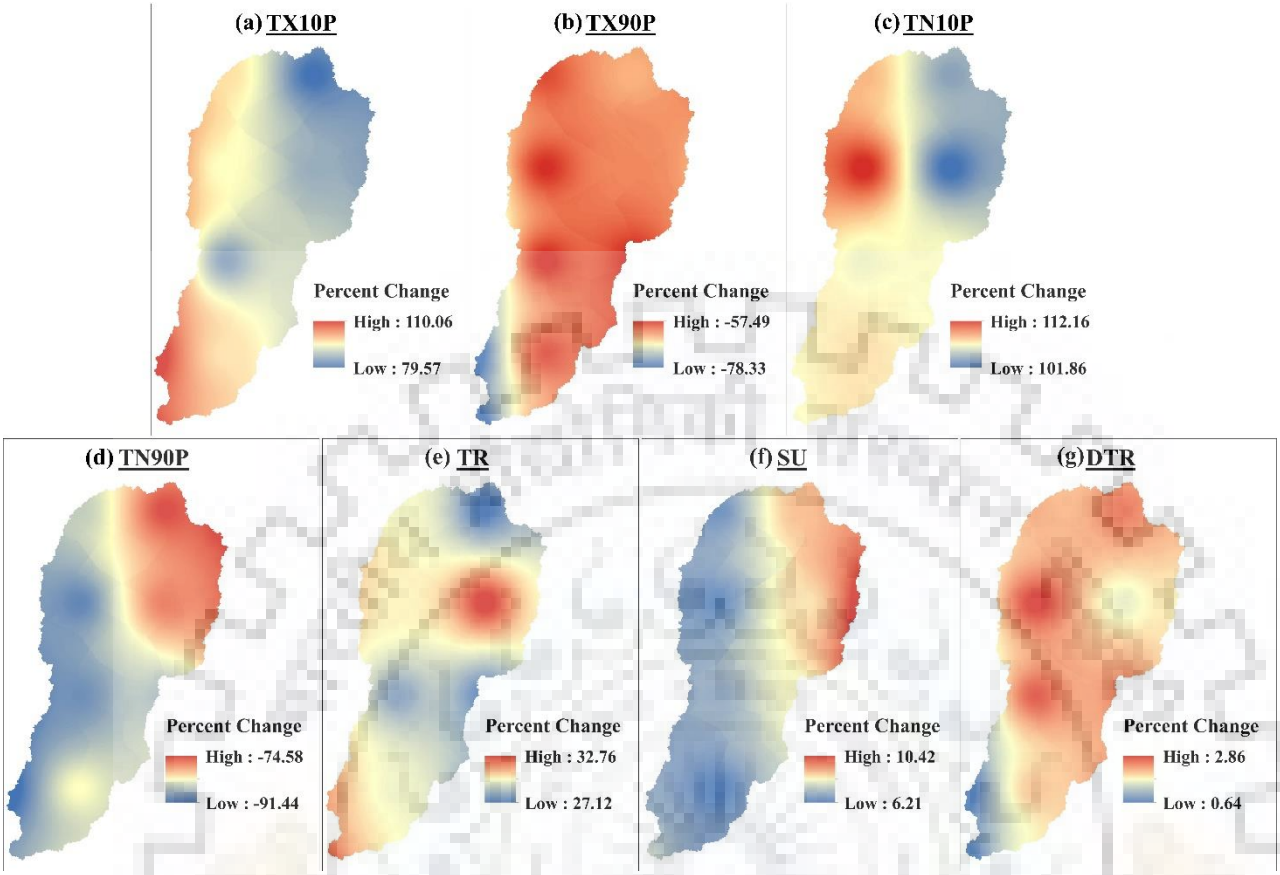

Figure 5.5 Spatiotemporal changes (%) in average temperature based indices for RCP 4.5 of four RCMs (CCCma, CSIRO, NorESM, MIROC5).

5.3.2.2 Climate projections under RCP 8.5

In similar lines, studies for RCP 8.5 have been performed as made for RCP 8.5. MMK results of all the indices for scenarios RCP 8.5 are represented in Tables 5.4 and 5.5 for all study periods. Linear trends of extreme value indices considering long term temperature and precipitation series for the three climate periods (CC1, CC2 and CC3) have been represented in Figures 5.6, 5.7(a), and 5.7(b). Also, the results of the spatial distribution of temporal changes (in percentage) of indices based on temperature and precipitation time series are represented in Figures 5.8 and 5.9 respectively.

The analysis of the results showed that almost all the grids exhibited more or less similar results in the case of MMK trend statistics. Hence only the results of any two representative stations have been displayed. A significant increasing trend was observed in the case of index TX10P, TN10P, TR and SU, while significant decreasing trends were observed in the case of TX90P, TN90P, and DTR for all the RCMs with few exceptions. Non-significant trends were found to exist in the case of WSDI and CSDI for all RCMs. Few exceptions were found in the MMK statistics values of different RCMs; in the case of index DTR CCCma and CSIRO showed a significant increasing trend while MIROC5

and NorESm showed a significant decreasing trend. Significant increasing trends were observed for all indices based on precipitation for all RCMs except for index CDD, CWD and RL. Significant decreasing trends were observed in the case of CDD for all RCMs except CSIRO, while no significant trend was observed for CWD for all RCMs. Also, for index RL, only CSIRO showed a significant increasing trend, while for index RM, MIROC5 and NorESM showed a significant increasing trend.

For the climate periods, significant increasing trends were observed during all three climate periods for almost all the RCMs in the case of TX10P, TN10P, TR, and SU. Significant decreasing trends were observed for index TX90P and TN90P for few models in period CC1 and CC2 and all RCMs in CC3. Only CCCma predicted a significant increasing trend for period CC1 and CC2 for index WSDI, while no trend was observed for CC3. No significant trend was observed for index CSDI. Conflicting results were observed for index DTR, where significant increasing trends were observed for climate period CC3 (MIROC5), while significant decreasing trends were observed for the period for MIROC5 and NorESM. While significant decreasing trends were observed for CC1 (CSIRO) and CC2 (MIROC5) as represented in Table 5.4.

It can be seen from Table 5.5 that significant increasing trends were observed for few RCMs in the case of the index of Rx1day, RX5day, PRCPTOT, R95PTOT, R99PTOT, SDII, RW and RH for climate period CC1 and CC2. No significant trends were obtained for index CWD and CDD for all the RCMs. For index RL, a significant increasing trend was obtained for CC1 (NorESM), while a significant decreasing trend was observed for period CC2 (CCCma). For index RM significant increasing trend for CC1 while a significant decreasing trend was observed for period CC2 (NorESM). A significant increasing trend was observed for period CC1 (MIROC5), while no trend was observed for period CC2. No significant trend was observed in the case of RVH for period CC1 and CC2. For period CC3, significant increasing trends were observed for RX1day, RX5day, PRCPTOT, R95PTOT, R99PTOT, SDII, RW, RRH, and RH for all RCMs. For index RVH, model CCCma showed a significant increasing trend. Significant decreasing trends were observed for index CDD for all RCMs except CSIRO. Conflicting results were obtained in the case of index RM, where CCCma showed a significant increasing trend while MIROC5 showed a significant increasing trend. To justify the results linear trends have also been represented in Figures 5.6, 5.7(a), and 5.7(b).

Linear trends of all the extreme value indices considering long term temperature and precipitation series have been presented in Figures 5.6, 5.7(a) and 5.7(b) for different climate periods, which further justify the trend results obtained in the study. The spatial distribution of temporal changes (in percentage) in precipitation and temperature-based indices for RCP 8.5 are shown in Figures 5.8 and 5.9, respectively.

Table 5.4 MMK statistics (Z) of indices based on temperature for RCP 8.5.

Entire period (2011-2100)										
RCM's	Grids	TX10P	TX90P	TN10P	TN90P	TR	SU	WSDI	CSDI	DTR
CCCma	Grid-A6	**7.70**	**-8.25**	**8.55**	**-3.89**	**9.57**	**2.40**	0.84	0.13	0.99
	Grid-A16	**7.69**	**-8.05**	**7.63**	**-3.78**	**9.45**	**2.31**	0.77	0.05	**2.41**
CSIRO	Grid-A9	**7.53**	**-7.55**	**8.02**	**-6.02**	**6.44**	**7.28**	-0.63	0.15	**3.55**
	Grid-A13	**9.86**	**-7.42**	**2.20**	**-6.36**	**6.72**	**5.83**	-0.18	0.14	**-3.00**
MIROC5	Grid-A12	**9.74**	**-8.33**	**3.37**	**-2.97**	**9.55**	**2.57**	1.17	0.25	**-6.98**
	Grid-A13	**14.67**	**-7.81**	**3.84**	**-3.87**	**8.89**	**2.47**	0.86	0.12	**-9.98**
NorESM	Grid-A14	**8.95**	**-6.19**	**7.94**	**-6.21**	**7.28**	0.53	**2.25**	0.13	**-6.15**
	Grid-A16	**8.97**	**-6.02**	**7.76**	**-6.20**	**8.67**	1.67	1.50	0.26	**-5.52**
Climate periods (CC1 , CC2, CC3)										
Periods	RCM's	TX10P	TX90P	TN10P	TN90P	TR	SU	WSDI	CSDI	DTR
CC1	CCCma	**2.91**	**-2.57**	**2.97**	**-2.30**	**2.84**	**2.06**	**2.57**	-0.40	-1.15
	CSIRO	**2.38**	-0.93	**3.01**	-1.04	1.02	1.75	0.36	0.18	**-2.79**
	MIROC5	**2.27**	0.02	0.50	**-4.96**	**2.79**	**5.93**	0.83	-0.17	-1.39
	NorESM	**2.52**	-1.75	**1.99**	**-2.05**	**4.40**	1.09	-0.41	-0.03	0.24
CC2	CCCma	**3.00**	-1.71	**6.24**	-1.89	**3.37**	**2.95**	**2.40**	-0.10	0.21
	CSIRO	**3.39**	**-4.19**	**4.16**	**-1.98**	**2.86**	-0.46	-0.90	-0.55	-0.18
	MIROC5	**3.69**	0.19	0.34	**-3.01**	**2.98**	**6.23**	1.37	-0.51	**-2.12**
	NorESM	**3.05**	-1.15	**2.23**	**-2.70**	**4.26**	**2.11**	-0.88	-0.53	0.27
CC3	CCCma	**9.53**	**-9.88**	**8.62**	**-3.63**	**7.35**	**2.45**	0.75	0.18	1.26
	CSIRO	**8.11**	**-7.65**	**7.40**	**-5.26**	**5.05**	**11.08**	-1.26	0.46	**2.67**
	MIROC5	**9.20**	**-8.29**	**2.83**	**-2.31**	**7.36**	**2.13**	0.97	0.28	**-6.22**
	NorESM	**8.62**	**-5.95**	**7.24**	**-5.71**	**8.77**	1.03	1.27	0.30	**-5.85**

Figures in bold specify significant values at 95% confidence (5% significance) level.

Table 5.5 MMK statistics (Z) of indices based on precipitation for RCP 8.5.

Entire period (2011-2100)														
RCMs	Grids	RX1day	RX5day	PRCPTOT	R95PTOT	R99PTOT	SDII	CWD	CDD	RW	RL	RM	RRH	RH	RVH
CCCma	Grid-A6	**3.49**	**3.76**	**4.11**	**4.72**	**4.47**	**4.50**	0.77	**-3.76**	1.74	1.15	-1.15	**3.00**	**4.45**	**3.89**
	Grid-A16	**4.04**	**3.18**	**2.89**	**4.34**	**4.39**	**4.53**	-1.20	**-2.75**	0.70	1.32	**2.20**	**2.52**	**2.48**	**3.67**
CSIRO	Grid-A9	**4.85**	**2.56**	**3.81**	**4.13**	**3.21**	**4.03**	-0.15	-0.94	**2.27**	1.60	-0.38	**3.50**	**3.61**	1.47
	Grid-A13	**4.38**	**2.77**	**3.72**	**4.21**	**4.46**	**4.23**	-0.40	-1.16	**2.32**	**2.69**	-0.40	**3.72**	**3.60**	0.47
MIROC5	Grid-A12	**5.14**	**6.30**	**5.17**	**5.81**	**7.22**	**6.05**	0.93	**-3.94**	**4.40**	1.76	**4.44**	**4.14**	**4.58**	**4.19**
	Grid-A13	**5.70**	**4.85**	**5.71**	**7.78**	**6.05**	**7.39**	0.39	**-4.24**	**5.23**	1.70	**3.36**	**4.12**	**5.99**	**5.52**
NorESM	Grid-A14	**4.31**	**5.19**	**4.22**	**4.98**	**4.12**	**4.92**	0.69	-1.11	**1.96**	-1.84	0.49	**2.69**	**3.49**	**2.56**
	Grid-A16	**6.29**	**7.47**	**3.48**	**3.81**	**10.58**	**4.76**	-0.32	**-4.31**	**2.85**	0.11	**2.62**	**3.06**	**3.28**	**2.69**
Climate periods (CC1 , CC2, CC3)														
Periods	RCMs	RX1day	RX5day	PRCPTOT	R95PTOT	R99PTOT	SDII	CWD	CDD	RW	RL	RM	RRH	RH	RVH
CC1	CCCma	**2.00**	**2.00**	**2.49**	1.53	1.61	1.50	0.00	-0.59	0.50	-0.87	-0.13	0.63	0.84	1.31
	CSIRO	**2.17**	0.46	1.64	1.57	**2.82**	1.39	0.86	0.12	**2.33**	0.83	**2.03**	1.46	1.17	1.43
	MIROC5	0.82	0.18	**1.99**	1.71	0.75	1.16	0.07	0.29	**2.85**	0.44	**2.50**	**2.31**	0.11	0.11
	NorESM	1.46	1.53	0.75	1.71	1.86	**2.32**	0.64	-0.16	**3.77**	**4.49**	**-4.06**	-0.13	**1.98**	0.34
CC2	CCCma	-0.29	0.36	-0.43	0.07	0.07	1.00	-1.58	1.36	-1.06	**-2.81**	-1.11	0.36	-0.09	-0.50
	CSIRO	**2.43**	1.43	1.57	1.21	**2.55**	1.18	-0.14	0.02	**2.11**	0.75	1.11	1.22	1.04	-0.10
	MIROC5	**2.16**	**2.32**	**2.64**	**2.53**	**2.43**	**2.39**	0.72	-0.16	**1.97**	1.87	1.55	1.87	**2.08**	1.47
	NorESM	**1.96**	**2.18**	1.29	**2.18**	**2.28**	**2.82**	0.68	0.80	-1.58	-1.83	**-3.26**	0.35	**2.06**	1.12
CC3	CCCma	**3.45**	**3.04**	**2.49**	**3.88**	**3.39**	**4.30**	-1.29	**-2.87**	0.23	1.65	**-2.40**	**3.30**	1.67	**2.65**
	CSIRO	**4.80**	**2.40**	**3.71**	**4.06**	**3.07**	**3.96**	-0.24	-0.94	**2.16**	1.52	-0.60	**3.42**	**3.50**	1.58
	MIROC5	**3.55**	**2.74**	**4.77**	**5.22**	**3.72**	**3.37**	0.42	**-4.47**	**6.50**	0.94	**4.18**	**3.28**	**3.29**	1.87
	NorESM	**2.74**	**2.78**	**3.82**	**4.33**	**3.44**	**5.01**	-0.14	**-2.31**	**2.82**	-1.29	1.35	**3.64**	**3.03**	1.10

Figures in bold specify significant values at 95% confidence (5% significance) level.

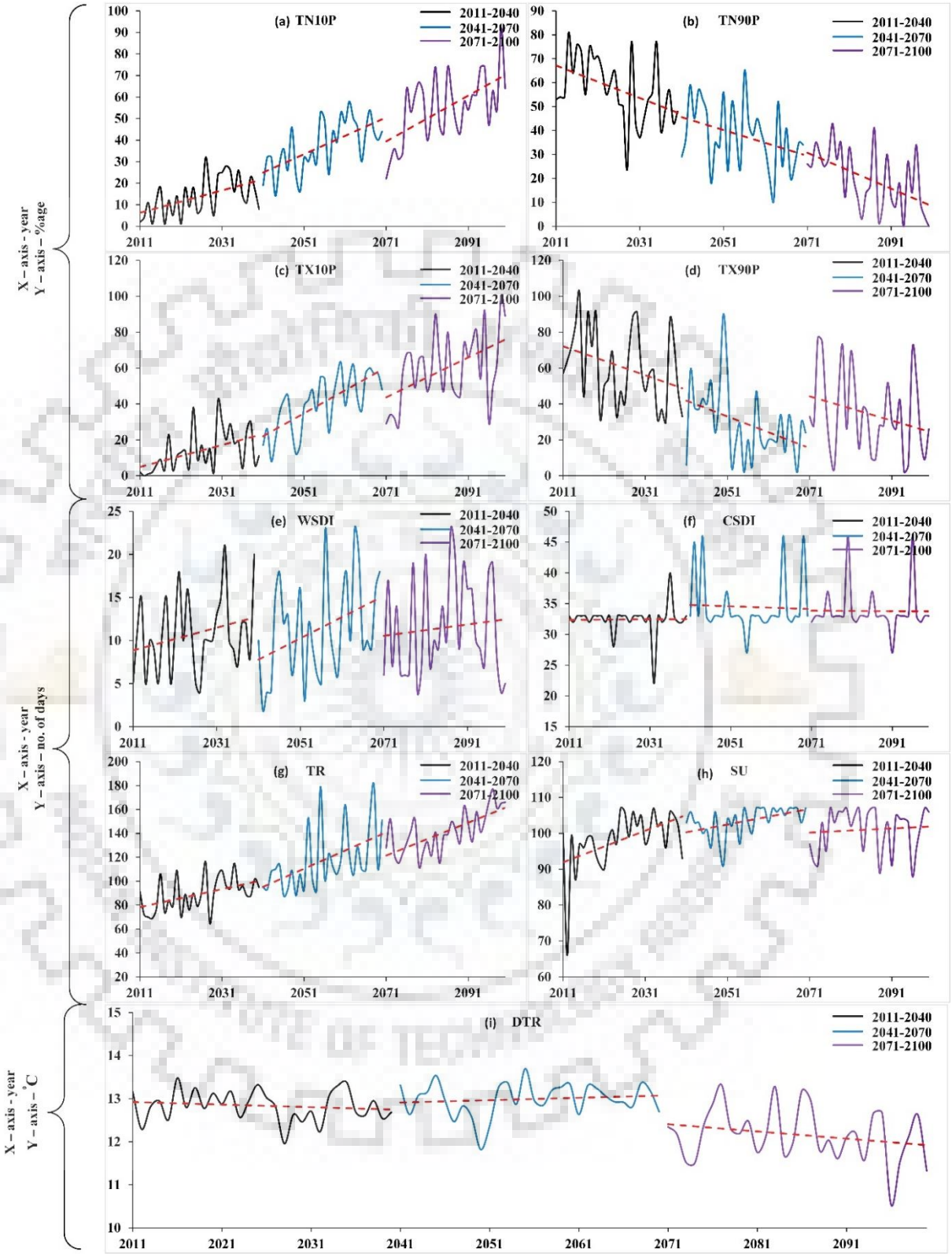

Figure 5.6 Linear trends for extreme value indices of long term temperature series for all climate periods for RCP 8.5.

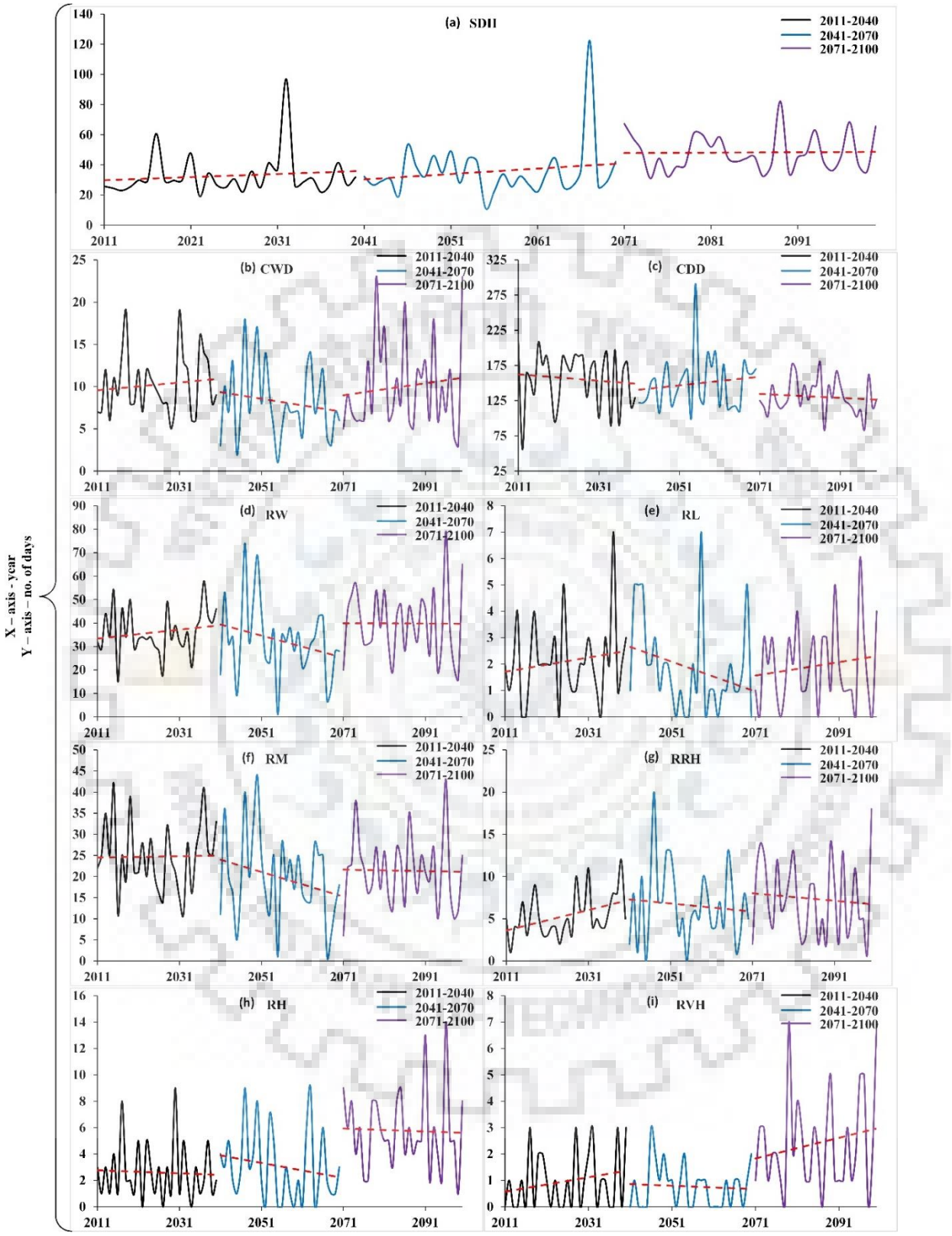

Figure 5.7(a) Linear trends for extreme value indices of long term precipitation series for all climate periods for RCP 8.5.

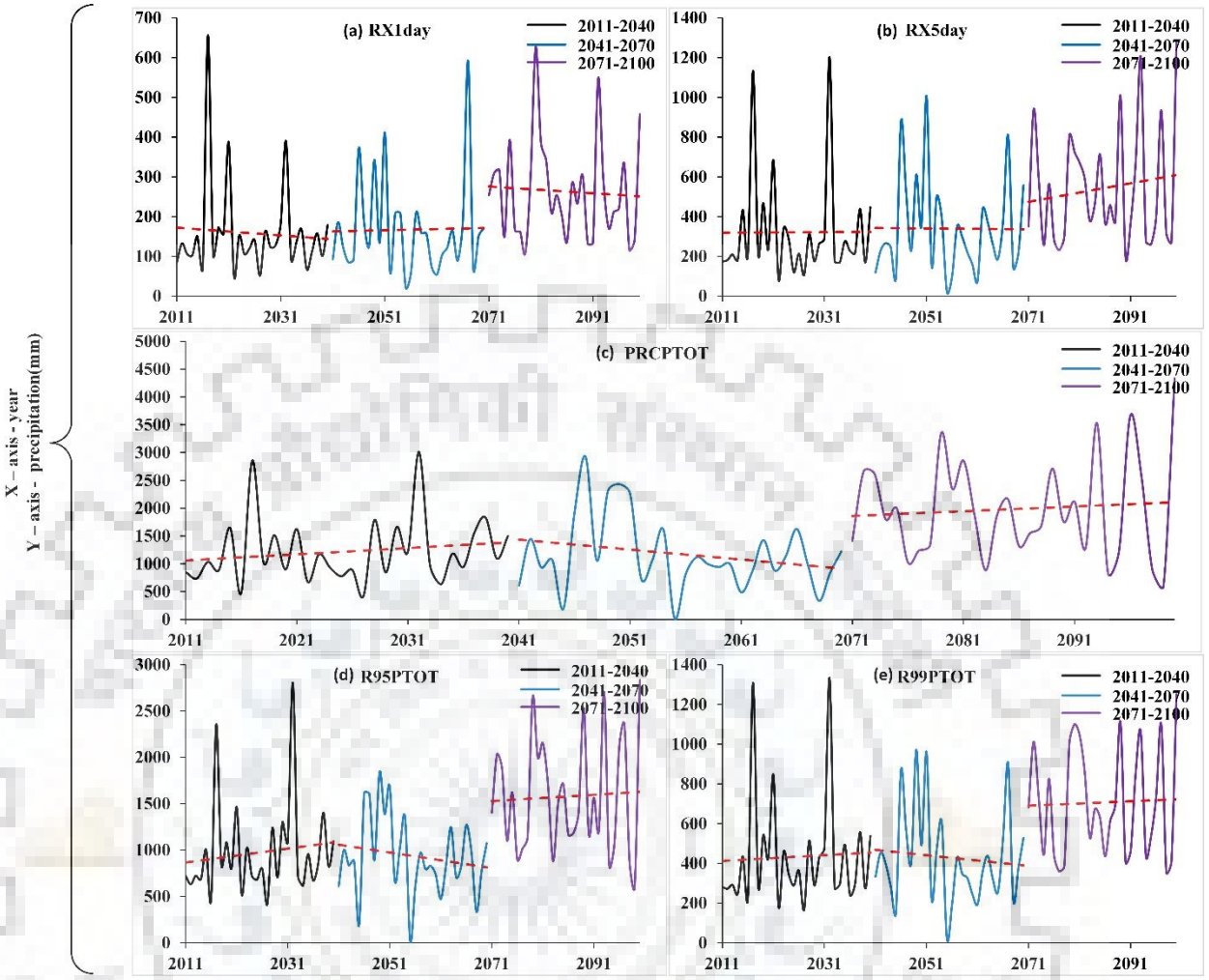

Figure 5.7(b) Linear trends for extreme value indices of long term precipitation series for all climate periods for RCP 8.5.

From the results discussed above for RCP 4.5, RCP 8.5, and from Figures 5.8 and 5.9, some inferences were drawn for the study area. Similar patterns of trends were observed for both the scenarios with a higher rate of change (in terms of percentage) in the case of RCP 8.5 as compared to RCP 4.5. An increase in the percentage of a number of cool days (TX10P) will be observed in the future, along with an increase in cool nights (TN10P), tropical nights (TR), and summer days (SU). Significant reductions in hot days (TX90P) and warm nights (TN90P) will be observed in the future. Also, a significant decrease in the Diurnal Temperature Range (DTR) was observed which explains that there will be a decrease in the difference of maximum and minimum temperature over the region. The trend for DTR in the case of RCP 8.5 had a stark contradiction with the results of RCP 4.5. However, even though all but one model predicted a decrease in DTR values, overall understanding points towards an increase in DTR in the future. It was also justified by the results obtained for different rainfall intensities, days with heavy rain (RH), very heavy rain (RVH) might increase as

per the study. The study also suggested that there will be an increase in total wet-day precipitation (PRCPTOT), along with very wet days (R95PTOT) and extremely wet days (R99PTOT) for the study area. Also, the consecutive dry days (CDD) might decrease in the future which may sound contradictory. Since the PRCPTOT is increasing dramatically, an increase in wet days (RW) along with days with heavy rainfalls (RRH, RH and RVH) sounds logical.

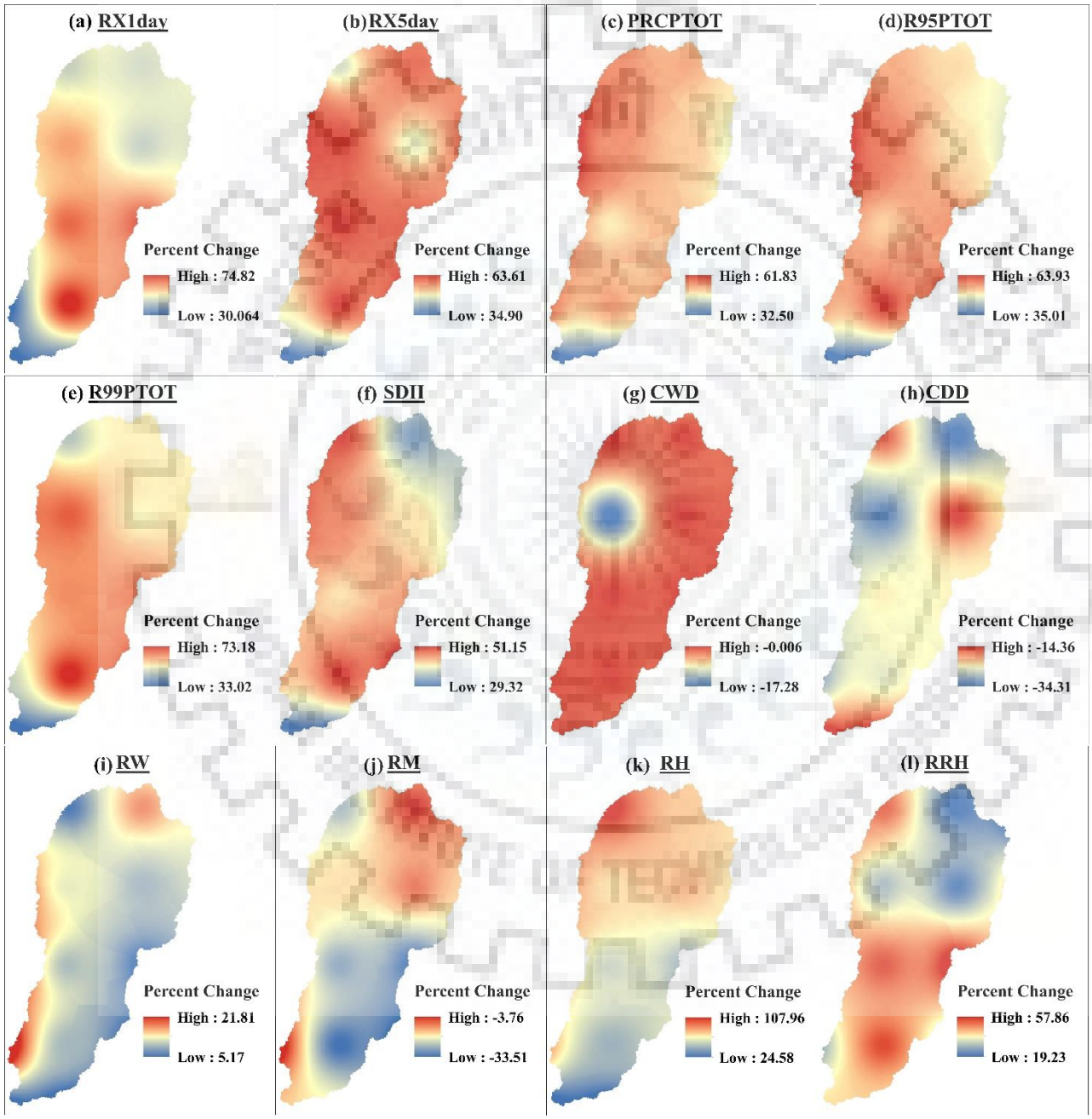

Figure 5.8 Spatiotemporal changes (%) in average precipitation based indices for RCP 8.5 of four RCMs (CCCma, CSIRO, NorESM, MIROC5).

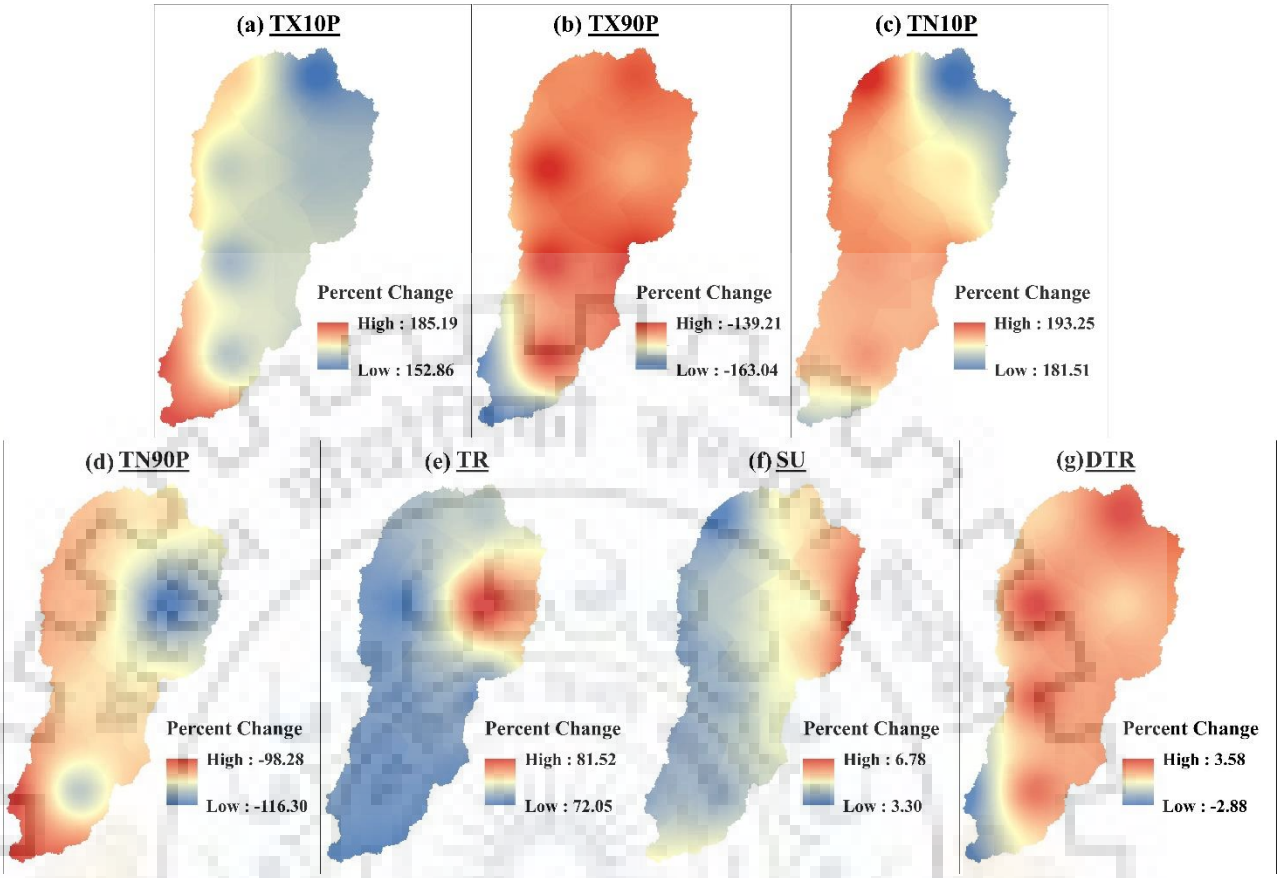

Figure 5.9 Spatiotemporal changes (%) in average temperature based indices for RCP 4.5 of four RCMs (CCCma, CSIRO, NorESM, MIROC5).

5.4 CONCLUDING REMARKS

For reproduction of meteorological parameters to study changes in extreme value indices in the future, regional climate model (RCMs) were evaluated in the study. Four RCMs were identified as the most suitable models to determine future times series data of precipitation and temperature (maximum and minimum) for the study viz. CCCma, CSIRO, MIROC5 and NorESM. The technique of distribution mapping was used to remove systematic biases that may be present in the data. MMK test statistic was used to evaluate the presence of any trend while the magnitude of the trend was quantified using Sen's slope estimator over the entire period (2011-2100) and for three climate periods, namely CC1 (2011-2041), CC2 (2041-2070) and CC3 (2071-2100). These tests were applied over two scenarios viz. RCP 4.5 and RCP 8.5. The overall result indicated an increase in the Diurnal Temperature Range (DTR) in the future along with an increase in days with heavy rainfalls in the case of both scenarios for the study area.

CHAPTER 6

LAND USE/LAND COVER DYNAMICS AND FUTURE PREDICTION

6.1 GENERAL

Rapid changes in land use/land cover (LULC) have been a significant concern of the 21st century, which has a direct impact on the survival of humanity. LULC change can be defined as the change in the biological and physical characteristics of the land. Primary reasons for these changes are due to various factors such as degradation of land, rise in urban settlement, deforestation, excessive agricultural practices as well conversion of forests and cultivable land into the urban or industrial lands (Tilman et al. 2011b; Setiawan and Yoshino 2012; Samal and Gedam 2014; Meshesha et al. 2016). In the recent past, dynamics of LULC have been investigated by many researchers across the globe using Remote Sensing (RS) and Geographic Information Systems (GIS) techniques (Weng 2002; Xiao et al. 2006; Schilling et al. 2009; Rozenstein and Karnieli 2011; Saadat et al. 2011; Khare et al. 2014).

Despite being a challenging task, the use of multi-temporal satellite images for the detection of LULC changes is quite common (Fan et al. 2008; Iqbal and Khan 2014; Qiang and Lam 2015). Change detection techniques have been used for various evaluations such as quantification of changes in urban settlement (assessment of urban sprawl), monitoring of changes in forest cover, assessment of changes in cultivable land, etc. (Rao and Pant 2001; Dinor et al. 2005; Kabba and Li 2011; Iqbal and Khan 2014; Niraula et al. 2015). The driving force behind LULC change is various environmental and development policies.

The conversion of LULC to meet increasing demographic demand such as conversion of forest area into agricultural to barren and subsequently into urban land results in soil erosion accelerated rate of surface runoff and depletion of groundwater level (Bishaw 2001; Ghani et al. 2010; Iqbal and Khan 2014; Kumar et al. 2017). Their combined effects, as well as mutual interaction among these anomalies, may result in land degradation in any area (Messinger 2003; Thormann et al. 2004; Niezgoda and Johnson 2005). According to a study by Piao et al. (2007), the annual river discharge across the globe has increased, and the land use land change is responsible for approximately 50% of this increase. The primary factor behind an increase in surface runoff is the change in vegetation

and evapotranspiration that further emphasizes the point that climate change and anthropogenic activities are the primary cause of land degradation leading to the increase in surface runoff. Farley et al. (2005) found that higher rates of evapotranspiration are directly related to the presence of denser forests in the region as compared to the presence of crunches or grasslands which directly influences water availability in the region for direct drainage. DeFries and Eshleman (2004) found that LULC change plays a pivotal role in impact studies of water quality and quantity. Hence, there is an urgent need to understand the changes in land use patterns and its impact on hydrology and water resources management. The conceptual framework behind causes, effects and impacts of land use/ land cover changes represented in Figure 6.1.

The increasing population was the main reason behind choosing Kharun watershed, which is part of the newly created state of Chhattisgarh in 2000. Increase in population growth has resulted in urban area expansion, mass industrialization and has also altered the traditional irrigation practices to meet the food demand of the growing population. Moreover, the government plans to include several villages nearby the capital city of Raipur (which lies in the watershed) for expansion. Several policies and plans have been executed to develop New Raipur is the state capital, which is approximately 10 km away from the existing city. However, in several cases, it has been observed that the policymakers often neglect these implications of land use land change over the region.

Keeping these points in view, the present study was conducted over the region of Kharun watershed. The primary objective of this chapter is to evaluate the LULC changes based on satellite-based remote sensing data and to generate the projection of LULC changes in the near future, using CA-Markov based model. Land-cover changes were investigated based on the temporal series of remote sensing multispectral satellite images of Landsat. The chapter presents the (i) identification of classes and distribution percentages of LULC; (ii) estimate the percentage changes in LULC of area between 1990 and 2015 at decadal and demi decadal-scale and quantify the rates of change; (iii) accuracy assessment of classified LULC; (iv) applying CA-Markov to predict LULC allocations in the near future of year 2030.

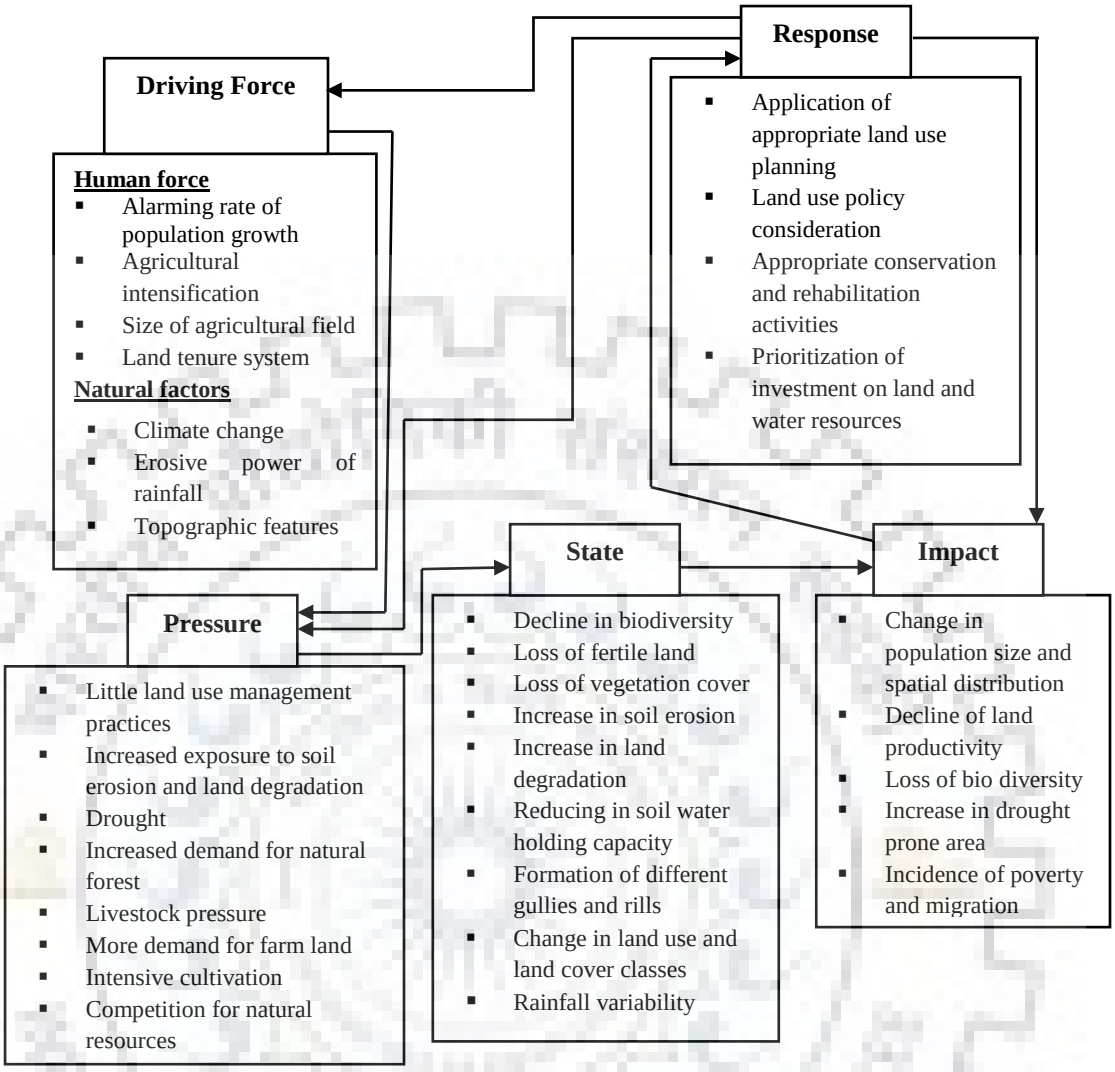

Figure 6.1 Conceptual framework behind causes, effects, and impacts of land use/land cover changes.

6.2 MATERIALS AND METHODS

6.2.1 Description of the Study Area

A detailed description of the study area already been discussed in Chapter 3.

6.2.2 Field Data Collection

Field visits were carried out in order to collect several ground truth points for the study area. During the field, data were collected from different locations to validate the detailed image. Ground truth points and their respective locations were recorded using Global Positioning System (GPS). Historical land cover data was assessed by interviewing the local population. Based on the interview and data collection, the study area was classified into five categories, viz. water bodies, urban area, and agricultural land, mixed forest, barren land, and sand/open rocks. The purpose of collecting the

ground truth points was to improve the accuracy of the LULC classification. For ground navigation during field visits, google maps were used.

6.2.3 Remote Sensing Data

For the study, satellite imageries were download from the United States Geological Survey (USGS) based website http://earthexplore.usgs.gov. The detail of satellite data is presented in Table 6.1. Historical satellite images from 1990 to 2015 having a uniform resolution of 30m were acquired in order to understand the LULC change dynamics for the study area. Keeping in view the clarity of the satellite images, images with not more than 10% of cloud cover were selected and downloaded from the website. The study area shared parts of 2 satellite imageries (path-row 142-45 and 142-46). Based on the availability LANDSAT 5 Thematic Mapper (TM) images for the years 1990, 1995, 2005 and 2010, LANDSAT 7 Enhanced Thematic Mapper (ETM) image for 2000 and LANDSAT 8 Operational Land Imager (OLI) and Thermal Infrared Sensor (TIRS) for 2015 were chosen. The obtained LANDSAT images were also corrected to remove the presence of any cloud cover in the images before further processing.

Table 6.1 Detailed description of the acquired satellite imageries.

S. No.	Images	Resolution	Sensor	Path	Rows	Acquisition date
1	Landsat5	30 m x 30 m	TM	142	45 and 46	2/5/1990
2	Landsat5	30 m x 30 m	TM	142	45 and 46	19/11/1995
3	Landsat7	30 m x 30 m	ETM	142	45 and 46	15/12/2000
4	Landsat5	30 m x 30 m	TM	142	45 and 46	19/11/2005
5	Landsat5	30 m x 30 m	TM	142	45 and 46	19/12/2010
6	Landsat8	30 m x 30 m	OLI_TIRS	142	45 and 46	23/12/2015

6.2.4 Methodology

Landsat satellite images are used to classify land use. All six images (1990, 1995, 2000, 2005, 2010 and 2015) were classified by employing supervised classification algorithm in this area. It is one of the most popular classification methods, which is usually suitable in the identification of a few classes. Geospatial tools ERDAS Imagine-2014 and ArcGIS 10.2 were used to process and prepare the LULC map. The overall methodology is given in Figure 6.2.

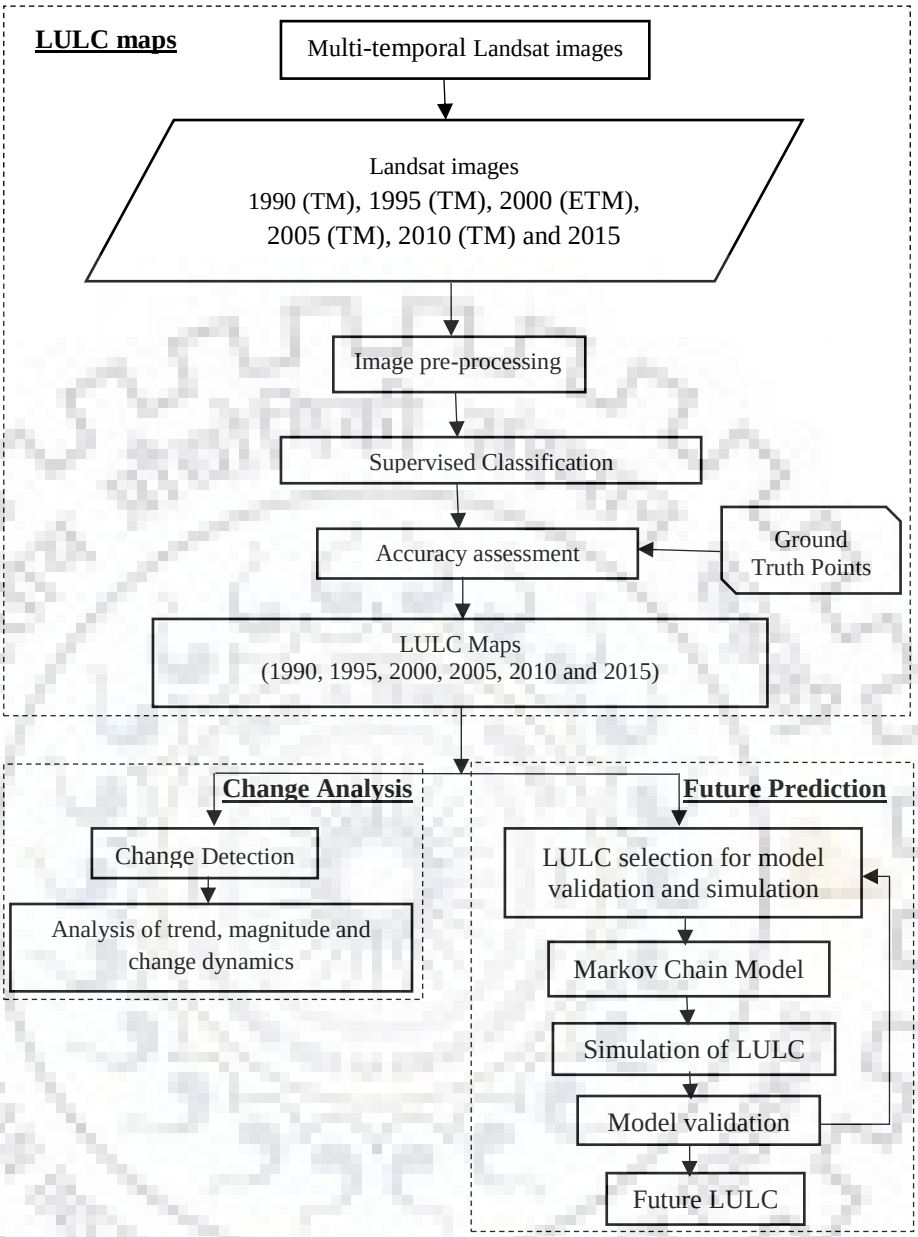

Figure 6.2 Flowchart showing general methodology for LULC classification and prediction.

6.2.4.1 Image Preprocessing

Before the pre-processing of the satellite images, individual bands were stacked, and the resulting satellite images were mosaicked for each path-row combination. Owing to the systematic mistakes and inaccuracy of the sensors, the pre-processing of the satellite imageries is an essential step in the land use mapping. Radiometric and geometric corrections were applied over satellite images to preprocess. Radiometric correction is applied over images from different periods to match their histograms, while in order to co-register the satellite images so that they can overlap perfectly

geometric correction is used. This is important because some of the essential methods are based on the comparison of the two images from different periods, e.g., supervised classification.

Before the analysis, the data was processed in ArcGIS10.2 and ERDAS IMAGINE 2014 environment. After the preliminary agreement that confirmed the correction of satellite images, a subset of the image was extracted that include area of interest (Kharun watershed). Satellite images of the extracted area are required radiometric correction for gain and bias correction before LULC classification. In this correction, digital number (DN) derived from the images is converted to the spectral radiance at the sensor by data calibration (Shalaby and Tateishi 2007; Hua et al. 2012).

$$L_{TOA} = \frac{(L_{MAX} - L_{MIN})}{(QCAL_{MAX} - QCAL_{MIN})} \times (DN - QCAL_{MIN}) + L_{MIN} \quad (6.1)$$

where L_{TOA} is the solar irradiance at the top of the atmosphere, L_{MAX} and L_{MIN} represent the maximum and minimum value, $QCAL_{MAX}$ and $QCAL_{MIN}$ are the maximum and minimum DN values (255 or 1). Moreover, the L_{MAX} and L_{MIN} are the gain and offset respectively available from the header file of the image.

Precise per-pixel registration of satellite data is a primary requisite of the change detection study, absence of which can result in the overestimation of the actual result (Dewan and Yamaguchi 2009). For change detection pixel by pixel analysis is carried out, anymiss-registration that is more than a single pixel can introduce anomaly in the result. To avoid this issue, the root-mean-square error (RMSE) between two dates must not exceed 0.5 pixel (Pandey and Khare 2017). In this study geometric correction was carried out using ground control points (GCPs) from topographic maps with a scale of 1:250,000 to geocode the image. The RMSE between the two images was found to be less than 0.5, which is acceptable.

6.2.4.2 Image classification and LULC class distribution

In order to perform the classification, a supervised classification method was applied in the ERDAS Imagine 2014 (a geospatial data processing tool). The ambiguous area and location in classification were recoded by taking help from topography map, ground truth points and by google map. There were six types of LULC identified in the study area, as (1) Water Bodies (2) Urban area (3) Agricultural land (4) Mixed Forest (5) Barren Land and (6) Sand and Open Rocks, description of these categories are given in Table 6.2.

Table 6.2 Detailed description of land use/land cover types.

S. No.	LULC classes	Description
1	Water bodies (WB)	Areas that have surface water. It includes ponds, streams, rivers, lakes, marshland and riverine vegetation found along riverbank and streams
2	Urban area (UA)	Urban and rural settlements, along with the areas having manmade constructions like roads, bridges, parking lots etc.
3	Agricultural land (AL)	Land allotted for crop cultivation both annual and perennial crops
4	Mixed forest (MF)	Area covered with dense/sparse natural forest and the areas having vegetative cover apart from agricultural land
5	Barren land (BL)	The area with very little or no vegetation cover on the surface of the land. It consists of vulnerable soil to erosion and degradation. It also includes bedrock, which is unable to support cultivation.
6	Sand and open rocks (SR)	The area with exposed rocks (due to quarrying) and the river sand (in the river floodplain

6.2.4.3 Accuracy assessment

In order to assess the accuracy of each LULC class, the kappa coefficient was used in this study. The efficiency of LULC classifications using the kappa coefficient is assessed by the equation below (Eq. 6.2).

$$Kappa\ coeffiecient: K_p = \frac{\eta_o - \eta_E}{1 - \eta_E} \tag{6.2}$$

where observed accuracy is denoted by η_o and the expected accuracy is denoted by η_E.

6.2.4.4 Change analysis

Once the images have been classified, and the accuracy of the classification is found to be satisfactory, change analysis is carried out considering classified images of any two different periods. In this study, the extent of change in the land use type between two periods was estimated.

The change in the magnitude of different LULC classes was performed using both ArcGIS10.2.2 and ERDAS IMAGINE 14 and finally using the following equation (Eq. 6.3).

$$\Delta A = (\%) = \frac{A_{t2} - A_{t1}}{A_{t1}} * 100 \tag{6.3}$$

where A_{t1} is the area of LULC types at the initial time, A_{t2} is the area of LULC types at the final time, ΔA (%) = percentage change in the area of LULC classes type between initial time A_{t1} and period A_{t2}.

6.2.4.5 Future prediction of LULC using Markov Chain model and Cellular Automata

A hybrid model of Markov Chain and Cellular Automata (CA-Markov) was opted in this study for the prediction of future LULC imagery. In order to predict a particular class, the Markov model considers both past changes as well as the rate of change. The initial state and the transition (or change) matrix is the primary requirement of the model. The transition matrix is defined as the matrix change matrix of the class developed during the conversion of LULC classes from one state to another (Halmy et al. 2015) given by Eq. 6.4

$$L = L_{ij} = \begin{bmatrix} L_{11} & L_{12} & \dots & L_{1n} \\ L_{21} & L_{21} & \dots & L_{2n} \\ \dots & \dots & \dots & \dots \\ L_{n1} & L_{n1} & \dots & L_{nn} \end{bmatrix} \quad (6.4)$$

where L denotes the transition probability of i^{th} and j^{th} state. The primary condition behind the Eq. 6.4 is that it should satisfy the equation below (Eq. 6.5).

$$\sum_{j=1}^{n} L_{ij} = 1 \quad 0 \le L_{ij} \le 1 \quad (6.5)$$

After obtaining the primary matrix and the change matrix (L_{ij}) for the Markov model, the Markov forecast model is given as:

$$L_n = L_{n-1} \qquad L_{ij} = L_{(0)} L_{ij}^n \quad (6.6)$$

where L_n is the transition probability at any given time, L_o is the primary matrix (Guan et al. 2011; Halmy et al. 2015).

Finally, in order to predict the future LULC of the study area, the output of the change matrix (obtained from the Markov chain) was used in the Cellular Automata (CA) model.

6.3 RESULTS AND DISCUSSIONS

6.3.1 Land Use/ Land Cover Map Development

Red, blue, green (RBG) and Near Infra-Red (NIR) bands were used for this study. These bands were stacked according to the standard color composite. For the sake of the analysis and ease, false-color composite (FCC) using bands 2, 3 and 4. From the studies carried out in the recent past, it was observed that to meet the food demand of the growing population, agricultural land has increased,

which has resulted in the reduction of forest areas (Lambin et al. 2003). Moreover, it was further observed due to an increase in urban migration and to settle the increased urban influx in urban areas, agricultural and forest areas have been converted into urban settlements, which has also resulted in an increase in the barren land in many parts of the globe. To assess the variation in the land use type in the study area, LULC maps were developed using supervised classification for the years 1990, 1995, 2000, 2005, 2010 and 2015. Six LULC classes were identified to represent the area in the best possible way; the statistics (percent land share) for each year are represented in Figure 6.3. Distribution of different classes developed for the year 1990-2015 has been represented in Table 6.3 and Table 6.4. The land use and land cover maps of the study area between 1990 and 2015 is represented in Figure 6.4. Accuracy of the developed maps was also evaluated using the kappa coefficient with the help of ground truth points obtained during the field survey, as shown in Table 6.4.

Based on the statistics it was observed that there is an overall increase in the urban area from 0.23% (1990) to 3.54% (2015) as well as in the proportion of barren land from 2.45% (1990) to 11.34% (2015) due to mass urbanization of the study area. From the field survey, it was also found that many farmers have sold their agricultural land for much higher profits near the urban settlement for real estate development. Hence, an increase share of barren land can be seen in recent years in the form of fallow land. As a result of an increase in the urban area and barren land, the subsequent reduction in agricultural land from 85.6% (1990) to 76.4% (2015) was observed along with a reduction in a mixed forest from 8.67% (1990) to 8.71% (2015). Due to increased quarrying in the region, the area described as sands and open rocks have increased from 1.19% (1990) to 1.82% (2015).

Table 6.3 Distribution of classes between 1990 and 2000.

CLASS	1990		1995		2000	
	Area		Area		Area	
	Sq. km.	%	Sq. km.	%	Sq. km.	%
Water bodies	78.53	1.89	103.38	2.49	114.44	2.76
Urban area	9.41	0.23	12.04	0.29	12.27	0.30
Agricultural land	3553.0	85.6	3546.9	85.4	3509.5	84.5
Mixed forest	360.09	8.67	335.24	8.07	265.15	6.39
Barren land	101.98	2.46	105.44	2.54	201.79	4.86
Sand and open rocks	49.31	1.19	49.31	1.19	49.00	1.18

Table 6.4 Distribution of classes between 2005 and 2015.

CLASS	2005		2010		2015	
	Area		Area		Area	
	Sq. km.	%	Sq. km.	%	Sq. km.	%
Water bodies	75.81	1.83	62.23	1.50	47.56	1.15
Urban area	23.64	0.57	82.68	1.99	147.16	3.54
Agricultural land	3516.9	84.7	3379.0	81.4	3173.8	76.4
Mixed forest	142.74	3.44	283.99	6.84	237.28	5.71
Barren land	325.64	7.84	284.08	6.84	470.94	11.34
Sand and open rocks	67.53	1.63	60.31	1.45	75.59	1.82

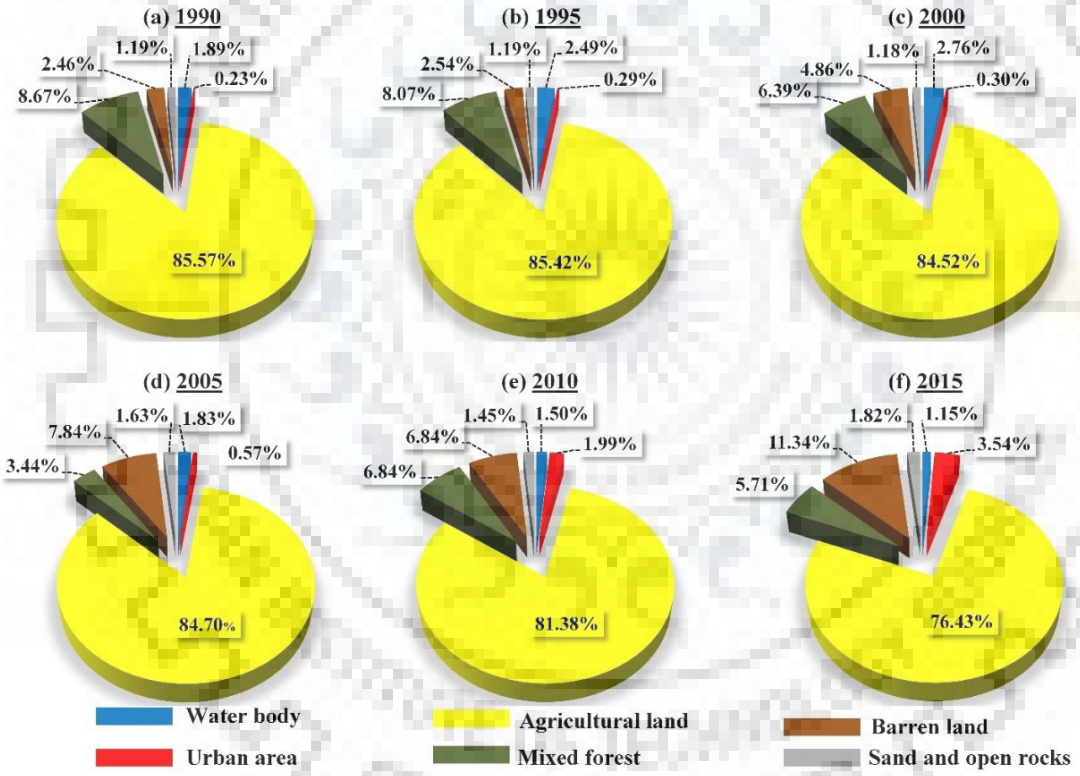

Figure 6.3 Percent of land distribution for various classes between 1990 and 2015.

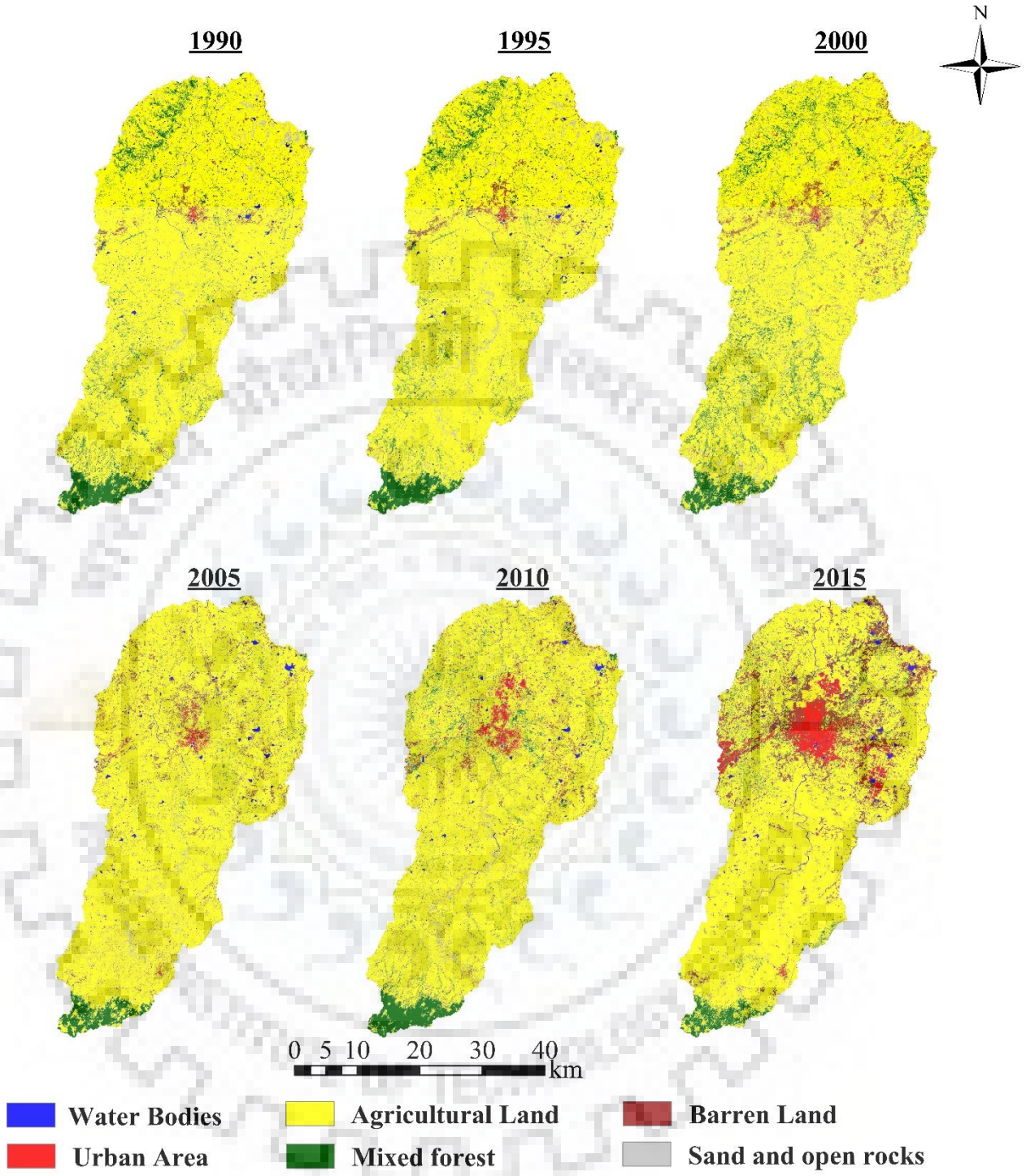

Figure 6.4 Land use/land cover maps of Kharun watershed between 1990 and 2015.

6.3.2 Accuracy Assessment

In order to measure the accuracy of the supervised classification, random control (representative) points were generated across each LULC map. Once these points were randomly generated, they were cross-checked with the reference GCPs collected during the field visit. Almost 350 GCPs were collected during the field visit. Moreover, the help of Google Earth in association with ERDAS imagine 2014 was also taken to verify the reference GCPs recorded using Global Positioning System (GPS). These control points were used for computing the accuracy of the LULC maps. The population error matrix of the LULC maps was used to generate accuracy statement statistics. The average overall accuracy was computed from observed accuracy (η_o) and the expected accuracy (η_E), as described in Eq. 6.2.

Around 180 random points were generated for each year (1990-2015). The location points of 2015 were collected by using the geographical positioning system (GPS) tool. The overall accuracy of all the LULC maps and Kappa statistics (K_p) of each class are presented in Table 6.4. From the Kappa statistics, it can be inferred that the overall accuracy for all the maps is between 78 - 87%, varying between different classes, which itself suggests that the maps have been classified satisfactorily.

Table 6.5 Kappa statistics (K_p) of all the classes for LULC maps between 1990 to 2015.

Accuracy type	LULC classes	1990	1995	2000	2005	2010	2015
Kappa coefficient (%age)	Water bodies	79	82	79	83	84	83
	Urban area	85	81	80	82	83	86
	Agricultural land	80	83	81	81	83	87
	Mixed forest	81	84	84	81	85	86
	Barren land	82	85	85	82	84	84
	Sand and open rocks	83	83	84	78	84	85

6.3.3 LULC Change Detection

Decadal, as well as demi-decadal change detection of LULC, was carried out to analyze the extent of change in land use and land cover of study area between 1990 and 2015. In order to have a better understanding, percent change in between two consecutive periods was computed along with percent change between two time periods keeping the base year of 1990 as constant, as shown in Figures 6.5 and 6.6, respectively. From Figures 6.5 and 6.6, it can be observed that the urban area has increased for each period but it increased by almost 250 % (59.03 km^2) between 2005 and 2010, which was most among all five years. Also, not much change was observed between 1990 and 2000, after which the urban area seems to increase rapidly. Between 2010 and 2015, the percent change was around

75% (64.47 km^2), even though the land area that has changed between 2010 and 2015 is more the percent change compared to 2005-2010 is less, which goes to explain that the rate of change has reduced in this period. A similar pattern of change was observed for barren land in the study area, with a maximum increase seen between 2010 and 2015 (65.78%). The percent change of barren land between 2005 and 2010 was -12.76% (-41.56 km^2). This may be due to massive real estate development and urban land expansion in the study area during that period, which turned barren/fallow land to urban land. Also, it was observed that agricultural land reduced continuously throughout the study period along with the mixed forest. Only exception was seen in the period of 2005 and 2010 when the share of mixed forest increases by almost 98% (141.24 km^2) due to massive afforestation drives and people awareness in the region but it again reduced by 16.45% (46.71 km^2) giving way to more of agricultural and urban land. The percent share of water bodies has also reduced in the study area.

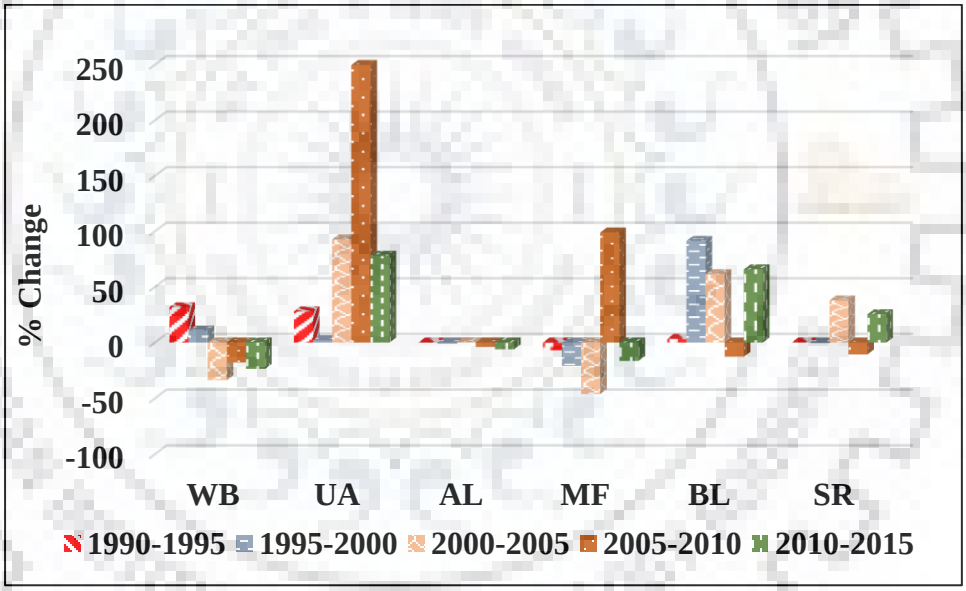

Figure 6.5 Demi-decadal percent change in LULC classes from 1990 to 2015.

As for the percent change in LULC classes with reference to the year 1990 as shown in Figure 6.6, it can be observed that the urban area has increased gradually since 1990 to 2015 from 27.9% between 1990 and 1995 to 1463% between 1990 and 2015, which is massive given a span of just 25 years. The percent share of barren land has also increased in the same manner, from 3.4% between 1990 and 1995 to 361.8% between 1990 and 2015. On the contrary water bodies, agricultural land and mixed forest have reduced gradually in the period. This clearly indicates that the floral region is giving way to urban settlement and barren land.

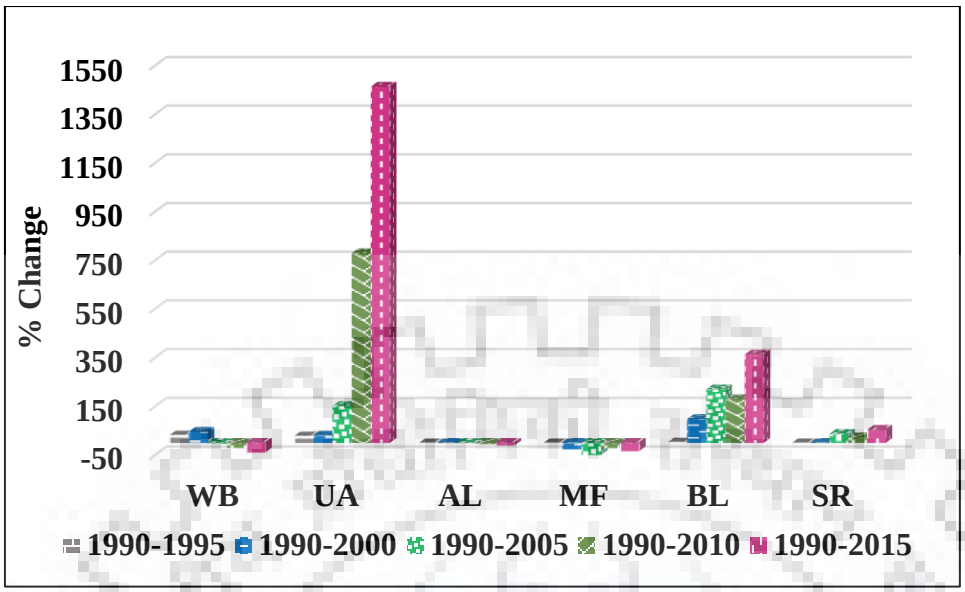

Figure 6.6 Percent change in LULC classes with reference to 1990.

Decadal changes of LULC classes between 1990 and 2015 indicate a spike in the percent change of urban area (573.82%) between 2000 and 2010 while increment was also observed between 1990 to 2000 and 2010 to 2015 as shown in Figure 6.7. Patterns similar to demi decadal changes were observed with an increase in barren land, sands, and open rocks accompanied by a decrease in water bodies, agricultural land and mixed forest.

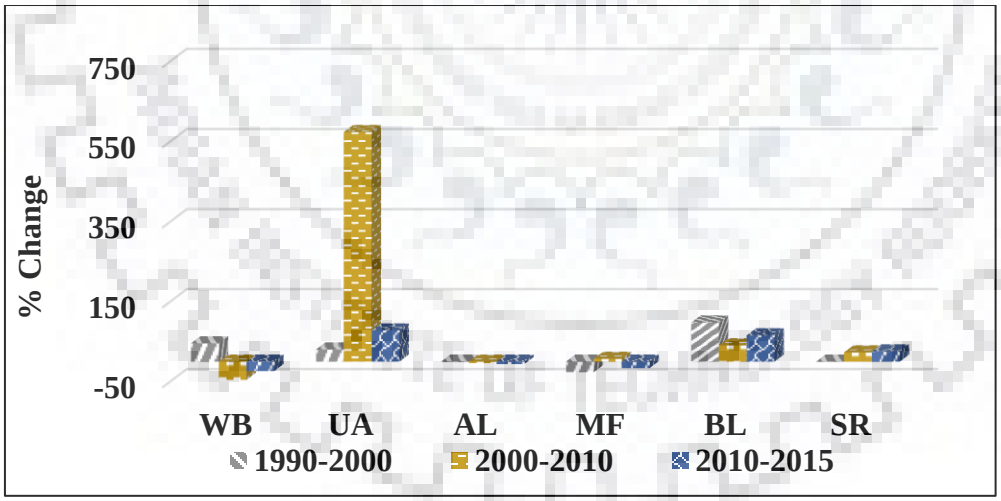

Figure 6.7 Decadal percent change in LULC classes from 1990 to 2015.

Not much abrupt changes were observed in the different classes between 1990 and 2000, but sudden changes in all the classes of the LULC maps were observed post-2000. The watershed lies in the state of Chhattisgarh (as discussed in Chapter 3), it received full statehood in the year 2000. The significant chunk of the urban area shown in various LULC maps is of Raipur city (Capital of

Chhattisgarh), and hence, due to massive urbanization owing to the fact the state capital was in Kharun watershed itself, this phenomenon of a sudden rise in an urban area can be explained. The percent change in different LULC classes with reference to the year 2000 was also computed as shown in Figure 6.8, which also shows that there is a gradual reduction in water bodies, agricultural land and mixed forest while there are a notable increase urban area and barren land. The urban area in the region increased by almost 1100% between 2000 and 2015, while barren land increased by almost 135% between that period.

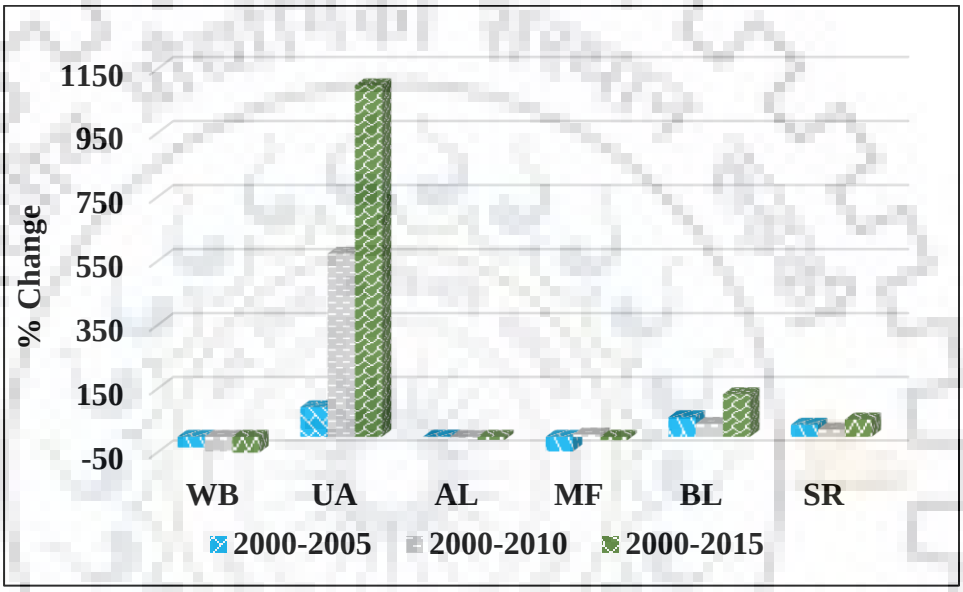

Figure 6.8 Percent change in LULC classes with reference to 2000.

6.3.4 Prediction of Future LULC and Change Detection from 1990 To 2030

Before the detection of changes in LULC distribution for the future, it is quite vital to know about the trend pattern of the past and present LULC changes. The information about the LULC pattern and the driving forces that are responsible for the change should be known before planning or execution of any policies in that region. By utilizing the knowledge of historical LULC changes, a change model of LULC can be developed in order to project the future map-making certain assumptions. In the present study, a combination of Cellular Automata and Markov Chain (CA-Markov) the model has been used for prediction of future LULC. The CA-Markov model is based on the transitional probability matrix. The reason behind using an integrated model was that the Markov model, which is a widely used model for future projection only provides the magnitude of change and does not provide direction of change. Hence, Cellular Automata (CA) model was also

incorporated with the Markov model since it provides the direction of change through spatial modeling (Petit et al. 2001).

Based on socio-economic information and land use planning of Kharun watershed from 1990 to 2005, three transition rules were opted for prediction of future LULC map of the year 2030. The first transition rule states that the factors which might influence the current LULC characteristic should not fluctuate considerably during the prediction of future LULC. The second rule considers speedy growth, which is based on the assumption that the LULC area changes rapidly while considering population growth, per capita living space, and floating population to meet the needs of the future scenario of 2030. The third rule ascertains ecological and farmland security, which means basic cropland and forestland cannot be converted into other categories and is considered as restricted area. By considering these three transition rules, LULC for the year 2030 was computed by applying the CA-Markov approach.

Initially, the model was validated by simulating the LULC distribution map of the year 2015, LULC maps of the year 1990 and 2005 were used for validation. Once the LULC map of 2015 was simulated, it was compared with the original classified LULC map as shown in Table 6.6. From the table, it can be observed that there is a close association between the classified and the simulated LULC of the year 2015 which gives further agree to the validation. The only notable anomaly found in the simulated LULC was that it slightly over predicted the class of water bodies (1.15% in classified, 3.20% in simulated). The projected LULC for the year 2030 indicates that there will be further increase in the urban area of the region, from 3.54% in 2015 to 6.73% in 2030. Also, the barren land in the area will further increase along with an increase in the water bodies. The projection for the year 2030 also indicated towards a further reduction in agricultural area from 76.43% in 2015 to 71.15% in 2030, while a slight decrease in the mixed forest was also observed. The percent land share of each class for the year 2030 is represented in Figure 6.9.

Table 6.6 Area statistics of the simulated (2015), classified (2015), and the projected (2030) LULC(s).

CLASS	Initial LULC (1990)		Final LULC (2005)		Classified LULC (2015)		Simulated LULC(2015)		Projected LULC (2030)	
	Area		Area		Area		Area		Area	
	Sq. km.	%	Sq. km.	%	Sq. km.	%	Sq. km.	%	Sq. km.	%
Water bodies	78.53	1.89	75.81	1.83	47.56	1.15	132.87	3.20	104.16	2.51
Urban area	9.41	0.23	23.64	0.57	147.16	3.54	193.08	4.65	279.57	6.73
Agricultural land	3552.96	85.57	3516.92	84.70	3173.75	76.43	3099.26	74.64	2954.39	71.15
Mixed forest	360.09	8.67	142.74	3.44	237.28	5.71	224.64	5.41	215.23	5.18
Barren land	101.98	2.46	325.64	7.84	470.94	11.34	438.90	10.57	557.16	12.42
Sand and open rocks	49.31	1.19	67.53	1.63	75.59	1.82	63.53	1.53	41.74	1.01

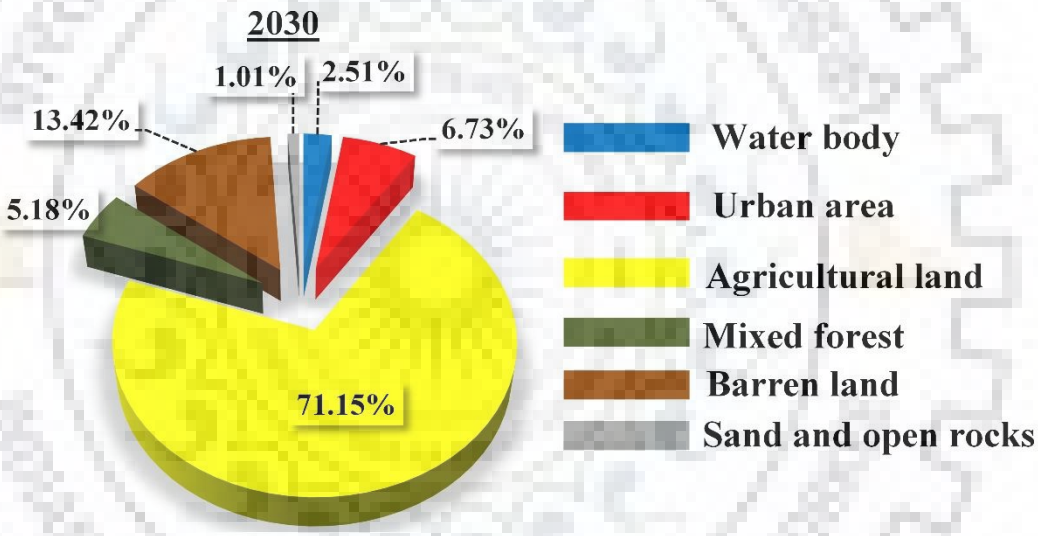

Figure 6.9 Percent of land distribution for various classes for projected LULC (2030).

Apart from the change in the magnitude of different LULC classes, one more critical aspect is the direction in which the change is happening. As discussed earlier the principal motive behind adopting an integrated model of CA-Markov was to get an understanding of the change in magnitude spatially as to how these changes in LULC class have taken place. The simulated LULC map for the projected the year 2030 is represented in Figure 6.10. As discussed earlier that the model was slightly over predicting the water body class for the simulated map of 2015 obtained from the LULC map of 1990 and 2015. Similar pattern has been observed for the simulated LULC map of the projected the year 2030, where the presence of blue pixels (representing water bodies) can be observed in certain places that belonged to some other class in previous LULC images. Besides the slight over prediction of water bodies, upon visualization, it can be said that the simulated LULC map for the projected

the year of 2030 is in accordance with the LULC maps of the past and such maps should be taken into account for the planning and also for the execution of policies in the future.

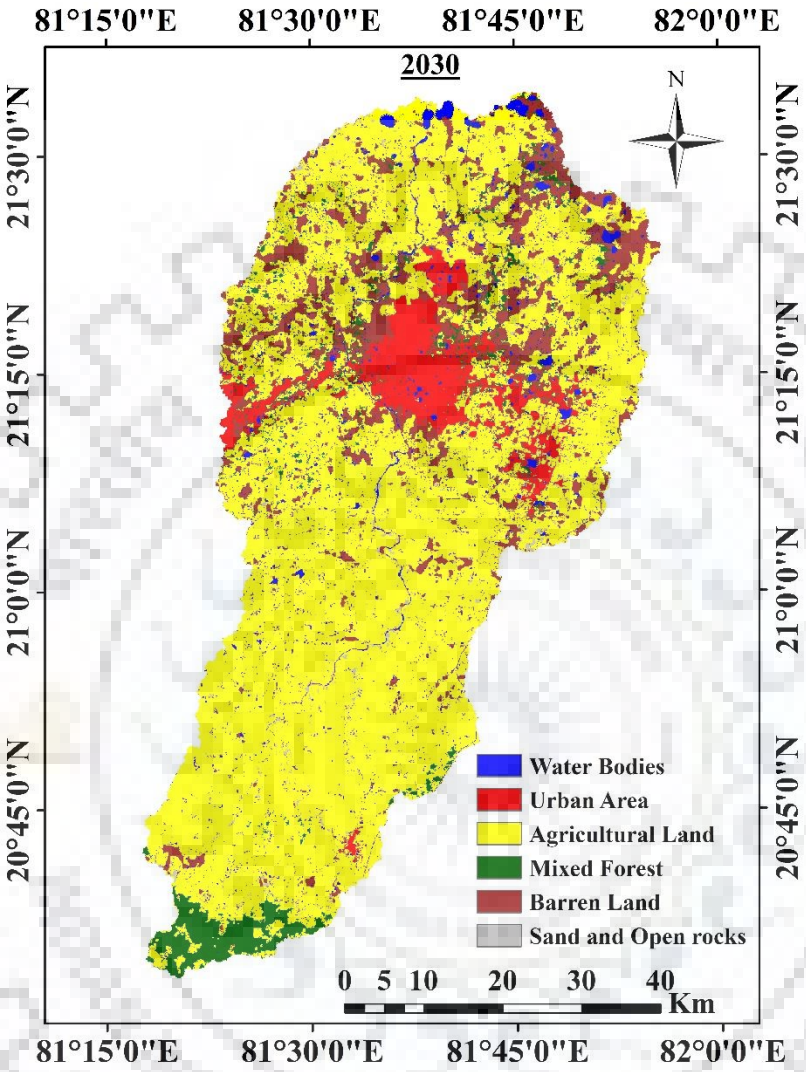

Figure 6.10 Simulated LULC map of the projected year 2030.

6.3.5 Causes of LULC Change Dynamics

Several natural and anthropogenic activities are the major causes of LULC change dynamics across the globe (Meyer and Turner 2003), having said that the extent of occurrence might differ from place to place. Population growth is one of the reasons for LULC change dynamics, but it cannot be stated with full authority that it is the sole reason for the change. Barbier and Burgess (1996) found out about the positive effects of population growth on the availability of resources. But, for a country like India, there is an immense pressure exerted over natural resources due to booming population growth and its implication can be seen in the form of erosion and soil degradation (Tripathi et al. 2004; Mondal et al. 2014). Natural causes such as climate change, as discussed in the

previous chapter, that have altered the rainfall intensities over the study area may worsen the situation of erosion in the study area. As for land degradation due to anthropogenic activities in the study area, the rate of LULC change has increased after the year 2000 (declaration of Chhattisgarh state). Since, the state capital lies in the Kharun watershed, the nearby areas of the city are giving way for further real estate development to accommodate the migrating population seeking newer/better job opportunities and livelihood. Mass migration towards the urban pockets of the study area may result in further change in land area in the region. In addition to his, a shortage of land resources might result in the conversion of cultivable (agricultural) land in the urban (paved) area and also to meet the food demand of growing population existing forest cover might give way to agricultural land.

6.3.6 The implication of LULC Change Dynamics

The gradual change in historical LULC classes is not susceptible to soil erosion and land degradation. However, rapid changes in LULC classes results in expansion of paved area (due to urbanization), and increase in barren and agricultural land which give rise to urban flooding and high level of soil erosion, particularly over the land surface without any vegetative cover (Schilling et al. 2009; Meshesha et al. 2016). Based on the historical classified images between 1990 and 2015 it can be inferred that there is a rise in urban area accompanied with the barren land for real estate development, upon analyzing the maps it was observed that the areas near the river banks are heavily urbanized (reduction in water bodies class) which will further deteriorate the riverfront in the study area. The conversion of lands with vegetation (mixed forest and agricultural land) into paved areas resulted in reduced infiltration and increased overland flow, which may become a root cause of urban flooding in the region. Also, an increase in barren land due to a reduction in vegetative cover will result in accelerated soil erosion in the region. The shifting of classes with vegetative cover into barren land is the primary source of intensive erosion, siltation in the river, floods and other water-borne diseases.

Rapid changes in LULC classes over the region can have severe implications in the region, the LULC changes in the region direct the attention towards increased urban settlement in the region along with intensive cropping to fulfill the food requirement of the population. Massive urbanization in the region results in the loss of biodiversity as well as degradation of existing land, a further increase in the migration towards the region exerts stress on policymakers to meet the needs of the increased population. Intensive cropping results in soil nutrient depletion of the agricultural fields which might

decrease crop productivity in the near future which will result in food insecurity in the region if the demands are not adequately met. A clear understanding of the implication of LULC dynamics can be achieved by referring to Figure 6.11 that details the conversion pattern of various LULC classes in the region and their further implications.

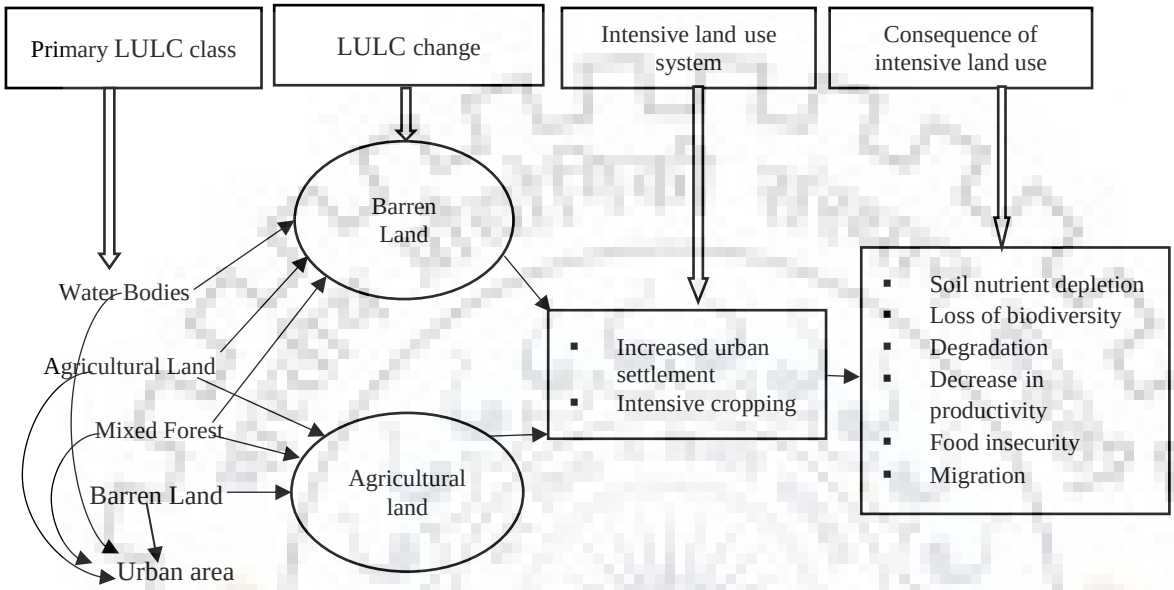

Figure 6.11 Conceptual linkage of cause and consequence of LULC change.

6.4 CONCLUDING REMARKS

Proper planning and policy making of any region requires a robust understating of LULC distribution for that area. The selective and micro information not only allows efficient land utilization management but also plays a vital role in future planning. In general, most of the towns and cities have altered their landscapes due to the increasing population in a haphazard and unplanned manner. So, in order to achieve sustainable development in any area, it is essential to understand the changing LULC patterns with time. By utilizing the knowledge of the present LULC scenario and learning from the mistakes in the past, one can hope for proper planning and sustainable development in the region. To achieve sustainable development, concerned agencies must provide a planning model so that the existing land can be utilized appropriately without damaging the natural vegetation. However, these types of planning models can only be conceptualized once the existing LULC changes and patterns are known. Keeping this view, the study of LULC change dynamics was carried out for the study area (Kharun watershed). LULC mapping was carried out for the region by using satellite imageries (LANDSAT 5, 7, and 8) by application of RS and GIS tools such as ERDAS Imagine and ArcGIS 2012. The LULC maps were classified into six different classes namely water

bodies, urban areas, agricultural land, barren land, mixed forest and sand/open rocks. The changes between different classes between 1990 and 2005 were evaluated at decadal as well as the demi-decadal level. Significant findings in the study stated that there is a decrease in vegetation (agricultural land and mixed forest) in the region, giving rise to an urban area and barren land. After the analysis of historical trend patterns in LULC, the LULC map for the near future (2030) was projected using the CA-Markov model. The model was validated and simulated with the classified LULC map of 2015. The projected LULC map of 2030 indicated the continuation of the same trend of the past. The model slightly over predicted the water body class for the simulated map of 2015 obtained from the LULC map of 1990 and 2015. Similar pattern were observed for the simulated LULC map of the projected the year 2030. The overestimation may due to different various sources of uncertainties such as input parameters, model processes and prediction uncertainties. If we add more number(s) of LULC periods data, these uncertainties may be reduced in future. These future projections indicate the expected changes in the near future. These LULC changes with respect to different classes in the near future will caution the concerned authorities for proper planning and management of the study area.

CHAPTER 7

HYDROLOGICAL SIMULATION UNDER LULC AND CLIMATE CHANGE SCENARIOS

7.1 GENERAL

In order to fulfill the water demand of the domestic, agricultural, and industrial sectors, it is mandatory to know the availability of water in that region. Understanding the current situation of water resource availability in the region and its variation due to historical physiographical and climate changes helps in sustainable planning and development. Enough shreds of evidence have been published in the past that directs attention towards the phenomenon of climate change and its implication over the hydrology and water resources (Ficklin et al. 2009; Liu et al. 2015; Niraula et al. 2015). Various studies have concluded that the significant factors that influence the climate system or effect global warming in one form or other are anthropogenic activities and emission of Green House Gases (GHGs) (Graham et al. 2007a; Zhu 2012; Omer et al. 2017; Veettil and Mishra 2016). Increasing the concertation of GHGs in the atmosphere rapidly modify the magnitude and frequency of hydro-climatic parameters. The projection of water availability on regional hydrology depends upon land use/land cover (LULC) and principal climatic variables (precipitation and temperature) from the regional climate model (RCMs).

In many parts of the globe, there has been a drastic change in the LULC classes for the last few decades and hence, change in the hydrological and ecological behavior of the area (Bronstert et al. 2002; Samal and Gedam 2012; Thakkar et al. 2017a). Due to human-made and natural activities, the change of runoff and water yield are very significant, a significant role in these changes is of LULC change dynamics and climate change on the overall hydrological conditions (Ficklin et al. 2009; Samal and Gedam 2014; Wu et al. 2016). Hence it becomes vital to know about the implication of changes in hydrology due to the combined effect of LULC and climate change (Srivastava et al. 2012; Zahabiyoun et al. 2013; Niraula et al. 2015; Thakkar et al. 2017b; Zope et al. 2017). Also, in order to project the changes in various hydrological components or other words changes in the water balance components, it is essential to know about the historical changes in climate and land use individually (Behera and Panda 2006; van Griensven and Meixner 2006; Khoi and Suetsugi 2014; Trang et al. 2017).

However, minimal studies are available that have studied water availability in a region by considering both LULC change dynamics and the effect of climate change. Moreover, hydrological simulation is not possible without a calibrated hydrological model set up for the region. In order to calibrate the model, many hydrological parameters cannot be measured directly in the field but must be obtained through a model calibration process. Model calibration is thus an essential task to obtain the optimal parameter values, which match simulations with observations as closely as possible. As already have been discussed in the earlier section, there are very few studies based on an assessment of hydrological responses under the dynamics of LULC and climate change over tropical watersheds. Keeping this issue in mind, hydrological impact assessment under land use and climate change scenarios were carried out over a tropical watershed (Kharun). Hence the aims of the study presented in this chapter are:

(A) Setup the semi-distributed hydrological model (SWAT) and check the suitability of the model over Kharun watershed.

(B) Computation of LULC change impact on water availability under constant climatic conditions.

(C) Evaluation and assessment of hydrological components (precipitation, evapotranspiration, and water yield) under future scenarios from 2011 to 2100 under IPCC AR5 representative concentration pathways (RCPs), moderate emission scenario (RCP 4.5) and high emission scenario (RCP 8.5).

The overall framework of the study detailing the SWAT model setup, description of LULC maps and climate data and impact assessment on water availability due to land use and climate change scenarios are represented in Figure 7.1.

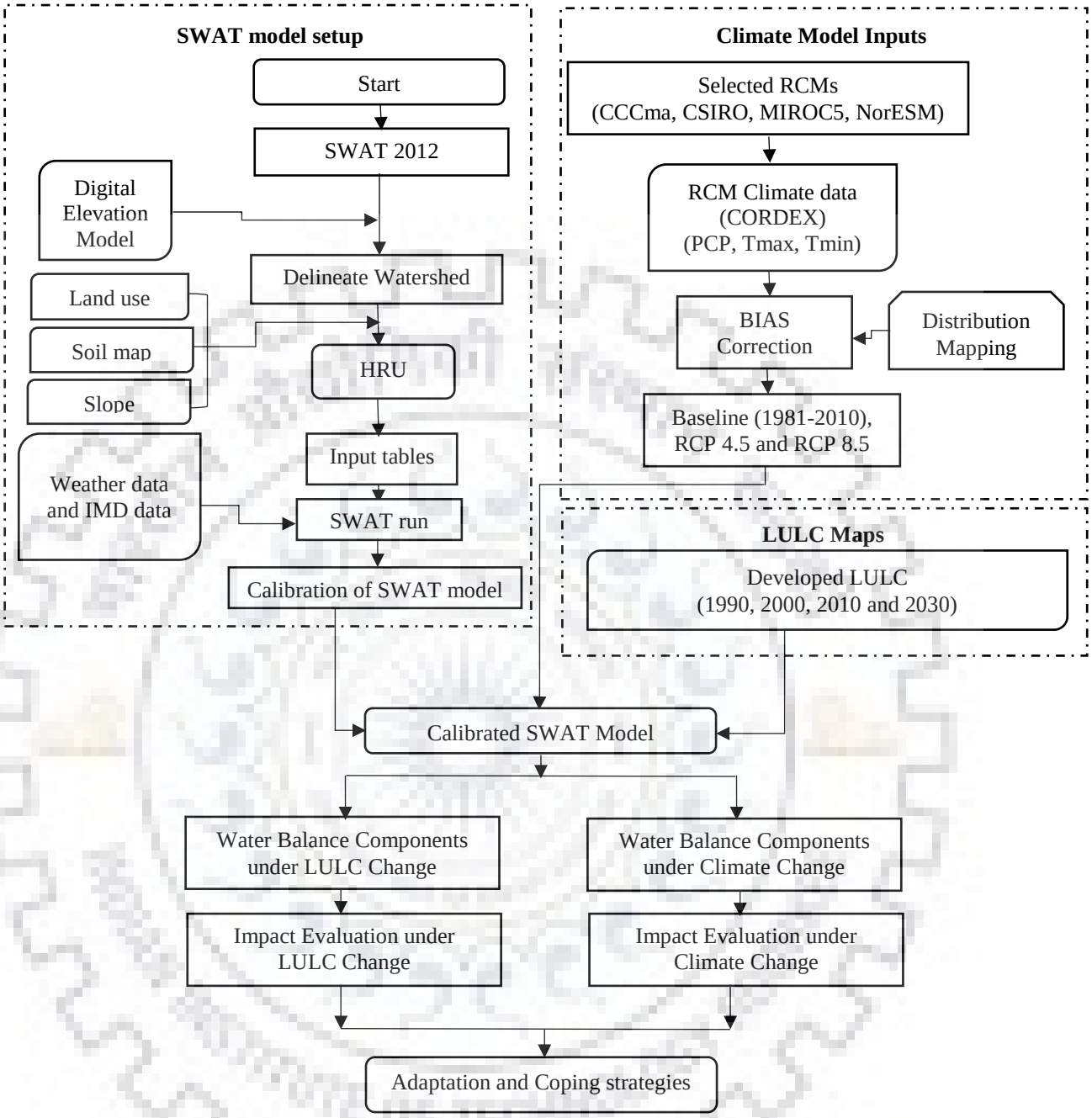

Figure 7.1 Framework of impact assessment on water availability due to land use and climate change scenarios.

7.2 MATERIALS AND METHODS

7.2.1 Description of the Study Area

Kharun (a tropical watershed) was chosen for determining the hydrological response simulation under different land use and climate change scenarios, the details of the study have already been discussed thoroughly in Chapter 3.

7.2.2 Data Used During Processing

7.2.2.1 Spatial data

Various types of spatial data are used as input for the simulation of the SWAT model. Spatial data that were used for SWAT model simulation in this study are:

(a) Digital Elevation model (DEM): DEM is the 3D representation of the study area's terrain. In the present study, a DEM of 30m resolution was used, it was provided by Shuttle Radar Topographic Mission (SRTM). The projection of DEM used in the study had a projection system of WGS_1984_UTM, Zone_44N.

(b) Soil Map: The digital soil map of the entire Earth was provided by Food and Agricultural Organization (FAO). The soil map was acquired at a scale of 1:5,000,000. The details of the soil types found in the study area have been discussed in Chapter 3.

(c) Land use map: The LULC data is essential for hydrological modeling. The LULC of an area is one of the significant factors which affect water yield, evapotranspiration and erosion in the watershed. For calibration and validation of the SWAT model the LULC map of 2010 was used. While LULC maps of 1990, 2000, 2010, and 2030 were used for computing water balance components for each LULC. All LULC maps (1990, 2000 and 2010) were developed using supervised classification and projected (2030) using CA-Markov model, as discussed in Chapter 6.

The distribution of different elevation, slope, land use classes, and soil map of Kharun watershed are presented in Figure 7.2.

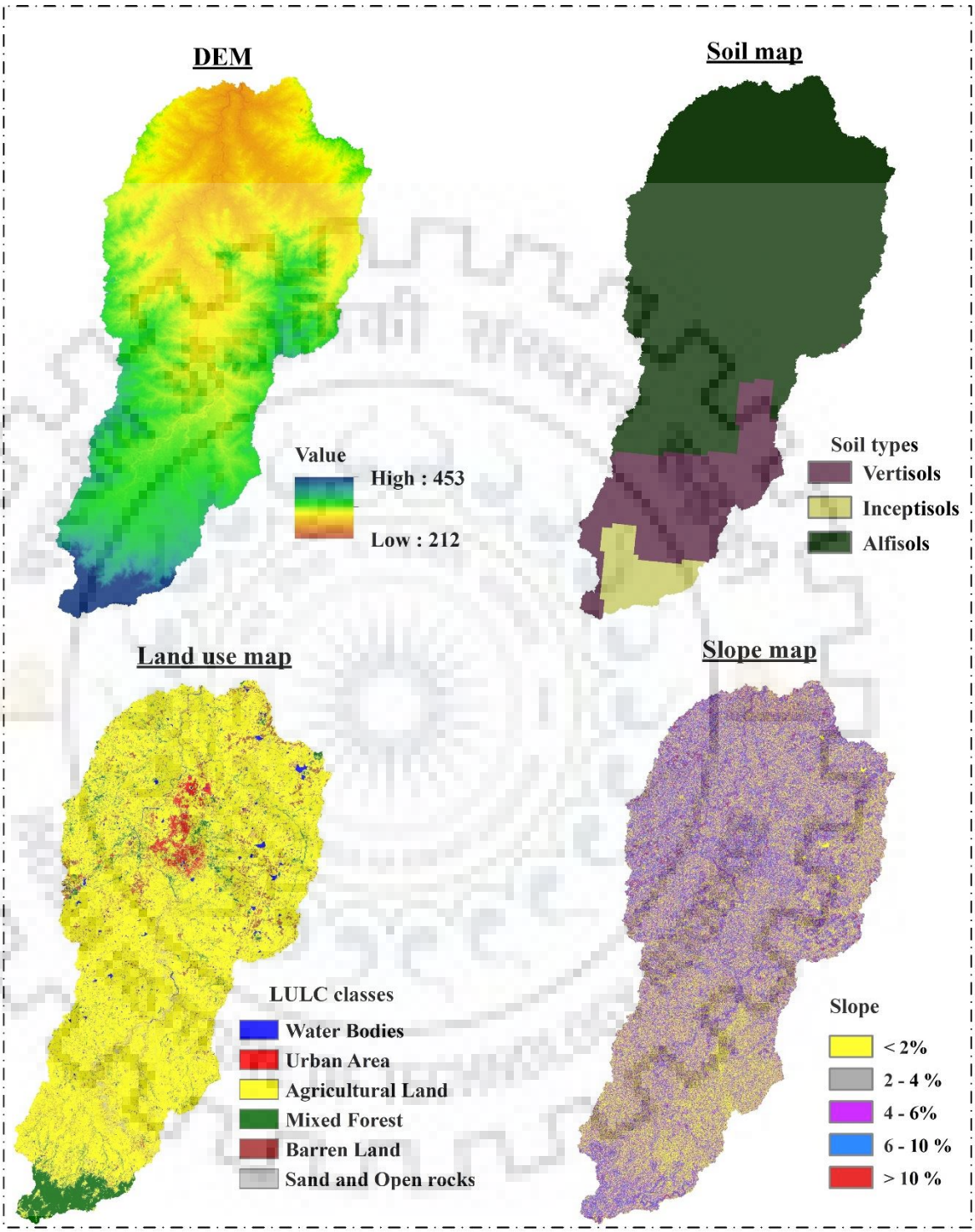

Figure 7.2 Spatial data (DEM, soil map, land use map, and slope map) used for hydrological modeling.

7.2.2.2 Hydro-meteorological data

(a) Discharge data: In order to calibrate and validate the modeled output, actual/observed data are required. Discharge data of Kharun watershed have been collected to calibrate and validate the model. Discharge data for 27 years was acquired from the Patherdihi Gauge discharge site of the Central Water Commission (CWC) on Kharun River. Further details of the data and location of the gauging site have been discussed in Chapter 3.

(b) Weather data: Gridded datasets of precipitation with high resolution ($0.25^{o} \times 0.25^{o}$) and resampled daily gridded datasets of temperature at the resolution of $0.25^{o} \times 0.25^{o}$ were used for the study. The data were acquired from the India Meteorological Department (IMD), the details of which, as well as the resampling technique, have been described thoroughly in Chapter 3.

(c) Regional climate data: To compute the variation in water balance components in the future, data of the Regional Climate Model (RCM) was used in this study. The spatial resolution of each RCM was $0.4^{o} \times 0.4^{o}$.

7.2.3 Hydrological Modelling Using SWAT

In the present study, Soil and Water Assessment Tool (SWAT) was used to simulate the water availability in the study area. SWAT is a semi-distributed, physically-based hydrological model operated at a daily or monthly time step (Arnold and Allen 1996; Neitsch et al. 2011). SWAT model possesses the ability to simulate crucial hydrological processes like past, present, and future hydro-climatic changes. In the SWAT model, changes in hydro-climatic futures can be simulated, considering different climate and land-use projections (Ullrich and Volk 2009).

For hydrological response, the model divides the main watershed into small sub-watersheds and sub-watersheds into small hydrological response units (HRU) connected through the drainage network (Green et al. 2006; Golmohammadi et al. 2017). HRU is the lumped unit that comprised of the unique combination of LULC, soils and slope area that allows routing of flows to the downstream sections (Neitsch et al. 2011). Spatial data and the hydro-meteorological data are the primary inputs of the SWAT. Hydro-meteorological inputs include climatic data such as precipitation, temperature (minimum and maximum), relative humidity, wind speed and solar radiation (Arnold et al. 1998). As discussed briefly in section 7.2.2.1, Digital elevation Model (DEM), Soil map, LULC map and slope map are spatial inputs that are required for hydrological modeling using SWAT (Singh et al. 2005; Arnold et al. 1998; Neitsch et al. 2011; Worku et al. 2017). The first step

in determining hydrological responses of a watershed is the delineation of the watershed in order to identify the watershed features such as gradient and slope length, characteristics of stream networks etc. The delineation of the watershed was done using the ArcSWAT interface (incorporated in ArcGIS 10.2) using DEM.

7.2.3.1 Model equations

For the process of simulation of the hydrological cycle, the water balance equation used in the SWAT model is given as (Wang et al. 2014a):

$$SW_t = SW_0 + \sum_{i=1}^{t}(R_{day} - Q_{surf} - E_a - W_{sweep} - W_{gw}) \quad (7.1)$$

In which SW_t means the final soil water content in mm; whereas, SW_0 means the initial soil water content in mm; time is represented by t in days; while R_{day} means precipitation volume in specific days of i in mm; the volume of runoff in specific day I is represented by Q_{surf} in mm; the volume of evapotranspiration happening in specific day i is represented by E_a (mm); W_{sweep} means the percolated water amount into the vadose zones through soil in day i in mm; W_{gw} represent volume of return flow volume in day i in mm.

Water yield

Water yield can be defined as the aggregated sum of water that leaves the Hydrological Response Unit (HRU) and enters the principle channel at a particular time step. For sustainable water resource management, one of the most crucial parameters that need to be evaluated is the water yield. Water yield within a watershed can be evaluated as (Wang et al. 2014a):

$$W_{yld} = Q_{surf} + Q_{gw} + Q_{lat} - T_{loss} \quad (7.2)$$

where W_{yld} is the water yield in mm; Q_{surf} refers to the surface runoff in mm; Q_{lat} denotes the lateral subsurface flow in mm; Q_{gw} is the groundwater contribution to streamflow (baseflow) and T_{loss} is the overall transmission loss (mm) in the channel due to transmission through the bed.

Surface Runoff

Three different options are present to predict the runoff process from the Hydrological Response Units (HRUs). Amongst them, the SCS curve was employed to predict runoff from daily rainfall, as per USDA-SCS 1972. SWAT being a comprehensive model have been used in various studies across

the globe to estimate runoff processes (Alibuyog et al. 2009; Sajikumar and Remya 2015a; Uniyal et al. 2015). Hence, in this present study, the simulation of surface runoff processes and estimation of peak runoff of HRUs were done in the SWAT model. In this study, SCS-CN was used to estimate runoff and is given by:

$$Q_{surf} = \frac{(P - I_a)^2}{(P - I_a) + S} \tag{7.3}$$

In which, Q_{surf} shows the volume of runoff depth in mm; while effective precipitation (mm) is represented by P; initial water abstraction (mm) is represented by I_a; maximum potential retention is represented by using S. However, water abstraction initially I_a is a function of optimum potential retention S. Hence,

$$I_a = \lambda S \tag{7.4}$$

where λ is a constant, its value lies between 0.2-0.5. In the present study, the value of λ was considered as 0.2.

Hence, Initial abstraction (I_a) can be rewritten as:

$$I_a = 0.2S \tag{7.5}$$

Rearranging Eq. 7.3 based on Eq. 7.4, we have:

$$Q_{surf} = \frac{(P - 0.2S)^2}{(P + 0.8S)} \tag{7.6}$$

The runoff occurs when the amount of precipitation exceeds 0.2 times the maximum potential retention ($P > 0.2S$). Generation of runoff depends upon various watershed characteristics such as the slope of the catchment, soil types, land-use practices, topography and also upon maximum potential retention. Hence, the maximum potential retention (S) is correlated with the curve number (a dimensionless parameter) moreover, is given as:

$$S = \left(\frac{25400}{CN}\right) - 254 \tag{7.7}$$

Once, the SWAT is modeled, calibrated and validated it yields various water balance components such as infiltration, percolation, evapotranspiration etc.

Base Flow

Groundwater contribution to streamflow or base flow is defined as that portion of streamflow that the stream sustains in the lean periods (between precipitation events). Groundwater flow is fed to the streams by delayed pathways. Baseflow is also denoted as groundwater recession flow, low-water flow, fair-weather runoff etc. The base flow can be estimated as (Schilling et al. 2009):

$$Q_{gwj} = Q_{gwj-1} \cdot e^{\left(-\alpha_{gw} \cdot \Delta t\right)} + W_{rchrg} \cdot \left(1 - e^{\left(-\alpha_{gw} \cdot \Delta t\right)}\right) \tag{7.8}$$

where Q_{gwj} means the groundwater flow (mm/day) in the main channel on any day j; α_{gw} is the base flow recession constant; W_{rchrg} is the amount of recharge (mm/day) that might enter the acquirer.

Lateral Subsurface Flow

Streamflow contribution that generates below the surface is called as lateral subsurface flow or interflow. Lateral subsurface flow is estimated simultaneously with redistribution in the soil profile. For each soil layer, to predict the lateral subsurface flow, a kinematic storage model is used. The model also keeps into account the variation in different soil parameters such as soil conductivity, slope, and soil water content. The later subsurface flow or in many cases the interflow is given as (Heuvelmans et al. 2004):

$$Q_{lat} = 0.024 \frac{\left(2S_v \cdot SC \cdot \sin\alpha\right)}{\left(\theta_d L\right)} \tag{7.9}$$

where Q_{lat} is the lateral subsurface flow in mm/day; S_v is the volume of soil water drained per unit area of saturated thickness in mm/day; SC is the saturated hydraulic conductivity in mm/hr; L is the length of the flow; α is the slope of land; θ_d is the drainable porosity; CN is the curve number of soil is discussed above.

Potential Evapotranspiration (PET)

Potential Evapotranspiration (or PET) is defined as the rate of evapotranspiration (ET_o) of a large area that occurs over a uniformly covered area having a vegetative cover with an unlimited water supply. It is based on the assumption that there will be no effect of micro-climatic processes like the effect of heat-storage or advection. PET can be estimated by three methods in the SWAT model,

namely the Hargreaves-Samani method (Hargreaves and Samani 1985), Priestley-Taylor method (Priestley and Taylor 1972), and Penman-Montieth method (Monteith 1965).

7.2.4 SWAT Model Setup

7.2.4.1 Watershed delineation

The first step in the simulation of hydrological processes using SWAT is the delineation of a watershed using DEM. It is necessary because the delineation process provides specific sub-watershed and watershed. In order to delineate the watershed, the DEM was imported into the ArcSWAT environment using ArcGIS 10.2. Watershed delineation comprises five primary steps, which include DEM setup, inlet, and outlet definition, the definition of stream, watershed outlet selection, definition, and calculation of each sub-watershed and watershed parameters, as shown in Figure 7.3.

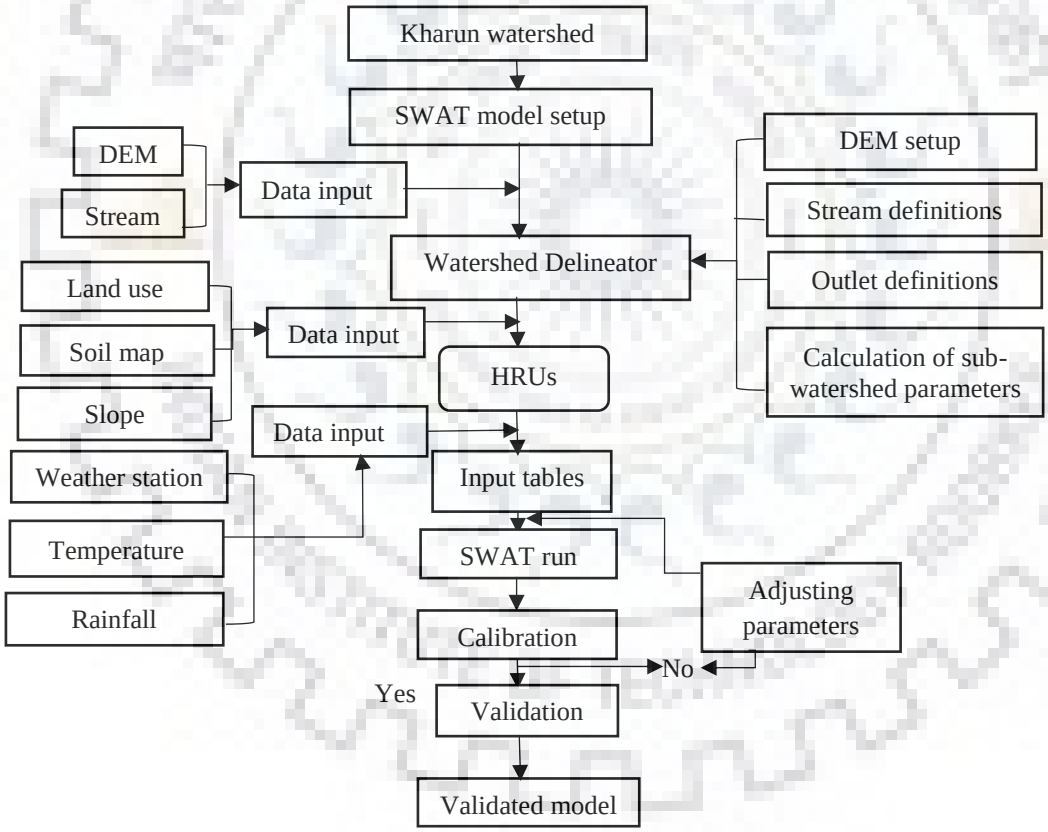

Figure 7.3 Detailed framework for SWAT model setup, calibration, and validation.

In the present study total, 27 sub-watersheds were delineated that are represented in Figure 7.4. Also, the reach of the river, as well as the location of modelled outlet and the location of Patherdihi gauging site, have been shown.

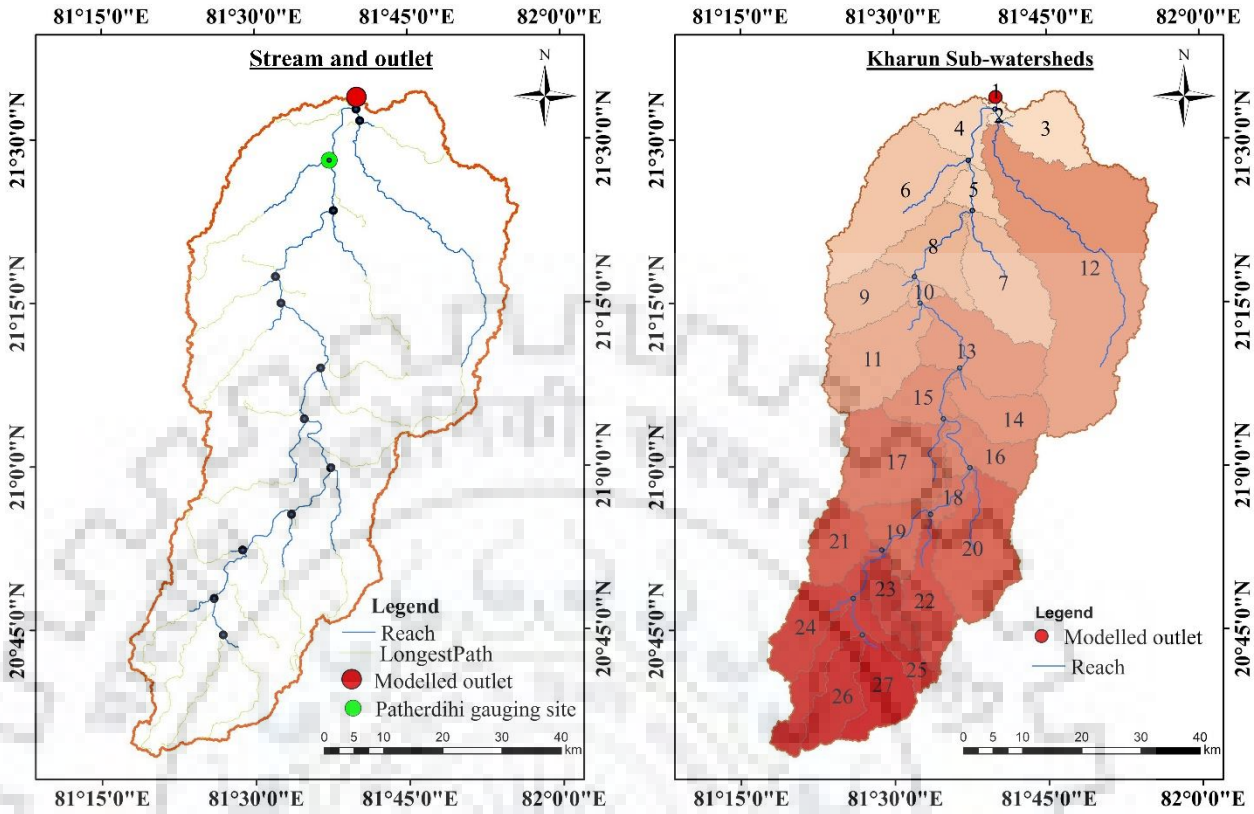

Figure 7.4 Description of stream networks, outlets, gauging site, and sub-watershed of Kharun watershed.

7.2.4.2 Hydrological Response Units (HRUs)

After the watershed delineation, Hydrological Response Units (HRUs) are generated. The HRUs may be defined as a cohesive unit made from the combination of land use, slope, and soil type of the region. The purpose of HRUs is to set up various soil layers, LULC map and soil maps into the SWAT project. Almost 100 % (99.07%) of the simulated area overlapped with the actual area, as represented in Table 7.1. As discussed earlier, the SWAT model employs LULC and soil data to determine HRUs of each sub-watershed. LULC categories (obtained by supervised classification) were used and a soil lookup table was used to identify various soil types. Reclassification of slope, soil and LULC maps were carried out. The different threshold for various parameters was considered for the study such as 20% for LULC, 10% for soil and 20% for slope. The determination of threshold values was based on multiple HRU delineation methods. The delineation process subdivided the watershed into 27 sub-watersheds as shown in Figure 7.4, and these sub-watersheds were further divided into 1124 HRUs for modeling purposes.

Table 7.1 Characteristics of gauging site.

Gauging Site	Latitude	Longitude	Actual Area (km^2)	Simulated Area (km^2)	Difference in Area (%)
Patherdihi	21º 20’ 28’ N	81º 35’48” S	4191	4152	0.93

7.2.4.3 Uncertainty and sensitivity analysis

A hydrological model should be capable of sufficiently predicting water balance components and to determine whether that hydrological model is robust or not, sensitivity analysis is carried out along with model calibration and validation. The purpose of carrying out sensitivity analysis is to know-how about the influence of various parameters over the predicted model. In the present study, the method of Latin Hypercube One Factor At a Time (LHOAT) was used for sensitivity analysis (Morris 1991) using SWAT-Calibration Uncertainties Program (SWAT-CUP). It is a widely used tool for the sensitivity evolution of a model that can also assess model calibration and parameter uncertainty (Van Liew et al. 2007; Narsimlu et al. 2015; Dakhlalla and Parajuli 2016).

Sequential Uncertainty Fitting Version 2 (SUFI-2) algorithm was used for the analysis and determination of uncertainties related to model calibration and validation and to identify the most sensitive input variables for the watershed (Abbaspour 2015). The value of *r*-factor as well as *p*-factor was used to assess the degree of uncertainty and goodness fit. *P*-factor is assessed by estimating the percentage of observed and simulated values bracketed by 95% prediction uncertainty. While the value of *r*-factor is assessed using an average thickness of percentage prediction uncertainty band (95ppu) and standard deviation of predicted and observed data (Abbaspour et al. 2007). The value of the *p*-factor lies between 0-100%, while the value of the *r*-factor is between zero and infinity (0 - ∞). The simulation correction is judged by the values of *r*-factor and *p*-factor that corresponds to the actual/observed and simulated/measured data. Hence, in order to evaluate the capability of the model calibration process and to evaluate the extent to which the simulated results deviated from these values, the *r*-factor and *p*-factor are employed.

7.2.4.4 Model performance evaluation

In the present study, model performance was evaluated using the coefficient of determination (R^2) and Nash-Sutcliffe efficiency (NSE) and Percent BIAS (PBIAS).

In general, the model is acceptable if the Coefficient of determination (R^2) is higher than 0.5, and calculated as:

$$R^2 = \left[\frac{\sum_{i=1}^{n} (O_i - O_{avr})(P_i - P_{avr})}{\left[\sum_{i=0}^{n} (O_i - O_{avr})^2 \sum_{i=1}^{n} (P_i - P_{avr})^2 \right]} \right]^2 \quad (7.10)$$

where the term O_i is i^{th} observed value, O_{avr} is the average observed value of total periods; P_i means the i^{th} modeled value and P_{avr} represents the average modeled value of the total periods.

According to Pandey et al. (2017), Nash-Sutcliffe efficiency (NSE) ranges from -∞ to 1, where 1 indicates perfect simulation against observed value. NSE was adopted as the parameter for the model evaluation in this study because it is known for its applicability and reliability in hydrological modeling (Tantawy et al. 2007; Legates and Mccabe 2013).

$$NSE = 1 - \left[\frac{\sum_{i=0}^{n} (O_i - P_i)^2}{\sum_{i=1}^{n} (O_i - O_{avr})^2} \right] \quad (7.11)$$

Percent Bias (PBIAS) indicated the underestimated or overestimated observed variable.

$$PBIAS = \left[\frac{\sum_{i=1}^{n} (O_i - P_i) * 100}{\sum_{i=1}^{n} (O_i)} \right] \quad (7.12)$$

where Q_o and Q_s represent the observed discharge and simulated discharge respectively.

In order to evaluate the performance of the calibrated and validated SWAT model, statistics of evaluation parameters in hydrology for the monthly time step are given in Table 7.2.

Table 7.2 Range of performance evaluation during calibration and validation.

Model used	value	Rating performance	Modeling stages	Reference
SWAT	**R^2**			
	>0.5	Very good	Calibration and validation	(Moriasi et al. 2007)
	<0.5	Unsatisfactory	Calibration and validation	(Moriasi et al. 2007)
	NSE			
	≥0.65	Very good	Calibration and validation	(Saleh et al. 2000)
	0.54 to 0.65	Adequate	Calibration and validation	(Saleh et al. 2000)
	>0.50	Satisfactory	Calibration and validation	(Saleh et al. 2000)
	PBIAS			
	<10%	Very good	Calibration and validation	(Van Liew et al. 2007)
	<10% to <15%	Good	Calibration and validation	(Van Liew et al. 2007)
	<15% to <25%	Satisfactory	Calibration and validation	(Van Liew et al. 2007)
	>25%	Unsatisfactory	Calibration and validation	(Van Liew et al. 2007)

7.3 RESULTS AND DISCUSSIONS

7.3.1 Model Sensitivity Analysis

After the SWAT model setup that includes delineation of the watershed, generation of HRUs, and writing of input table using meteorological and spatial data, the SWAT run was executed. However, before the interpretation of the modeled results, it is mandatory to know about the most sensitive parameters that may affect the runoff generation in the model (Kannan et al. 2007; Chapi et al. 2015). For this purpose, a sensitivity analysis was performed. During the sensitivity analysis, the value range (Minimum, maximum and fitted value) of different parameters was identified using the SWAT user's manual (Neitsch et al. 2011; Abbaspour 2015). As discussed earlier, the LHOAT technique was adopted for performing one-at-a-time sensitivity analysis (van Griensven et al. 2006; Green and van Griensven 2008). For this purpose, 27 hydrological parameters were selected initially, out of which 15 parameters were found to be most sensitive and their values were adjusted based on an acceptable agreement between observed and simulated values. The ranking and description of the most sensitive parameters have been represented in Table 7.3. In this table, the parameter with the least rank is the most sensitive parameter and vice-versa. The list of sensitive parameters along with their minimum, maximum and fitted value has been represented in Table 7.4.

Table 7.3 Description and ranking of the most sensitive parameters.

Rank	Parameter Name	Definition
1	V__ALPHA_BF.gw	Baseflow alpha factor (days)
2	R__EPCO.bsn	Plant uptake compensation factor
3	R__RCHRG_DP.gw	Deep aquifer percolation fraction
4	R__SOL_Z(..).sol	Maximum rooting depth of soil profile
5	V__GW_DELAY.gw	Groundwater delay (days)
6	R__ESCO.bsn	Soil evaporation compensation factor
7	R__BIOMIX.mgt	Biological mixing efficiency
8	V__GWQMN.gw	Threshold depth of water in the shallow aquifer required for return flow to occur (mm)
9	R__SURLAG.bsn	Surface runoff lag time
10	R__SOL_BD(..).sol	Moist Bulk Density
11	R__CH_K2.rte	Effective hydraulic conductivity in main channel alluvium
12	R__SOL_AWC(..).sol	Available water capacity of the soil layer
13	R__GW_REVAP.gw	Groundwater "revap" coefficient.
14	R__CN2.mgt	SCS runoff curve number
15	R__SOL_K(..).sol	Saturated hydraulic conductivity

Table 7.4 Minimum (Min.), maximum (Max.), and the fitted values of sensitive parameters.

S. No.	Parameter Name	Change type	Min.	Max.	Fitted value
1	ALPHA_BF.gw	Replace	0	1	0.69
2	EPCO.bsn	Relative	0	1	0.36
3	RCHRG_DP.gw	Relative	0	1	0.35
4	SOL_Z.sol	Relative	0	3500	1606.5
5	GW_DELAY.gw	Replace	0.34	3.46	2.76
6	ESCO.bsn	Relative	0	1	0.9
7	BIOMIX.mgt	Relative	0	1	0.94
8	GWQMN.gw	Replace	0	2	1.11
9	SURLAG.bsn	Relative	0.05	24	0.79
10	SOL_BD(..).sol	Relative	0.9	2.5	1.9
11	CH_K2.rte	Relative	0.01	500	209.51
12	SOL_AWC.sol	Relative	0.11	0.23	0.23
13	GW_REVAP.gw	Relative	0.02	0.2	0.18
14	CN2.mgt	Relative	-0.3	0.1	-0.27
15	SOL_K.sol	Relative	0	2000	70

7.3.2 Calibration and Validation of the SWAT Model

Both graphical, as well as statistical tests, were carried out during the calibration of the model. For calibration and validation, the entire discharge data series 27 (1987-2014) series was broken into three parts. The first three years (1987-1990) was opted for the warmup period of the SWAT model. For the calibration of the SWAT model, data from 1990 to 2005 (15 years) were considered, while the rest of the data was used for validation. Calibration of the model was performed by automatic calibration technique using the Sequential Uncertainty Fitting Version 2 (SUFI-2) Algorithm in SWAT-CUP 2012 version of 5.1.6.2. The most sensitive parameters (Table 7.3) were calibrated with 500 combinations of 3 iterations between 1990 and 2005. Validation of the model was done similarly by using the outputs from the calibration process. The results of the calibration and validation of the model have been represented in Figure 7.5 and Figure 7.6 respectively. Upon visual interpretation of the results, it can be inferred that there is a close match between the observed discharge data at the outlet and the simulated/modeled discharge obtained from the SWAT model. It can be observed that the peaks are matching perfectly in almost all the years barring few exceptions, which further suggests that the model can very well estimate the peak floods in the region. Also, it was found that for almost all the years, the peaks representing the simulated discharge are taller than the peaks representing the observed/actual discharge, although it is quite similar. Hence, it can be inferred that the model is slightly over-predicting the streamflow in the watershed.

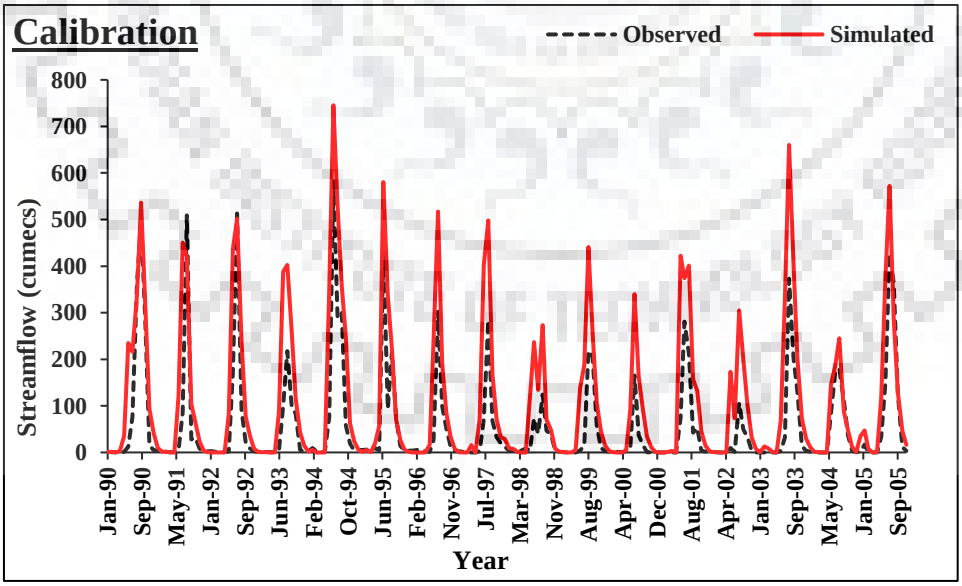

Figure 7.5 Calibration plot of simulated and observed discharge at the outlet.

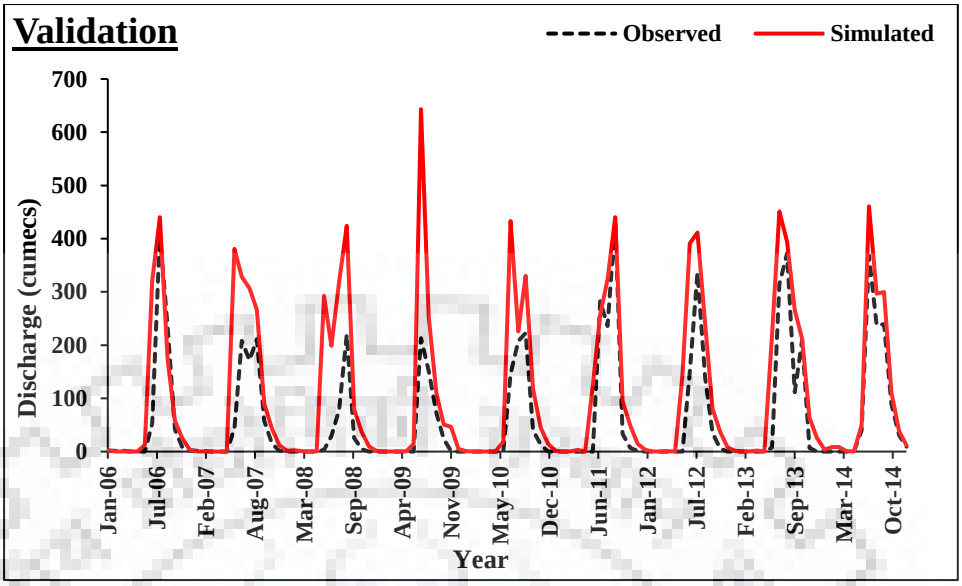

Figure 7.6 Validation plot of simulated and observed discharge at the outlet.

Apart from the visual interpretation of the observed and simulated discharge, the model performance was evaluated based on p-factor, r-factor, coefficient of determination (R^2), Nash-Sutcliffe efficiency (NSE), and Percent BIAS (PBIAS) as shown in Table 7.5. As per Moriasi et al. (2007), if the value NSE and R^2 is greater than 0.65 (Table 7.2), it confirms that the model performance is very good. It also suggests that if the value of PBIAS is less than 10%, the model performance is very good. The values obtained for each model performance parameter are well within the acceptable range which itself explains that the model has a strong predictive capability. Hence, depending upon the calibration and validation results of the SWAT, it can be concluded that the SWAT is applicable over Kharun watershed.

Table 7.5 Values of model performance parameters at the outlet.

S. No.	Evaluation	Duration	*p*-factor	*r*-factor	R^2	NSE	PBIAS (%)
1	Calibration	1990-2005	0.23	0.32	0.84	0.8	-9.4
2	Validation	2006-2014	0.18	0.35	0.85	0.79	-9.2

7.3.3 Model Application Under Land Use and Climate Change Scenarios

In this study, the effects of LULC and climate changes on water balance components were evaluated by comparing the SWAT outputs of 29 simulations. Four simulations were performed under the dynamics of LULC (1990, 2000, 2010, and 2030), whereas 25 runs were conducted under different climatic conditions (Figure 7.7). Two GHGs scenarios (RCP 4.5 and RCP 8.5) from four climate models (representative RCMs) were selected to assess the climate change impact over the study area.

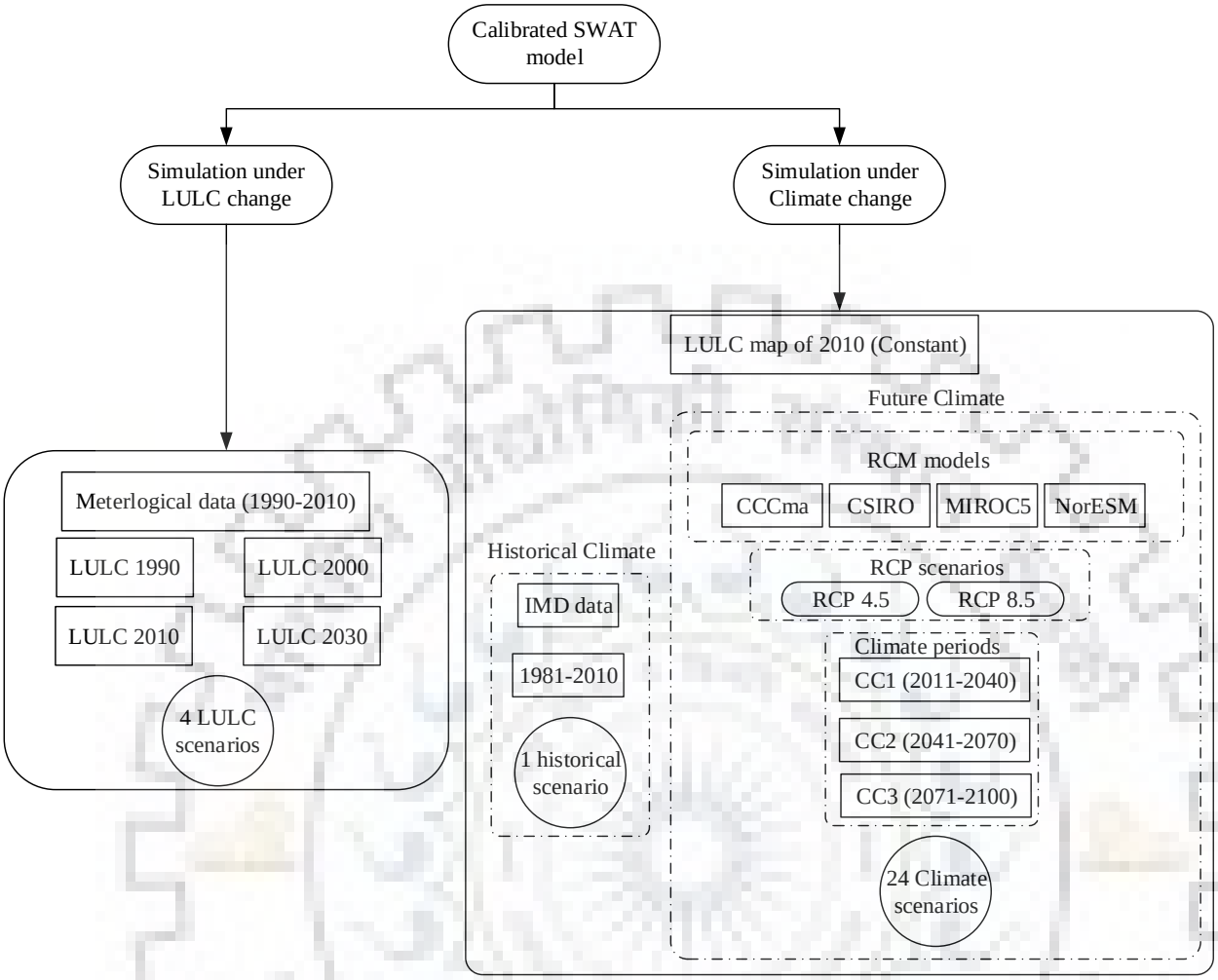

Figure 7.7 Flowchart illustrating 29 simulations under varying land use and climate change scenarios.

7.3.3.1 Impact of LULC change over water balance components

The calibrated SWAT model was used to simulate the impact of LULC change over water balance components. As discussed earlier, the water balance components of the Kharun watershed were simulated under four different land-use periods, 1990, 2000, 2010, and predicted land use 2030. LULC class distribution and changes are given in Table 7.6. Based on the analysis it was observed that not much changes were observed between 1990 and 2000, the only significant difference was the increase in land share of water bodies which increased from 75.83 km^2 (1.89%) to 114.44 km^2 (2.76%), while the share of barren land nearly doubled from 101.98 km^2 (2.46%) to 201.79 km^2 (4.86%). However, in the next decade, things seemed to deviate from their natural course. The share of water bodies reduced from 2.76% to just 1.5% (62.23 km^2), and agricultural land reduced from 3509.5 km^2 (84.5%) to 3379 km^2 (81.4%). These changes in the share of water bodies and agricultural land were the result of a rise in urban areas from 12.27 km^2 (0.30%) to 82.68 km^2

(1.99%). Similar trends were also seen between 2010 and projected the year of 2030, where there was a further reduction in agricultural land and mixed forest accompanied by an increasingly urban area and barren land. These changes are a result of extensive real estate development in the study area due to the declaration of the state of Chhattisgarh, details of which have been discussed briefly in Chapter 6.

Table 7.6 Land use/land cover distribution of the years 1990, 2000, 2010 and 2030.

CLASS	1990		2000		2010		2030	
	Area		Area		Area		Area	
	Sq. km.	%	Sq. km.	%	Sq. km.	%	Sq. km.	%
Water bodies	78.53	1.89	114.44	2.76	62.23	1.50	104.16	2.51
Urban area	9.41	0.23	12.27	0.30	82.68	1.99	279.57	6.73
Agricultural land	3553.0	85.6	3509.5	84.5	3379.0	81.4	2954.39	71.15
Mixed forest	360.09	8.67	265.15	6.39	283.99	6.84	215.23	5.18
Barren land	101.98	2.46	201.79	4.86	284.08	6.84	557.16	12.42
Sand and open rocks	49.31	1.19	49.00	1.18	60.31	1.45	41.74	1.01

Impact study of LULC change dynamics on hydrological components was carried out by utilizing various LULC scenarios. The results indicated that, over time, there is an increase in water yield while there is a reduction in Evapotranspiration (ET). The change in LULC influence the surface properties such as curve number (CN) values and evapotranspiration properties. Change in surface parameter values due to changed LULC is the root cause of change in the water balance components. In order to compute the LULC change impact only, the period of climate data has been fixed for the simulation. In this study, fixed climatic period data from 1990 to 2010 has been considered to simulate the SWAT model for impact assessment study considering LULC change. The average annual values of water balance (water yield, actual evapotranspiration) are given in Table 7.7. Water yield includes surface runoff, groundwater, lateral flow as well as transmission losses in the channel (Eq. 7.2). Table 7.6 indicates that increase in settlement (urban area and barren land) and a decrease in vegetation (agricultural land and mixed forest), which results in increased water yield and reduces ET. Based on the interpretation of results, it can be observed that ET reduced with time due to a decrease in vegetation, earlier it used to be 326.71 mm in 1990, but it declined to 298.39 mm during the projected the year of 2030. Similarly, the increase in paved area and flat surfaces due to the increase in urban areas and barren land due to urbanization resulted in increased runoff and decreased groundwater storage, which leads to an increase in overland flow. These changes in overland flow are directly reflected over the water yield which increased from 781.58 mm in 1990 to 881.84 mm

in the projected the year of 2030 which further supports the argument. The average annual values of evapotranspiration and water yield of sub-watershed due to LULC change are shown in Figure 7.8 and Figure 7.9, respectively. During the last two decades (2010-2030), LULC change increased water yield by 45.88 mm and accounted for 5.48% of the total change (881.84 mm). Moreover, ET decreases by 4.19% in the same duration.

Table 7.7 Average annual water balance components under 1990, 2000, 2010, and 2030 LULC.

LULC	Precipitation (mm)	ET (mm)	Water Yield (mm)
1990	1115.04	326.71	781.58
2000	1115.04	318.47	810.93
2010	1115.04	311.44	835.96
2030	1115.04	298.39	881.84

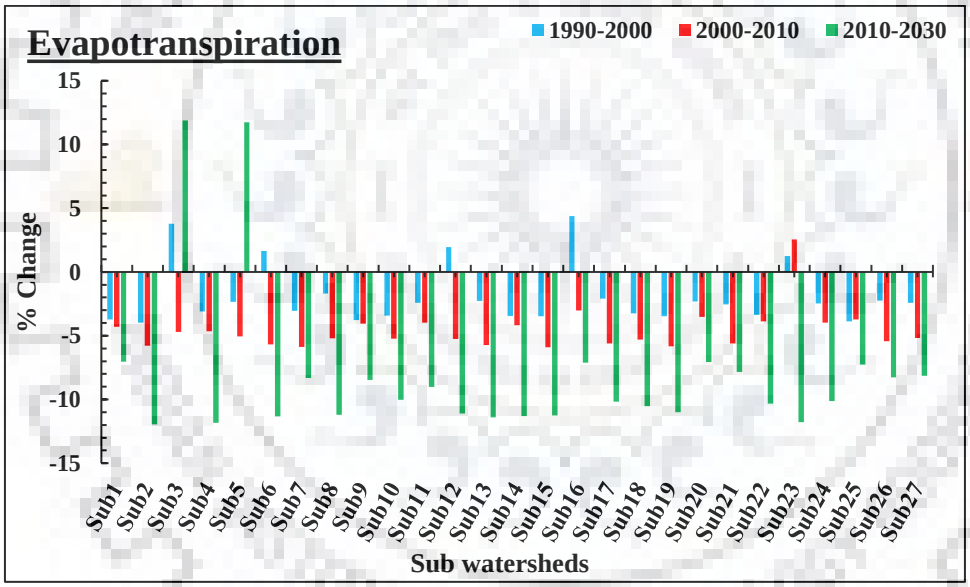

Figure 7.8 Comparison of decadal changes in evapotranspiration due to LULC change.

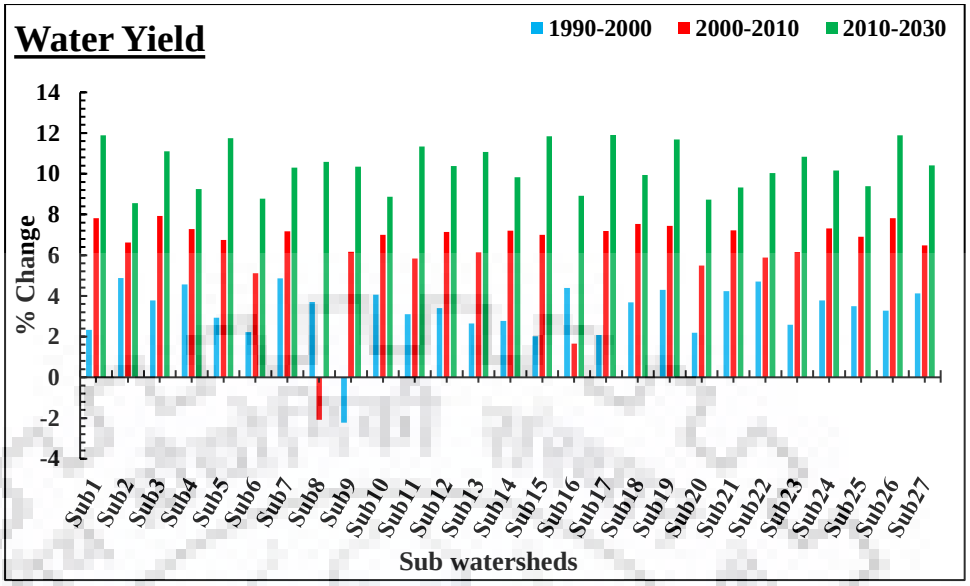

Figure 7.9 Comparison of decadal changes in water yield due to LULC change.

7.3.3.2 Impact of climate change over water balance components

7.3.3.2.1 Precipitation projection under RCP scenarios

Precipitation is the critical component of hydrological modeling along with the temperature. To model any hydrological process, it is mandatory to know about the precipitation characteristic of a region since it is the only source of water availability in most of the regions. Hence, the variability of precipitation over Kharun watershed was estimated to know about the effects of climate change in the region. Detail discussion about the historical trends and long term changes in precipitation have been discussed in Chapter 4, while the variation in rainfall trends in the future has been discussed in detail in Chapter 5. For a hydrological simulation of Kharun watershed due to climate change, observed dataset (IMD precipitation) was compared with the simulated precipitation values obtained from four Representative Climate Models (RCMs), namely CCCma, CSIRO, MIROC5 and NorESM. The comparative result of precipitation variation of observed precipitation (IMD) with the simulated RCM data during the baseline period (1981-2010) has been represented in Figure 7.10. It was found that the average annual precipitation for different RCMs was 1004 mm (CCCma), 1237 mm (CSIRO), 1089 mm (MIROC5), and 1316 mm (NorESM) while the actual average annual precipitation as per IMD was 1151 mm for the region. MIROC5 was found to produce the closest result with a minimum difference of 5.6%, while the maximum difference was seen in the case of NorESM (-11.6%) regarding IMD data. To have a better understanding Figure 7.10 can be referred which shows the comparison of precipitation variation of observed precipitation data (IMD) with the simulated RCM data for the baseline period of 1981-2010.

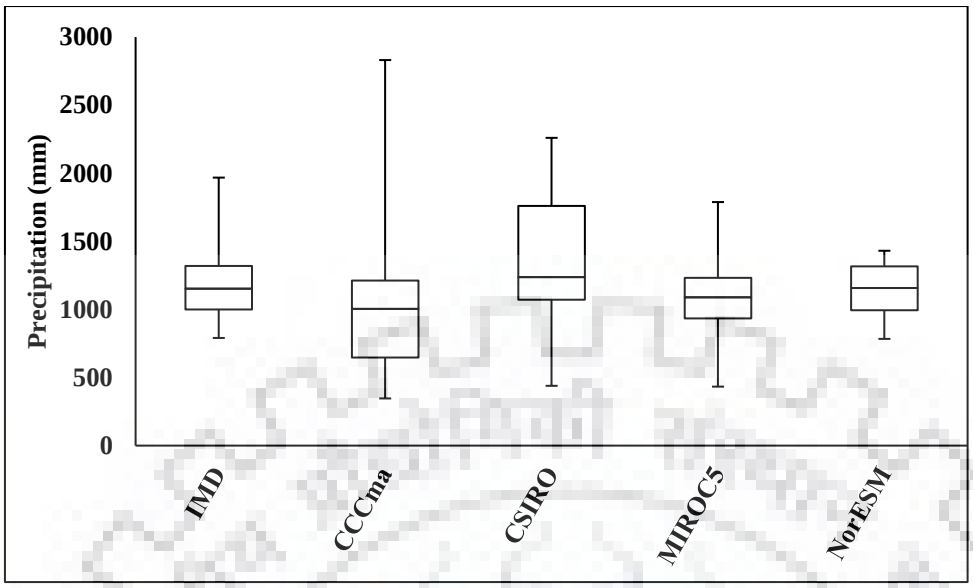

Figure 7.10 Comparison of precipitation variation of observed precipitation (IMD) with the RCM data during the baseline period (1981-2010).

Apart from the comparison of observed precipitation of IMD datasets and simulated precipitation from the four RCMs for the baseline scenario, future climate projections in the case of RCP 4.5 and RCP 8.5 were also compared. Three distinct climate periods of 30 years each were chosen for the purpose, namely, CC1 (2011-2040), CC2 (2041-2070) and (2071-2100). Prima facie, it was observed that the average annual precipitation is increasing with the increase in time for all the RCMs in both the RCP projection. For example, in the case of RCP 4.5 for RCM MIROC5, the annual average precipitation in CC1 was 1201 mm and 1536mm in CC3, while for the IMD baseline scenario, it was 1151 mm. Also, the notable point is related to this observation was that the average annual precipitation of MIROC5 during baseline (1981-2010) was 1089 mm. Hence, it can be inferred that the annual average precipitation in the case of MIROC5 increased by almost 10% in CC1 and by 41% in CC3. Similar patterns were observed for CCCma, CSIRO, and NorESM (Figure 7.11) and all the RCMs of the RCP 8.5 scenario (Figure 7.12). Hence, it can be inferred that the average annual precipitation for the region is on the rise with passing time. It also signifies that the average annual precipitation during period CC1 is less as compared to the baseline period, but increased progressively in the periods CC2 and CC3. Variation in average monthly precipitation was also computed for the climate periods (CC1, CC2 and CC3) for all the RCMs under RCP 4.5 and RCP 8.5, the results have been represented in Figure 7.13 and Figure 7.14 respectively.

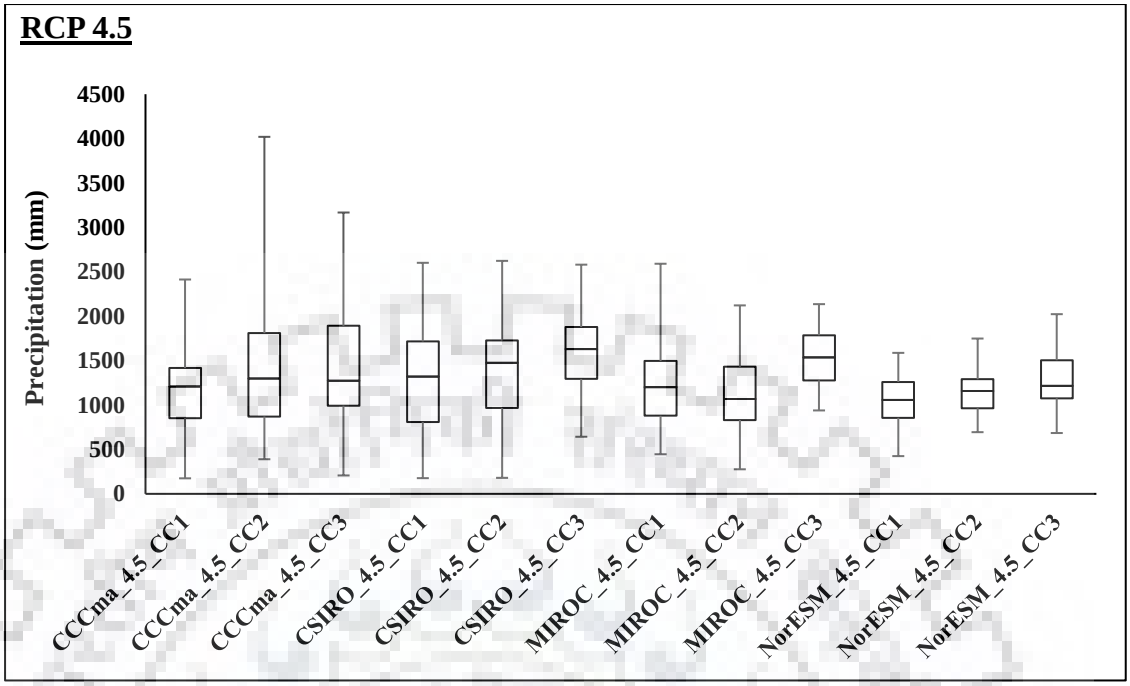

Figure 7.11 Variation in precipitation of climate periods: CC1 (2011-2040), CC2 (2041-2070) and CC3 (2071-2100) for RCP 4.5.

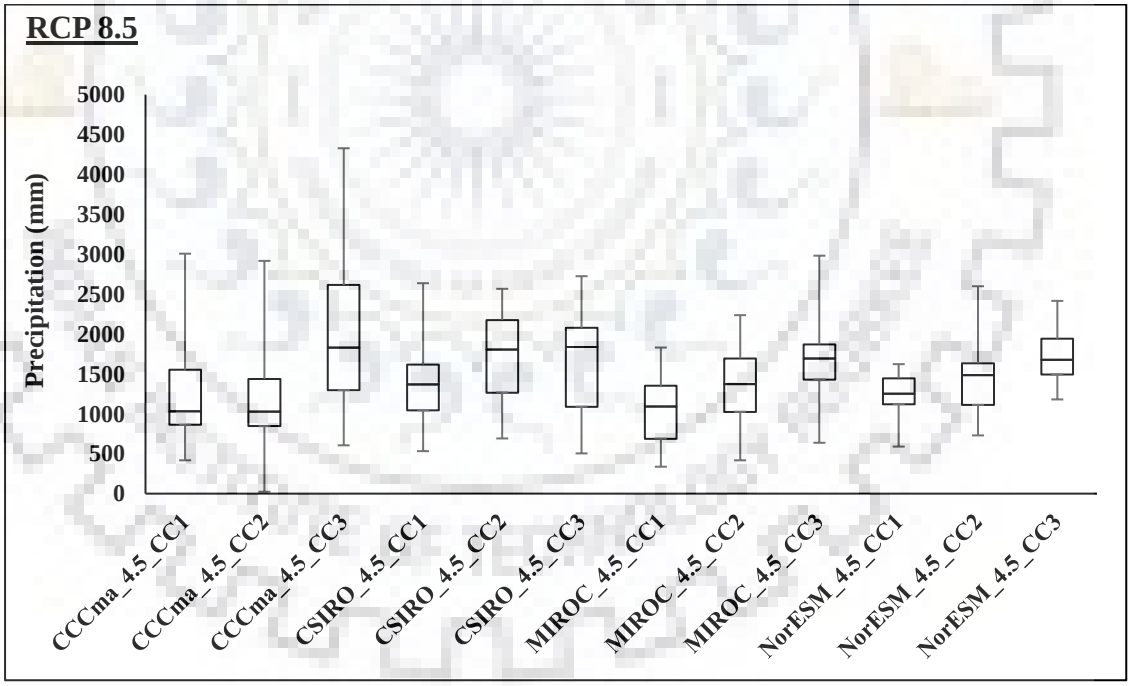

Figure 7.12 Variation in precipitation of climate periods: CC1 (2011-2040), CC2 (2041-2070) and CC3 (2071-2100) for RCP 8.5.

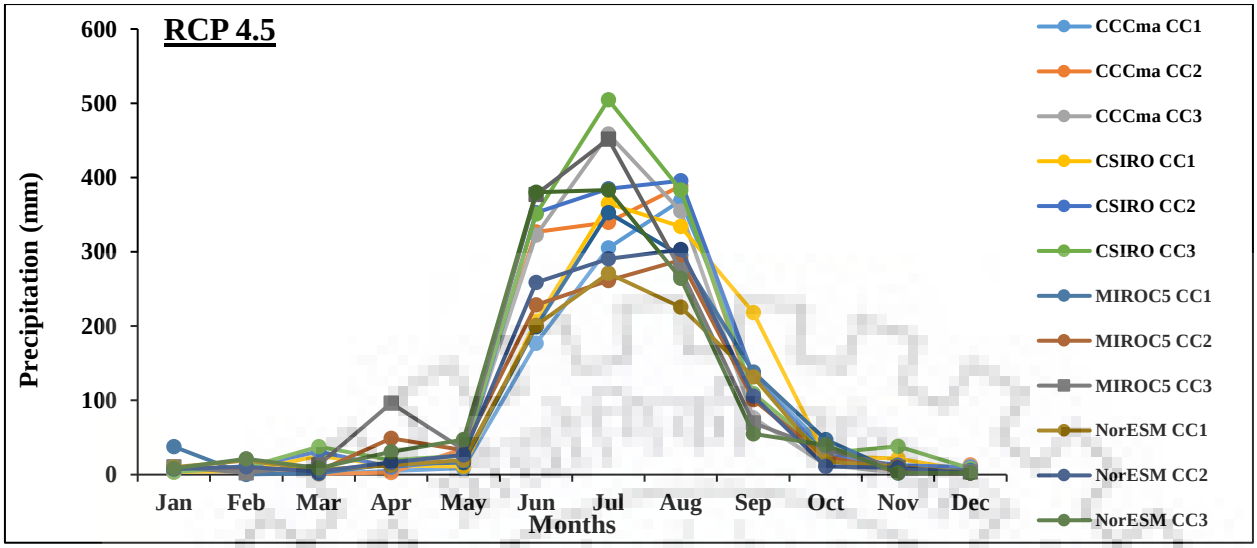

Figure 7.13 Comparison of projected average monthly precipitation (RCP 4.5).

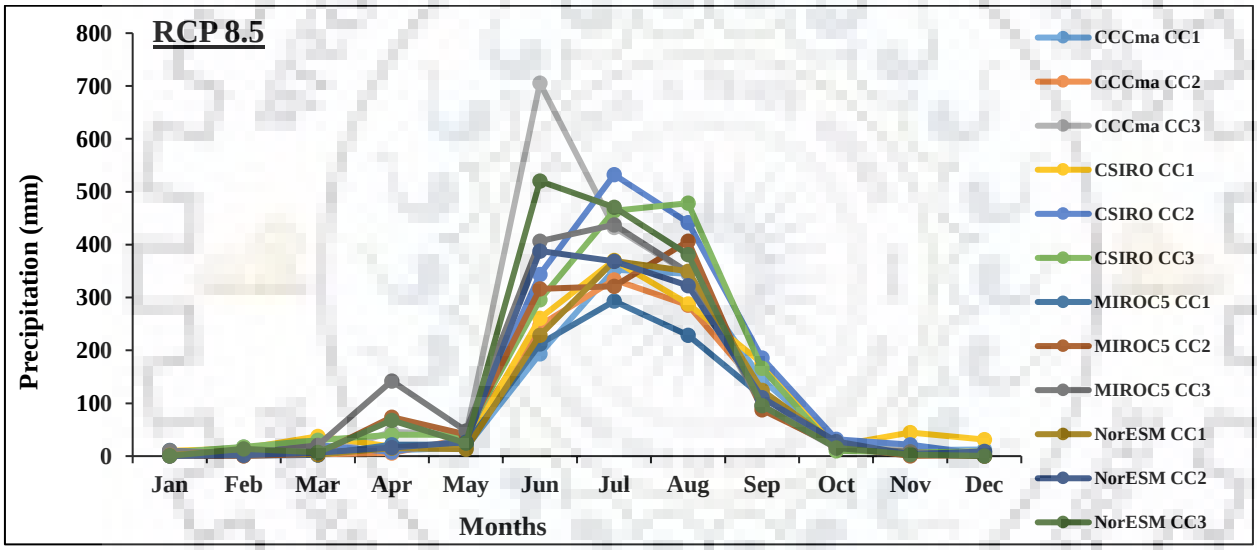

Figure 7.14 Comparison of projected average monthly precipitation (RCP 8.5).

7.3.3.2.2 Temporal changes in water balance components

As discussed in the previous section, 25 SWAT simulations were carried out to determine the temporal changes in water balance components over Kharun watershed. For this purpose, SWAT simulation was carried out over the calibrated SWAT model initially using IMD data (1981-2010) as a baseline. Before this 24 SWAT simulations were carried out for the future climate periods, i.e., CC1 (2011-2040), CC2 (2041-2070), and CC3 (2071-2100) considering both RCP 4.5 and RCP 8.5 scenarios. The results of the water balance components obtained from SWAT simulation of the baseline period were compared with the results of water balance components obtained for each climate period for all the RCMs (CCCma, CSIRO, MIROC5 and NorESM). The percent change in water balance components of all future climate simulations scenarios (CC1, CC2 and CC3)

concerning the baseline scenario (IMD) have been represented in Table 7.8 and their variations can be seen visually from Figure 7.15 (precipitation), Figure 7.16 (evapotranspiration) and Figure 7.17 (water yield).

It was observed that concerning the simulation under IMD, climate scenarios of the CSIRO model resulted in an increase in almost all of the hydrological components during all three climate periods and both RCP scenarios. The overall finding of the results suggested that there is a temporal increase in all the three water balance components in both RCP scenarios. In RCP 4.5, the maximum increase in precipitation was observed in CC3 (29.02%) of the CSIRO climate model. Similarly, in RCP 8.5, the maximum increase was found in CC3 (56.02%) of the CCCma model. For both RCP scenarios reduction in precipitation was observed in period CC1 (2011-2040) by -16.83% for NorESM and by -16.29% for MIROC5. The simulation result suggests that the evapotranspiration (ET) in the region is going to increase between 2011 and 2100 but when compared to IMD simulation as a reference, it was observed that the ET has decreased. The maximum change in ET was obtained in CC3. For RCP 4.5, it was 3.99% (MIROC5) and for RCP 8.5, it was 7.26% (MIROC5). While the minimum change in ET was observed in CC1. The maximum increase in water yield was observed in CC3, 37.36% for CSIRO (RCP 4.5), and 77.10% for CCCma (RCP 8.5).

Table 7.8 Percent changes in water balance components of all simulation scenarios w.r.t. baseline.

Climate models	CC1			CC2			CC3		
	PCP	ET	WYLD	PCP	ET	WYLD	PCP	ET	WYLD
RCP 4.5									
CCCma	-5.05	-25.39	3.29	11.20	-22.96	25.58	14.08	-27.56	24.82
CSIRO	10.51	-11.73	19.92	24.83	-3.22	36.66	29.02	0.63	37.36
MIROC5	-0.26	-12.26	4.40	-8.94	-8.70	-9.12	25.75	3.99	34.92
NorESM	-16.83	-11.28	-19.36	-6.29	-8.04	-5.74	12.28	1.03	16.82
RCP 8.5									
CCCma	0.87	-23.41	10.91	-4.05	-25.69	4.79	56.02	-14.53	77.10
CSIRO	15.68	-3.83	23.88	47.30	0.08	67.39	27.44	6.62	32.63
MIROC5	-16.29	-15.94	-16.73	14.07	-7.60	23.14	33.24	7.26	41.48
NorESM	2.58	-8.34	7.25	14.86	-1.48	21.65	37.87	3.92	49.48

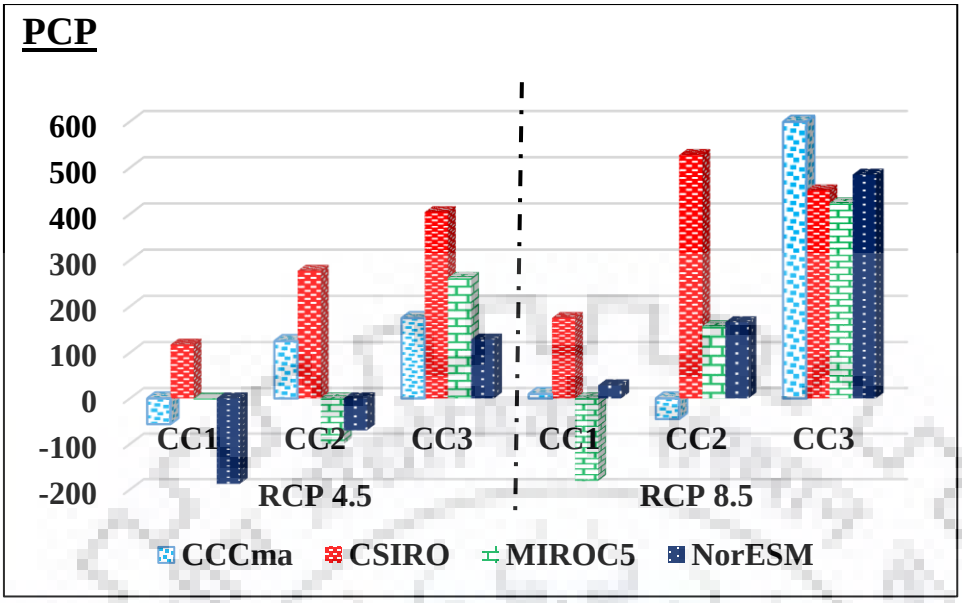

Figure 7.15 Comparison of simulated annual average precipitation (PCP) of climate periods with respect to simulated baseline (IMD) data.

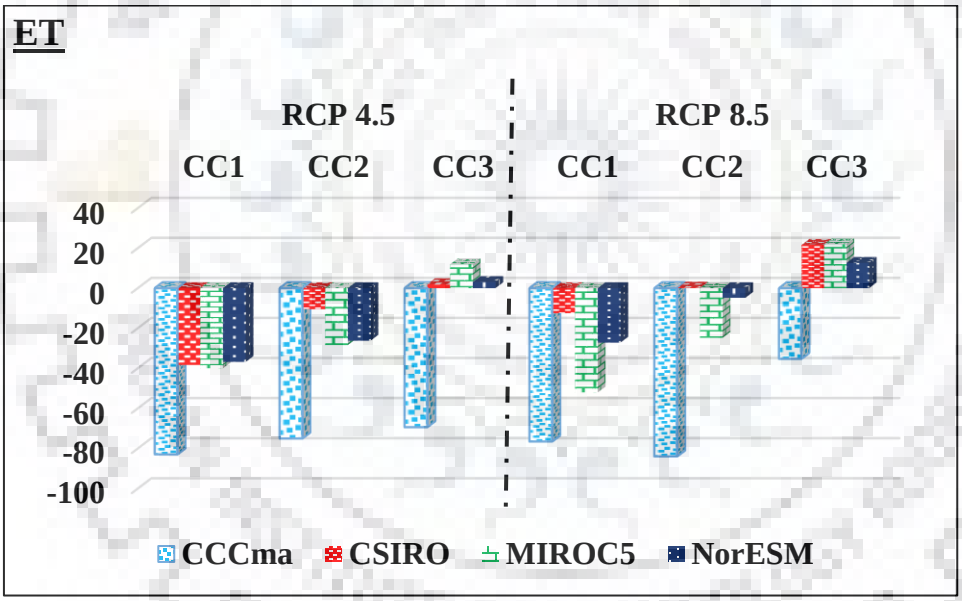

Figure 7.16 Comparison of simulated annual average Evapotranspiration (ET) of climate periods with respect to simulated baseline (IMD) data.

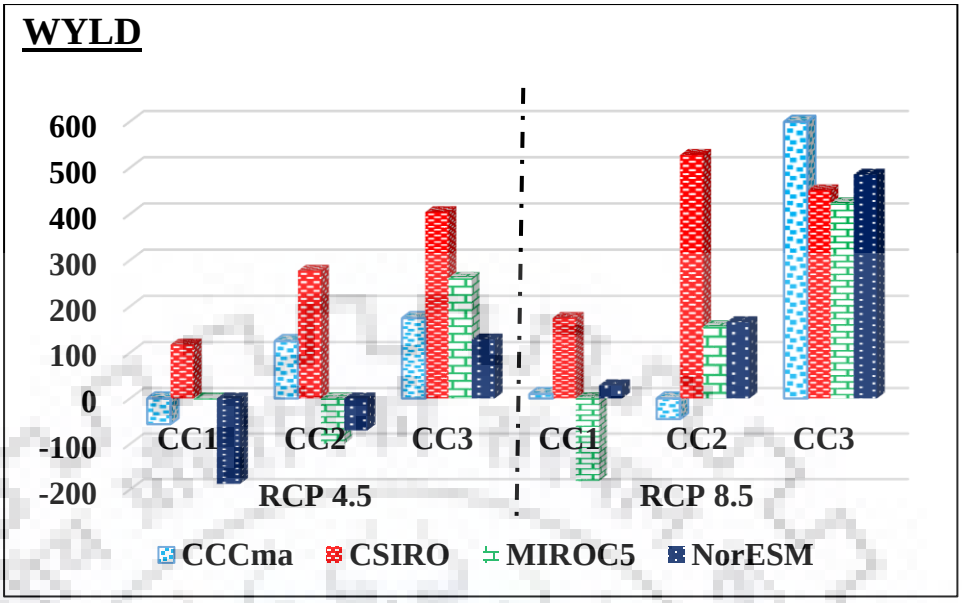

Figure 7.17 Comparison of simulated annual average Water Yield (WYLD) of climate periods with respect to simulated baseline (IMD) data.

To have a better understanding of temporal variations of water balance components over Kharun watershed due to climate change, spatial maps were plotted. Figure 7.18 shows the spatial variation of water balance components across all watersheds in the Kharun watershed during the base period (1981-2010), considering IMD data for the simulation. Similarly, temporal variations of all the water balance components were also plotted, Figure 7.19 and Figure 7.20 shows the variation of precipitation across all the sub-watershed of all four climate models for all the three climate periods (CC1, CC2 and CC3) for RCP 4.5 and RCP 8.5 respectively. Similarly, the sub-watershed wise variation of evapotranspiration of all the climate models for all three climate periods for RCP 4.5 and RCP 8.5 is presented in Figure 7.21 and Figure 7.22 respectively. Also, Figure 7.23 and Figure 7.24 presents the sub-watershed wise variation of water yield of all the climate models for all the three climate periods for RCP 4.5 and RCP 8.5, respectively.

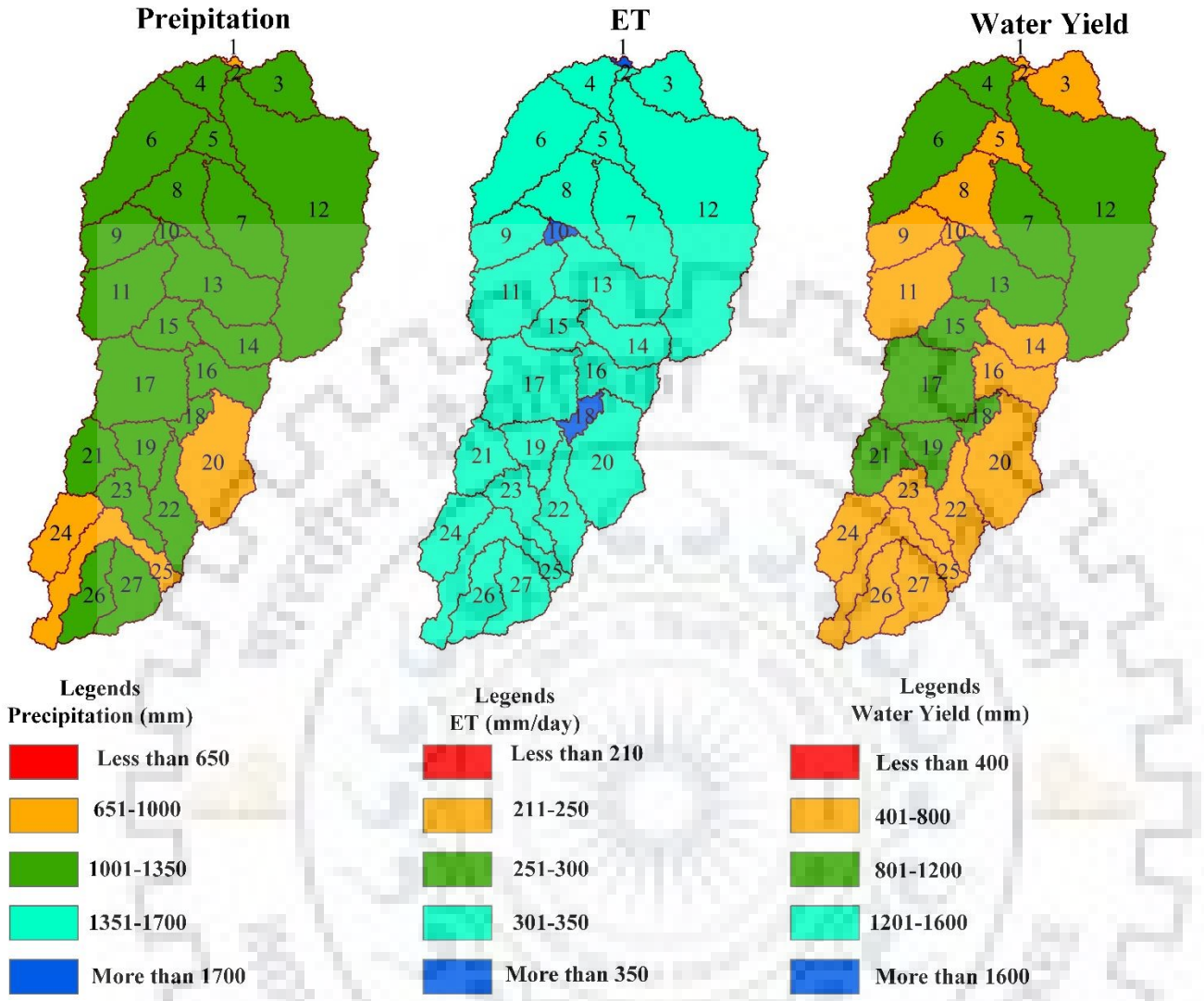

Figure 7.18 Sub-watershed wise variation of water balance components during the baseline period (1981-2010).

Based on the analysis of Figures 7.19 - 7.24, it is observed that the sub-watersheds present in the southern part of the Kharun watershed are bound to receive lesser rainfall (precipitation) as compared to the northern reaches of the watershed for both RCP scenarios (RCP 4.5 and RCP 8.5). As a result of which there will be more water yield in the northern sub-watersheds of the region, as signified by Figure 7.23 and Figure 7.24. It was also observed that there is a temporal increase in all the water balance components across most of the sub-watersheds.

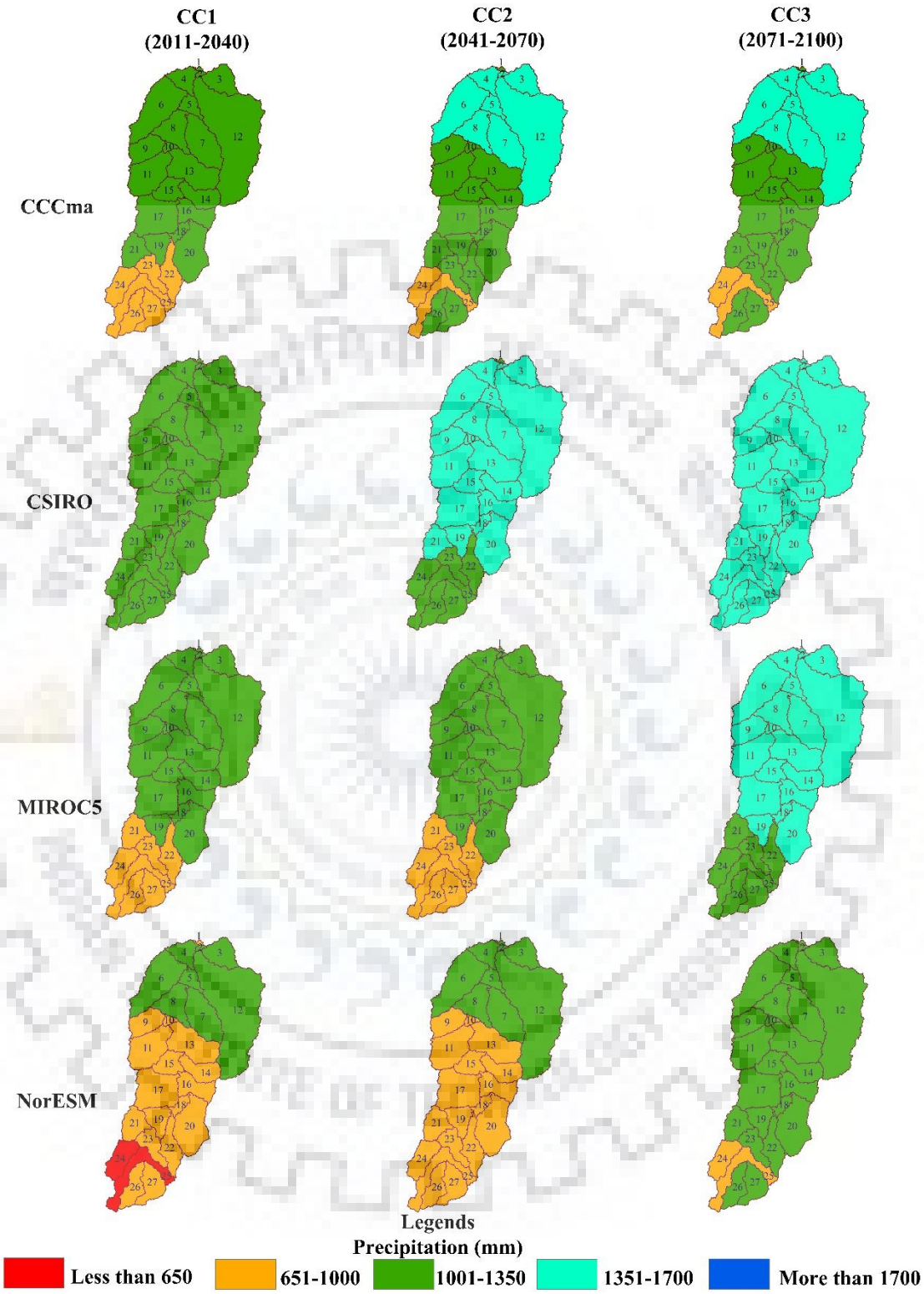

Figure 7.19 Sub-watershed wise variation of simulated precipitation during all climate periods for RCP 4.5.

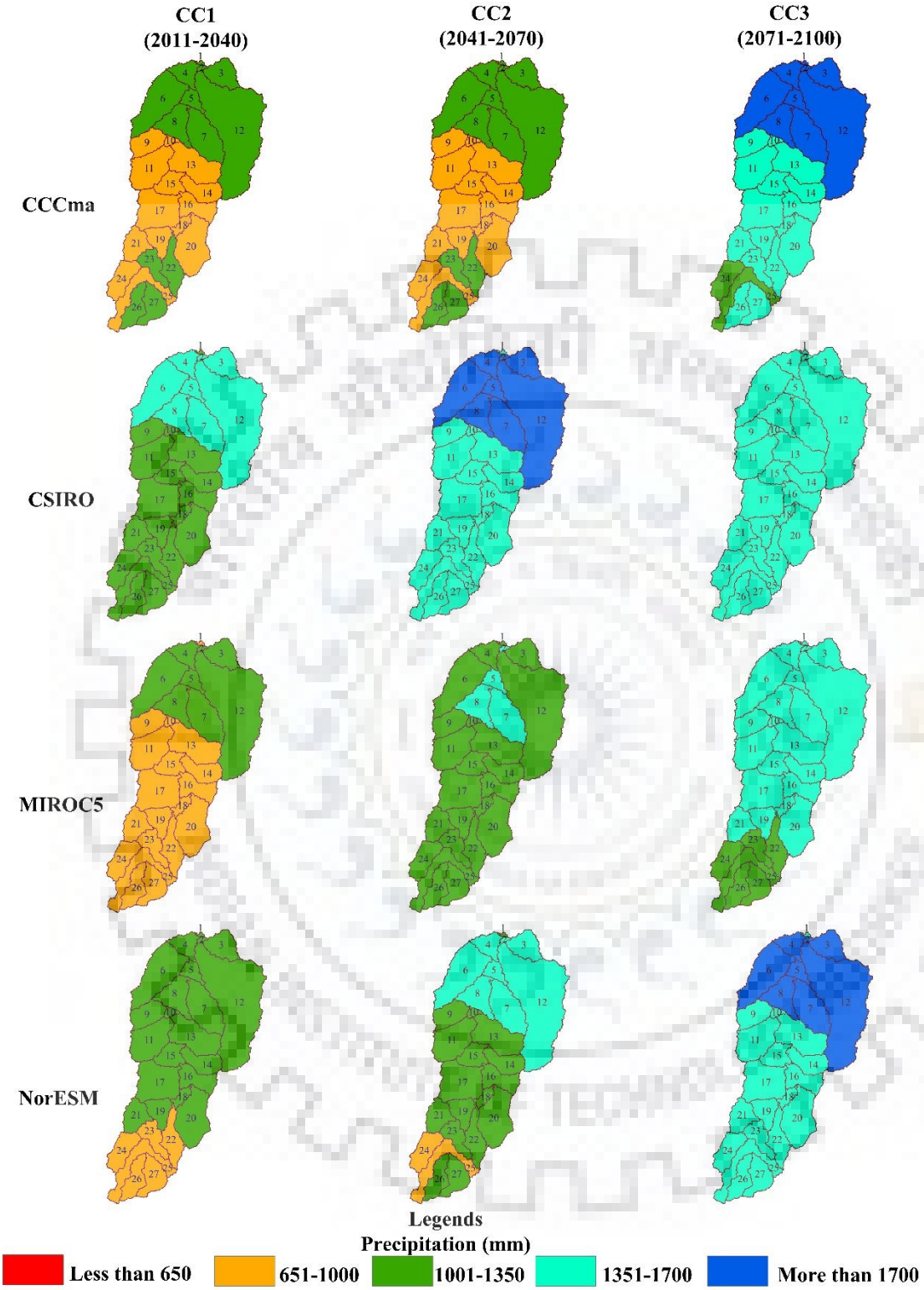

Figure 7.20 Sub-watershed wise variation of simulated precipitation during all climate periods for RCP 8.5.

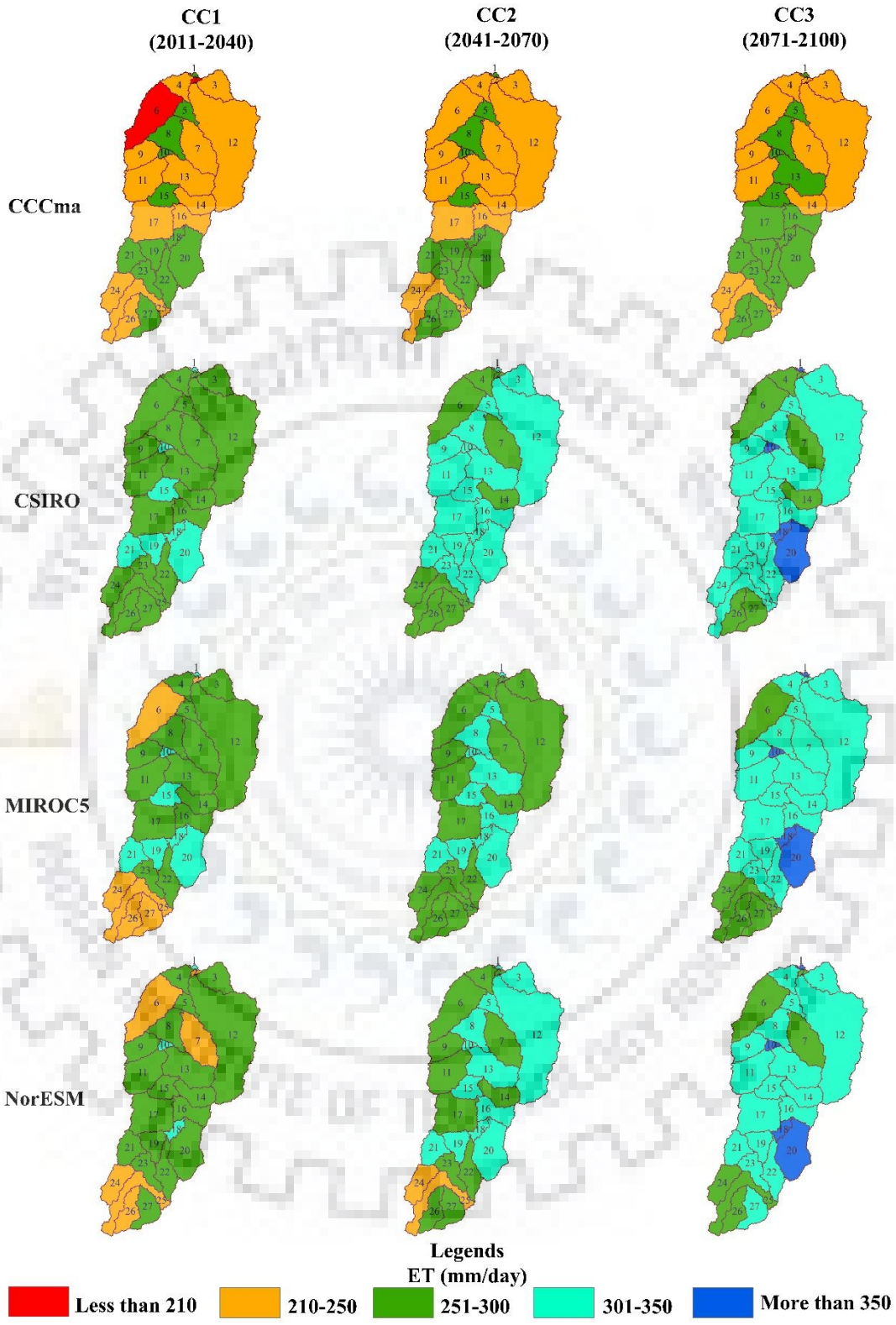

Figure 7.21 Sub-watershed wise variation of simulated evapotranspiration during all climate periods for RCP 4.5.

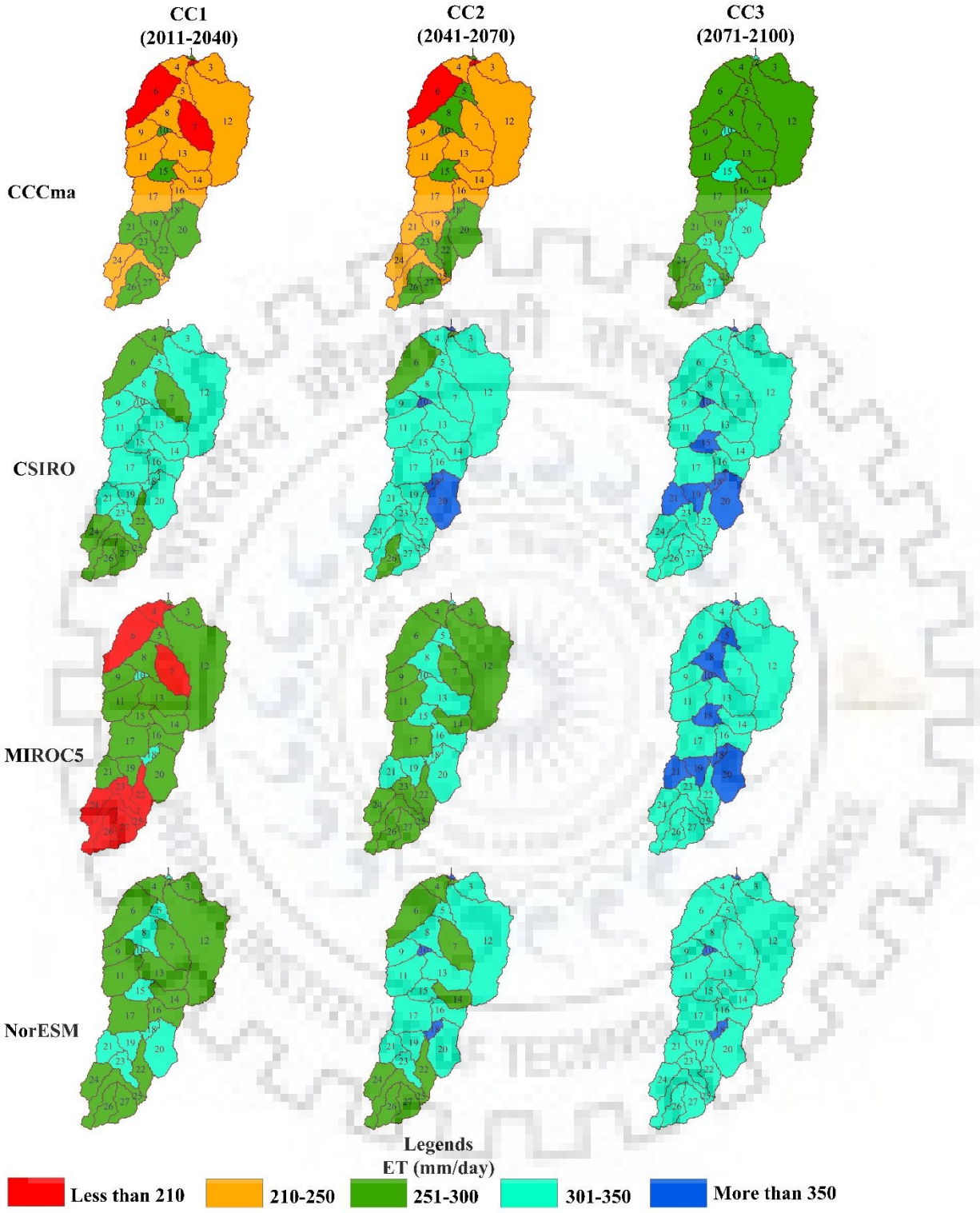

Figure 7.22 Sub-watershed wise variation of simulated evapotranspiration during all climate periods for RCP 8.5.

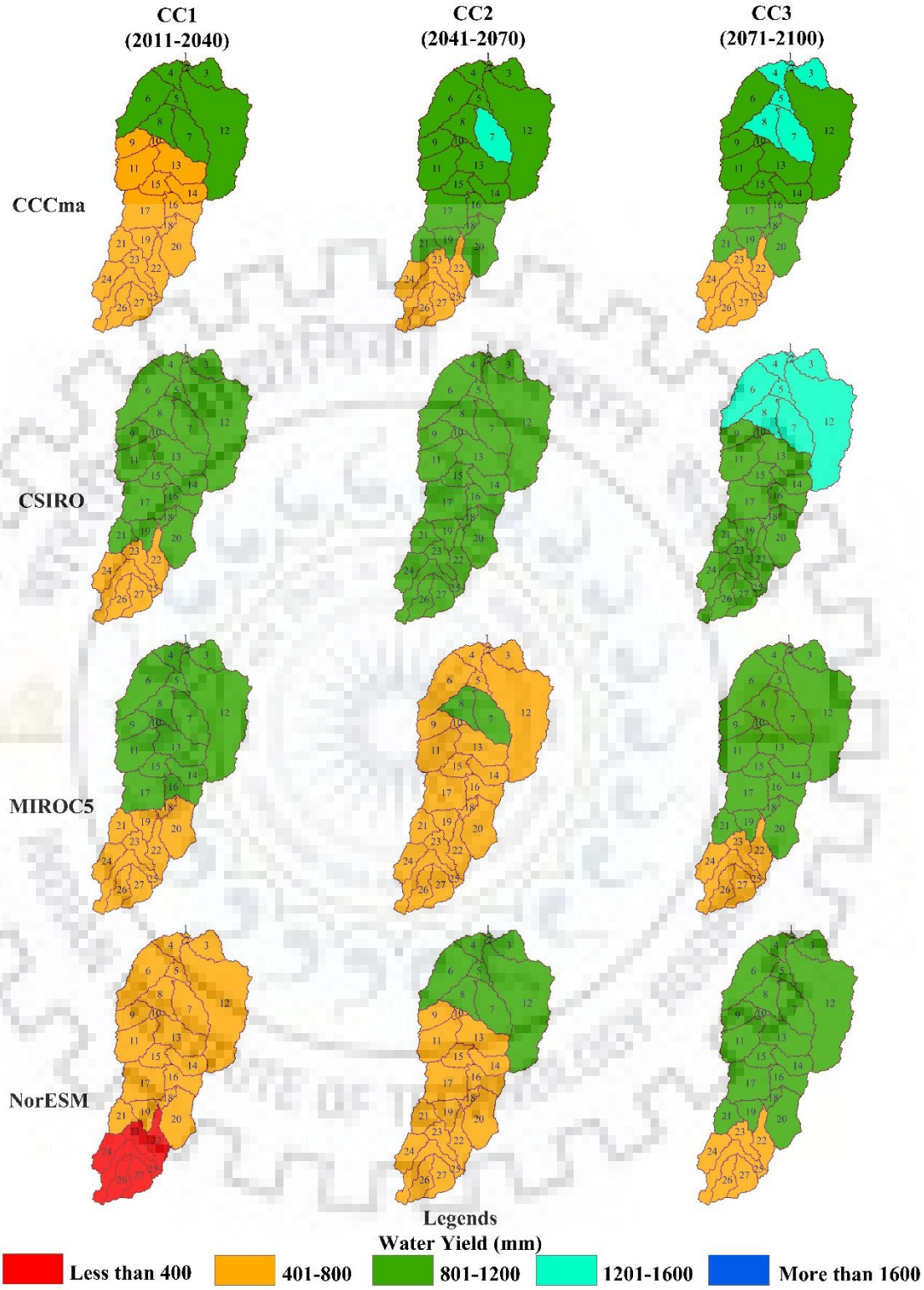

Figure 7.23 Sub-watershed wise variation of simulated water yield during all climate periods for RCP 4.5.

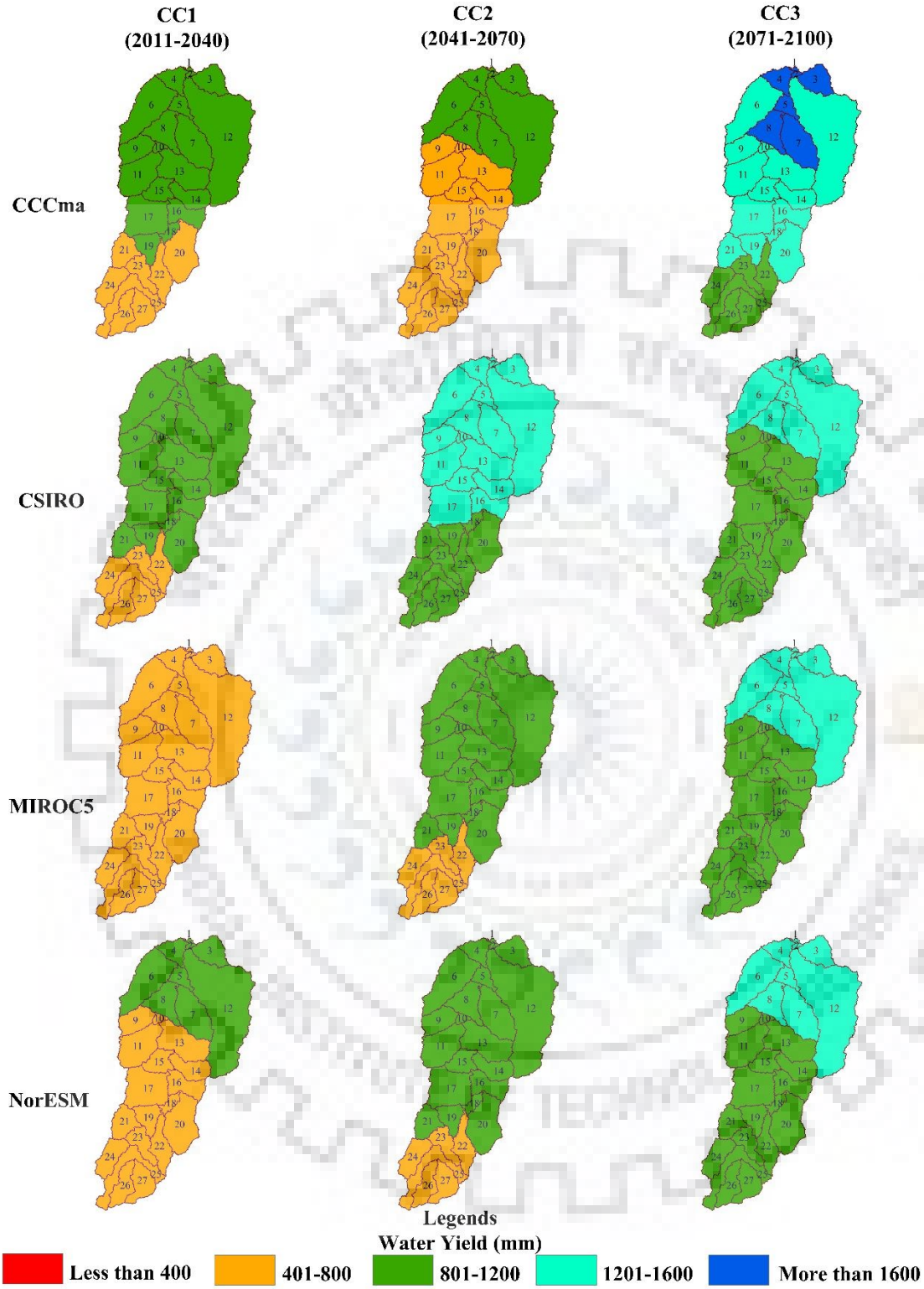

Figure 7.24 Sub-watershed wise variation of simulated water yield during all climate periods for RCP 8.5.

7.3.4 Adaptation and Coping Strategies Towards Climate Change

According to IPCC AR5, the global climate has changed and will keep on changing with the passing time. Its impact can be seen over precipitation, temperature, and other water balance components. However, the trends may differ from region to region as the variation in orography and circulation pattern differs locally. Due to anthropogenic activities and increased GHGs concentration, the surface temperature of the earth and the rate of precipitation is fast changing. An adverse effect of climate change is affecting global food security, water availability and ecosystem. To minimize this, it is vital to reduce the emission of GHGs concentration in the atmosphere. Moreover, proper adaptation and coping strategies may prevent or reduce the adverse effect of climate change. Overall, the present study suggests that change in climate will continue and might accelerate in the future, despite differences in the underlying expectations regarding economic development (scenario storylines) and model uncertainty.

Furthermore, Representative Concentration Pathways (RCP), moderate (RCP 4.5) and high (RCP 8.5) were considered from latest greenhouse trajectories of IPCC AR5 to assess the vulnerability within the area i.e. Kharun watershed. An ensemble of global climate models of the watershed indicates that annual mean temperature most likely to rise from 1.98ºC (RCP 4.5) to 3.18ºC (RCP 8.5) by the 21st century (Figure 7.25 and Figure 7.26). Precipitation in the watershed may increase by about 23% (RCP 4.5) to 35% (RCP 8.5) in the next 100 years (Figure 7.27 and Figure 7.28). Moreover, extreme events of precipitation in the late 21st century can be observed from the ensembles of RCMs output. There is enough evidence that the expected changes in climate positively affect water resources and agriculture. There is a need to propose adaptation and coping strategies in water resources and extreme events (flood) for the watershed.

Therefore, it can be summarized that the vulnerability considering the various sources of uncertainty such as RCPs and RCMs. They will undoubtedly affect the future climate in the watershed in the following ways:

- The temperature will increase up to 3.5ºC under high GHGs concentration.
- Increase in temperature will stimulate the evapotranspiration and contribute to the intensification of the hydrological cycle.
- A rise in temperature will affect food production and uncertainty in crop yield.
- It is most likely that the increase in total precipitation will continue.

- During the mid of the 21st century, extreme values will frequently occur which will trigger flooding and soil erosion on a massive scale.

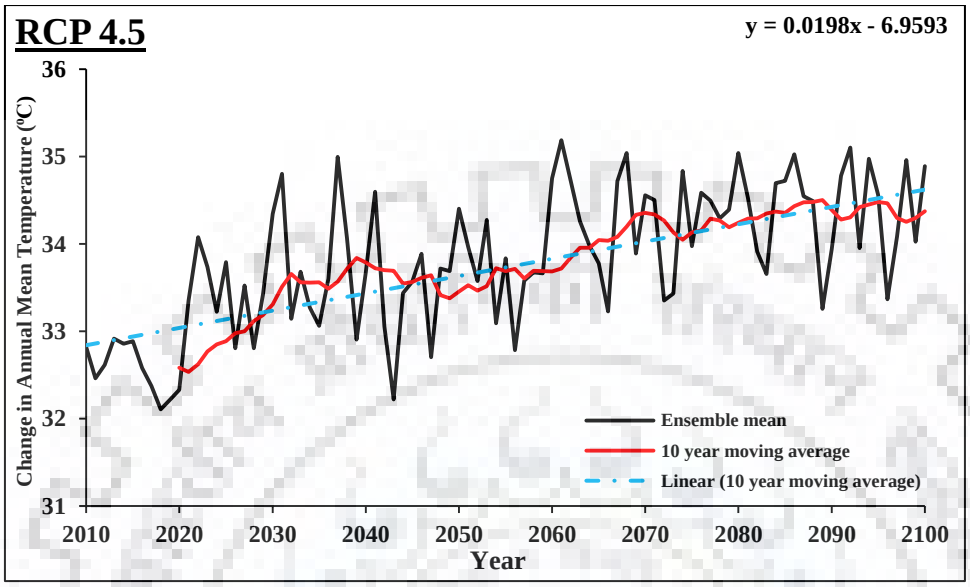

Figure 7.25 Change in mean annual temperature of watershed averaged considering RCMs output ensemble for RCP 4.5.

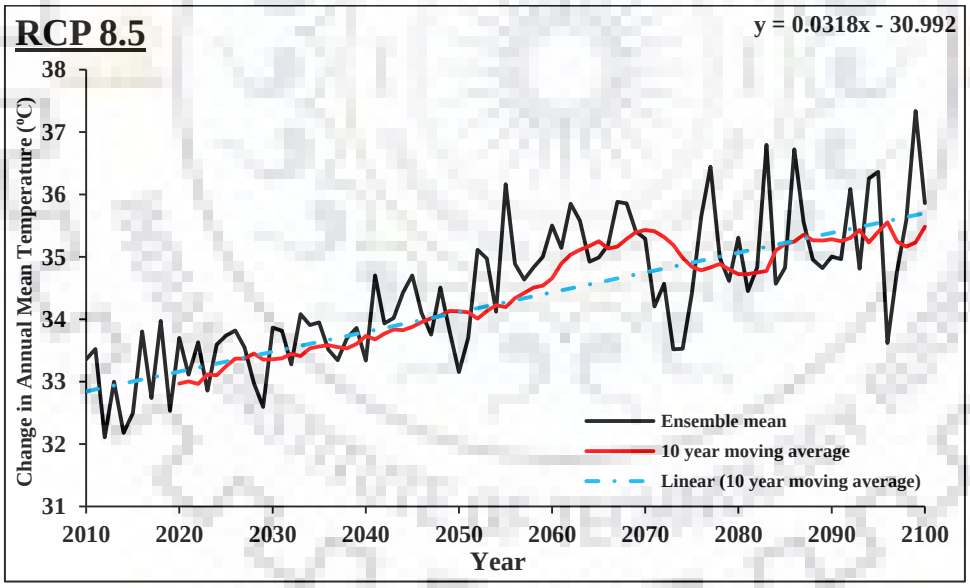

Figure 7.26 Change in mean annual temperature of watershed averaged considering RCMs output ensemble for RCP 8.5.

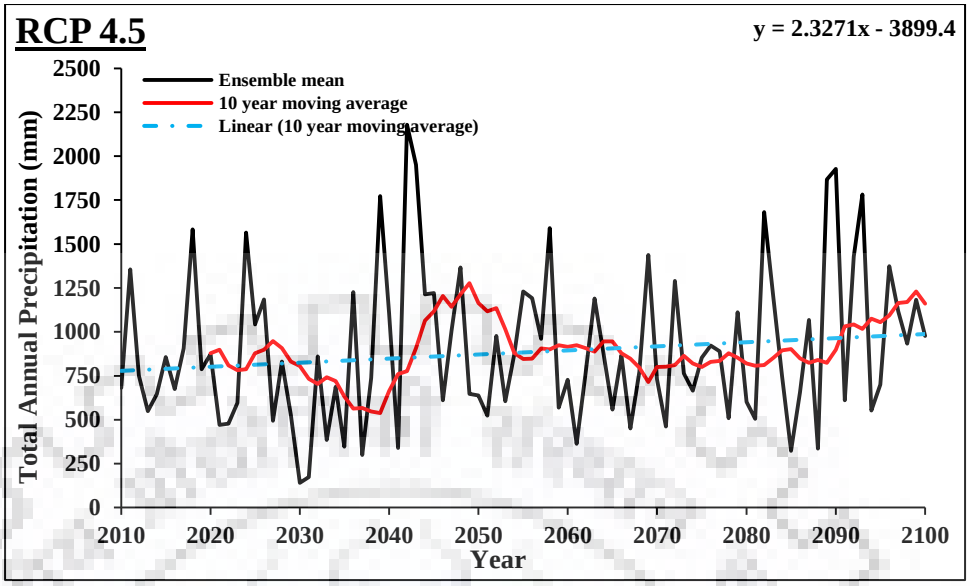

Figure 7.27 Change in total annual precipitation of watershed averaged considering RCMs output ensemble for RCP 4.5.

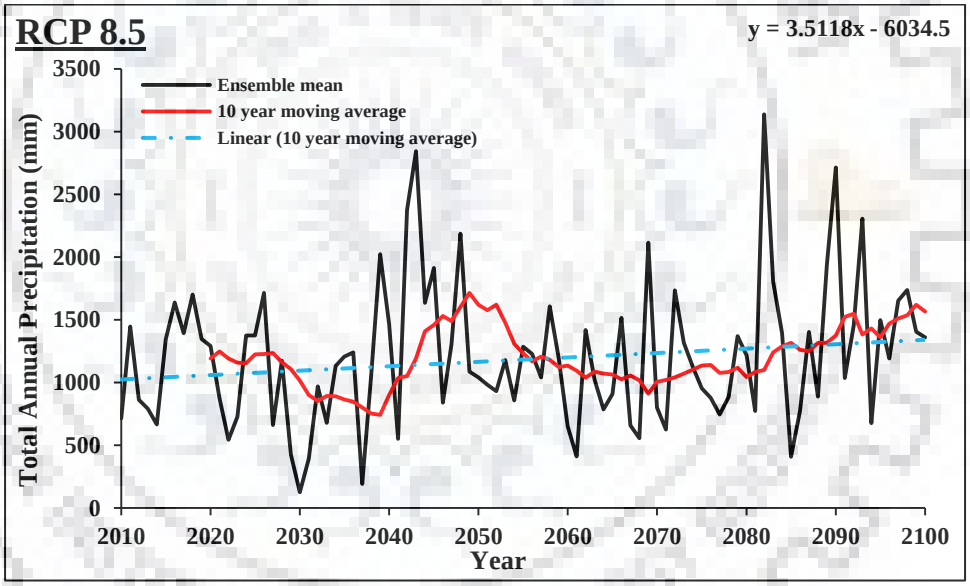

Figure 7.28 Change in total annual precipitation of watershed averaged considering RCMs output ensemble for RCP 8.5.

The IPCC AR5 (2013) gives suggestions regarding adaption, capacity enhancement, and vulnerability. The primary recommendation concludes that reduction of the vulnerability of any country towards climate change demands an increased ability to adapt and cope with its effects. Both coping and adaptation have become essential in reducing the risks of climate change. In order to avoid or reduce the negative impacts of climate-driven changes in water resources on farming systems and to exploit potential positive effects, a range of technological and management options

are available. The basic principles and elements of adaptation strategies are (Kelly and Adger 2000; Nyong et al. 2007; Adger 2007; Epule et al. 2017):

1. Assessment and development of flood management, including risk analysis and environmental and social impact assessment;

2. Provide warnings of the flood to the general public and civil defense in advance;

3. Monitor the hydrologic regime and related climate factors, especially in the region most likely to suffer from the adverse effects of climate change

4. Develop long-term strategies and practical implementation programs for agricultural water use under scarcity conditions with competing demands for water;

5. Land management techniques and amendment in policy to manage the natural vegetation and expansion of urbanization;

6. Crop substitution to reduce dependence on irrigation or to increase water availability. Some crops use less water or are more resistant to heat, so they cope better with dry conditions than others. Also, the choice of crops may contribute to adaptation in terms of "evapotranspiration management," in particular for rain-fed agriculture. In regions, a large proportion of the water that falls as precipitation is evaporated and transpired again by the vegetation. Through the appropriate selection of crop types, evapotranspiration from agriculture may be reduced, which could lead to increased runoff and a generally enhanced availability of water for other crops or purposes.

7. Changes in farming systems to make them more resilient against higher variability in climatic conditions. Diversification of production may thus be a way for farmers to increase their management flexibility and adaptive capacity. Also, organic farming approaches may enhance the capacity of agricultural soils to perform under changing and more adverse climatic conditions.

8. Changes in land use and landscape management may help conserve water, for instance, replacing arable land by grassland. To reduce the sensitivity of farming systems to flood damage, a change of land use in flood risk areas might be necessary. For instance, crop farming in flood risk areas may be replaced by extensive grassland management.

9. Initiate case-studies to establish whether there are linkages between climate changes and the current occurrences of droughts and floods in certain regions.

10. Furthermore, an integrated approach called Integrated Water Resources Management (IWRM) tool might be proposed to maximize economic and social welfare equitably without compromising the sustainability of vital ecosystems under climate change as suggested in many studies (Al Radif 1999; Shah and Koppen 2006; Mersha et al. 2016). It is defined as a process which promotes the coordinated development and management of water, land and related resources in order. However, the potential impacts of climate change and increasing climate variability needs to be sufficiently incorporated in the IWRM plans. IWRM is an excellent tool for coping with natural climate variability and the prerequisite for adapting to the highly uncertain consequences of global warming and associated climate change. The research community needs to introduce the concept and basic overview of IWRM tools in the adaptation of climate change impact and recommend it as a potential tool for implementation. IWRM seems to provide more flexibility and adaptive capacity than conventional water resources management approaches. As such, IWRM has to deal with all-natural resources, not only water but also soils, surface water and groundwater, water quantity, quality as well as ecological aspects of water.

In general, water resource management uses both an analytical framework, explicitly identifying the components and different steps in the analysis process, and a computational framework, establishing a capacity for data processing and quantitative comparison of alternatives. Based on scenarios for climate change, demography, economic development, and spatial planning, projections of the water demand for irrigation, drinking water supply, industrial water supply and environmental requirements are made.

Moreover, agriculture may benefit from adaptation measures taken in the water management sector. A need for further research exists both with respect to the integrated impacts of CO_2 increase and climate change on farming systems and with respect to adaptation strategies that can improve the sustainability and resilience of farming systems under more variable climatic conditions. Issues for research include spatial resolution in vulnerability mapping, technological and management-based adaptation measures.

7.4 CONCLUDING REMARKS

This study investigated the effect of dynamics in LULC change and the effect of considerable historical and future climate variability on water availability of Kharun watershed as it plays a crucial role in the sustainable development of water resources planning and management. To mimic the watershed characteristic, it was essential to calibrate the model. The following conclusions can be drawn from the study presented in this chapter:

- Parameters, namely Base Alpha Factor (ALPHA_BF), Plant uptake compensation factor (EPCO), and Deep aquifer percolation fraction (RCHRG_DP), were found to be the most sensitive parameters for the Kharun watershed.
- For monthly simulations, the values of R^2, NSE, and PBIAS were found to be 0.84, 0.8 and -9.4% during calibration, and 0.85, 0.79 and -9.2% during validation, respectively. The results indicated satisfactory model performance for Kharun watershed. Based on these results, it was concluded that the SWAT model could be successfully employed for the hydrological simulation purposes over Kharun watershed.
- In order to compute the hydrological components under the dynamics of LULC, fixed climatic period data from 1990 to 2010 was considered to simulate the impact of LULC change for 1990, 2000, 2010, and 2030. Results indicate that an increase in settlement (urban and barren land) for real estate development, accompanied by a decrease in vegetation (agricultural land and mixed forest), resulted in an increase in the water yield but the evapotranspiration (ET) reduced due to reduction of vegetation. It was observed that ET reduced with time due to a decrease in vegetation, earlier it used to be 326.71 mm in 1990 but it declined to 298.39 mm during the projected the year of 2030. Due to an increase in overland flow, the water yield increased from 781.58 mm in 1990 to 881.84 mm in the projected the year of 2030. During the last two decades (2010-2030), LULC change increased water yield by 45.88 mm and accounted for 5.48% of the total change (881.84 mm). Moreover, ET decreased by 4.19% in the same duration.
- For both RCP scenarios, reduction in precipitation was observed in period CC1 (2011-2040) by -16.83% for NorESM and by -16.29% for MIROC5. The simulation result suggests that the evapotranspiration (ET) in the region is going to increase between 2011 and 2100 but when compared to IMD simulation as a reference, it was observed that the ET has decreased. The maximum change in ET was obtained in CC3. For RCP 4.5, it was 3.99% (MIROC5)

and for RCP 8.5, it was 7.26% (MIROC5). While the minimum change in ET was observed in CC1. The maximum increase in water yield was observed in CC3, 37.36% for CSIRO (RCP 4.5) and 77.10% for CCCma (RCP 8.5).

CHAPTER 8

SUMMARY AND CONCLUSIONS

8.1 SUMMARY

The present research has been carried out to ascertain the water availability and its distribution under the impact of climate change and anthropogenic interventions in Kharun watershed, India. Water is the most crucial aspect of human life and is affected the most due to change in the climate. Climate change intensifies the process of hydrological cycle which subsequently has severe effects on the intensity and frequency of extreme events. Increased evaporation, sea-level rise, prolonged droughts and unpredictable precipitation are just a few results of climate variability that directly affect the water availability in any region. The change in meteorological distribution influences the ecosystem and landscape change and will continue to do so in the near future. However, the root cause of variation in precipitation rate and temperature in Kharun watershed is the rapid urbanization of the region and climate change. For future planning and management of the available water resources, it becomes quite essential to have a clear understanding of the distribution and variability of meteorological parameters.

To investigate the long term changes in the hydrological balance of an area (basin/watershed), it is essential to know about the history, climatology, topography and demography of that area. Kharun watershed was opted for the present study. Raipur, the capital city of Chhattisgarh, lies within the watershed, and the Kharun River bisects the capital due west of the city. Massive urbanization and industrialization have been observed after the formation of Chhattisgarh state. Due to real estate development, forest areas and agricultural land have given way to residential and industrial complexes. These large scale development and urbanization have altered the hydrological balance in the region. To investigate the extent of imbalances caused by the alteration in the hydrological balance, this study was carried out in one of the major watersheds in the tropical region of Chhattisgarh.

8.2 CONCLUSIONS

The salient findings and conclusions drawn from the present study are discussed below.

8.2.1 Shift and Trends in Meteorological Variables

The ecosystem and landscape change mainly influence long term changes in meteorological distribution. However, changes in precipitation rate and temperature are the main causes of climate change, which drastically varies the flow in the river. For the planning and management of water resources, it is quite essential to understand the distribution and variability of meteorological parameters. Trend detection was carried out for long term temperature (maximum, minimum, and mean) and precipitation data by applying regression analysis, MMK test, and the magnitude of change has been found out using Sen's slope estimator over 22 grids in and around the study area. Apart from finding the nature and extent of trend, the magnitude of change was also computed to quantify the change in terms of the respective units of the parameters. Similar statistics were also performed over 23 indices of meteorological extremes computed from long term precipitation and temperature time series, 18 extreme precipitation and temperature indices out of 27 developed by ETCCDMI were considered for the study. Additionally, five more indices were proposed in the study, which is based on the precipitation intensity indices suggested by IMD. Also, the Cumulative sum (Cusum) and sequential Mann-Kendall (SQMK) test were applied to identify the climatic shift (change year) over the meteorological time series.

1. Significant findings of the study state that there is an increase in average maximum temperature during summer (0.19ºC), post-monsoon (0.21ºC), and winter (0.61ºC) seasons. Significant reduction in average yearly minimum temperature (-0.68ºC) was observed over the study area, similar reduction in average minimum temperature during summer (-0.39ºC), monsoon (-0.60ºC) and post-monsoon (-0.32ºC) season. The most significant reduction in average minimum temperature was seen during the winter season (-1.10ºC). The annual precipitation seems to be decreasing over the study area by almost 210 mm for 115 years. Similar trends were also seen for summer (16.85 mm), post-monsoon (3.26 mm), and winter (2.69 mm).
2. After the computation of long term variation in meteorological extremes, it can be inferred that the gap between the minimum and maximum temperature seems to be increasing over the study period at an average rate of 0.09ºC/decade (4.6%), which explains the increasing trend in Diurnal Temperature Range (DTR). This precisely explains the fact that the days are

getting hotter, and the nights are getting colder and its effects can be seen over the rainfall intensities in the region. As per the results obtained, there was reduction observed in the number of light rainy days (-10.2%), moderate rainy days (-17.8%), rather heavy and heavy rainy days (-25.5 and -18.4%). The number of cumulative dry days in the study area has increased by 19.5%, which in itself explains the reduction in rainy days. As the trend statistics of temperature and precipitation extremes tend to get severe after shift (as discussed in Chapter 4), the phenomenon due to the variation in these extreme indices will have a more adverse effect on the study area.

8.2.2 Climate Models and Future Trend Analysis

For reproduction of meteorological parameters to study changes in extreme value indices in the future, the Regional Climate Model (RCMs) was evaluated in the study. Four RCMs were identified as the most suitable models to determine future times series data of precipitation and temperature (maximum and minimum) for the study viz. CCCma, CSIRO, MIROC5 and NorESM. The technique of distribution mapping was used to remove systematic biases that may be present in the data. MMK test statistic was used to evaluate the presence of any trend while the magnitude of the trend was quantified using Sen's slope estimator over the entire period (2011-2100) and for three climate periods, namely CC1 (2011-2041), CC2 (2041-2070) and CC3 (2071-2100). These tests were applied over two scenarios viz. RCP 4.5 and RCP 8.5.

For the study area, it was observed that the annual rainfall in the future would increase by almost 29% (especially in period CC3). Also, a reduction in the number of CWD (10%) accompanied by an increase in CDD (-17%) was observed for the future, which further emphasizes the point of increase in high-intensity rainy days (RRH by 51%) in the future. A similar phenomenon was observed for both the scenarios (i.e., RCP 4.5 and RCP 8.5). The study also suggested that climate change will have considerable effects on the region. In the future, the nights will become warmer (increase in TR by 81%), and the days will get hotter (increase in SU by 6%) while the DTR will increase by almost 2.6% in the future for both RCP scenarios. The overall result indicated an increase in the Diurnal Temperature Range (DTR) in the future, along with an increase in days with heavy rainfalls in the case of both scenarios for the study area.

8.2.3 Land Use/Land Cover Dynamics and Future Prediction

The study of land use/land cover (LULC) change dynamics was carried out over the Kharun watershed. LULC mapping was carried out for the region by using satellite imageries (LANDSAT 5, 7, and 8) by application of RS and GIS tools such as ERDAS Imagine and ArcGIS 2012. The LULC maps were classified into six different classes namely water bodies, urban areas, agricultural land, barren land, mixed forest and sand/open rocks. The changes between different classes between 1990 and 2015 were evaluated at decadal as well as the demi-decadal level. Significant findings in the study stated that there is a decrease in vegetation (agricultural land and mixed forest) in the region, giving rise to the urban area and barren land. In 25 years (1990-2015), the urban area increased by almost 1450%, which is very high for an agricultural watershed, also in that period, the land share of agricultural land and mixed forest depleted by approx. 20% and 50%, respectively. This clearly indicates that the floral region is giving way to urban settlement and barren land.

After the analysis of historical trend patterns in LULC, the LULC map for the near future (2030) was projected using the CA-Markov model. The model was validated and simulated with the classified LULC map of 2015. The projected LULC map of 2030 indicated the continuation of the same trend of the past. It was found that the urban areas in the region will increase by almost 47.36%, while the agricultural land will further deplete by 7.5%, and the mixed forest in the region will shrink by 10% in the near future. These future projections indicate the expected changes in the near future. Therefore, the LULC changes concerning different classes in the near future will caution the concerned authorities for proper planning and management of the study area.

8.2.4 Hydrological Simulation Under LULC and Climate Change Scenarios

This study investigated the effect of dynamics in LULC change and the effect of significant historical and future climate variability on water availability of Kharun watershed as it plays a crucial role in the sustainable development of water resources planning and management. To mimic the basin characteristic, it was essential to calibrate the model. The following conclusions can be drawn from the study:

1. Parameters, namely Baseflow Alpha Factor (ALPHA_BF), Plant uptake compensation factor (EPCO), and Deep aquifer percolation fraction (RCHRG_DP), were found to be the most sensitive parameters for the Kharun watershed.

2. For monthly simulations, the values of R^2, NSE and PBIAS were found to be 0.84, 0.8 and -9.4% during calibration, and 0.85, 0.79 and -9.2% during validation, respectively. The results indicated satisfactory model performance for the basin. Based on these results, it was concluded that the SWAT model could be successfully employed for hydrological simulation purposes over Kharun watershed.
3. In order to compute the hydrological components under the dynamics of LULC, fixed climatic period data from 1990 to 2010 was considered to simulate the impact of LULC change for 1990, 2000, 2010, and 2030. Results indicate that an increase in settlement (urban and barren land) for real estate development, accompanied by a decrease in vegetation (agricultural land and mixed forest), resulted in an increase in the water yield but the evapotranspiration (ET) reduced due to the reduction of vegetation. It was observed that ET reduced with time due to a decrease in vegetation, earlier it used to be 326.71 mm in 1990 but it declined to 298.39 mm during the projected the year of 2030. Due to an increase in overland flow, the water yield increased from 781.58 mm in 1990 to 881.84 mm in the projected the year of 2030. During the last two decades (2010-2030), LULC change increased water yield by 45.88 mm and accounted for 5.48% of the total change (881.84 mm). Moreover, ET decreases by 4.19% in the same duration.
4. For both RCP scenarios, reduction in precipitation was observed in period CC1 (2011-2040) by -16.83% for NorESM and by -16.29% for MIROC5. The simulation result suggests that the evapotranspiration (ET) in the region is going to increase between 2011 and 2100 but when compared to IMD simulation as a reference, it was observed that the ET has decreased. The maximum change in ET was obtained in CC3. For RCP 4.5, it was 3.99% (MIROC5) and for RCP 8.5, it was 7.26% (MIROC5). While the minimum change in ET was observed in CC1. The maximum increase in water yield was observed in CC3, 37.36% for CSIRO (RCP 4.5) and 77.10% for CCCma (RCP 8.5).
5. To address the issue of hydrological imbalance due to LULC and climate change in the study area, Kharun watershed some adaptation and coping strategies were proposed. These measures included land management techniques, crop substitution (to reduce dependency on irrigation) and alteration in farming systems, changes in land use, and landscape management to help conserve water and Integrated Water Resources Management (IWRM) techniques. IWRM techniques, with the help of localized case studies, might help in ensuring proper water usability for the social and economic development of the study area.

8.3 RESEARCH CONTRIBUTIONS

The research contributions of the present study are summarized below:

1. Historical trends in meteorological parameters (precipitation and temperature) along with the trends of various extreme value indices over Kharun watershed were evaluated using MMK, and their trends were quantified using Sen's slope estimator. Apart from the existing 18 (out of 23) indices, an additional five (5) extreme value indices were proposed in the present study to determine the variation in various rainfall intensities due to climate change. Detection of climate shift in the region was carried out using Sequential Mann-Kendall (SQMK) and Cumulative Sum (CUSUM) test statistics.
2. Future trends ever in extreme value indices based on precipitation and temperature were evaluated using Regional Climate Models (RCM). BIAS correction was applied over the RCMs using distribution mapping techniques.
3. LULC mapping was carried out using the Landsat TM, ETM and OLI_TRS satellite images utilizing geospatial tools viz. GIS and ERDAS Imagine. The development in the different classes of LULC was evaluated from 1990 to 2015. Understanding of trend patterns was demonstrated and predicated for the year 2030 using the CA-Markov model.
4. Development of model setup (SWAT) for Kharun watershed and its calibration using SWAT-CUP. Projection of water balance components (precipitation, evapotranspiration, and water yield) was investigated by integrating bias-corrected climate data with the calibrated model under high and moderate emission scenarios from 2011 to 2100 as well under LULC changes. To estimate the changes in the hydrological response under the dynamics of LULC and projection of virtual water for three climatic periods of the 21st century under climate change scenarios. Adaptation and coping strategies were suggested in the study area.

8.4 RESEARCH LIMITATIONS

Limitations of the present study are given below:

1. Only four climate models were considered to predict long term trend changes and for the projection of water balance components in the present study.

2. No change in the soil layer and LULC were considered over the long term period in the projection of water availability.
3. In general, adaptation provides an essential strategy to reduce negative consequences. Therefore, it does not imply that the proposed adaptation can overcome all climate change effects.
4. During the hydrological modeling of Kharun watershed, small structures along the river have been neglected due to the unavailability of proper data.
5. Combined effect of LULC change and climate change could not be analyzed in the present study.

8.5 SCOPE FOR FUTURE STUDIES

There are few limitations in the study which can be overcome shortly listed as:

1. In order to reduce the uncertainty in the future projection of hydrological components, some more climate models and projections may be considered in the study to reduce the uncertainty.
2. Due to the unavailability of proper data, the effects of the minor hydraulic structure were not considered in the present study, which may be considered in future studies.
3. CA-Markov model was used for future land use prediction, other methods such as multi-layer perceptron neural network, logistic regression, or modified machine-learning procedures can be adopted to have a better understanding.
4. To set up the model, limited SWAT parameters were considered in the study that may be extended in the future study.
5. Since the soil loss data was not available for the study area, the study of sediment yield in the watershed could not be done. Future studies can be conducted over the study area by treating it as an ungauged watershed.

REFERENCES

Ab. Ghani, A., and Azamathulla, H. M. (2014). "Development of GEP-based functional relationship for sediment transport in tropical rivers." *Neural Computing and Applications*, 24(2), 271–276.

Abbaspour, K. C. (2015). "SWAT-CUP: SWAT Calibration and Uncertainty Programs- A User Manual,Department of Systems Analysis,Intergrated Assessment and Modelling (SIAM),EAWAG. Swiss Federal Institute of Aqualtic Science and Technology,Duebendorf,Switzerland." *User Manual*, 100p.

Abbaspour, K. C., Yang, J., Maximov, I., Siber, R., Bogner, K., Mieleitner, J., Zobrist, J., and Srinivasan, R. (2007). "Modelling hydrology and water quality in the pre-alpine/alpine Thur watershed using SWAT." *Journal of Hydrology*, 333(2–4), 413–430.

Adger, W. N. (2007). "Social Capital, Collective Action, and Adaptation to Climate Change." *Economic Geography*, (Ipcc).

Aguilar, E., Peterson, T. C., Obando, P. R., Frutos, R., Retana, J. A. (2005). "Changes in precipitation and temperature extremes in Central America and northern South America, 1961–2003." *Journal of Geophysical Research*, 110(D23), D23107.

Al-sharif, A. A. A., and Pradhan, B. (2014). "Monitoring and predicting land use change in Tripoli Metropolitan City using an integrated Markov chain and cellular automata models in GIS." *Arabian Journal of Geosciences*, 7(10), 4291–4301.

Alexander, L. V., Zhang, X., Peterson, T. C., Caesar, J., Gleason, B. (2006). "Global observed changes in daily climate extremes of temperature and precipitation." *Journal of Geophysical Research Atmospheres*, 111(5), 1–22.

Alibuyog, N. R., Ella, V. B., Reyes, M. R., Srinivasan, R., Heatwole, C., and Dillaha, T. (2009). "Predicting the Effects of Land Use on Runoff and Sediment Yield in Selected Sub-watersheds of the Manupali River Using the ArcSWAT Model." *International Agricultural Engineering Journal*, 18, 15–25.

Anandhi, A., and Nanjundiah, R. S. (2014). "Performance evaluation of AR4 Climate Models in simulating daily precipitation over the Indian region using skill scores." *Theoretical and Applied Climatology*, 119(3–4), 551–566.

Anderson, T. W. (1952). “Theory of certain" Goodness of fit" criteria based on stochastic processes.” *Ann. Math. Stat.*, 23, 193–212.

Arnell, N. W. (1999). “The Effect of Climate Change on Hydrological Regimes in Europe.pdf.” *Global Environmental Change*, 9(1), 5–23.

Arnold, J. G., and Allen, P. M. (1996). “Estimating hydrologic budgets for three Illinois watersheds.” *Journal of Hydrology*, 176(1–4), 57–77.

Arnold, J. G., Srinivasan, R., Muttiah, R. S., and Williams, J. R. (1998). “Large area Hydrologic Modeling and Assessment Part I: Model development ‘Basin scale model called SWAT (Soil and Water speed and storage, advanced software debugging policy to meet the needs, and the management to the tank model).’” *American Water Resources Association*, 34(February), 73–89.

Arora, M., Goel, N. K., and Singh, P. (2005). “Evaluation de tendances de température en Inde.” *Hydrological Sciences Journal*, 50(1), 81–93.

Asres, R. S., Tilahun, S. A., Ayele, G. T., and Melesse, A. M. (2016). “Analyses of land use/land cover change dynamics in the upland watersheds of Upper Blue Nile Basin.” *Landscape Dynamics, Soils and Hydrological Processes in Varied Climates*, Springer, 73–91.

Azamathulla, H. M., and Zahiri, A. (2012). “Flow discharge prediction in compound channels using linear genetic programming.” *Journal of hydrology*, Elsevier, 454, 203–207.

Balamurugan, B., Das, B., Zhang, W. Y., Skomski, R., and Sellmyer, D. J. (2014). “Hf-Co and Zr-Co alloys for rare-earth-free permanent magnets.” *Journal of Physics Condensed Matter*, 26(6).

Barbier, E. B., and Burgess, J. C. (1996). “Economic analysis of deforestation in Mexico.” *Environment and Development Economics*, Cambridge University Press, 1(2), 203–239.

Basistha, A., Arya, D. S., and Goel, N. K. (2008). “Spatial distribution of rainfall in Indian Himalayas - A case study of Uttarakhand Region.” *Water Resources Management*, 22(10), 1325–1346.

Behera, S., and Panda, R. K. (2006). “Evaluation of management alternatives for an agricultural watershed in a sub-humid subtropical region using a physical process based model.” *Agriculture, Ecosystems and Environment*, 113(1–4), 62–72.

Bharati, L., and Jayakody, P. (2011). “Hydrological impacts of inflow and land-use changes in the Gorai River catchment, Bangladesh.” *Water International*, 36(3), 357–369.

Bhaskar, N. R., Parida, B. P., and Nayak, A. K. (1997). “Flood estimation for ungauged catchments using the GIUH.” *Journal of water resources planning and management*, American Society of Civil Engineers, 123(4), 228–238.

Bhavani, P., Chakravarthi, V., Roy, P. S., Joshi, P. K., and Chandrasekar, K. (2017). “Long-term agricultural performance and climate variability for drought assessment: a regional study from Telangana and Andhra Pradesh states, India.” *Geomatics, Natural Hazards and Risk*, Taylor & Francis, 8(2), 822–840.

Bishaw, B. (2001). “Deforestation and Land Degredation in the Ethiopian Highlands: A Strategy for Physical Recovery.” *Northeast African Studies*, 8(1), 7–25.

Boyles, R. P., and Raman, S. (2003). “Analysis of climate trends in North Carolina (1949-1998).” *Environment International*, 29(2–3), 263–275.

Bronstert, A., Niehoff, D., and Brger, G. (2002). “Effects of climate and land-use change on storm runoff generation: Present knowledge and modelling capabilities.” *Hydrological Processes*, 16(2), 509–529.

Burns, D. A., Klaus, J., and McHale, M. R. (2007). “Recent climate trends and implications for water resources in the Catskill Mountain region, New York, USA.” *Journal of Hydrology*, 336(1–2), 155–170.

Byakatonda, J., Parida, B. P., and Kenabatho, P. K. (2015). “Climate Variability and Trends in Meteorological Time Series in Semi-Arid Botswana.” *Preceding of the 10 th Alexander von Humboldt International Conference Addis Ababa, Ethiopia*, 18–20.

Camici, S., Brocca, L., Melone, F., and Moramarco, T. (2013). “Impact of Climate Change on Flood Frequency Using Different Climate Models and Downscaling Approaches.” *Journal of Hydrologic Engineering*, 19(8), 04014002.

Caramelo, L., and Manso, M. D. (2007). “A study of precipitation variability in the Duero Basin (Iberian Peninsula).” 339(October 2006), 327–339.

Chandrakar, A., Khare, D., and Krishan, R. (2017). "Assessment of Spatial and Temporal Trends of Long Term Precipitation over Kharun Watershed, Chhattisgarh, India." *Environmental Processes*, Environmental Processes, 4(4), 959–974.

Chapi, K., Rudra, R. P., Ahmed, S. I., Khan, A. A., Gharabaghi, B., Dickinson, W. T., and Goel, P. K. (2015). "Spatial-temporal dynamics of runoff generation areas in a small agricultural watershed in southern Ontario." *Journal of Water Resource and Protection*, Scientific Research Publishing, 7(01), 14.

Chatterjee, S., Khan, A., and Barman, N. K. (2014). "Research article application of sequential mann-kendall test for detection of approximate significant change point in surface air temperature for kolkata weather observatory , west bengal , india." *International Journal of Current Research*, 6(2), 5319–5324.

Chattopadhyay, S., and Jha, M. K. (2016). "Hydrological response due to projected climate variability in Haw River watershed, North Carolina, USA." *Hydrological Sciences Journal*, Taylor & Francis, 61(3), 495–506.

Chen, H., Xu, C. Y., and Guo, S. (2012). "Comparison and evaluation of multiple GCMs, statistical downscaling and hydrological models in the study of climate change impacts on runoff." *Journal of Hydrology*, Elsevier B.V., 434–435, 36–45.

Cheung, W. H., Senay, G. B., and Singh, A. (2008). "Trends and spatial distribution of annual and seasonal rainfall in Ethiopia." *International journal of climatology*, Wiley Online Library, 28(13), 1723–1734.

Christensen, O. B., Gutowski, W. J., Nikulin, G., and Legutke, S. (2013). "1 Introduction The data must comply 100 % with the DRS and CVs . 2 File format 3 Grids." (Dmi), 1–23.

Chu, T. W., and Shirmohammadi, A. (2004). "Swat m." 47(4), 1057–1074.

Dakhlalla, A. O., and Parajuli, P. B. (2016). "Evaluation of the Best Management Practices at the Watershed Scale to Attenuate Peak Streamflow Under Climate Change Scenarios." *Water Resources Management*, 30(3), 963–982.

De, U. S., and Rao, G. S. P. (2004). "Urban climate trends—the Indian scenario." *Journal of Indian Geophysical Union*, 8(3), 199–203.

DeFries, R., and Eshleman, K. N. (2004). “Land-use change and hydrologic processes: a major focus for the future.” *Hydrological processes*, Wiley Online Library, 18(11), 2183–2186.

Dettinger, M. D., Cayan, D. R., Meyer, M. K., and Jeton, A. (2004). “Simulated hydrologic responses to climate variations and change in the Merced, Carson, and American River basins, Sierra Nevada, California, 1900-2099 *.” *Climatic Change*, 62(1–3), 283–317.

Dewan, A. M., and Yamaguchi, Y. (2009). “Using remote sensing and GIS to detect and monitor land use and land cover change in Dhaka Metropolitan of Bangladesh during 1960-2005.” *Environmental Monitoring and Assessment*, 150(1–4), 237–249.

Diaconis, P., and Efron, B. (1985). “Institute of Mathematical Statistics is collaborating with JSTOR to digitize, preserve, and extend access to The Annals of Statistics. ® www.jstor.org.” *Annals of Statistics*, 13(3), 845–874.

Dibike, Y. B., and Coulibaly, P. (2005). “Hydrologic impact of climate change in the Saguenay watershed: Comparison of downscaling methods and hydrologic models.” *Journal of Hydrology*, 307(1–4), 145–163.

Dinor, J., Azazi Zakaria, N., Abdullah, R., and Ab Ghani, A. (2005). “Deforestation Effect to the Runoff Hydrography at Sungai Padas Catchment.” *2nd International Conference on Managing Rivers in the 21st Century*, 351–359.

Duhan, D., and Pandey, A. (2013). “Statistical analysis of long term spatial and temporal trends of precipitation during 1901-2002 at Madhya Pradesh, India.” *Atmospheric Research*, Elsevier B.V., 122, 136–149.

Duhan, D., and Pandey, A. (2015). “Statistical downscaling of temperature using three techniques in the Tons River basin in Central India.” *Theoretical and Applied Climatology*, 121(3–4), 605–622.

Easton, Z. M., Fuka, D. R., White, E. D., Collick, A. S., Biruk Ashagre, B., McCartney, M., Awulachew, S. B., Ahmed, A. A., and Steenhuis, T. S. (2010). “A multi basin SWAT model analysis of runoff and sedimentation in the Blue Nile, Ethiopia.” *Hydrology and Earth System Sciences*, 14(10), 1827–1841.

Epule, T. E., Ford, J. D., Lwasa, S., and Lepage, L. (2017). "Climate change adaptation in the Sahel." *Environmental Science and Policy*, Elsevier, 75(May), 121–137.

Errasti, I., Ezcurra, A., Sáenz, J., and Ibarra-Berastegi, G. (2011). "Validation of IPCC AR4 models over the Iberian Peninsula." *Theoretical and Applied Climatology*, 103(1), 61–79.

Evans, J. P., and McCabe, M. F. (2010). "Regional climate simulation over Australia's Murray-Darling basin: A multitemporal assessment." *Journal of Geophysical Research Atmospheres*, 115(14), 1–15.

Ezber, Y., Lutfi Sen, O., Kindap, T., and Karaca, M. (2007). "Climatic effects of urbanization in Istanbul: a statistical and modeling analysis." *International Journal of Climatology: A Journal of the Royal Meteorological Society*, Wiley Online Library, 27(5), 667–679.

Fan, F., Wang, Y., and Wang, Z. (2008). "Temporal and spatial change detecting (1998-2003) and predicting of land use and land cover in Core corridor of Pearl River Delta (China) by using TM and ETM+ images." *Environmental Monitoring and Assessment*, 137(1–3), 127–147.

Farley, K. A., Jobbágy, E. G., and Jackson, R. B. (2005). "Effects of afforestation on water yield: a global synthesis with implications for policy." *Global change biology*, Wiley Online Library, 11(10), 1565–1576.

Fazzini, M., Bisci, C., and Billi, P. (2015). "Landscapes and landforms of Ethiopia." *Choice Reviews Online*, 53(02), 53-0795-53–0795.

Fennessy, M. J. (1994). "The simulated Indian monsoon: a GCM sensitivity study." *Journal of Climate*.

Ficklin, D. L., Luo, Y., Luedeling, E., and Zhang, M. (2009). "Climate change sensitivity assessment of a highly agricultural watershed using SWAT." *Journal of Hydrology*, Elsevier B.V., 374(1–2), 16–29.

Fischer, G., Tubiello, F. N., van Velthuizen, H., and Wiberg, D. A. (2007). "Climate change impacts on irrigation water requirements: Effects of mitigation, 1990-2080." *Technological Forecasting and Social Change*, 74(7), 1083–1107.

Franczyk, J. (2000). "The Effects of Climate Change and Urbanization on the Runoff of the Rock Creek Basin."

Frei, C., Christensen, J. H., Déqué, M., Jacob, D., Jones, R. G., and Vidale, P. L. (2003). "Daily precipitation statistics in regional climate models: Evaluation and intercomparison for the European Alps." *Journal of Geophysical Research: Atmospheres*, 108(D3), n/a-n/a.

Fu, G., Liu, Z., Charles, S. P., Xu, Z., and Yao, Z. (2013a). "A score-based method for assessing the performance of GCMs: A case study of southeastern Australia." *Journal of Geophysical Research Atmospheres*, 118(10), 4154–4167.

Fu, G., Yu, J., Yu, X., Ouyang, R., Zhang, Y., Wang, P., Liu, W., and Min, L. (2013b). "Temporal variation of extreme rainfall events in China, 1961-2009." *Journal of Hydrology*, Elsevier B.V., 487, 48–59.

Gan, T. Y., Ito, M., Hülsmann, S., Qin, X., Lu, X. X., Liong, S. Y., Rutschman, P., Disse, M., and Koivusalo, H. (2016). "Possible climate change/variability and human impacts, vulnerability of drought-prone regions, water resources and capacity building for Africa." *Hydrological Sciences Journal*, 61(7), 1209–1226.

Garbrecht, J., Van Liew, M., and Brown, G. O. (2004). "Trends in Precipitation, Streamflow, and Evapotranspiration in the Great Plains of the United States." *Journal of Hydrologic Engineering*, 9(5), 360–367.

Gassman, P. W., Reyes, M. R., Green, C. H., and Arnold, J. G. (2007). "T s w a t : h d , a , f r d." 50(4), 1211–1250.

Gebremicael, T. G., Mohamed, Y. A., Betrie, G. D., van der Zaag, P., and Teferi, E. (2013). "Trend analysis of runoff and sediment fluxes in the Upper Blue Nile basin: A combined analysis of statistical tests, physically-based models and landuse maps." *Journal of Hydrology*, 482, 57–68.

Gessesse, B., Bewket, W., and Bräuning, A. (2015). "Model-Based Characterization and Monitoring of Runoff and Soil Erosion in Response to Land Use/land Cover Changes in the Modjo Watershed, Ethiopia." *Land Degradation and Development*, 26(7), 711–724.

Ghani, A. A., Ali, R., Zakaria, N. A., Hasan, Z. A., Chang, C. K., and Ahamad, M. S. S. (2010). "A temporal change study of the Muda River system over 22 years." *Intl. J. River Basin Management*, Taylor & Francis, 8(1), 25–37.

Ghani, A. A. B., Zakaria, N. A., and Kassim, M. (2008). "Sediment deposition in a rigid monsoon drain." *International Journal of River Basin Management*, 6(1), 23–30.

Ghosh, S. (2010). "SVM-PGSL coupled approach for statistical downscaling to predict rainfall from GCM output." *Journal of Geophysical Research Atmospheres*, 115(22), 1–18.

Gocic, M., and Trajkovic, S. (2013). "Analysis of changes in meteorological variables using Mann-Kendall and Sen's slope estimator statistical tests in Serbia." *Global and Planetary Change*, Elsevier B.V., 100, 172–182.

Golmohammadi, G., Rudra, R., Dickinson, T., Goel, P., and Veliz, M. (2017). "Predicting the temporal variation of flow contributing areas using SWAT." *Journal of Hydrology*, Elsevier, 547, 375–386.

Gosain, A. K., Rao, S., and Arora, A. (2011). "Climate change impact assessment of water resources of India." *Current Science*, 101(3), 356–371.

Gosain, A. K., Rao, S., and Basuray, D. (2006). "SPECIAL SECTION: CLIMATE CHANGE AND INDIA Climate change impact assessment on hydrology of Indian river basins." *Current Science*, 90(3).

Graham, L. P., Andreáasson, J., and Carlsson, B. (2007a). "Assessing climate change impacts on hydrology from an ensemble of regional climate models, model scales and linking methods - A case study on the Lule River basin." *Climatic Change*, 81(SUPPL. 1), 293–307.

Graham, L. P., Hagemann, S., Jaun, S., and Beniston, M. (2007b). "On interpreting hydrological change from regional climate models." *Climatic Change*, 81(SUPPL. 1), 97–122.

Green, C. H., and van Griensven, A. (2008). "Autocalibration in hydrologic modeling: Using SWAT2005 in small-scale watersheds." *Environmental Modelling and Software*, 23(4), 422–434.

Green, C. H., Tomer, M. D., Di Luzio, M., and Arnold, J. G. (2006). "Hydrologic evaluation of the soil and water assessment tool for a large tile-drained watershed in Iowa." *Transactions of the ASABE*, American Society of Agricultural and Biological Engineers, 49(2), 413–422.

Griensven, A., and Meixner, T. (2006). "Methods to quantify and identify the sources of uncertainty for river basin water quality models." *Water Science and Technology*, 53(1), 51–59.

Griensven, A., Meixner, T., Grunwald, S., Bishop, T., Diluzio, M., and Srinivasan, R. (2006). "A global sensitivity analysis tool for the parameters of multi-variable catchment models." *Journal of Hydrology*, 324(1–4), 10–23.

Guan, D., Li, H., Inohae, T., Su, W., Nagaie, T., and Hokao, K. (2011). "Modeling urban land use change by the integration of cellular automaton and Markov model." *Ecological Modelling*, Elsevier B.V., 222(20–22), 3761–3772.

Guo, H., Hu, Q., and Jiang, T. (2008). "Annual and seasonal streamflow responses to climate and land-cover changes in the Poyang Lake basin, China." *Journal of Hydrology*, 355(1–4), 106–122.

Guy, B. T., Dickinson, W. T., and Rudra, R. P. (1987). "The roles of rainfall and runoff in the sediment transport capacity of interrill flow." *Transactions of the ASAE*, American Society of Agricultural and Biological Engineers, 30(5), 1378–1386.

Haddeland, I., Heinke, J., Biemans, H., Eisner, S., Flörke, M., Hanasaki, N., Konzmann, M., Ludwig, F., Masaki, Y., Schewe, J., Stacke, T., Tessler, Z. D., Wada, Y., and Wisser, D. (2014). "Global water resources affected by human interventions and climate change." *Proceedings of the National Academy of Sciences*, 111(9), 3251–3256.

Halmy, M. W. A., Gessler, P. E., Hicke, J. A., and Salem, B. B. (2015). "Land use/land cover change detection and prediction in the north-western coastal desert of Egypt using Markov-CA." *Applied Geography*, Elsevier Ltd, 63, 101–112.

Hamed, K. H., and Rao, A. (1998). "A modified Mann-Kendall trend test for autocorrelated data." *Journal of Hydrology*, 204(1–4), 182–196.

Hargreaves, G., and Samani, Z. (1985). "Reference Crop Evapotranspiration from Temperature." *Applied Engineering in Agriculture*, 1(2), 96–99.

Hassan, Z., Harun, S., and Malek, M. A. (2012). "Application of ANNs Model with the SDSM for the Hydrological Trend Prediction in the Sub-catchment of Kurau River, Malaysia." *Journal of Environment Science and Engineering B*, 1(May 2014), 577–585.

Hay, L. E., Clark, M. P., Wilby, R. L., Gutowski, W. J., Leavesley, G. H., Pan, Z., Arritt, R. W., and Takle, E. S. (2002). "Use of Regional Climate Model Output for Hydrologic Simulations." *Journal of Hydrometeorology*, 3(5), 571–590.

Heo, J., Yu, J., Giardino, J. R., and Cho, H. (2015). "Impacts of climate and land-cover changes on water resources in a humid subtropical watershed: a case study from East Texas, USA." *Water and Environment Journal*, Wiley Online Library, 29(1), 51–60.

Heuvelmans, G., Muys, B., and Feyen, J. (2004). "Evaluation of hydrological model parameter transferability for simulating the impact of land use on catchment hydrology." *Physics and Chemistry of the Earth*, 29(11-12 SPEC. ISS.), 739–747.

Holland, G., Done, J., Bruyere, C., Cooper, C. K., and Suzuki, A. (2010). "Model investigations of the effects of climate variability and change on future Gulf of Mexico tropical cyclone activity." *Offshore Technology Conference*, Offshore Technology Conference.

Hu, Z., and Lo, C. P. (2007). "Modeling urban growth in Atlanta using logistic regression." *Computers, Environment and Urban Systems*, 31(6), 667–688.

Hua, L., He, X., Yuan, Y., and Nan, H. (2012). "Assessment of runoff and sediment yields using the AnnAGNPS model in a three-gorge watershed of China." *International Journal of Environmental Research and Public Health*, 9(5), 1887–1907.

Huang, J., Zhang, J., Zhang, Z., Xu, C., Wang, B., and Yao, J. (2011). "Estimation of future precipitation change in the Yangtze River basin by using statistical downscaling method." *Stochastic Environmental Research and Risk Assessment*, Springer, 25(6), 781–792.

Huong, H. T. L., and Pathirana, A. (2013). "Urbanization and climate change impacts on future urban flooding in Can Tho city, Vietnam." *Hydrology and Earth System Sciences*, 17(1), 379–394.

Ipcc. (2013). "Climate Change 2013: The Physical Science Basis. Contribution of Working Group I to the Fifth Assessment Report of the Intergovernmental Panel on Climate Change." *Intergovernmental Panel on Climate Change, Working Group I Contribution to the IPCC Fifth Assessment Report (AR5)(Cambridge Univ Press, New York)*, 1535.

IPCC. (2007a). “Climate Change 2007 - The physical science basis: contribution of working group I to the fourth assessment rep.” *Bulletin fuer Angewandte Geologie*, 18(2), 5–19.

IPCC. (2007b). *Climate Change 2007: impacts, adaptation and vulnerability: contribution of Working Group II to the fourth assessment report of the Intergovernmental Panel. Genebra, Suíça*.

IPCC. (2017). “Ocean circulation: Thermohaline circulation.” *Theoretical and Applied Climatology*, Elsevier B.V., 4(2), 1549-1555.

Iqbal, M. F., and Khan, I. A. (2014). “Spatiotemporal Land Use Land Cover change analysis and erosion risk mapping of Azad Jammu and Kashmir, Pakistan.” *Egyptian Journal of Remote Sensing and Space Science*, Elsevier B.V., 17(2), 209–229.

Iskander, S. M., Rajib, M. A., and Rahman, M. M. (2014). “Trending Regional Precipitation Distribution and Intensity: Use of Climatic Indices.” *Atmospheric and Climate Sciences*, 04(03), 385–393.

Jain, S. K., and Kumar, V. (2012). “Trend analysis of rainfall and temperature data for India.” *Current Science (Bangalore)*, 102(1), 37–49.

Jain, S. K., Kumar, V., and Saharia, M. (2013). “Analysis of rainfall and temperature trends in northeast India.” *International Journal of Climatology*, 33(4), 968–978.

Jaiswal, R. K., Saxena, R., and Mukherjee, S. (1999). “Application of remote sensing technology for land use/land cover change analysis.” *Journal of the Indian Society of Remote Sensing*, 27(2), 123–128.

Jat, M. K., Khare, D., Garg, P. K., and Shankar, V. (2009). “Remote sensing and GIS-based assessment of urbanisation and degradation of watershed health.” *Urban Water Journal*, 6(3), 251–263.

Jha, M., Pan, Z., Tackle, E. S., and Gu, R. (2004). “Impacts of climate change on streamflow in the Upper Mississippi River Basin: A regional climate model perspective.” *Journal of Geophysical Research D: Atmospheres*, 109(9), 1–12.

Jhajharia, D., and Singh, V. P. (2011). “Trends in temperature, diurnal temperature range and sunshine duration in Northeast India.” *International Journal of Climatology*, 31(9), 1353–1367.

Johnson, F., and Sharma, A. (2009). "Measurement of GCM skill in predicting variables relevant for hydroclimatological assessments." *Journal of Climate*, 22(16), 4373–4382.

Kabba, V. T. S., and Li, J. (2011). "Analysis of Land Use and Land Cover Changes, and Their Ecological Implications in Wuhan, China." *Journal of Geography and Geology*, 3(1).

Kampata, J. M., Parida, B. P., and Moalafhi, D. B. (2008). "Trend analysis of rainfall in the headstreams of the Zambezi River Basin in Zambia." *Physics and Chemistry of the Earth*, 33(8–13), 621–625.

Kamusoko, C., Aniya, M., Adi, B., and Manjoro, M. (2009). "Rural sustainability under threat in Zimbabwe - Simulation of future land use/cover changes in the Bindura district based on the Markov-cellular automata model." *Applied Geography*, Elsevier Ltd, 29(3), 435–447.

Kang, I. S., Jin, K., Wang, B., Lau, K. M., Shukla, J., Krishnamurthy, V., Schubert, S., Wailser, D., Stern, W., Kitoh, A., Meehl, G., Kanamitsu, M., Galin, V., Satyan, V., Park, C. K., and Liu, Y. (2002). "Intercomparison of the climatological variations of Asian summer monsoon precipitation simulated by 10 GCMs." *Climate Dynamics*, 19(5–6), 383–395.

Kannan, N., White, S. M., Worrall, F., and Whelan, M. J. (2007). "Sensitivity analysis and identification of the best evapotranspiration and runoff options for hydrological modelling in SWAT-2000." *Journal of Hydrology*, 332(3–4), 456–466.

Kay, A. L., Davies, H. N., Bell, V. A., and Jones, R. G. (2009). "Comparison of uncertainty sources for climate change impacts: Flood frequency in England." *Climatic Change*, 92(1–2), 41–63.

Keller, M. (2009). "Climate Risks and Development Projects." *Assessment Report for a Community-Level Project in Guduru, Oromia, Ethiopia*, (November), 1–35.

Kelly, P. M., and Adger, W. N. (2000). "Theory and practice in assessing vulnerability to climate change and facilitating adaptation." *Climatic Change*, 47(4), 325–352.

Kenabatho, P. K., Parida, B. P., and Moalafhi, D. B. (2012). "The value of large-scale climate variables in climate change assessment: The case of Botswana's rainfall." *Physics and Chemistry of the Earth*, Elsevier Ltd, 50–52, 64–71.

Kendall, M. G. (1975). "Rank correlation measures." *Charles Griffin, London*, 202, 15.

Khare, D., Patra, D., Mondal, A., and Kundu, S. (2014). "Impact of landuse/land cover change on run-off in a catchment of Narmada river in India." *Applied Geomatics*, 7(1), 23–35.

Khoi, D. N., and Suetsugi, T. (2014). "The responses of hydrological processes and sediment yield to land-use and climate change in the Be River Catchment, Vietnam." *Hydrological Processes*, 28(3), 640–652.

Kioutsioukis, I., Melas, D., and Zerefos, C. (2010). "Statistical assessment of changes in climate extremes over Greece (1955-2002)." *International Journal of Climatology*, 30(11), 1723–1737.

Kiran, V. S. S. (2013). "Change Detection In Landuse/Landcover Using Remote Sensing & G. I. S Techniques: A Case Study Of Mahananda Catchment, West Bengal." *International Journal Of Research In Management Studies*, 2, 68–72.

Klein Tank, A. M. G., and Können, G. P. (2003). "Trends in Indices of daily temperature and precipitation extremes in Europe, 1946-99." *Journal of Climate*, 16(22), 3665–3680.

Kodra, E., Ghosh, S., and Ganguly, A. R. (2012). "Evaluation of global climate models for Indian monsoon climatology." *Environmental Research Letters*, 7(1).

Kondratyev, K. Y., and Cracknell, A. P. (2017). *Observing global climate change*. CRC Press.

Kothawale, D. R., Revadekar, J. V., and Kumar, K. R. (2010). "Recent trends in pre-monsoon daily temperature extremes over India." *Journal of Earth System Science*, 119(1), 51–65.

Kruger, A. C., and Shongwe, S. (2004). "Temperature trends in South Africa: 1960-2003." *International Journal of Climatology*, 24(15), 1929–1945.

Kucukmehmetoglu, M., and Geymen, A. (2008). "Measuring the spatial impacts of urbanization on the surface water resource basins in Istanbul via remote sensing." *Environmental Monitoring and Assessment*, 142(1–3), 153–169.

Kuemmerle, T., Radeloff, V. C., Perzanowski, K., and Hostert, P. (2006). "Cross-border comparison of land cover and landscape pattern in Eastern Europe using a hybrid classification technique." *Remote Sensing of Environment*, 103(4), 449–464.

Kuhnle, R. A., Bingner, R. L., Foster, G. R., and Grissinger, E. H. (1996). "Effect of land use changes on sediment transport in Goodwin Creek." *Water Resources Research*, 32(10), 3189–3196.

Kumar, M., Ramanathan, A., Rao, M. S., and Kumar, B. (2006). “Identification and evaluation of hydrogeochemical processes in the groundwater environment of Delhi, India.” *Environmental Geology*, 50(7), 1025–1039.

Kumar, N., Tischbein, B., Kusche, J., Laux, P., Beg, M. K., and Bogardi, J. J. (2017). “Impact of climate change on water resources of upper Kharun catchment in Chhattisgarh, India.” *Journal of Hydrology: Regional Studies*, Regional Environmental Change, 13, 189–207.

Kumar, P., Wiltshire, A., Mathison, C., Asharaf, S., Ahrens, B., Lucas-Picher, P., Christensen, J. H., Gobiet, A., Saeed, F., Hagemann, S., and Jacob, D. (2013). “Downscaled climate change projections with uncertainty assessment over India using a high resolution multi-model approach.” *Science of the Total Environment*, Elsevier B.V., 468–469, S18–S30.

Kunkel, K. E. (2003). “North American Trends in Extreme Precipitation - Springer.” *Natural Hazards*, 29(2), 291–305.

Lafon, T., Dadson, S., Buys, G., and Prudhomme, C. (2013). “Bias correction of daily precipitation simulated by a regional climate model: A comparison of methods.” *International Journal of Climatology*, 33(6), 1367–1381.

Lambin, E.F., Geist, H.J. and Lepers, E., 2003. "Dynamics of land-use and land-cover change in tropical regions." *Annual review of environment and resources*, 28(1), pp.205-241.

Lázaro, R., Rodrigo, F. S., Gutiérrez, L., Domingo, F., and Puigdefábregas, J. (2001). “Analysis of a 30-year rainfall record (1967-1997) in semi-arid SE spain for implications on vegetation.” *Journal of Arid Environments*, 48(3), 373–395.

Legates, D. R., and Mccabe, G. J. (2013). “A refined index of model performance: A rejoinder.” *International Journal of Climatology*, 33(4), 1053–1056.

Lenhart, T., Eckhardt, K., Fohrer, N., and Frede, H.-G. (2002). “Comparison of two different approaches of sensitivity analysis.” *Physics and Chemistry of the Earth, Parts A/B/C*, Elsevier, 27(9–10), 645–654.

Li, L., Xu, C. Y., Zhang, Z., and Jain, S. K. (2014). “Validation of a new meteorological forcing data in analysis of spatial and temporal variability of precipitation in India.” *Stochastic Environmental Research and Risk Assessment*, 28(2), 239–252.

Li, Y. G., He, D., Hu, J. M., and Cao, J. (2015). "Variability of extreme precipitation over Yunnan Province, China 1960-2012." *International Journal of Climatology*, 35(2), 245–258.

Liang, L., Li, L., and Liu, Q. (2011). "Precipitation variability in Northeast China from 1961 to 2008." *Journal of Hydrology*, Elsevier B.V., 404(1–2), 67–76.

Van Liew, M. W., Veith, T. L., Bosch, D. D., and Arnold, J. G. (2007). "Suitability of SWAT for the Conservation Effects Assessment Project: Comparison on USDA Agricultural Research Service Watersheds." *Journal of Hydrologic Engineering*, 12(2), 173–189.

Lin, Y. P., Hong, N. M., Wu, P. J., Wu, C. F., and Verburg, P. H. (2007). "Impacts of land use change scenarios on hydrology and land use patterns in the Wu-Tu watershed in Northern Taiwan." *Landscape and Urban Planning*, 80(1–2), 111–126.

Linden, P. Van Der. (2007). "Climate Change 2007: Impacts, Adaptation and Vulnerability. Contribution of Working Group II to the Fourth Assessment Report of the Intergovernmental Panel on Climate Change." *Intergovernmental Panel on Climate Change*, 4, 982.

Liu, G. H., Luan, Z. Q., Yan, B. X., Guo, Y. D., and Wang, Z. X. (2015). "Response of hydrological processes to land use change and climate variability in the upper Naoli River watershed, northeast China." *Water Resources*, 42(4), 438–447.

Liu, L., Liu, Z., Ren, X., Fischer, T., and Xu, Y. (2011). "Hydrological impacts of climate change in the Yellow River Basin for the 21st century using hydrological model and statistical downscaling model." *Quaternary International*, Elsevier Ltd and INQUA, 244(2), 211–220.

Liu, M., and Lu, J. (2015). "Predicting the impact of management practices on river water quality using SWAT in an agricultural watershed." *Desalination and Water Treatment*, Taylor & Francis, 54(9), 2396–2409.

Loaiciga, H. A., Valdes, J. B., Vogel, R., Garvey, J., and Schwarz, H. (1996). "Global warming and the hydrologic cycle." *Journal of Hydrology*, 174(1–2), 83–127.

Longobardi, A., and Villani, P. (2010). "Trend analysis of annual and seasonal rainfall time series in the Mediterranean area." *International Journal of Climatology*, 30(10), 1538–1546.

Loukas, A., and Quick, M. C. (1996). "Spatial and temporal distribution of storm precipitation in southwestern British Columbia." *Journal of Hydrology*, 174(1–2), 37–56.

Lynch, A. H., and Arcsym, M. (2000). “Response of the seasonal carbon cycle in high latitudes to.” 105, 897–908.

Mall, R. K., Gupta, A., Singh, R., Singh, R. S., and Rathore, L. S. (2006a). “Jun06-Water-Cc-Cgc-India-Cursci.” 90(12).

Mall, R. K., Singh, R., Gupta, A., Srinivasan, G., and Rathore, L. S. (2006b). “Impact of climate change on Indian agriculture: A review.” *Climatic Change*, 78(2–4), 445–478.

Mansell, M. G. (1997). “The effect of climate change on rainfall trends and flooding risk in the West of Scotland.” *Nordic hydrology*, 28(1), 37–50.

Marengo, J. A., Rusticucci, M., Penalba, O., and Renom, M. (2010). “An intercomparison of observed and simulated extreme rainfall and temperature events during the last half of the twentieth century: Part 2: Historical trends.” *Climatic Change*, 98(3), 509–529.

Marhaento, H., Booij, M. J., Rientjes, T. H. M., and Hoekstra, A. Y. (2017). “Attribution of changes in the water balance of a tropical catchment to land use change using the SWAT model.” *Hydrological Processes*, 31(11), 2029–2040.

Matondo, J. I., and Msibi, K. M. (2001). “Estimation of the impact of climate change on hydrology and water resources in Swaziland.” *Water International*, 26(3), 425–434.

Matondo, J. I., Peter, G., and Msibi, K. M. (2004). “Evaluation of the impact of climate change on hydrology and water resources in Swaziland: Part I.” *Physics and Chemistry of the Earth*, 29(15-18 SPEC.ISS.), 1181–1191.

McAlpine, C. A., Syktus, J., Deo, R. C., Lawrence, P. J., McGowan, H. A., Watterson, I. G., and Phinn, S. R. (2007). “Modeling the impact of historical land cover change on Australia’s regional climate.” *Geophysical Research Letters*, 34(22), 1–6.

Mearns, L. O., Hulme, M., Carter, T. R., Leemans, R., Lal, M., and Whetton, P. (2001). “Climate Scenario Development (Chapter 13). In Climate Change 2001: The Scientific Basis, Contribution of Working Group I to the Third Assessment Report of the IPCC.” 583–638.

Meehl, G. A., Stocker, T. F., Collins, W. D., Friedlingstein, P., Gaye, T., Gregory, J. M., Kitoh, A., Knutti, R., Murphy, J. M., and Noda, A. (2007). “Global climate projections.” Cambridge, UK, Cambridge University Press.

Mehrotra, R., Sharma, A., Kumar, D. N., and Reshmidevi, T. V. (2013). "Assessing future rainfall projections using multiple GCMS and a multi-site stochastic downscaling model." *Journal of Hydrology*, Elsevier B.V., 488, 84–100.

Memarian, H., Kumar Balasundram, S., Bin Talib, J., Teh Boon Sung, C., Mohd Sood, A., and Abbaspour, K. (2012). "Validation of CA-Markov for Simulation of Land Use and Cover Change in the Langat Basin, Malaysia." *Journal of Geographic Information System*, 04(06), 542–554.

Mendis, W. T. G., and Wadigamangawa, A. (1996). "Integration of Remote Sensing and GIS for Land Use/Land Cover Mapping in Nil Wala Basin. GIS Development."

Mersha, A. N., De Fraiture, C., Mehari, A., Masih, I., and Alamirew, T. (2016). "Integrated Water Resources Management: Contrasting principles, policy, and practice, Awash River Basin, Ethiopia." *Water Policy*, 18(2), 335–354.

Meshesha, T. W., Tripathi, S. K., and Khare, D. (2016). "Analyses of land use and land cover change dynamics using GIS and remote sensing during 1984 and 2015 in the Beressa Watershed Northern Central Highland of Ethiopia." *Modeling Earth Systems and Environment*, Springer International Publishing, 2(4), 1–12.

Messinger, T. (2003). "Comparison of storm response of streams in small, unmined and valley-filled watersheds, 1999–2001, Ballard Fork, West Virginia." *US Geological Survey*, 2, 4303.

Meyer, W. B., and Turner, B. L. (2003). "Human Population Growth and Global Land-Use/Cover Change." *Annual Review of Ecology and Systematics*, 23(1), 39–61.

Miao, C., Duan, Q., Sun, Q., Huang, Y., Kong, D., Yang, T., Ye, A., Di, Z., and Gong, W. (2014). "Assessment of CMIP5 climate models and projected temperature changes over Northern Eurasia." *Environmental Research Letters*, IOP Publishing, 9(5).

Min, S. K., Zhang, X., Zwiers, F. W., and Hegerl, G. C. (2011). "Human contribution to more-intense precipitation extremes." *Nature*, Nature Publishing Group, 470(7334), 378–381.

Minale, A., and Rao, K. (2011). "Hydrological Dynamics and Human Impact on Ecosystems of Lake Tana, Northwestern Ethiopia." *Ethiopian Journal of Environmental Studies and Management*, 4(1).

Mirza, M. Q., Warrick, R. a., Ericksen, N. J., and Kenny, G. J. (1998). "Trends and persistence in precipitation in the Ganges, Brahmaputra and Meghna river basins." *Hydrological Sciences Journal*, 43(6), 845–858.

Mishra, S. S., and Nagarajan, R. (2010). "Morphometric analysis and prioritization of sub-watersheds using GIS and remote sensing techniques: a case study of Odisha, India." *International Journal of Geomatics and Geosciences*, Integrated Publishing Association, 1(3), 501.

Mishra, S. S., and Nagarajan, R. (2013). "Hydrological drought assessment in Tel river basin using standardized water level index (SWI) and GIS based interpolation techniques." *International Journal of Conceptions on Mechanical and Civil Engineering*, 1(1), 2–5.

Mitsova, D., Shuster, W., and Wang, X. (2011). "A cellular automata model of land cover change to integrate urban growth with open space conservation." *Landscape and Urban Planning*, Elsevier B.V., 99(2), 141–153.

Modarres, R., and de Paulo Rodrigues da Silva, V. (2007). "Rainfall trends in arid and semi-arid regions of Iran." *Journal of Arid Environments*, 70(2), 344–355.

Mondal, A., Khare, D., and Kundu, S. (2015). "Spatial and temporal analysis of rainfall and temperature trend of India." *Theoretical and Applied Climatology*, 122(1–2), 143–158.

Mondal, A., Khare, D., Kundu, S., Meena, P. K., Mishra, P. K., and Shukla, R. (2014). "Impact of Climate Change on Future Soil Erosion in Different Slope, Land Use, and Soil-Type Conditions in a Part of the Narmada River Basin, India." *Journal of Hydrologic Engineering*, 20(6), C5014003.

Monteith, J. L. (1965). "Evaporation and environment." *Symposia of the society for experimental biology*, Cambridge University Press (CUP) Cambridge, 205–234.

Moriasi, D. N., Arnold, J. G., Van Liew, M. W., Bingner, R. L., Harmel, R. D., and Veith, T. L. (2007). "Curriculum for the Academy Profession Degree Programme in Multimedia Design and Communication - National part, 2017." *American Society of Agricultural and Biological Engineers*, 50(3), 885–900.

Morris, M. D. (1991). "Factorial sampling plans for preliminary computational experiments." *Technometrics*, Taylor & Francis Group, 33(2), 161–174.

Moss, R. H., Edmonds, J. A., Hibbard, K. A., Manning, M. R. (2010). "The next generation of scenarios for climate change research and assessment." *Nature*, Nature Publishing Group, 463(7282), 747–756.

Muller, M. (2007). "Adapting to climate change: Water management for urban resilience." *Environment and Urbanization*, 19(1), 99–113.

Murty, P. S., Pandey, A., and Suryavanshi, S. (2014). "Application of semi-distributed hydrological model for basin level water balance of the Ken basin of Central India." *Hydrological Processes*, 28(13), 4119–4129.

Nagarajan, R., Mukherjee, A., Roy, A., and Khire, M. V. (1998). "Technical note Temporal remote sensing data and GIS application in landslide hazard zonation of part of Western ghat, India." Taylor & Francis.

Narsimlu, B., Gosain, A. K., and Chahar, B. R. (2013). "Assessment of Future Climate Change Impacts on Water Resources of Upper Sind River Basin, India Using SWAT Model." *Water Resources Management*, 27(10), 3647–3662.

Narsimlu, B., Gosain, A. K., Chahar, B. R., Singh, S. K., and Srivastava, P. K. (2015). "SWAT model calibration and uncertainty analysis for streamflow prediction in the Kunwari River Basin, India, using sequential uncertainty fitting." *Environmental Processes*, Springer, 2(1), 79–95.

Neitsch, S. L., Arnold, J. G., Kiniry, J. R., and Williams, J. R. (2011). "Theoretical documentation SWAT."

New, M., Hewitson, B., Stephenson, D. B., Tsiga, A., Kruger, A., Manhique, A. (2006). "Evidence of trends in daily climate extremes over southern and west Africa." *Journal of Geophysical Research Atmospheres*, 111(14), 1–11.

Nicholls, N., and Collins, D. (2006). "Observed Climate Change in Australia over the past Century." *Energy & Environment*, 17(1), 1–12.

Niezgoda, S. L., and Johnson, P. A. (2005). "Improving the urban stream restoration effort: identifying critical form and processes relationships." *Environmental management*, Springer, 35(5), 579–592.

Niraula, R., Meixner, T., and Norman, L. M. (2015). "Determining the importance of model calibration for forecasting absolute/relative changes in streamflow from LULC and climate changes." *Journal of Hydrology*, Elsevier B.V., 522, 439–451.

Nyong, A., Adesina, F., and Osman Elasha, B. (2007). "The value of indigenous knowledge in climate change mitigation and adaptation strategies in the African Sahel." *Mitigation and Adaptation Strategies for Global Change*, 12(5), 787–797.

Ojha, C. S. P. (2013). "Downscaling of Precipitation for Lake Catchment in Arid Region in India using Linear Multiple Regression and Neural Networks." *The Open Hydrology Journal*, 4(1), 122–136.

Ojha, C. S. P., Goyal, M. K., and Adeloye, A. J. (2010). "Downscaling of Precipitation for Lake Catchment in Arid Region in India using Linear Multiple Regression and Neural Networks." 122–136.

Ojha, R., Kumar, D. N., Sharma, A., and Mehrotra, R. (2013). "Assessing GCM Convergence for India Using the Variable Convergence Score." *Journal of Hydrologic Engineering*, 19(6), 1237–1246.

Ojha, R., Nagesh Kumar, D., Sharma, A., and Mehrotra, R. (2012). "Assessing Severe Drought and Wet Events over India in a Future Climate Using a Nested Bias-Correction Approach." *Journal of Hydrologic Engineering*, 18(7), 760–772.

Omer, A., Wang, W., Basheer, A. K., and Yong, B. (2017). "Integrated assessment of the impacts of climate variability and anthropogenic activities on river runoff: a case study in the Hutuo River Basin, China." *Hydrology Research*, 48(2), 416–430.

Pai, D. S., Sridhar, L., Rajeevan, M., Sreejith, O. P., Satbhai, N. S., and Mukhopadyay, B. (2014). "Development of a new high spatial resolution (0 . 25 ° × 0 . 25 °) Long Period (1901-2010) daily gridded rainfall data set over India and its comparison with existing data sets over the region." *Mausam*, 65(1), 1–18.

Panchal, R. A., Suryanarayana, T. M. V, and Parekh, F. P. (2013). "Rainfall-Runoff modeling using ANN at Dharoi sub-basin." *Climate Change Impacts on Water Resources Systems*, 135.

Pandey, B. K., Gosain, A. K., Paul, G., and Khare, D. (2017). "Climate change impact assessment on hydrology of a small watershed using semi-distributed model." *Applied Water Science*, Springer Berlin Heidelberg, 7(4), 2029–2041.

Pandey, B. K., and Khare, D. (2017). "Analyzing and modeling of a large river basin dynamics applying integrated cellular automata and Markov model." *Environmental Earth Sciences*, Springer Berlin Heidelberg, 76(22), 1–12.

Pandey, B. K., and Khare, D. (2018). "Identification of trend in long term precipitation and reference evapotranspiration over Narmada river basin (India)." *Global and Planetary Change*, Elsevier, 161(December 2017), 172–182.

Parekh, F. P., and Suryanarayana, T. M. V. (2012). "Impact of climatological Parameters on yield of wheat using neural network fitting." *International Journal of Modern Engineering Research*, Citeseer, 2(5), 3534–3537.

Parida, B. P. (1999). "Modelling of Indian summer monsoon rainfall using a four-parameter Kappa distribution." *International Journal of Climatology*, 19(12), 1389–1398.

Partal, T., and Kahya, E. (2006). "Trend analysis in Turkish precipitation data." *Hydrological Processes*, 20(9), 2011–2026.

Parth Sarthi, P., Ghosh, S., and Kumar, P. (2015). "Possible future projection of Indian Summer Monsoon Rainfall (ISMR) with the evaluation of model performance in Coupled Model Inter-comparison Project Phase 5 (CMIP5)." *Global and Planetary Change*, Elsevier B.V., 129, 92–106.

Patel, N. R., Suryanarayana, T. M. V, and Shete, D. T. (2018). "Analyzing extreme events using standardized precipitation index during the 20th century for Surat District, India." *Application of Geographical Information Systems and Soft Computation Techniques in Water and Water Based Renewable Energy Problems*, Springer, 41–50.

Patricola, C. M., and Cook, K. H. (2010). “Northern African climate at the end of the twenty-first century: An integrated application of regional and global climate models.” *Climate Dynamics*, 35(1), 193–212.

Pavan, V., Tomozeiu, R., Cacciamani, C., and di Lorenzo, M. (2008). “Daily precipitation observations over Emilia-Romagna: Mean values and extremes.” *International Journal of Climatology*.

Penalba, O. C., and Robledo, F. A. (2010). “Spatial and temporal variability of the frequency of extreme daily rainfall regime in the La Plata Basin during the 20th century.” *Climatic Change*, 98(3), 531–550.

Perkins, S. E., Pitman, A. J., Holbrook, N. J., and McAneney, J. (2007). “Evaluation of the AR4 climate models’ simulated daily maximum temperature, minimum temperature, and precipitation over Australia using probability density functions.” *Journal of Climate*, 20(17), 4356–4376.

Petit, C., Scudder, T., and Lambin, E. (2001). “Quantifying processes of land-cover change by remote sensing: Resettlement and rapid land-cover changes in south-eastern Zambia.” *International Journal of Remote Sensing*, 22(17), 3435–3456.

Piao, S., Friedlingstein, P., Ciais, P., de Noblet-Ducoudré, N., Labat, D., and Zaehle, S. (2007). “Changes in climate and land use have a larger direct impact than rising CO2 on global river runoff trends.” *Proceedings of the National academy of Sciences*, National Acad Sciences, 104(39), 15242–15247.

Pingale, S. M., Khare, D., Jat, M. K., and Adamowski, J. (2014). “Spatial and temporal trends of mean and extreme rainfall and temperature for the 33 urban centers of the arid and semi-arid state of Rajasthan, India.” *Atmospheric Research*, Elsevier B.V., 138, 73–90.

Pisinaras, V., Petalas, C., Gikas, G. D., Gemitzi, A., and Tsihrintzis, V. A. (2010). “Hydrological and water quality modeling in a medium-sized basin using the Soil and Water Assessment Tool (SWAT).” *Desalination*, Elsevier B.V., 250(1), 274–286.

Prakasam, Cji. (2010). “Land use and land cover change detection through remote sensing approach: A case study of Kodaikanal taluk, Tamil nadu.” *International journal of Geomatics and Geosciences*, Integrated Publishing Association, 1(2), 150.

Priestley, C. H. B., and Taylor, R. J. (1972). “On the assessment of surface heat flux and evaporation using large-scale parameters.” *Monthly weather review*, 100(2), 81–92.

Qiang, Y., and Lam, N. S. N. (2015). “Modeling land use and land cover changes in a vulnerable coastal region using artificial neural networks and cellular automata.” *Environmental Monitoring and Assessment*, 187(3).

Qingsong Zhu, Jiaming Mai, and Ling Shao. (2015). “A Fast Single Image Haze Removal Algorithm Using Color Attenuation Prior.” *IEEE Transactions on Image Processing*, IEEE, 24(11), 3522–3533.

Radić, V., and Clarke, G. K. C. (2011). “Evaluation of IPCC models’ performance in simulating late-Twentieth-Century climatologies and weather patterns over North America.” *Journal of Climate*, 24(20), 5257–5274.

Al Radif, A. (1999). “Integrated water resources management (IWRM): An approach to face the challenges of the next century and to avert future crises.” *Desalination*, 124(1–3), 145–153.

Rahmani, V., Hutchinson, S. L., Harrington Jr, J. A., Hutchinson, J. M. S., and Anandhi, A. (2015). “Analysis of temporal and spatial distribution and change-points for annual precipitation in Kansas, USA.” *International Journal of Climatology*.

Rai, P. K., Chahar, B. R., and Dhanya, C. T. (2017). “GIS-based SWMM model for simulating the catchment response to flood events.” *Hydrology Research*, 48(2), 384–394.

Raju, K. S., and Kumar, D. N. (2014). “Ranking of global climate models for India using multicriterion analysis.” *Climate Research*, 60(2), 103–117.

Rao, K. S., and Pant, R. (2001). “Land use dynamics and landscape change pattern in a typical micro watershed in the mid elevation zone of central Himalaya, India.” *Agriculture, Ecosystems and Environment*, 86(2), 113–124.

Rozenstein, O., and Karnieli, A. (2011). “Comparison of methods for land-use classification incorporating remote sensing and GIS inputs.” *Applied Geography*, Elsevier, 31(2), 533–544.

Rusticucci, M., and Barrucand, M. (2004). "Observed trends and changes in temperature extremes over Argentina." *Journal of Climate*, 17(20), 4099–4107.

Saadat, H., Adamowski, J., Bonnell, R., Sharifi, F., Namdar, M., and Ale-Ebrahim, S. (2011). "Land use and land cover classification over a large area in Iran based on single date analysis of satellite imagery." *ISPRS Journal of Photogrammetry and Remote Sensing*, International Society for Photogrammetry and Remote Sensing, Inc. (ISPRS), 66(5), 608–619.

Sajikumar, N., and Remya, R. S. (2015a). "Impact of land cover and land use change on runoff characteristics." *Journal of Environmental Management*, Elsevier Ltd, 161, 460–468.

Sajikumar, N., and Remya, R. S. (2015b). "Impact of land cover and land use change on runoff characteristics." *Journal of Environmental Management*, Elsevier Ltd, 161, 460–468.

Saleh, A., Arnold, J. G., Gassman, P. W., Hauck, L. M., Rosenthal, W. D., Williams, J. R., and Mcfarland, A. M. S. (2000). "A swat u n b r w." 43(5), 1077–1087.

Samal, D. R., and Gedam, S. S. (2012). "Impact of land use dynamics on stream flow: A case study in upper Bhima basin, Maharashtra, India." *International Geoscience and Remote Sensing Symposium (IGARSS)*, IEEE, 7165–7168.

Samal, D. R., and Gedam, S. S. (2014). "Assessing the impact of land use change on stream flow in a semi-urban river basin, Maharashtra, India." *International Journal of Hydrology Science and Technology*, 3(4), 351.

Samal, D. R., Gedam, S. S., and Nagarajan, R. (2015). "GIS based drainage morphometry and its influence on hydrology in parts of Western Ghats region, Maharashtra, India." *Geocarto International*, Taylor & Francis, 30(7), 755–778.

Sanjay, J. (2018). "IITM Coordinated CORDEX South Asia- Downscaled climate change Projections for the Hindu Kush Himalayan region." (October).

Sanjay, J., Krishnan, R., Shrestha, A. B., Rajbhandari, R., and Ren, G. Y. (2017). "Downscaled climate change projections for the Hindu Kush Himalayan region using CORDEX South Asia regional climate models." *Advances in Climate Change Research*, Elsevier Ltd, 8(3), 185–198.

Santhi, C., Kannan, N., Arnold, J. G., and Di Luzio, M. (2008). "Spatial calibration and temporal validation of flow for regional scale hydrologic modeling." *Journal of the American Water*

Resources Association, 44(4), 829–846.

Sato, T., Kimura, F., and Kitoh, A. (2007). "Projection of global warming onto regional precipitation over Mongolia using a regional climate model." *Journal of Hydrology*, 333(1), 144–154.

Saulnier, G. M., Beven, K., and Obled, C. (1997). "Including spatially variable effective soil depths in TOPMODEL." *Journal of Hydrology*, 202(1–4), 158–172.

Schilling, K. E., Jha, M. K., Zhang, Y. K., Gassman, P. W., and Wolter, C. F. (2009). "Impact of land use and land cover change on the water balance of a large agricultural watershed: Historical effects and future directions." *Water Resources Research*, 45(7), 1–12.

Seneviratne, S. I., Nicholls, N., Easterling, D., Goodess, C. M., Kanae, S., Kossin, J., Luo, Y., Marengo, J., Mc Innes, K., and Rahimi, M. (2012). "Changes in climate extremes and their impacts on the natural physical environment." *Managing the risks of extreme events and disasters to advance climate change adaptation: Special report of the Intergovernmental Panel on Climate Change*, Cambridge University Press, 109–230.

Setiawan, Y., and Yoshino, K. (2012). "Change detection in land-use and land-cover dynamics at a regional scale from MODIS time-series imagery." *ISPRS Annals of the Photogrammetry, Remote Sensing and Spatial Information Sciences*, 1(September), 243–248.

Shah, T., and Koppen, B. van. (2006). "Is India Ripe for Integrated Water Resources Management? Fitting Water Policy to National Development Context." *Economic and Political Weekly*, 41(31), 3413–3421.

Shalaby, A., and Tateishi, R. (2007). "Remote sensing and GIS for mapping and monitoring land cover and land-use changes in the Northwestern coastal zone of Egypt." *Applied Geography*, 27(1), 28–41.

Sharma, C. S., Panda, S. N., Pradhan, R. P., Singh, A., and Kawamura, A. (2016). "Precipitation and temperature changes in eastern India by multiple trend detection methods." *Atmospheric Research*, Elsevier B.V., 180, 211–225.

She, D., Shao, Q., Xia, J., Taylor, J. A., Zhang, Y., Zhang, L., Zhang, X., and Zou, L. (2015). "Investigating the variation and non-stationarity in precipitation extremes based on the concept of event-based extreme precipitation." *Journal of Hydrology*, Elsevier B.V., 530, 785–798.

Shifteh Some'e, B., Ezani, A., and Tabari, H. (2012). "Spatiotemporal trends and change point of precipitation in Iran." *Atmospheric Research*, Elsevier B.V., 113, 1–12.

Shrestha, A. B., Bajracharya, S. R., Sharma, A. R., Duo, C., and Kulkarni, A. (2017). "Observed trends and changes in daily temperature and precipitation extremes over the Koshi river basin 1975–2010." *International Journal of Climatology*, 37(2), 1066–1083.

Shrestha, A. B., Wake, C. P., Mayewski, P. A., and Dibb, J. E. (1999). "Maximum temperature trends in the Himalaya and its vicinity: An analysis based on temperature records from Nepal for the period 1971-94." *Journal of Climate*, 12(9), 2775–2786.

Shukla, R., and Khare, D. (2011). "Historical trend investigation of temperature variation in Indira Sagar Canal command area in Madhya Pradesh (1901 – 2005)." 2(2009), 5–13.

Da Silva, V. D. P. R. (2004). "On climate variability in Northeast of Brazil." *Journal of Arid Environments*, 58(4), 575–596.

Singh, A., Rudra, R., and Yang, W. H. (2005). "Adapting SWAT for riparian wetlands in an Ontario watershed." *3rd International SWAT Conference Proceedings*, 123–131.

Singh, J., Knapp, H., and Demissie, M. (2004). "Hydrologic modeling of the Iroquois River watershed using HSPF and SWAT. ISWS CR 2004-08." *Champaign, Ill.: Illinois State Water Survey*, 61820, 343–360.

Singh, S., Ghosh, S., Sahana, A. S., Vittal, H., and Karmakar, S. (2017). "Do dynamic regional models add value to the global model projections of Indian monsoon?" *Climate Dynamics*, Springer Berlin Heidelberg, 48(3–4), 1375–1397.

Singh, V., Goyal, M. K., and Chu, X. (2015). "Multicriteria Evaluation Approach for Assessing Parametric Uncertainty during Extreme Peak and Low Flow Conditions over Snow Glaciated and Inland Catchments." *Journal of Hydrologic Engineering*, 21(1), 04015044.

Sinha, M. K. (2015). "Achieving inclusive growth from large water resources projects." *NDCWWC Journal (A Half Yearly Journal of New Delhi Centre of WWC)*, NEW DELHI CENTRE World Water Council, 4(2), 21–26.

Smeeton, N. C. (1985). "Early history of the kappa statistic." *Biometrics*, 41, 795.

Solomon, S., Qin, D., Manning, M., Averyt, K., and Marquis, M. (2007). *Climate change 2007-the physical science basis: Working group I contribution to the fourth assessment report of the IPCC*. Cambridge university press.

Srinivas, C. V., Hariprasad, D., Bhaskar Rao, D. V., Anjaneyulu, Y., Baskaran, R., and Venkatraman, B. (2013). "Simulation of the Indian summer monsoon regional climate using advanced research WRF model." *International Journal of Climatology*, 33(5), 1195–1210.

Srivastava, P. K., Han, D., Rico-Ramirez, M. A., Bray, M., and Islam, T. (2012). "Selection of classification techniques for land use/land cover change investigation." *Advances in Space Research*, COSPAR, 50(9), 1250–1265.

Su, F., Duan, X., Chen, D., Hao, Z., and Cuo, L. (2013). "Evaluation of the global climate models in the CMIP5 over the Tibetan Plateau." *Journal of Climate*, 26(10), 3187–3208.

Sun, W., Mu, X., Song, X., Wu, D., Cheng, A., and Qiu, B. (2016). "Changes in extreme temperature and precipitation events in the Loess Plateau (China) during 1960-2013 under global warming." *Atmospheric Research*, Elsevier B.V., 168, 33–48.

Tabari, H., and Hosseinzadeh Talaee, P. (2011). "Analysis of trends in temperature data in arid and semi-arid regions of Iran." *Global and Planetary Change*, Elsevier B.V., 79(1–2), 1–10.

Tabari, H., Marofi, S., Aeini, A., Talaee, P. H., and Mohammadi, K. (2011). "Trend analysis of reference evapotranspiration in the western half of Iran." *Agricultural and Forest Meteorology*, Elsevier B.V., 151(2), 128–136.

Tantawy, M. M., Ouda, S. A., and Khalil, F. A. (2007). "Irrigation optimization for different sesame varieties grown under water stress conditions." *Journal of Applied Sciences Research*, 3(1), 7–12.

Teng, J., Chiew, F. H. S., Timbal, B., Wang, Y., Vaze, J., and Wang, B. (2012). "Assessment of an analogue downscaling method for modelling climate change impacts on runoff." *Journal of Hydrology*, Elsevier B.V., 472–473, 111–125.

Teutschbein, C., and Seibert, J. (2012). "Bias correction of regional climate model simulations for hydrological climate-change impact studies: Review and evaluation of different methods." *Journal of Hydrology*, Elsevier B.V., 456–457, 12–29.

Thakkar, A. K., Desai, V. R., Patel, A., and Potdar, M. B. (2017a). "Impact assessment of watershed management programmes on land use/land cover dynamics using remote sensing and GIS." *Remote Sensing Applications: Society and Environment*, Elsevier, 5, 1–15.

Thakkar, A. K., Desai, V. R., Patel, A., and Potdar, M. B. (2017b). "Application of remote sensing in analysis of impact assessment using biomass vigour changes of watersheds." *Journal of Environmental Biology*, Triveni Enterprises, 38(4), 543.

Thormann, M. N., Bernier, L. P. Y., Foster, N. W., Schindler, D. W., and Beall, F. D. (2004). "Land-use practices and changes-forestry." Citeseer.

Tilman, D., Balzer, C., Hill, J., and Befort, B. L. (2011a). *Global food demand and the sustainable intensification of agriculture*. *Proceedings of the National Academy of Sciences*.

Tilman, D., Balzer, C., Hill, J., Befort, B. L., Sheng Yue, Paul Pilon (2011b). "Global food demand and the sustainable intensification of agriculture." *Theoretical and Applied Climatology*, Elsevier B.V., 104(3–4), 217–227.

Trang, N. T. T., Shrestha, S., Shrestha, M., Datta, A., and Kawasaki, A. (2017). "Evaluating the impacts of climate and land-use change on the hydrology and nutrient yield in a transboundary river basin: A case study in the 3S River Basin (Sekong, Sesan, and Srepok)." *Science of the Total Environment*, Elsevier B.V., 576, 586–598.

Tripathi, M. P., Panda, R. K., Raghuwanshi, N. S., and Singh, R. (2004). "Hydrological modelling of a small watershed using generated rainfall in the soil and water assessment tool model." *Hydrological Processes*, 18(10), 1811–1821.

Tripathi, M. P., Raghuwanshi, N. S., and Rao, G. P. (2006). "Effect of watershed subdivision on simulation of water balance components." *Hydrological Processes*, 20(5), 1137–1156.

Trömel, S., and Schönwiese, C. D. (2007). "Probability change of extreme precipitation observed from 1901 to 2000 in Germany." *Theoretical and Applied Climatology*, 87(1–4), 29–39.

Ullrich, A., and Volk, M. (2009). "Application of the Soil and Water Assessment Tool (SWAT) to predict the impact of alternative management practices on water quality and quantity." *Agricultural Water Management*, 96(8), 1207–1217.

UN Habitat. (2011). “Planning for Climate Change - A strategic, values-based approach for urban planners.”

Uniyal, B., Jha, M. K., and Verma, A. K. (2015). “Assessing Climate Change Impact on Water Balance Components of a River Basin Using SWAT Model.” *Water Resources Management*, 29(13), 4767–4785.

Vallam, P., and Qin, X. S. (2017). “Climate change impact assessment on flow regime by incorporating spatial correlation and scenario uncertainty.” *Theoretical and Applied Climatology*, Theoretical and Applied Climatology, 129(1–2), 607–622.

Varikoden, H., Mujumdar, M., Revadekar, J. V., Sooraj, K. P., Ramarao, M. V. S., Sanjay, J., and Krishnan, R. (2018). “Assessment of regional downscaling simulations for long term mean, excess and deficit Indian Summer Monsoons.” *Global and Planetary Change*, Elsevier, 162(November 2017), 28–38.

Veettil, A. V., and Mishra, A. K. (2016). “Water security assessment using blue and green water footprint concepts.” *Journal of Hydrology*, Elsevier B.V., 542, 589–602.

W. D. Rosenthal, R. Srinivasan, and J. G. Arnold. (2013). “Alternative River Management Using a Linked GIS-Hydrology Model.” *Transactions of the ASAE*, 38(3), 783–790.

Wakode, H. B., Dutta, D., Desai, V. R., Baier, K., and Azzam, R. (2013). “Morphometric analysis of the upper catchment of Kosi River using GIS techniques.” *Arabian Journal of Geosciences*, Springer, 6(2), 395–408.

Wang, G., Yang, H., Wang, L., Xu, Z., and Xue, B. (2014a). “Using the SWAT model to assess impacts of land use changes on runoff generation in headwaters.” *Hydrological Processes*, 28(3), 1032–1042.

Wang, Q., Zhang, M., Wang, S., Ma, Q., and Sun, M. (2014b). “Changes in temperature extremes in the Yangtze River Basin, 1962-2011.” *Journal of Geographical Sciences*, 24(1), 59–75.

Wang, W., and Ding, J. (2003). “Wavelet Network Model and Its Application to the Prediction of Hydrology.” *Forecast*, 1(1), 67–71.

Weng, Q. (2002). “Land use change analysis in the Zhujiang Delta of China using satellite remote sensing, GIS and stochastic modelling.” *Journal of environmental management*, 64(3), 273–284.

Wilby, R. L., and Harris, I. (2006). “A framework for assessing uncertainties in climate change impacts: Low-flow scenarios for the River Thames, UK.” *Water Resources Research*, 42(2), 1–10.

Worku, T., Khare, D., and Tripathi, S. K. (2017). “Modeling runoff–sediment response to land use/land cover changes using integrated GIS and SWAT model in the Beressa watershed.” *Environmental Earth Sciences*, Springer Berlin Heidelberg, 76(16), 1–14.

Wu, Y., Li, S., and Yu, S. (2016). “Monitoring urban expansion and its effects on land use and land cover changes in Guangzhou city, China.” *Environmental Monitoring and Assessment*, 188(1), 1–15.

Xiao, J., Shen, Y., Ge, J., Tateishi, R., Tang, C., Liang, Y., and Huang, Z. (2006). “Evaluating urban expansion and land use change in Shijiazhuang, China, by using GIS and remote sensing.” *Landscape and Urban Planning*, 75(1–2), 69–80.

Xu, C. Y., and Singh, V. P. (2004). “Review on regional water resources assessment models under stationary and changing climate.” *Water Resources Management*, 18(6), 591–612.

Xu, C. yu, Gong, L., Jiang, T., Chen, D., and Singh, V. P. (2006). “Analysis of spatial distribution and temporal trend of reference evapotranspiration and pan evaporation in Changjiang (Yangtze River) catchment.” *Journal of Hydrology*, 327(1–2), 81–93.

Xu, K., Milliman, J. D., and Xu, H. (2010). “Temporal trend of precipitation and runoff in major Chinese Rivers since 1951.” *Global and Planetary Change*, Elsevier B.V., 73(3–4), 219–232.

Xu, Z. X., Takeuchi, K., and Ishidaira, H. (2003). “Monotonic trend and step changes in Japanese precipitation.” *Journal of Hydrology*, 279(1–4), 144–150.

Yang, T., Li, H., Wang, W., Xu, C. Y., and Yu, Z. (2012). “Statistical downscaling of extreme daily precipitation, evaporation, and temperature and construction of future scenarios.” *Hydrological Processes*, 26(23), 3510–3523.

You, Q., Kang, S., Aguilar, E., Pepin, N., Flugel, W. A., Yan, Y., Xu, Y., Zhang, Y., and Huang, J. (2011). "Changes in daily climate extremes in China and their connection to the large scale atmospheric circulation during 1961-2003." *Climate Dynamics*, 36(11–12), 2399–2417.

Zahabiyoun, B., Goodarzi, M. R., Bavani, A. R. M., and Azamathulla, H. M. (2013). "Assessment of Climate Change Impact on the Gharesou River Basin Using SWAT Hydrological Model." *Clean - Soil, Air, Water*, 41(6), 601–609.

Zakaria, N. A., Ghani, A. A., Abdullah, R., Sidek, L. M., Kassim, A. H., and Ainan, A. (2004). "MSMA–a new urban stormwater management manual for Malaysia." *Available at redac. eng. usm. my/html/publish/2004_06. pdf. Accessed on*, 15(3), 2008.

Zhai, P., Zhang, X., Wan, H., and Pan, X. (2005). "Trends in total precipitation and frequency of daily precipitation extremes over China." *Journal of Climate*, 18(7), 1096–1108.

Zhang, X., Aguilar, E., Sensoy, S., Melkonyan, H., Tagiyeva, U. (2005). "Trends in Middle East climate extreme indices from 1950 to 2003." *Journal of Geophysical Research Atmospheres*, 110(22), 1–12.

Zhang, X., Wan, H., Zwiers, F. W., Hegerl, G. C., and Min, S. K. (2013). "Attributing intensification of precipitation extremes to human influence." *Geophysical Research Letters*, 40(19), 5252–5257.

Zhao, Y., Zou, X., Cao, L., and Xu, X. (2014). "Changes in precipitation extremes over the Pearl River Basin, southern China, during 1960-2012." *Quaternary International*, Elsevier Ltd, 333, 26–39.

Zhou, B., Xu, Y., Wu, J., Dong, S., and Shi, Y. (2016). "Changes in temperature and precipitation extreme indices over China: Analysis of a high-resolution grid dataset." *International Journal of Climatology*, 36(3), 1051–1066.

Zhu, J. (2012). "Impact of Climate Change on Extreme Rainfall across the United States." *Journal of Hydrologic Engineering*, 18(10), 1301–1309.

Zope, P. E., Eldho, T. I., and Jothiprakash, V. (2017). "Hydrological impacts of land use–land cover change and detention basins on urban flood hazard: a case study of Poisar River basin, Mumbai, India." *Natural Hazards*, Springer Netherlands, 87(3), 1267–1283.

List of Publication/conferences

Publications

1. **Ayush Chandrakar**, Deepak Khare, Radha Krishan, "Assessment of Spatial and Temporal Trends of Long Term Precipitation over Kharun Watershed, Chhattisgarh, India", in Environmental Processes, 4(4) , 959-974, Springer, 2017. (SCOPUS indexed).
2. **Ayush Chandrakar**, Deepak Khare, Radha Krishan, "Identification of long term Changes in meteorological extremes over a tropical watershed, Central India" submitted to Journal of Meteorological Applications, Royal Meteorological Society. (Manuscript id: - MET-19-0117). (under review)
3. **Ayush Chandrakar**, Deepak Khare, Radha Krishan, "Climate shift and its impact on indices of climatic extremes over a small watershed", submitted to Journal of Environmental Monitoring and Assessment, Springer. (Manuscript id: - EMAS-D-19-01023). (under review)

Conferences

1. **Ayush Chandrakar**, Deepak Khare, Radha Krishan, Santosh S Palmate, "Assessing Spatiotemporal Trends of Long Term Temperature over Kharun Watershed Chhattisgarh, India", in American Geophysical Union, Fall meeting 2018, Washington, DC, USA, 2018.
2. **Ayush Chandrakar,** Brij K. Pandey, Radha Krishan, Deepak Khare, Tesfa Worku, "Hydrological Simulation of an Ungauged Catchment (Kharun Watershed) using SWAT", in International Conference on Sustainable Technologies for Intelligent Water Management. (STIWM), Roorkee, 2018.

Publication/Conference outside research area

1. Radha Krishan, Bhaskar R. Nikam, Santosh M. Pingale, **Ayush Chandrakar**, Deepak Khare, "Analysis of Trends in Rainfall and Dry/Wet Years over a century in Eastern Ganga Canal Command", 25(4), 561-574 in Journal of Meteorological Applications, 2018.
2. Radha Krishan, Deepak Khare, Bhaskar R Nikam, **Ayush Chandrakar**, , "Impact of Climate Shift on Rainfall and Temperature Trend in Eastern Ganga Canal Command", in International Journal of Environmental and Ecological Engineering, 2018
3. Radha Krishan**, Ayush Chandrakar**, Bhaskar R Nikam, Deepak Khare, "Analysis of Trends in Rainfall over a Century in Eastern Ganga Canal Command", in International Conference on Hydraulics, Water Resources and Coastal Engineering (Hydro2016), Pune, 2016.